DANMARKS OG GRØNLANDS GEOLOGISKE UNDERSØGELSE RAPPORT 2019/25

Investigating the discrepancy between gas and liquid Permeability in the Gassum and Skagerrak Formations

Hanne D. Holmslykke, Rikke Weibel, Kathrine Hedegaard
Sachin Karan & Annette Elisabeth Rosenbom

GEOLOGICAL SURVEY OF DENMARK AND GREENLAND
DANISH MINISTRY OF CLIMATE, ENERGY AND UTILITIES

GEUS

DANMARKS OG GRØNLANDS GEOLOGISKE UNDERSØGELSE RAPPORT 2019/25

Investigating the discrepancy between gas and liquid permeability in the Gassum and Skagerrak Formations

GEOTHERM – Geothermal energy from sedimentary reservoirs – Removing obstacles for large scale utilization

Innovation Fund Denmark: project 6154-00011B
(Final report in WP3)

Hanne D. Holmslykke, Rikke Weibel, Kathrine Hedegaard
Sachin Karan & Annette Elisabeth Rosenbom

GEOLOGICAL SURVEY OF DENMARK AND GREENLAND
DANISH MINISTRY OF CLIMATE, ENERGY AND UTILITIES

GEUS

Dansk sammendrag

Den danske undergrund rummer sandstensreservoirer, der er velegnede til indvinding af geotermisk energi i store dele af landet. Potentialet er stort, men der er en række udfordringer forbundet med efterforskning og udnyttelse af ressourcen, hvoraf estimering af reservoirkvaliteten og især reservoirets permeabilitet er en af de væsentligste begrænsende faktorer. Denne GEOTHERM rapport belyser forhold omkring bestemmelse af permeabilitet.

Permeabilitet er et mål for et porøst mediums gennemtrængelighed for gas eller væske som følge af en trykforskel. Permeabilitet er en af de vigtigste parameter til vurdering af et geotermisk reservoirs ydeevne, og pålidelige estimater af et reservoirs permeabilitet er derfor yderst vigtig. Selvom det er et reservoirs væske permeabilitet, der er interessant, er det ofte gas-permeabiliteten, der måles i laboratoriet, da væske-permeabiliteten er omkostningstung, vanskelig og tidskrævende at måle. I teorien er permeabiliteten uafhængig af hvilken fluid (gas eller væske), der anvendes ved permeabilitetsmålingen. Dette har dog vist sig ikke altid at være tilfældet, idet væske-permeabiliteten ofte er betydeligt lavere end gas-permeabiliteten. Derfor er der i dette projekt udført en række detaljerede laboratorieforsøg med henblik på at undersøge forskellen mellem gas- og væske-permeabiliteten for kernemateriale fra Skagerrak og Gassum Formationerne i boringer fra Nordjylland. Resultaterne viser, at der i et log-log plot er en lineær sammenhæng mellem gas- og væske-permeabiliteten, samt at denne sammenhæng ser ud til være forskellig for de to undersøgte geologiske formationer. Det anbefales, at de lineære sammenhænge indgår i fremtidige estimeringer af brine-permeabiliteter af sandsten i områder, hvor de nævnte formationer udgør de geotermiske reservoirer. Det anbefales endvidere at tilsvarende analyser udføres for de øvrige geotermiske reservoirer, Bunter Sandsten og Haldager Sandsten formationerne samt for Skagerrak og Gassum formationerne i den øvrige del af landet.

Extended summary

This report summarises the results of the research project “Investigating the discrepancy between gas and liquid permeability in the Gassum and Skagerrak Formations”. The project is part of WP3 in the project GEOTHERM – Geothermal energy from sedimentary reservoirs – Removing obstacles for large scale utilization, funded by the Innovation Fund Denmark (IFD). The objective is to increase our understanding of the observed difference between measured gas and liquid permeability in order to improve our prediction of the permeability of a geological reservoir from geophysical well logs combined with data obtained from measurements of permeability in the laboratory.

Permeability represents the ability of rock material to conduct fluid flow and is one of the most important properties of porous media when evaluating a geothermal project. Since liquid permeability may be difficult and time consuming to measure accurately, often the gas permeability is measured in the laboratory to estimate reservoir permeability even though it is the liquid permeability that is of interest for evaluation of the reservoir performance. In theory, the permeability is independent of the fluid used for the permeability measurements. However, this is not always so, and often the permeability to liquid is significantly lower than that to gas. Therefore, a detailed series of laboratory experiments have been conducted to investigate the discrepancy between measured gas and liquid permeability for sandstone core specimens from the Skagerrak and the Gassum Formation in the North Jutland region.

In this study, gas and Klinkenberg permeability are measured and compared with measured brine and Milli-Q water permeability for sandstones with as large a variability in permeability, average grain size, clay mineral type and abundances as possible. Klinkenberg permeability is a gas slippage corrected permeability that in theory should represent equivalent liquid permeability. Detailed characterisation of the core material is made by nuclear magnetic resonance (NMR) to give an indication of the pore size of the core material, mercury-injection capillary pressure (MICP) to estimate the distribution of the pore throat radii of the specimens, by BET (Brunauer, Emmett and Teller) to determine the specific surface area of the specimens and by petrographic analysis to estimate the average grain size, clay content and mineralogy. The effluent from the liquid permeability measurements is filtered and analysed for major cations and the residue from the filtration is analysed by scanning electron microscopy (SEM) for identification of fines released from the core specimen during the liquid permeability determination.

The results show that the permeability to liquid is always lower than that to gas, even the Klinkenberg permeability. Thus, the ratio between measured gas (k_g) and Klinkenberg (k_K) permeability to brine (k_b) permeability is k_g/k_b = 1.6 - 70 and k_K/k_b = 0.5 – 29, respectively, while the ratios to Milli-Q water ($k_{Milli\text{-}Q}$) permeability is $k_g/k_{Milli\text{-}Q}$ = 2.3 – 140 and $k_K/k_{Milli\text{-}Q}$ = 0.5 – 37, respectively. A linear correlation on a log-log scale is observed for the Klinkenberg/gas, brine/gas, brine/Klinkenberg, Milli-Q water/gas, Milli-Q water/Klinkenberg and Milli-Q water/brine permeabiilties, respectively with r^2 > 0.9650. The following correlations are found when the permeabilities are inserted in the units mD:

Brine vs gas permeability:

Gassum Fm: $\log(k_b) = 1.0591 \log(k_g) - 0.4652$ $r^2 = 0.9959$

Skagerrak Fm: $\log(k_b) = 1.3428 \log(k_g) - 1.3615$ $r^2 = 0.9774$

Brine vs Klinkenberg permeability

Gassum Fm: $\log(k_b) = 1.0178 \log(k_K) - 0.3073$ $r^2 = 0.9929$

Skagerrak Fm: $\log(k_b) = 1.1188 \log(k_K) - 0.9191$ $r^2 = 0.9890$

Milli-Q water vs gas permeability:

Gassum Fm: $\log(k_{Milli\text{-}Q}) = 1.2166 \log(k_g) - 0.8779$ $r^2 = 0.9843$

Skagerrak Fm: $\log(k_{Milli\text{-}Q}) = 1.7453 \log(k_g) - 1.6895$ $r^2 = 0.9774$

Milli-Q water vs Klinkenberg permeability

Gassum Fm: $\log(k_{Milli\text{-}Q}) = 1.1982 \log(k_K) - 0.7424$ $r^2 = 0.9894$

Skagerrak Fm: $\log(k_{Milli\text{-}Q}) = 1.1247 \log(k_K) - 1.0688$ $r^2 = 0.9651$

Milli-Q water vs brine permeability:

Gassum Fm: $\log(k_{Milli\text{-}Q}) = 1.0564 \log(k_b) - 0.1656$ $r^2 = 0.9963$

Skagerrak Fm: $\log(k_{Milli\text{-}Q}) = 1.0231 \log(k_b) - 0.1866$ $r^2 = 0.9947$

Interestingly, a clear distinction between the Gassum and the Skagerrak Formation is observed in the correlation between the permeabilities to different fluids (e.g. gas/brine or Klinkenberg/Milli-Q water). In contrast, nearly all of the data follow the same trend in the correlation between the permeabilities with the same fluid (gas/Klinkenberg and Milli-Q water/brine) and here no difference is observed for the data from the two different geological formations investigated in this study.

Even though the mineralogy may affect the permeability, no clear correlation is observed between the abundance of clay minerals and the discrepancy between the gas/Klinkenberg and the liquid permeability. Thus, our data indicate that the mineralogy may to some extend account for the smaller variation in the permeability around the regression lines, rather than for the larger difference between the gas/Klinkenberg and the liquid permeability. However, the controlling factor(s) for the difference between the gas/Klinkenberg permeability and the liquid permeability remains unknown and further detailed investigations of the results of this study is proceeding. We expect that the numerical modelling and the discrepancies between measured and simulated pressure can be used to analyze and deduce the reasoning for the inconsistencies for the various plugs and enable us to conduct a more sound based estimation of the brine and Milli-Q water permeability from the gas permeability of the plug.

We recommend that the observed linear correlations between brine permeability and gas or Klinkenberg permeability for the Gassum and the Skagerrak Formations are included in future estimates of brine permeability of sandstone in areas where the mentioned formations constitute the geothermal reservoirs. It is also recommended that similar analyses are carried out for other Danish geothermal reservoirs i.e. the Bunter Sandstone and Haldager Sandstone Formations as well as for the Skagerrak and Gassum Formations in the rest of the country.

Content

1. Introduction 6

2. Materials and methods 7

2.1 Work-flow diagram of analytical procedures 7
2.2 Sample material and fluid 8
2.3 Experimental procedure 10
2.3.1 Permeability 10
2.3.2 Liquid permeability 10
2.4 Material characterisation 12
2.4.1 He-porosity and grain density 12
2.4.2 Nuclear magnetic resonance (NMR) 12
2.4.3 Mercury-injection capillary pressure (MICP) 13
2.4.4 Specific surface area (BET) 13
2.4.5 Optical- and scanning electron microscopy 13

3. Results and discussion 15

3.1 Liquid permeability calculations 15
3.2 Gas versus Klinkenberg permeability 17
3.3 Liquid versus gas and Klinkenberg permeability 18
3.4 Milli-Q water permeability versus brine permeability 25
3.5 Numerical modelling 30
3.5.1 Theoretical assumptions behind permeability estimation 30
3.5.2 Conceptual model 31
3.5.3 Results and discussion 32

4. Recommendations for further studies 35

5. Conclusions 36

6. References 37

Appendices
Appendix A: Overview of results
Appendix B: Conventional core analysis (gas and Klinkenberg permeability) results
Appendix C: Liquid permeability results
Appendix D: NMR results
Appendix E: MICP results
Appendix F: BET results
Appendix G: Water chemistry
Appendix H: Mineralogical overview

1. Introduction

This report summarises the results and finalizes the reporting of Milestone 3.6b as part of WP3 in the project GEOTHERM – Geothermal energy from sedimentary reservoirs – Removing obstacles for large scale utilization, funded by the Innovation Fund Denmark (IFD). In this part of the project, a detailed investigation of the observed discrepancy between measured gas and liquid permeabilities of core material from sandstone reservoirs is carried out.

Direct use of geothermal energy for heating purposes is rapidly growing worldwide (Lund and Boyd, 2016) . A key parameter when assessing the properties of a geothermal reservoir is the permeability, i.e. the capacity for flow through the porous material. In theory, the permeability is solely related to the pore geometry of the rock and is independent of the fluid used for the permeability measurements. The objective is to increase our understanding of the observed difference between measured gas and liquid permeability in order to improve our prediction of the permeability of a geological reservoir from geophysical well logs combined with “hard” data obtained from measurements of permeability on small pieces of cylindrical core samples (typically c. 2.5 cm in diameter and c. 5 cm in length). As liquid permeability may be difficult and time consuming to measure accurately, it is often mainly the gas permeability that is measured in the laboratory although it is the liquid permeability that is of interest for evaluation of the reservoir performance. In theory, the liquid permeability can be inferred from the gas permeability (Klinkenberg, 1941). However, it is now clear that this is not always the case and the reason for this is poorly understood (Rosenbrand et al., 2015b; Duan and Yang, 2014; Al-Bulushi et al., 2012; Loosveldt et al., 2002). Currently, we know that the relationship is complex and highly dependent on e.g. the mineralogical composition of the specific reservoir sandstone under study. Furthermore, in complex geological materials, such as porous sandstones, the measured permeability of the porous medium varies considerably depending on the composition of the fluid flowing in the pore network (Cardoso and Balaban, 2015; Rosenbrand et al., 2015b; Wang et al., 2015). The rock/liquid/gas permeability interrelation may to some extent be explained by existing theory such as the Klinkenberg effect (Klinkenberg, 1941) and the diffuse double layer (DLVO) theory (Rosenbrand et al., 2015b; Rosenbrand et al., 2014). This is, however, not always a sufficient explanation, and especially in sandstones with complex mineralogical composition, the common theory fails in the description of laboratory results. Therefore, in this study the discrepancy between measured gas and liquid permeabilities of core materials from sandstone reservoirs is carried out on a variety of different sandstones. The project consists of the following tasks:

- Thorough laboratory core flooding experiments designed to measure the permeability of selected core material using gas, brine and Milli-Q water as the flooding fluid.
- Characterisation of changes in the chemical composition of the effluent from the liquid permeability measurements and collection of potential fines released during the flooding experiments.
- Detailed characterisation of the core material (Nuclear magnetic resonance (NMR), specific surface area (BET), mercury-injection capillary pressure (MICP), optical and scanning electron microscopy (SEM)).
- Numerical modelling of the experiments.

2. Materials and methods

2.1 Work-flow diagram of analytical procedures

A series of laboratory experiments have been conducted (Figure 2.1) to investigate the discrepancy between measured gas and liquid permeability for sandstone core specimens from the Skagerrak and the Gassum Formation in the North Jutland region. Gas and Klinkenberg permeability were measured and compared with measured brine and Milli-Q water permeability. Detailed characterisation of the core material is made by nuclear magnetic resonance (NMR) to give an indication of the pore size of the specimen, mercury-injection capillary pressure (MICP) to estimate the distribution of the pore throat radii of the specimens, BET to determine the specific surface area of the specimens and by petrographic analysis (SEM and thin section) to estimate the clay content and mineralogy. The effluent from the liquid permeability measurements is collected, filtered and analysed for major cations. The residue from the filtration is analysed by SEM for identification of fines released from the core specimen during the liquid permeability determination.

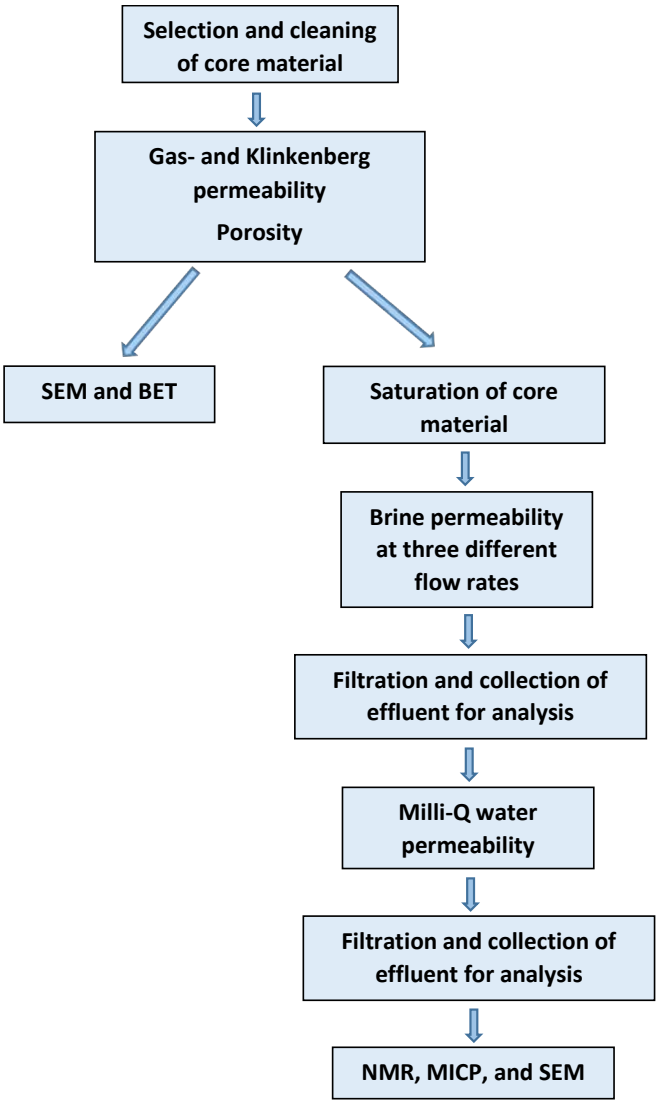

Figure 2.1 *Work-flow diagram of the analytical procedure in this study*

2.2 Sample material and fluid

In all, 20 sandstone specimens were plugged (1”) from cores of the Skagerrak and the Gassum Formation in the North Jutland region (Table 2.1). A careful selection had the scope of representing variations in grain size, sorting, porosity, permeability, clay content and mineralogy. The Triassic Skagerrak Formation and the Upper Triassic – Lower Jurassic Gassum Formation are potential geothermal reservoir rocks in large parts of Denmark (Figure 2.2). The Skagerrak Formation represents sandstones deposited mainly by braided streams in an arid climate, whereas the Gassum Formation represents sandstones deposited in shallow marine and paralic environments under humid climatic conditions (Weibel et al., 2017; Olivarius and Nielsen, 2016; Nielsen, 2003). The grain sizes and degree of sorting varies due to differences in depositional environments. The dominant clay mineral types vary between these two formations due to climatic differences affecting the early diagenetic changes (Weibel et al., 2017). The samples were selected in pairs so that sandstones with similar average grain size represented different types and/or abundances of clay minerals. In a similar way, paired sandstones with similar average grain sizes, but different porosity and permeability were selected.

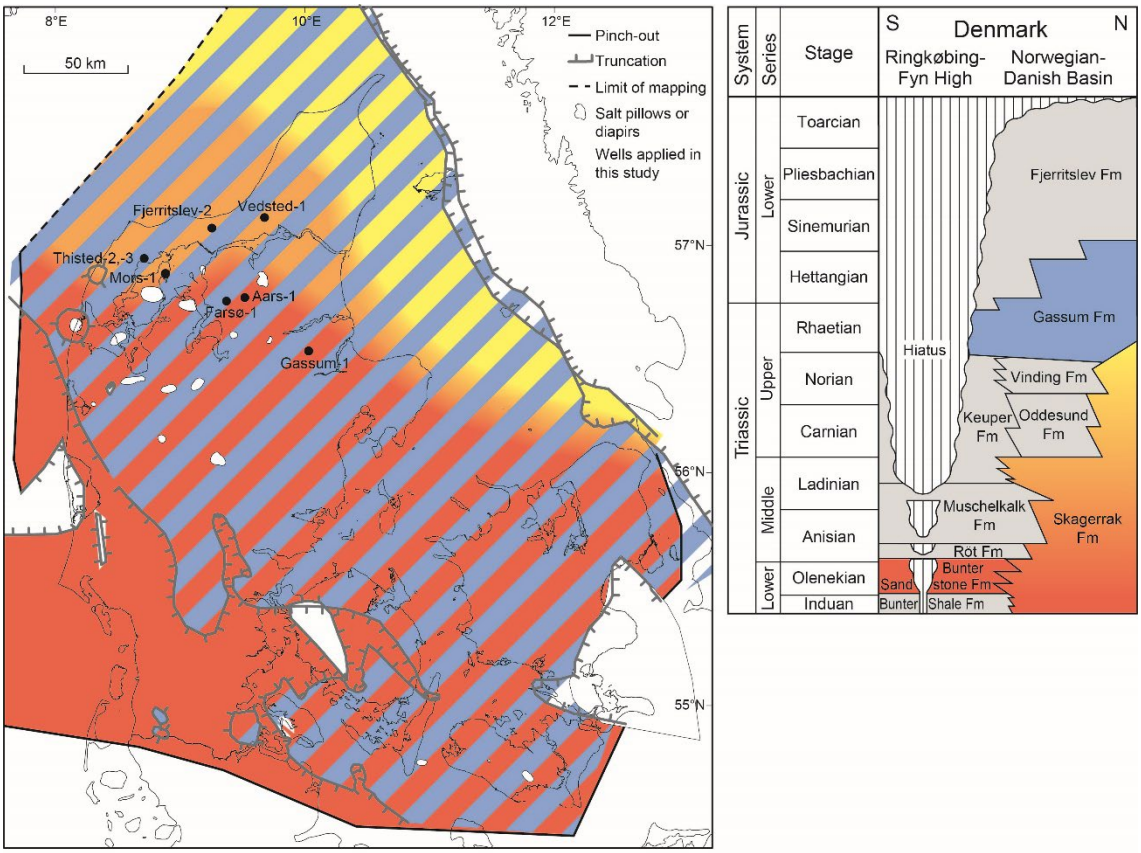

Figure 2.2 *Location of the wells from which core material was selected for permeability measurements and distribution of geothermal reservoirs: Skagerrak (yellow – orange), and Gassum (blue) formations. Modified from (Weibel et al., 2017).*

Table 2.1 *Overview of plug specimens used in the study. The table shows the type of analysis performed with each plug specimen.*

Sample id	Lab id	Formation	Well	Depth	CCAL	Liquid perm		Effluent	Filter	NMR		MICP	BET	SEM
				m		Brine	DW	analysis	material	Brine	DW			
Ve1-Ga2009.96A	8A	Gassum	Vedsted-1	2009.96	x							x	x	x
Ve1-Ga2009.96C	8C	Gassum	Vedsted-1	2009.96	x	x	x	x	x	x	x			
Ve1-Ga2010.17B	9B	Gassum	Vedsted-1	2010.17	x	x	x	x	x	x	x			
Ve1-Ga2010.17C	9C	Gassum	Vedsted-1	2010.17	x							x	x	x
Aa1-Ga3325.03A	11A	Gassum	Aars-1	3325.03	x							x	x	x
Aa1-Ga3325.03B	11B	Gassum	Aars-1	3325.03	x	x	x	x	x	x	x			
Aa1-Ga3326.49A	13A	Gassum	Aars-1	3326.49	x							x	x	x
Aa1-Ga3326.49B	13B	Gassum	Aars-1	3326.49	x	x	x	x	x	x	x			
Aa1-Ga3318.20A	20	Gassum	Aars-1	3318.20	x	x	x	x	x	x	x			
Aa1-Ga3352.22A	14	Gassum	Aars-1	3352.22	x	x	x	x	x	x	x			
Aa1-Ga3352.22B	14A	Gassum	Aars-1	3352.22	x							x	x	x
Aa1-Ga3353.05A	16	Gassum	Aars-1	3353.05	x	x	x	x	x	x	x			
Aa1-Ga3320.80A	21A	Gassum	Aars-1	3320.80	x	x	x	x	x	x	x			
Aa1-Ga3320.80B	21B	Gassum	Aars-1	3320.80	x							x	x	x
Aa1-Ga3275.38A	22A	Gassum	Aars-1	3275.38	x	x	x	x	x	x	x			
Aa1-Ga3275.38B	22B	Gassum	Aars-1	3275.38	x							x	x	x
Aa1-Ga3318.10A	10	Gassum	Aars-1	3318.10	x	x	x	x	x	x	x			
Aa1-Ga3318.10B	10A	Gassum	Aars-1	3318.10	x							x	x	x
Aa1-Ga3325.52A	12A	Gassum	Aars-1	3325.52	x	x	x	x	x	x	x			
Aa1-Ga3325.52B	12B	Gassum	Aars-1	3325.52	x							x	x	x
Mo1-Sk5034.24A	15	Skagerrak	Mors-1	5034.24	x	x	x	x	x	x	x			
Mo1-Sk5034.24B	15A	Skagerrak	Mors-1	5034.24	x							x	x	x
Mo1-Sk5089.57A	3	Skagerrak	Mors-1	5089.57	x	x	x	x	x	x	x			
Mo1-Sk5089.57B	3A	Skagerrak	Mors-1	5089.57	x							x	x	x
Th2-Sk2919.35A	4	Skagerrak	Thisted-2	2919.35	x							x	x	x
Th2-Sk2919.35B	4A	Skagerrak	Thisted-2	2919.35	x	x	x	x	x	x	x			
Th2-Sk2923.05A	5	Skagerrak	Thisted-2	2923.05	x	x	x	x	x	x	x			
Th2-Sk2923.05B	5A	Skagerrak	Thisted-2	2923.05	x							x	x	x
Th2-Sk2761.63A	6	Skagerrak	Thisted-2	2761.63	x	x	x	x	x	x	x			
Th2-Sk2761.63B	6A	Skagerrak	Thisted-2	2761.63	x							x	x	x
Fr2-Sk1051.00	23	Skagerrak	Frederikshavn-2	1051.00	x	x	x	x	x					
Ga1-Sk3124.90A	2	Skagerrak	Gassum-1	3124.90	x	x	x							
Ga1-Sk3124.90B	2A	Skagerrak	Gassum-1	3124.90	x							x	x	x
Ga1-Sk3032.42A	1	Skagerrak	Gassum-1	3032.42	x	x	x	x	x	x	x			
Ga1-Sk3032.42B	1A	Skagerrak	Gassum-1	3032.42	x							x	x	x
Ve1-Sk2062.92A	7A	Skagerrak	Vedsted-1	2062.92	x							x	x	x
Ve1-Sk2062.92B	7B	Skagerrak	Vedsted-1	2062.92	x	x	x	x	x	x	x			

CCAL: Conventional cor eanalysis e.g. porosity, gas- and Klinkenberg permeabiilty
NMR: Nuclear megnetic resonance
MICP: Mercury injection capillary pressure
BET: specific surface area
SEM: Scanning electron microscope

Table 2.2 *Chemical composition of the synthetic Skagerrak and Gassum brines used for the liquid permeability tests. The brines are modified from Laier (1982) and (Laier, 2008), respectively.*

Element	Skagerrak g/L	Gassum g/L
Na	57	70
K	3	1.8
Mg	8.1	2.3
Ca	36	33
Sr	0.95	0.90
HCO_3^-	0.08	0.02
Br^-	-	1.1
SO_4^{2-}	0.27	0.25

The chemical composition of the synthetic Skagerrak and Gassum Formation brine applied in the liquid permeability measurements were modified from Laier (1982, 2008) and shown in Table 2.2. The saturation indices for relevant minerals were checked using the geochemical modelling tool PHREEQC (Parkhurst and Appelo, 2013) to ensure that unwanted precipitation of minerals (e.g. calcite) did not occur in the brine prior to the liquid permeability measurements.

2.3 Experimental procedure

2.3.1 Permeability

2.3.1.1 Gas permeability (uncorrected)

The plug specimen was mounted in a Hassler core holder, and a confining pressure of 400 psig (27.6 barg) was applied to the sleeve. The uncorrected permeability to gas was measured by flowing nitrogen gas (N_2) through a plug specimen of known dimensions at differential pressures between 0 and 1 bara. No back pressure was applied. The readings of the digital gas permeameter were checked regularly by routine measurement of permeable steel reference plugs (Core Laboratories™ gas permeability reference plug set).

2.3.1.2 Klinkenberg permeability (corrected)

The Klinkenberg (slip) corrected gas permeability, also referred to as the equivalent liquid permeability, was calculated from gas permeability measurements. The procedure was the same as described above, but performed at three different mean pressures and with a back pressure at the effluent end of the core holder. Nitrogen gas pressures at 3, 5 and 8 bara were applied at the upstream end of the plug, and the downstream pressure was regulated until a suitable flow rate was obtained. During the measurements, the differential pressure across the plug specimen was kept approximately constant around 250 mbara in order to maintain a similar flow regime during the three measurements. When a steady state was reached, the upstream pressure, differential pressure across the plug, and the flow reading was recorded. A linear regression of permeability on an inverse mean pressure plot was performed for the three measurements, and the intercept on the permeability axis was the Klinkenberg corrected gas permeability. The readings of the digital gas permeameter were checked regularly by routine measurement of permeable steel reference plugs (Core Laboratories™ gas permeability reference plug set).

2.3.2 Liquid permeability

A series of fluid permeability experiments was performed such that each specimen was flooded with synthetic brine at three different flow rates following flooding with milli-Q water at the same three flow rates. The specimens from the Skagerrak Formation were flooded with the synthetic Skagerrak brine, while the specimens from the Gassum Formation were

flooded with the synthetic Gassum brine. Prior to testing, the specimens were cleaned in methanol to remove any salt precipitation; and the He-porosity, N_2-gas permeability and Klinkenberg permeability measured (section 2.3.1.1and 2.3.1.2). The specimens were then kept in vacuum (at -1 mbar) and subsequently pressure-saturated (at 110 bar for three days) in degassed brine (Table 2.2). The saturation state of the specimen was verified using the Archimedes test.

Upon testing, a brine saturated specimen was placed in a Viton sleeve in a hydrostatic core holder and a confining pressure of 27.6 bar (400 psi) was applied (Figure 2.3). The fluid permeability was measured under hydrostatic conditions at 25°C using first synthetic brine succeeded by Milli-Q water as the flooding fluid while imposing a backpressure of c. 2 bar. The pressure gradient across the sample was measured with two pressure transducers placed upstream and downstream of the core holder, respectively. For both fluids, the permeability was measured at three different flow rates ranging from 0.08 ml/h to 119 ml/h corresponding to pore velocities between 0.25 cm/h and 90 cm/h, and subsequently the flow rate was decreased to the lowest flow rate. Enough time at each flow rate was allowed to ensure a stable pressure gradient across the sample (generally one hour) before changing the flow rate. Prior to permeability measurements with Milli-Q water, the core specimen was flushed with Milli-Q water at the lowest test rate or lower until the electrical conductivity (EC) of the effluent was below 500 µS/cm after which the Milli-Q water permeability measurement was initiated. During permeability measurements with either fluids, the EC gauge was bypassed.

The viscosities of the Gassum and the Skagerrak brines were determined experimentally. First, Milli-Q water, with a viscosity of 0.89 cP, was flooded through a 13.2 m long thin tube mounted instead of the core holder, and the inner diameter of the tube was calculated using Poiseuille's equation. Secondly, brine was flooded through the tube and Poiseuille's equation again used to calculate the viscosity of the brine.

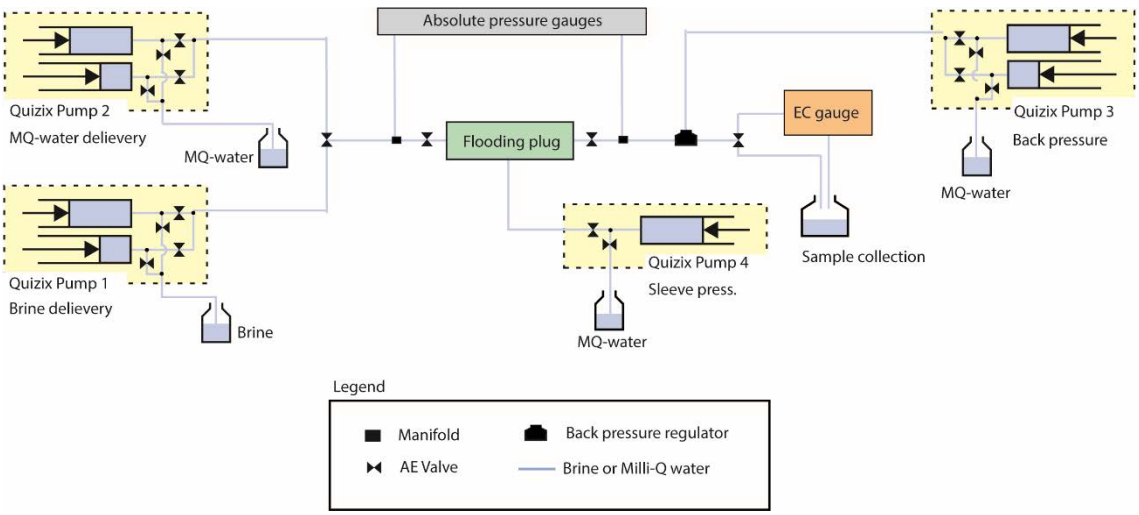

Figure 2.3: *Experimental setup for measuring the liquid permeability.*

During permeability measurements, the effluent was collected, such that one collective sample was obtained for each specimen containing the effluent from permeability measurements at three velocities with either brine or Milli-Q water. The brine and Milli-Q water effluents were

passed through a 0.45 µm and 0.22 µm membrane filter, respectively, and split into two separate polyethylene vials. Samples for analysis for cations received 1 vol% of 7M HNO_3 and were kept refrigerated until inductively coupled plasma mass spectroscopy (ICP-MS) analysis. The applied instrument was a PerkinElmer Elan6100DRC Quadrupol with a standard deviation of 3-15% depending on the element measured. Samples for anion analysis (chloride and sulphate) were frozen until ion-chromatography analysis. The applied instrument was a Metrohm IC, 819 detector, column Metrosep A sup. 5 – 150/4.0 with a quantification limit of 0.05 mg/L. The filters was flushed with 200 ml Milli-Q water to remove any salts and the types of fines were identified by SEM analysis. Following the liquid permeability measurement, the core specimens were characterised by NMR, MICP, BET and thin section analysis.

2.4 Material characterisation

2.4.1 He-porosity and grain density

The porosity was determined by the difference between the measured grain volume and measured bulk volume at room temperature. The Helium porosity technique based on Boyle's Law was used for the determination of grain volume, applying a double chambered Helium porosimeter with digital readout. The specimen bulk volume was measured by total submersion of the plug specimen in a mercury bath using Archimedes principle. Grain density was calculated from the grain volume measurement and the weight of the cleaned, dry specimen.

The Helium porosimeter was calibrated using a set of steel plugs (Core Laboratories™ volume reference plug set) before the measurement of plug samples was initiated. The bulk volume apparatus was checked using a steel plug with known volume.

2.4.2 Nuclear magnetic resonance (NMR)

The NMR technique is based on the magnetization decay of fluid molecules and gives an indication of the pore size of the specimen. The hydrogen nuclei (protons) in the pore fluid are aligned with static and oscillating magnetic fields and the relaxation time after the removal of the magnetic field is measured. The NMR relaxation response of a single fluid filled pore can be expressed by the exponential decay of the transverse magnetization signal, called $1/T_2$. T_2 is a characteristic time that represents the magnetic decay of the protons within the fluid after their polarization. The T_2 relaxation time indicates the size of pores containing the protons. Relaxation times are short in small pores since the hydrogen molecules are near the grain surface where the interaction with surface charges promotes the relaxation. Likewise, relaxation times are longer in larger pores.

NMR measurements were made using a GeoSpec2 NMR Core Analyzer at frequency of 2.25 MHz, temperature of 35°C and atmospheric pressure. T_2 relaxations were measured using the Carr-Purcel-Meiboom-Gill (CPMG) pulse sequences. The Raw NMR data were acquired

with the Lithometrix (Green imaging technologies, INC.) software and the T_2 relaxation spectra were generated using the WinDXP (Oxford Instruments, UK) and Lithometrix (Green imaging technologies, INC.) softwares. All measurements were conducted to a targeted Signal to Noise Ratio of 200. The recycle delay (repetition time) was selected at 7.5 s, number of echoes at 4545, and the CPMG inter echo spacing (τ) at 55 µs. NMR measurements were made on samples saturated with first Milli-Q water and subsequently on the same samples saturated with brine.

2.4.3 Mercury-injection capillary pressure (MICP)

The distribution of the pore throat radii of the specimens were determined by mercury-injection capillary pressure (MICP) tests. These tests are based on the principle that mercury is a near-perfect non-wetting liquid that will only infiltrate the rock pores when a pressure is applied. Larger pores are saturated at low pressure, and as the pressure stepwise increases to 50.000 psi the mercury progressively invades pores with smaller pore throats until the entire connected pore system will be completely saturated. The MICP measurements were performed with a Quantachrome Poremaster® GT 60 instrument.

2.4.4 Specific surface area (BET)

The specific surface area of the samples was obtained with the nitrogen adsorption method using the Autosorb iQ gas sorption system from Quantachrome Instruments. BET-analysis provides specific surface area evaluation by nitrogen multilayer adsorption measured as a function of relative pressure. The technique encompasses external area and pore area evaluations to determine the total specific surface area in m^2/g.

2.4.5 Optical- and scanning electron microscopy

Polished thin sections were prepared from end trims of the plugs impregnated with blue epoxy for easy identification of porosity. The polished thin sections were examined in transmitted and reflected light microscope. Supplementary studies of crystal morphologies and paragenetic relationships were performed on platinum-coated rock chips mounted on stubs and on carbon-coated thin sections using a Zeiss Sigma 300VP scanning electron microscope equipped with a field emission gun and using either secondary electron detector (SE) or back-scatter electron detector (BCS). Fines on filters from fluid experiments were platinum-coated and analysed with the SE detector.

The mean grain diameter in each thin section was obtained by measurement of minimum 100 grains intersecting three or more arbitrary straight lines. Since thin section grain-size analysis underestimates the dimensions relative to sieving analysis the long axis diameter of the measured grains are applied for calculation of mean grain size and degree of sorting. The grain size nomenclature was applied according to the Wentworth Class (Wentworth, 1922). Sorting was defined as graphic standard deviation (Folk, 1966) calculated from the

thin section grain-size distribution. The sorting classes are defined for eight relative phi classes that range from very well to poorly sorted. Modal compositions of the sandstones were obtained by point counting minimum 500 points in each thin section, excluding the porosity.

3. Results and discussion

The results of the gas, Klinkenberg and liquid permeability measurements, and the NMR, MICP and BET analyses are summarised in appendix A, while appendices B-H gives detailed results of the conventional core analysis, the liquid permeability measurements, NMR, MICP, BET, and the chemical composition of the effluent from the liquid permeability measurements and a mineralogical overview, respectively.

3.1 Liquid permeability calculations

An example of the results from the liquid permeability measurements is shown in Figure 3.1. The left hand side of the figure shows the measured differential pressure at the different flow rates using brine as the flooding fluid. Initially, the differential pressure increases slowly after initiating flow in the plug but at the following changes in the flow rate an immediate response is seen in the differential pressure. For all flow rates, the differential pressure becomes stable relatively fast (within hours for the first flow rate and for the following flowrates within in minutes).

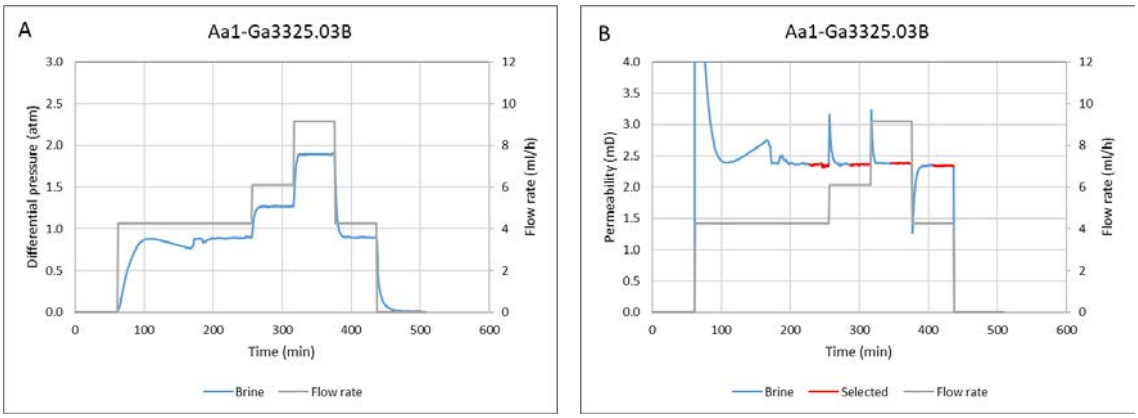

Figure 3.1 *Results of the brine permeability measurements for plug Aa1-Ga3325.03B (plug 11B). A: Measured differential pressure and flow rate and B: Calculated brine permeability. The brine permeability for each flow rate is determined by averaging the permeability measurements marked with red for each flow rate.*

The measured differential pressure is subsequently used to calculate the liquid permeability by Darcy's law:

$$Q = -\frac{kA\Delta P}{\mu L} \tag{1}$$

where Q is the flow velocity, k is the permeability, A is the cross-sectional area to flow, ΔP is the pressure gradient across the sample, μ is the fluid viscosity and L is the length of the sample. Typically, Darcy's law is valid only under conditions that satisfy Darcian of laminar

flow. To distinguish between laminar and non-laminar flow, the Reynolds number, Re, is typically used. The Reynolds number for flow through porous media is defined by:

$$Re = \frac{v d \rho}{\mu} \tag{2}$$

where v is the pore velocity (m/s), d is a characteristic dimension of the porous material (m) (e.g. a mean pore dimension or a mean grain diameter), ρ is the fluid density(kg/m^3) and μ is the fluid viscosity (kg/m^2/s). Typically, any flow with a Reynolds number less than one is laminar and it would be valid to apply Darcy's law. Assuming a mean pore size equal to the maximum measured pore throat diameter obtained from mercury injection capillary test as the characteristic dimension (Bloomfield and Williams, 1995), Reynolds number is significantly below 1 in all our experiments. Thus, it is likely that all the liquid permeability test were performed under conditions of laminar flow.

An example of the calculated brine permeability is shown in Figure 3.1B. For each flow rate the brine permeability was calculated as the average of minimum 30 measurements with constant differential pressure (marked with red in Figure 3.1B). For example, for plug Aa1-Ga3325.03B (11B) the brine permeability was calculated to be 2.35 mD at 7 cm/h, 2.36 at 10 cm/h, 2.38 at 15.1 cm/h and 2.34 when retuning to 7 cm/h again.

To obtain an overall brine permeability for each plug, combining the permeability of all the flow rates by which the brine permeability was performed, QμL/A was plottet against ΔP for the last 30 measurements at each flow rate (Figure 3.2). According to equation 1, the slope of the regression line equals the permeability. For plug Aa1-Ga3325.03B (plug 11B) the overall brine permeability equals 2.37 mD.

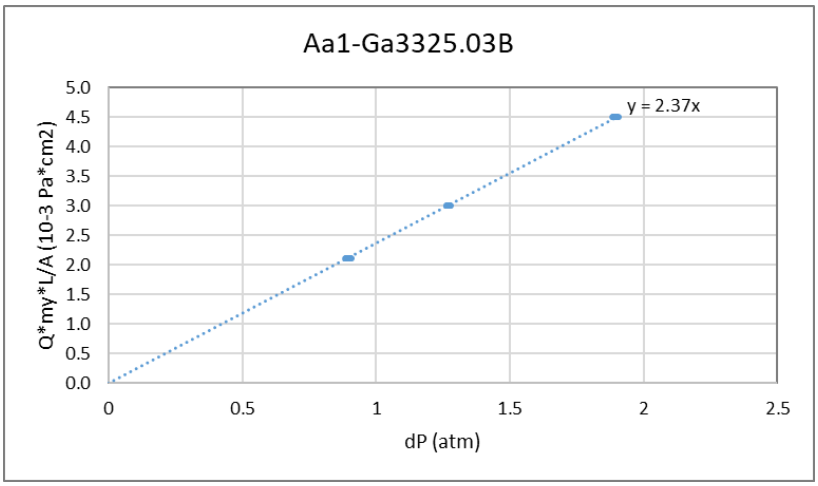

Figure 3.2 *Determination of an overall brine permeability for plug Aa1-Ga3325.0B (plug 11B) by combining the brine permeabilities calculated for each of the flow rates by which the permeability measurements were performed.*

3.2 Gas versus Klinkenberg permeability

The results of the gas and Klinkenberg permeability are shown in appendix B. The measured gas permeability for the tested sandstone plugs varies between 0.3 and 557 mD while the measured Klinkenberg permeability ranges between 0.04 to 502 mD. As expected, the measured Klinkenberg permeability is lower than the measured gas permeability for all samples. Generally, the Klinkenberg to gas permeability ratio is 0.6 to 0.9.

Klinkenberg (Klinkenberg, 1941) discovered that the permeability of a medium to gas is higher than that to water, and he attributed this phenomenon to “slip flow” between gas molecules and solid walls. While liquids have a zero velocity at a grain surface, gases exhibited some finite velocity at the same grain surface (slippage). This slippage results in a higher flow rate for the gas as compared to the liquid. By definition, the Klinkenberg permeability is corrected for this slippage between gas molecules and solid walls and as such should represent equivalent liquid permeability.

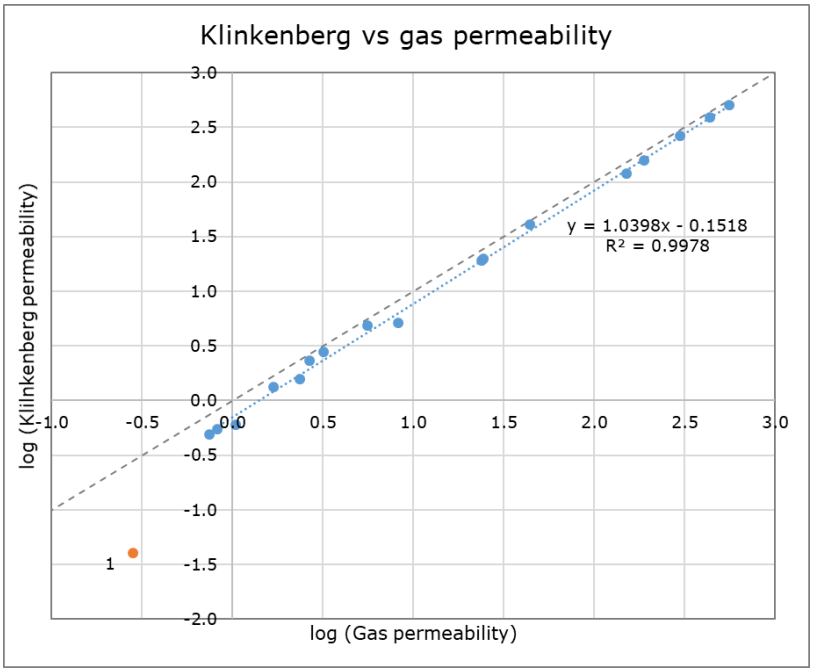

Figure 3.3 *Correlation between measured Klinkenberg permeability (in mD) and gas permeability (in mD) for all samples analysed in this study. The dashed line indicate the ratio 1:1.*

The correlation between the measured Klinkenberg permeability and gas permeability is shown in Figure 3.3. On a log-log plot the measurements fall on a straight line (r^2 = 0.9978) close to but lower than the 1:1 ratio indicating that the measured Klinkenberg permeability is lower than the measured gas permeability. Nearly all of the data follows the same trend and no difference is observed for the data from the two different geological formations investigated in this study. The slope of the line is slightly larger than one reflecting that the difference between gas and Klinkenberg permeability becomes smaller at higher permeability. This is in line with previous studies showing that the slippage effect becomes smaller at higher permeability (Wang et al., 2019; Duan and Yang, 2014; Klinkenberg, 1941).

The permeability of plug 1 does not follow the general trend of the data as a significantly lower Klinkenberg permeability is measured compared to the gas permeability. This could be due to a larger slippage effect in this sample compared to the other samples. Besides having a very small permeability, plug 1 also has the lowest pore throat diameter as measured by MICP (appendix A). Both low permeability and small pore sizes are known to increase the slippage effect (Duan and Yang, 2014; Klinkenberg, 1941).

3.3 Liquid versus gas and Klinkenberg permeability

The results of the liquid permeability measurements are shown in appendix C and summarized with other results in this study in appendix A. The measured brine permeability varies between 0.11 mD and 342 mD for the Gassum Formation and between 0.004 mD and 85 mD for the Skagerrak Formation. The Milli-Q water permeability measurements varies between 0.07 mD 81 mD for the Gassum Formation and 0.002 mD and 44 mD for the Skagerrak Formation. The measured permeability for both liquids are lower than the measured gas and Klinkenberg permeability for all samples.

The correlation between the measured brine permeability and the measured gas and Klinkenberg permeability is shown in Figure 3.4. The measured brine permeability correlates linearly with both the measured gas and Klinkenberg permeability on a log-log plot ($r^2 > 0.97$). Also the Milli-Q water permeability correlates linearly with both the measured gas and Klinkenberg permeability on a log-log plot ($r^2 > 0.97$) for both the Skagerrak and Gassum formations (Figure 3.5). This is in line with previous studies on both sandstones (Mahesar et al., 2017; Chen et al., 2016; Bloomfield and Williams, 1995) and carbonate (Al-Bulushi et al., 2012). In this study, a clear distinction is observed for the Gassum and the Skagerrak formations. Thus, a least squares regression (the best fit line indicated in Figure 3.4 and Figure 3.5) has the following form for the two formations when the permeabilities are given in mD:

<u>Brine vs gas permeability:</u>

Gassum Fm: $\log(k_b) = 1.0591 \log(k_g) - 0.4652$ $r^2 = 0.9959$

Skagerrak Fm: $\log(k_b) = 1.3428 \log(k_g) - 1.3615$ $r^2 = 0.9774$

<u>Brine vs Klinkenberg permeability</u>

Gassum Fm: $\log(k_b) = 1.0178 \log(k_K) - 0.3073$ $r^2 = 0.9929$

Skagerrak Fm: $\log(k_b) = 1.1188 \log(k_K) - 0.9191$ $r^2 = 0.9890$

<u>Milli-Q water vs gas permeability:</u>

Gassum Fm: $\log(k_{Milli\text{-}Q}) = 1.2166 \log(k_g) - 0.8779$ $r^2 = 0.9843$

Skagerrak Fm: $\log(k_{Milli\text{-}Q}) = 1.7453 \log(k_g) - 1.6895$ $r^2 = 0.9774$

<u>Milli-Q water vs Klinkenberg permeability</u>

Gassum Fm: $\log(k_{Milli\text{-}Q}) = 1.1982 \log(k_K) - 0.7424$ $r^2 = 0.9894$

Skagerrak Fm: $\log(k_{Milli\text{-}Q}) = 1.1247 \log(k_K) - 1.0688$ $r^2 = 0.9651$

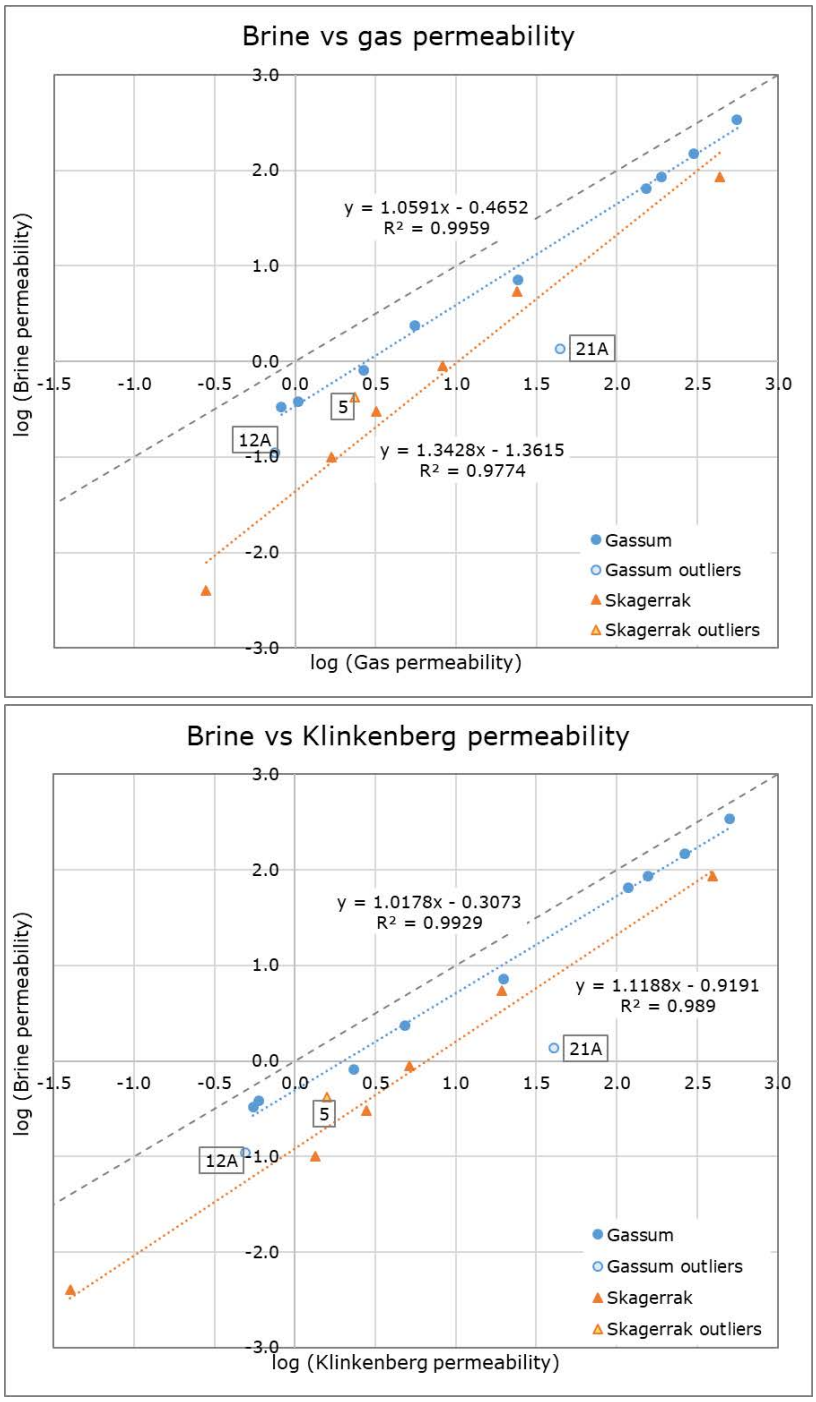

Figure 3.4 *Correlation between measured brine permeability (in mD) and gas permeability(in mD) (top) and measured brine permeability (in mD) and Klinkenberg permeability (in mD) (bottom) for samples from the Gassum Formation (circle) and Skagerrak Formation (triangle). The dashed line indicate the ratio 1:1.*

Generally, a larger reduction between the liquid and both the gas and the Klinkenberg permeability is observed for the Skagerrak Formation as compared to the Gassum Formation. Furthermore, the regression lines in Figure 3.4 and Figure 3.5 for the Gassum Formation are nearly parallel to the 1:1 ratio between the liquid and the gas and Klinkenberg permeability. whereas the reduction in the liquid permeability relative to gas and Klinkenberg permeability show a larger dependency on the permeability for the Skagerrak Formation. Thus, a larger

reduction in the liquid permeability is observed at the lower permeabilities for the Skagerrak Formation, particularly relative to the gas permeability.

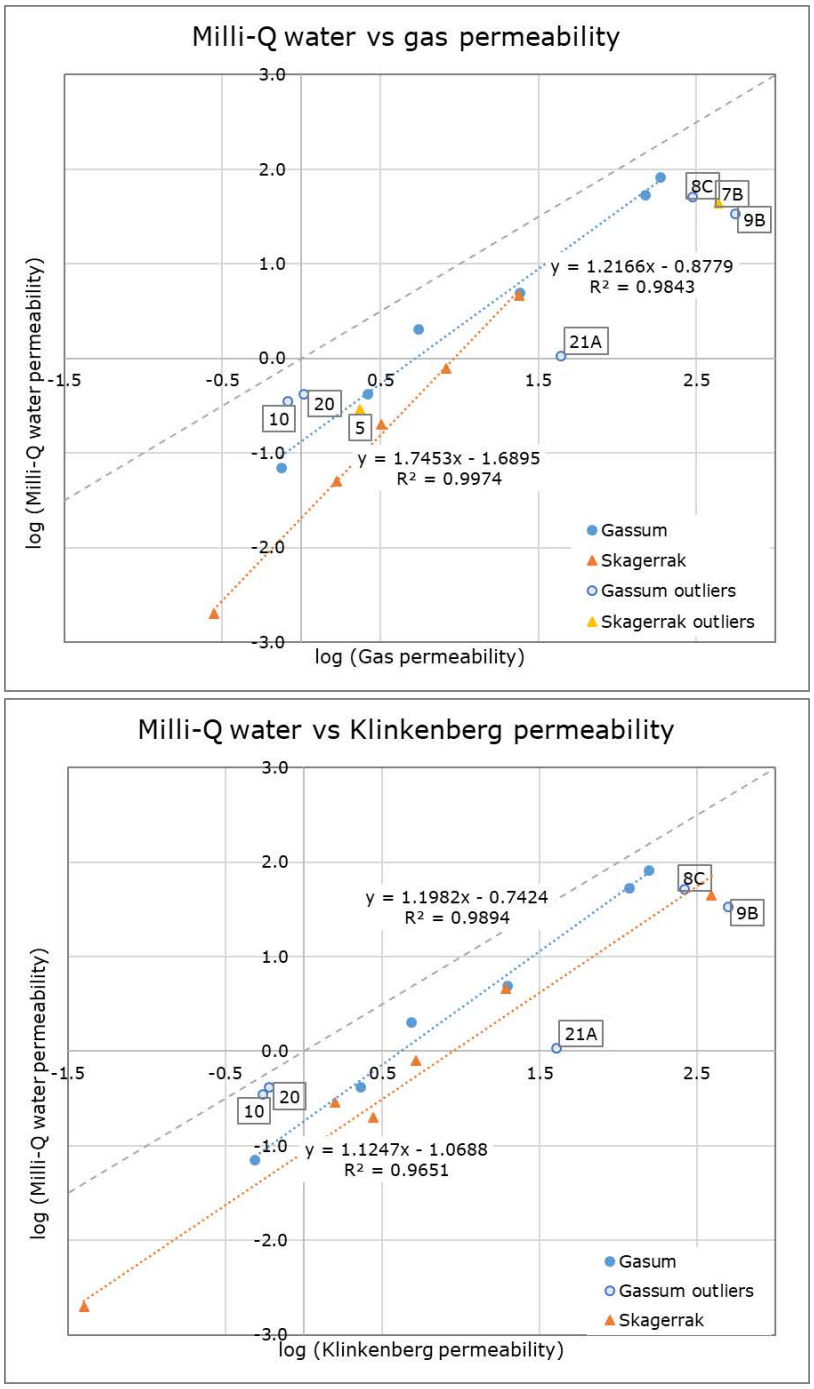

Figure 3.5 *Correlation between measured Milli-Q water permeability (in mD) and gas permeability (in mD) (top) and measured Milli-Q permeability (in mD) and Klinkenberg permeability (in mD) (bottom) for samples from the Gassum Formation (circle) and Skagerrak Formation (triangle). The dashed line indicate the ratio 1:1.*

A few plugs are identified as outliers and do not follow the general trend in Figure 3.4 and Figure 3.5. The plugs 8C and 9B are very short plugs (only c. 2 cm in length) and therefore the effects may affect the permeability measurements for these plugs resulting in a higher

uncertainty. The plugs 5 and 10 are the most inhomogeneous plugs which may also affect the permeability. Drilling mud is identified in plug 21A. As drilling mud mostly consist of smectite which is known to swell when in contact with liquid (Civan, 2015), this may explain the significantly lower permeability to liquid compared to that to gas for this plug. Besides having a low permeability, plug 12A also has a very small pore throat diameter and therefore may be more affected by a potential reduction of the pore throat diameter by a layer of immobile water in the liquid permeability measurements. Plug 7B shows, unlike the other plugs, a continuous decrease in the liquid permeability measurements for the three different flow rates (appendix C) and therefore the overall liquid permeability for this plug is very uncertain. The plug has a high content of kaolinite which may possibly detach from the surface when in contact with Milli-Q water and block the pore throats (Rosenbrand et al., 2015b). This needs, however, to be investigated in further detail.

A reduction in the permeability when using liquid as the flooding fluid as compared to gas is previously observed (Wang et al., 2019; Rosenbrand et al., 2015a; Duan and Yang, 2014; Tanikawa and Shimamoto, 2009; Baraka-Lokmane, 2002; Loosveldt et al., 2002; Klinkenberg, 1941). Gas slip contributes to a higher apparent permeability to gas, due to non-zero velocity on the pore fluid interface (Klinkenberg, 1941). This may not account for all of the observed difference between the permeability to liquid and to gas in this study since the Klinkenberg permeability is still significantly larger than both the brine and the Milli-Q water permeability. In fact, the gas slip appears to only affect the liquid permeability marginally (Figure 3.3, Figure 3.4 and Figure 3.5).

Several explanations have been proposed for the observed difference between the Klinkenberg and the liquid permeability, including interaction of clay with the liquid (Rosenbrand et al., 2015a; Baraka-Lokmane, 2002; Luffel et al., 1993; Jones and Owens, 1980), reduction of effective pore size caused by the adhesion of water molecules to e.g. clay particle surface or iron-oxides/hydroxides (Wang et al., 2019; Rosenbrand et al., 2015a; Duan and Yang, 2014; Andreassen and Fabricius, 2010; Solymar et al., 2003; Luffel et al., 1993; Heid et al., 1950), and chemical reactions caused by the undersaturation of samples during liquid permeability measurements (Baraka-Lokmane, 2002).

The swelling of clay, primarily smectite, is known to reduce the permeability (Civan, 2015). Clay swelling is a result of an increase in interlayer spacing in clay particles and is controlled primarily by the composition of aqueous solutions with which the clay comes into contact. Two different clay swelling processes have been identified 1) Crystalline swelling and 2) osmotic swelling (Civan, 2015). Crystalline swelling occurs when clays are exposed to concentrated brines or aqueous solutions containing large quantities of divalent or multivalent ions; this is caused by the formation of molecular water layers on the surface of clay minerals and leads to less swelling and less damage than osmotic swelling. Osmotic swelling occurs when clays are exposed to dilute solutions or solutions containing larger quantities of Na^+ cations; this is caused by the formation of an electric double layer on the surface of clay minerals and leads to more swelling and hence more damage. These phenomena create repulsive forces that separate the clay flakes from each other. In our experiments, most of the samples are selected so they do not contain smectite, except for plug number 23 containing randomly interlayered smectite/chlorite and plug number 1 containing mixed-layer ordered smectite/chlorite. Random smectite/chlorite has a higher content of smectite compared to mixed-

layer smectite/chlorite and therefore is likely to swell more. In line with this, fluid permeability measurements were not possible to conduct for plug 23 containing randomly interlayered smectite probably due to clay swelling, while liquid flow was still possible for plug 1 containing mixed-layer ordered smectite/chlorite.

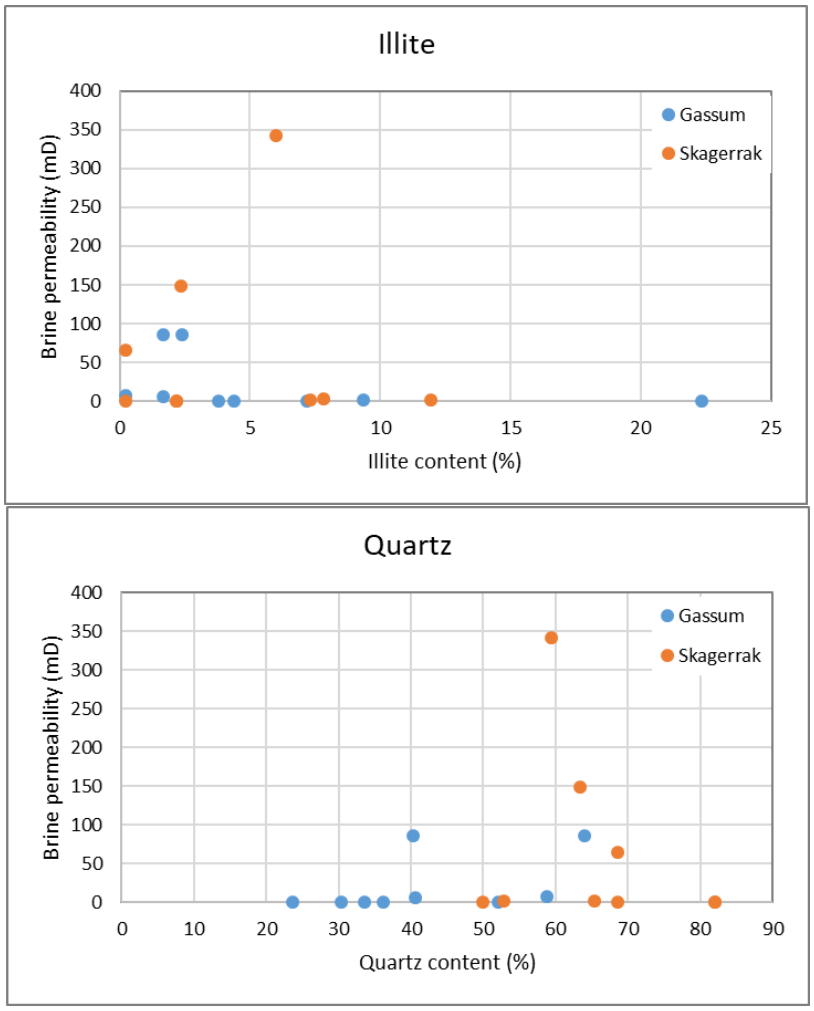

Figure 3.6 *Correlation between the brine permeability and the content of selected minerals.*

Delicate clay minerals, such as fibrous illite that grow perpendicular to the grain surface, may collapse onto the grain surface during drying (Luffel et al., 1993). It has been proposed that the reversible collapse of fibrous illite during drying may cause a higher permeability to gas (which is measured on dry samples) than to liquid (Rosenbrand et al., 2015a; Luffel et al., 1993). However, no clear correlation between the illite content and the difference between Klinkenberg permeability and the brine permeability is observed in this study (Figure 3.6).

Baraka-Lokmane et al. (2009) found a positive correlation between the permeability to brine and the quartz content in rock samples from three sandstone reservoirs and used among other parameters the quartz content to predict the brine permeability. Although the difference between the Klinkenberg permeability and the brine permeability appears to be larger at higher quartz content, no clear correlation is observed in this study.

Thus, although the liquid permeability may be affected by the clay content and mineralogy of the sandstone, our data indicate that the clay content and mineralogy may to some extend account for the variation in the permeability around the regression line in Figure 3.4 and Figure 3.5, rather than for the larger difference between the Klinkenberg and the liquid permeability.

It has also been suggested that the difference between the Klinkenberg permeability and the liquid permeability is governed experimentally by the subsaturation of the flooding fluid with respect to certain minerals during the liquid permeability measurements (Baraka-Lokmane, 2002). Particularly when using Milli-Q water as the flooding fluid, this may be relevant, but also to some degree when flooding with brine. In the reservoir, the brine is in chemical equilibrium with the most reactive minerals, such as carbonate and sulphates. Although a large effort is done in making the synthetic Gassum and Skagerrak brines, used in the flooding experiments in this study, resembling the naturally occurring brines as much as possible, a complete match is not possible. For example, the content of carbonate in the naturally occurring brine is very difficult to measure accurately due to degassing of CO_2 during sampling. Furthermore, for practical reasons Fe^{2+} is not added to the synthetic brines since this would precipitate as Fe^{3+} in the presence of oxygen.

Figure 3.7 shows the depletion or addition of major ions in the effluents from the liquid permeability measurements. For the measurements with brine no major changes is observed in the chemical composition of the brine during the flooding of the sandstones, except for sulphate, which appears to increase in all samples. Sulphate is present in low concentration in the brine and therefore the apparent increase in the sulphate concentration could be due to uncertainty in the sulphate measurements as a result of the high dilution requirements due to the high salinity of the brines. In any case, addition of sulphate to the effluent indicates a dissolution of sulphate bearing minerals, which may increase rather than decrease the brine permeability.

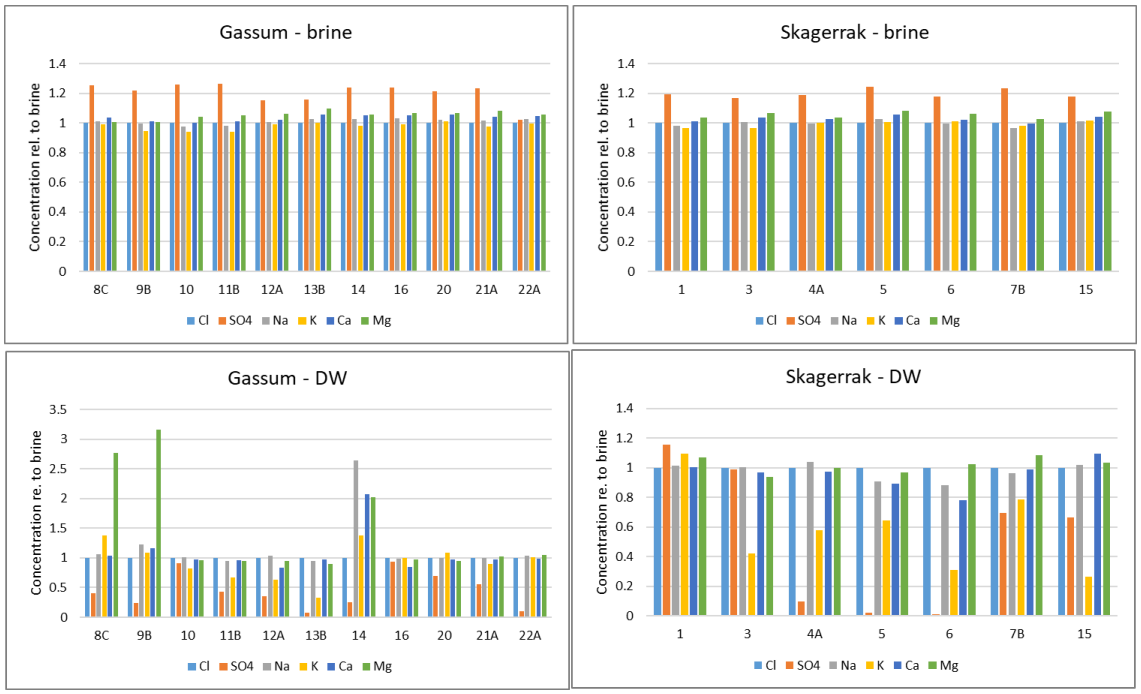

Figure 3.7 *The concentration of major ions in the effluent from the liquid permeability measurements relative to the concentration in the Gassum and the Skagerrak brine. A value of 1 indicates no changes in the concentration, while a positive and a negative value indicate addition or depletion of the element, respectively.*

As expected, larger changes in the chemical composition of the effluent from the Milli-Q water permeability measurements are observed (Figure 3.7). Due to the short period of time the core materials were flushed during the permeability measurements, it is, however, uncertain, whether potential chemical reactions may be significant enough to account for the difference between the Klinkenberg and the liquid permeability. Thus, while chemical reactions between the flooding fluid and the core material may occur during the liquid permeability measurements, these reactions are considered to be partly responsible for the scattering around the regression line in Figure 3.4 and Figure 3.5, rather than for the larger difference between the Klinkenberg and the liquid permeability.

Several authors have suggested that liquid-layer theory can account for the observed lower liquid permeability compared to Klinkenberg permeability (Wang et al., 2019; Rosenbrand et al., 2015a; Duan and Yang, 2014). Adhesion of water molecules to the mineral surface may reduce the effective pore size and thereby the pore volume that is available to brine flow as compared to gas flow. An immobile water layer would have a greater effect in smaller pores. However, Figure 3.8 shows that in our experiments the reduction in the Klinkenberg permeability appears to be larger in the samples with the larger pore throat radius.

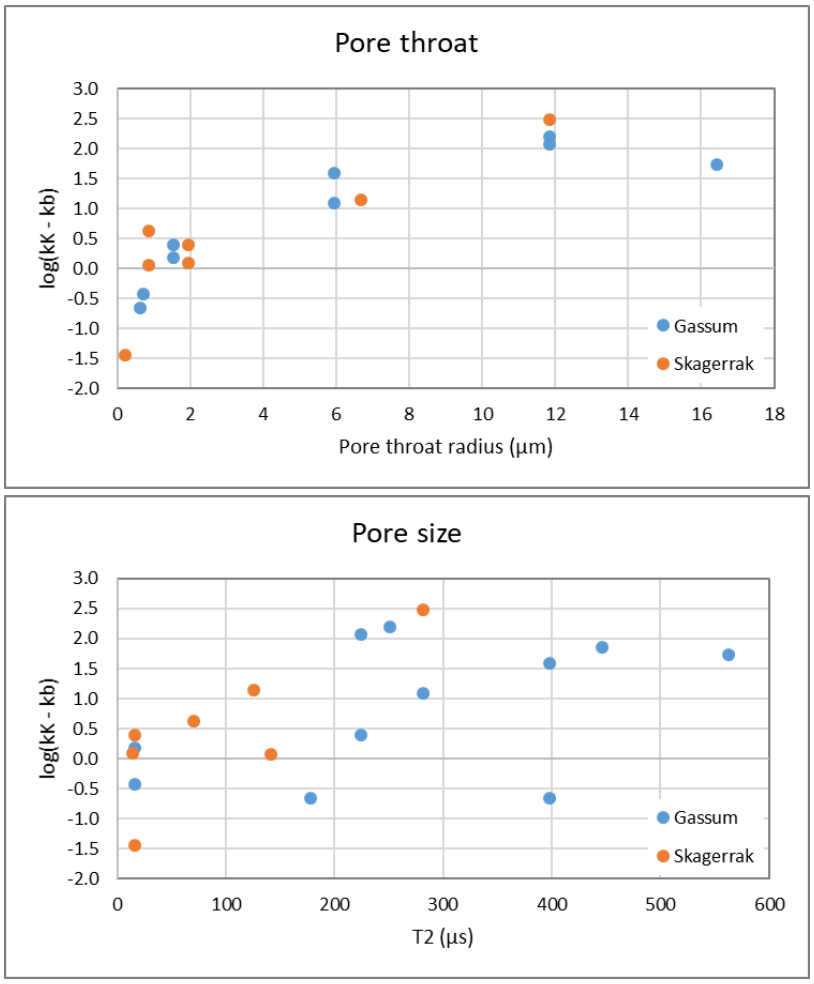

Figure 3.8 *Correlation between the log to the difference between Klinkenberg permeability in mD (k_K) and brine permeability in mD (k_b) and pore throat radius (top) and the pore size (bottom).*

3.4 Milli-Q water permeability versus brine permeability

The correlation between the permeability to Milli-Q water and that to brine is shown in Figure 3.9 for the data from the Gassum and the Skagerrak Formation. The Milli-Q water permeability is lower than the brine permeability for all measurements ($K_b/k_{Milli\text{-}Q}$ = 0.9 - 10). For both formations the measurements lie on a straight line (r^2 = 0.9963 and r^2 = 0.9947, respectively) in a log-log plot. Interestingly, no significant difference is observed for the two sandstone formations. The slope of the lines are slightly larger than one reflecting that the difference between Milli-Q water and brine permeability becomes smaller at higher permeability. A least squares regression (the best fit line indicated in Figure 3.9) has the following form for the two formations when the permeabilities are given in mD:

<u>Milli-Q water vs brine permeability:</u>

Gassum Fm: $\log(k_{Milli\text{-}Q}) = 1.0564 \log(k_b) - 0.1656$ $r^2 = 0.9963$

Skagerrak Fm: $\log(k_{Milli\text{-}Q}) = 1.0231 \log(k_b) - 0.1866$ $r^2 = 0.9947$

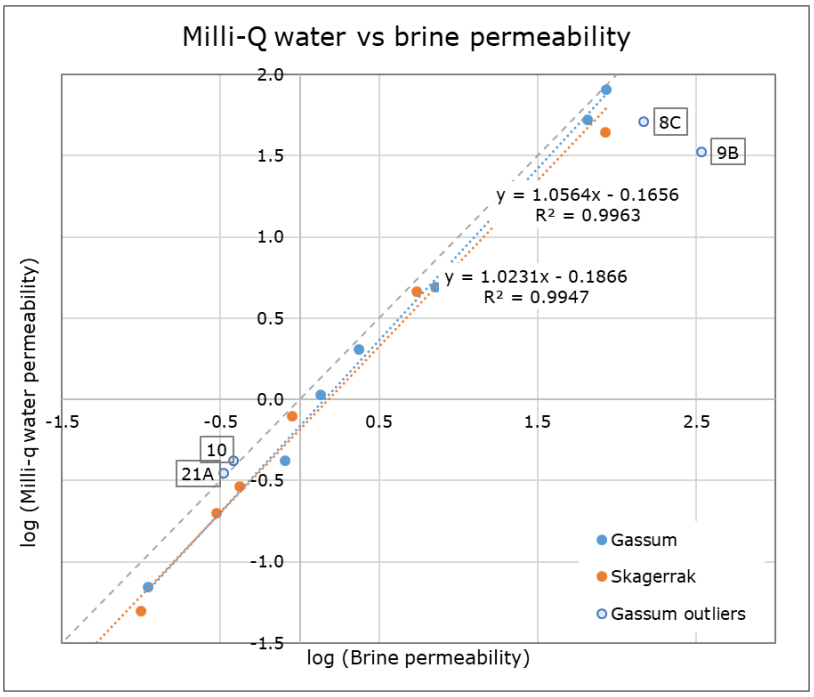

Figure 3.9 *Correlation between measured Milli-Q water permeability and brine for samples from the Gassum Formation (circle) and Skagerrak Formation (triangle). The dashed line indicate the ratio 1:1.*

Several authors have suggested that mobilization of colloidal particles, such as kaolinite causes permeability reduction and that the DLVO theory (Derjaguin and Landau, 1941) can be used to predict particle mobilization resulting from an increase in the electrical double layer repulsion force among particles and the pore walls (Schembre and Kovscek, 2005; Khilar and Fogler, 1984). Kaolinite particles are flat plates that are typically encountered in small stacks, or booklets, in sandstones. Initially kaolinite is assumed to be located on the surface of quartz grains (Schembre and Kovscek, 2005; Khilar et al., 1990). Under the experimental conditions, both the quartz grains and the kaolinite particles have a negative surface potential (Kia et al., 1987). The surface potential attracts oppositely charged ions; some of these may be bound to the surface whereas the others form a diffuse layer, which shields the surface potential. According to the DLVO theory, the magnitude of the electrical double layer repulsion between two negatively charged surfaces depends on the separation between the surfaces, the surface potentials, and the diffuse double layer thickness, which can be characterised by the Debye length:

$$\kappa^{-1} = \sqrt{\frac{\varepsilon_0 \varepsilon_r k_b T}{2 N_A e^2 I}} \qquad (3)$$

where ε_0 is the dielectric permittivity of a vaccum, ε_r is the relative dielectric permittivity of a solution, k_b is the Boltzman constant, T is the temperature, N_A is Avogadro's constant, e is the charge of an electron and I is the ionic strength of the solution given as the sum of the product of the concentration c and charge i of all the ions in the solution, i.e. $I = ½\Sigma c_i z_i^2$. Reducing salinity reduces I and increases the Debye length (cf. Eq. (3)), which can result in particle mobilisation (Schembre and Kovscek, 2005; Khilar et al., 1990). These particles may

block pore throats and thereby reduce the permeability. In our samples, the kaolinite crystals form long chains of face-to-face arranged booklets in the open pore space. Only a limited amount of kaolinite is trapped in quartz overgrowths, therefore the detachment of kaolinite booklets from the quartz surface is unlikely. However, since the surface of kaolinite is negatively charged, detachment between kaolinite crystals in a similar way as the previously described detachment of kaolinite from quartz may be possible. Another possibility is that the kaolinite particles simply take up more space in the pore space when the plug is flushed with Milli-Q water due to a separation of the kaolinite particles.

To investigate if fines migrations may occur in our liquid permeability experiments, the effluent from the experiment was filtered and the residue investigated in scanning electron microscope. Results show that fine particles from effluents from plugs of the Gassum Formation are mainly kaolinite and very rarely silica/quartz (Figure 3.10 and Figure 3.11). Artefact comprises Fe-Cr-Ni flakes and organic fibres. Fe-Cr-Ni precipitates on the filters from brine samples. Occasionally, uranium-thorium containing clusters have been identified in filtered water samples (Figure 3.11). Fine particles from effluents from the Skagerrak Formation contains rare albite and kaolinite (Figure 3.10) even though kaolinite has not been identified in the sandstone plugs from the Thisted-2 and Mors-1 cores.

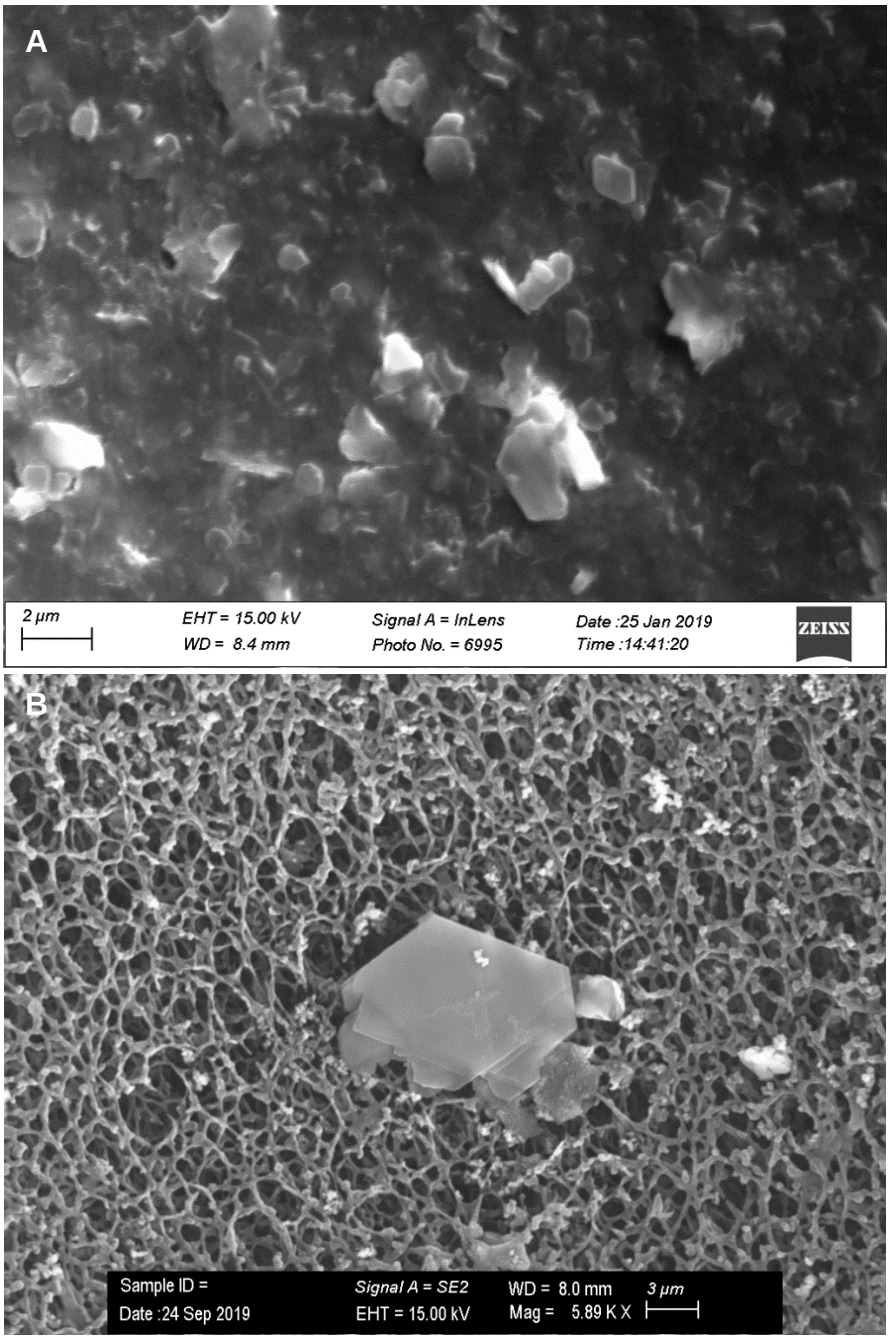

Figure 3.10 *Kaolinite: A. Common kaolinite from the effluent from the Gassum Formation. B. Rare kaolinite from the effluent from the Skagerrak Formation*

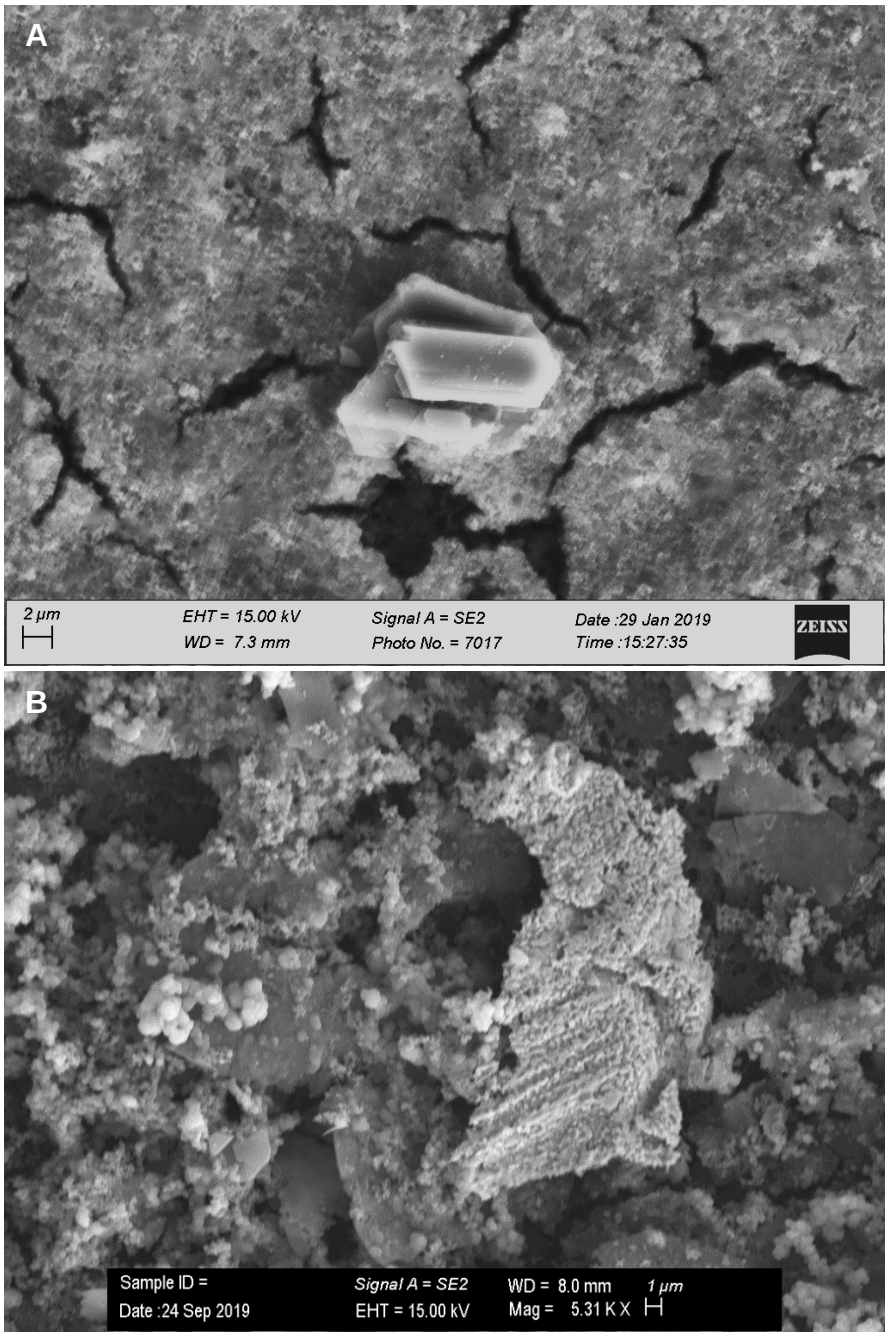

Figure 3.11 *A. Albite crystals from the Gassum Formation. B. Cluster of uranium-thorium formed during the experiment with Skagerrak Formation.*

Although kaolinite appears to be released and migrate through the core material in our experiments, no clear correlation is observed between Milli-Q water permeability and the kaolinite content (Figure 3.12) and the role of kaolinite needs to be investigated in further details.

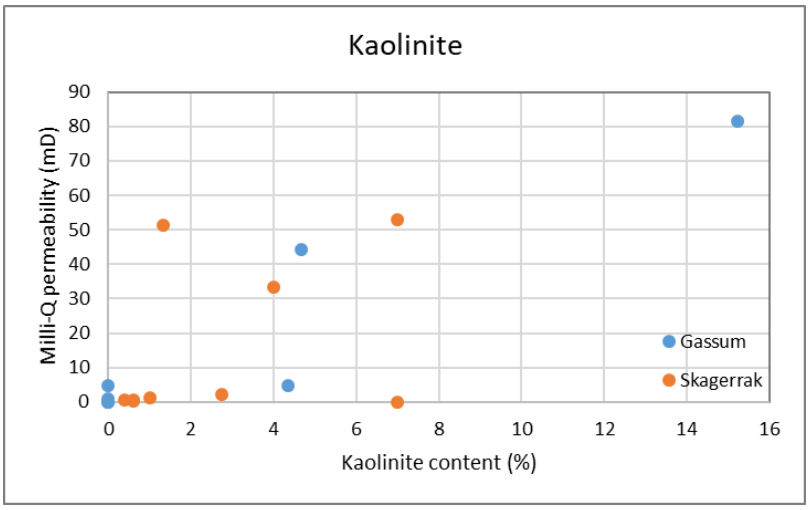

Figure 3.12 *Correlation between the Milli-Q permeability and the content of kaolinite.*

3.5 Numerical modelling

To help identify the factors responsible for the observed discrepancies between the measured permeability of a plug simulations of flow through the plugs is conducted using the modelling tool COMSOL Multiphysics and its Darcy flow equation. As an initial step in our exploitation, a numerical flow simulation accounting for the dynamical changes in flow and viscosity during the experiment on plug 21A from the Gassum Formation were conducted.

3.5.1 Theoretical assumptions behind permeability estimation

By assuming no changes take place within the plug during the experiment (Figure 3.13), the gas permeability (PermG) can be converted into

- a Klinkenberg permeability (PermKL) by adding a constant *kl*
- a Brine permeability (PermB) by multiplying it with a factor *kb* accounting for the viscosity of the Brine (µBrine)
- a Milli-Q permeability ($Perm_{Milli\text{-}Q}$) by multiplying it with a factor *kMilli-Q* account for the viscosity of the Milli-Q ($\mu_{Milli\text{-}Q}$)

$$PermG = PermKL + kl = kb(\mu Brine - 1) * PermB = kdw(\mu DW - 1) * PermDW \quad (4)$$

For each flow step in the experiment, the permeability can be estimated by:

$$Perm = \mu * L * Q/(\pi * R^2 * (P1 - P2)), \quad (5)$$

where µ is the viscosity of the fluid, L is the length of the core plug, Q is the flow rate set at the inlet, R is the radius of the core plug, P1 is the pressure at the inlet and P2 is the pressure at the outlet.

Assuming no changes to the properties of the plug, similar PermB and PermMilli-Q estimates should be obtained from the four flow steps in the experiment (Figure 3.13; PermB1 = PermB2…=PermMilli-Q 1=...). Dynamic flow experiments on core plugs could provide the constants *kb* and *kMilli-Q* facilitating the convergent of measured gas permeability to brine and Milli-Q permeability if the plug was not exposed to changes during the experiment. With property changes of a plug being the rule rather than the exception, this initial work was focusing on how to delineate causes for changes in the plug during the experiment. I.e., a clarification of whether changes are associated with:

- the plug media
- the plug dimensions (too short…)
- drilling mud
- transport of iron and clay particles
- the flow rate
- the change in fluid and viscosity (from brine to Milli-Q water)

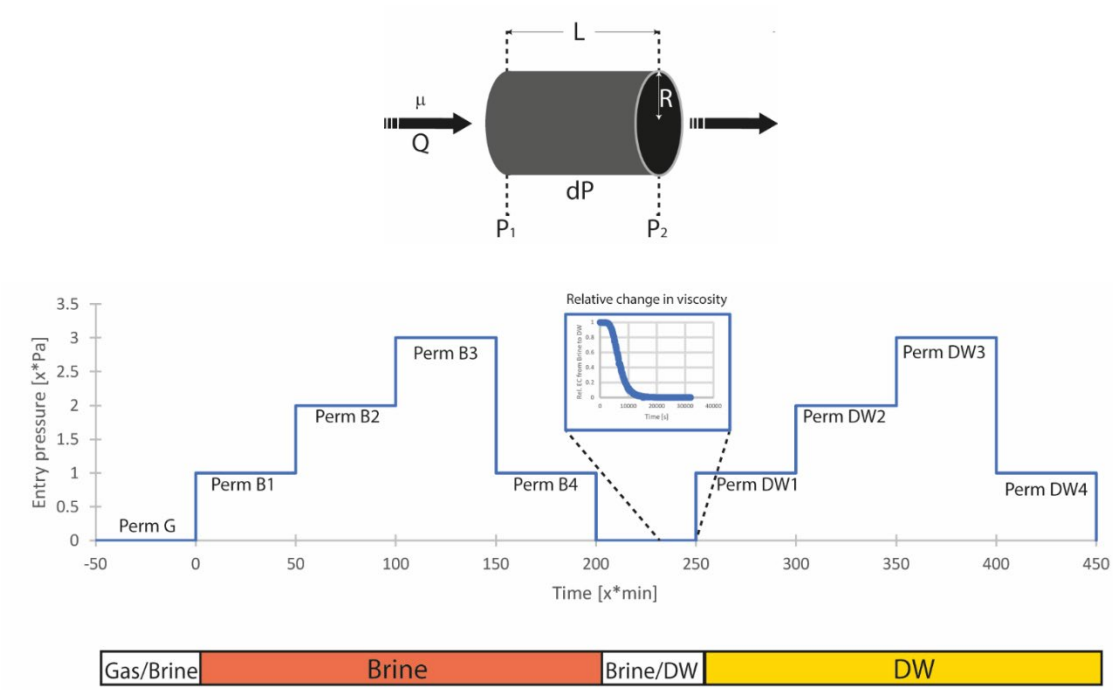

Figure 3.13: *Conceptual model of the plug (top) and pressure at P1 over time (bottom). The insertion shows the relative change in viscosity when flushing the brine-saturated plug with Milli-Q water (DW). The x-denotation is used to imply that the values are relative to the applied flow rate.*

3.5.2 Conceptual model

The plug was be set up according to the illustration in Figure 3.13. At the edges of the plug parallel to the flow direction, a no flow boundary is specified (pressurised with 400 psi as in the experiment) while the boundary at the outlet, P2, has a time varying pressure according

to measured pressure during the experiment. The reason for using a time varying specified boundary at P2 is that during the experiments, a back pressure of 2 bar was applied.

A varied specified flux is defining the inlet, P1, according to the applied flowrates during the experimental setup. The described setup was a generic setup for all plugs analysed. The permeability is constant during the entire simulation to mimic theoretical conditions. That is when no internal changes occur within the plug.

For the current plug, Gassum 21A, the flow rate is specified according to Table 3.1. The flushing of the plug with Milli-Q water began at time 309 min. with flow rate 1 and was completed at time 614 min. The viscosity of the of the diluted brine was assumed to be linear correlated with the dilution factor. Subsequently, the experiment continued with varying flow rate using Milli-Q water.

Table 3.1. *Applied fluxes at the given time periods*.

	Flux, Q (m s^{-1})	Start time (min)	End time (min)
Flow rate 1	4.05E-06	0	130
Flow rate 2	6.09E-06	130	190
Flow rate 3	1.01E-05	190	250
Flow rate 1	4.05E-06	250	674
Flow rate 2	6.09E-06	674	734
Flow rate 3	1.01E-05	734	794
Flow rate 1	4.05E-06	794	876

3.5.3 Results and discussion

The inlet pressure (P1) both simulated and measured are shown in Figure 3.14. It is evident that around time 70 min., the simulated and measured P1 are similar. This pattern continues until the flow rate increases at time 130 min. Hereafter, the measured and simulated P1 deviate slightly so that observed pressures are generally underestimated and at the largest applied flow rate at time 190 min, the offset increases. Once the flow rate decreases at time 250 min., the simulated and measured P1 are similar again. The reason for the measured pattern is yet not clear, but could be due to mechanically forced bending of illite due to the high flow rate. Thus, with increasing flow rates, the illite particles tend to lay more down; a process that is reversible when returning to the lowest flow rate again.

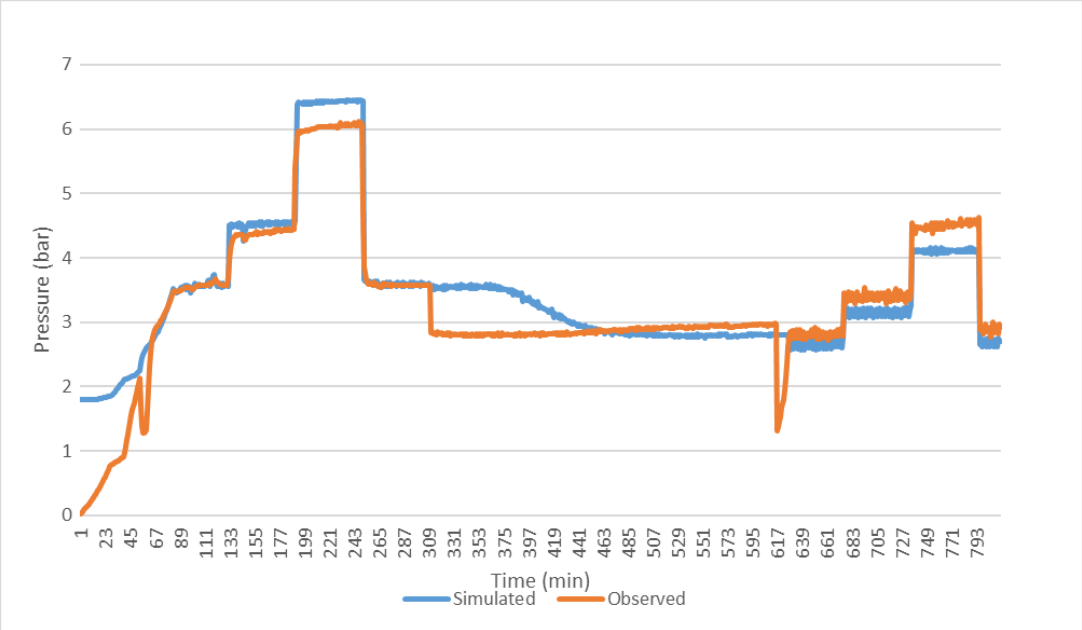

Figure 3.14 *Simulated and measured pressure at the inlet, P1, over time for Gassum 21A plug.*

The flushing of the plug with Milli-Q water and the gradual change of viscosity from brine to Milli-Q water is initiated at time 309 min. ending at time 614 min. Within this timespan, the simulated pressure is higher compared to the measured pressure until approximately time 450 min. The reason for this discrepancy is likely due to the choice in model conceptualization. The simulated pressure at the outlet is time varying based on the measured pressures and reflects that the viscosity of incoming water changes abruptly. In the model, however, the described change in viscosity (Figure 3.13) is taking place simultaneously in the whole plug, which is not the case in the real plug, where Milli-Q water starting at the inlet P1 graduately will replace the brine and over time reach the outlet P2. At around time 450 min., the simulated and measured pressures are again similar. Though the simulated pressure is slightly underestimated compared to measured pressure. As was the case with brine, the offset between simulated and measured pressures for the period with Milli-Q water flooding increases at higher flow rates. Similarly, the offset seems to decrease once the flow rates are changed back to the lowest flow rate at time 794 min. It is noted that the offsets during flushing with Milli-Q water are opposite compared to the offsets during flushing with brine. Thus, measured pressure are underestimated by the model. Since the deviations were apparent at the beginning of the simulations, it indicates that the properties of the plug could have changed after being flushed with Milli-Q . As drilling mud has been identified in this plug, a plausible explanation for the observed pattern could be the swelling of the smectite in the drilling mud when in contact with Milli-Q water. In smectite the negative charge of the clay platelets is balanced by means of the positive charge of the cations present in the interlayer locations, including K^+, Na^+, Ca^{2+} and Mg^{2+}. This feature helps keep the stack of clay platelets together. However, when exposed to low ionic strength aqueous solutions, interlayer cations adsorb water molecules from the aqueous solution to form thick envelopes of water films over the clay platelets. This process causes the expansion of the interlayer and thus clay swelling (Civan, 2015).

We expect that these discrepancies between measured and simulated pressure can be used to analyze and deduce the possible causes for the inconsistencies with regard to permeability for the various plugs and in the future delineate how to deduce the factors *kd* and *kMilli-Q* described above enable us to conduct a more sound based estimation of the brine and Milli-Q water permeability from the gas permeability of the plug.

4. Recommendations for further studies

Although the obtained gas-liquid correlations of the present study can be used in future brine-permeability estimates of sandstones reservoirs further investigations may refine the correlations and increase our understanding of the discrepancy between the gas and liquid permeability in the Danish sandstone reservoirs. Recommendations to further investigations are:

- Investigation of the gas-liquid correlation for the Bunter Sandstone Formation and the Haldager Sandstone Formation as well as for the Skagerrak and Gassum Formations in the rest of the country. In this study, a clear distinction is observed between the gas-liquid correlation for Gassum and the Skagerrak formations. In future studies it could be relevant to investigate how the other two important potential Danish geothermal reservoirs fit into this correlation.
- To look into more details the effect of the ratio between pore throat size and the size of the kaolinite particles. It is plausible that larger kaolinite particles in a reservoir with smaller pore throats are more likely to affect the permeability than small kaolinite particles in a reservoir with larger pore throats.

5. Conclusions

In this study, a detailed series of laboratory experiments have been conducted to investigate the discrepancy between measured gas and liquid permeability for sandstone core specimens from the Skagerrak and Gassum Formations in the North Jutland region. Gas and Klinkenberg permeability is measured and compared with measured brine and Milli-Q water permeability. Detailed characterisation of the core material by NMR, MICP, BET and SEM is made and the effluent from the liquid permeability measurements is analysed for major cations. The residue from the filtration of the effluent is analysed by SEM for identification of fines released from the core specimen during the liquid permeability determination.

The results show that the permeability to the different fluids decrease in the order $k_g > k_K > k_b > k_{MILLI\text{-}Q}$ where the subscript g, K, b and Milli-Q denotes gas, Klinkenberg, brine and Milli-Q water, respectively. A linear correlation in a log-log diagram is observed for the Klinkenberg/gas, brine/gas, brine/Klinkenberg, Milli-Q/gas, Milli-Q/Klinkenberg and Milli-Q/brine permeabiilties, respectively with $r^2 > 0.9650$. Interestingly, for the correlation between the permeabilities with the same fluid (gas/Klinkenberg and Milli-Q/brine) no distinction is observed between the two sandstone formation, whereas a clear distinction between the Gassum and the Skagerrak Formation is observed for the correlation between the permeabilities to different fluids (e.g. gas/brine or Klinkenberg/Milli-Q).

Even though the mineralogy may affect the permeability, no clear correlation is observed between the mineralogy and the discrepancy between the gas/Klinkenberg and the liquid permeability. Thus, our data indicate that the mineralogy may to some extend account for the smaller variation in the permeability around the regression lines, rather than for the larger difference between the gas/Klinkenberg and the liquid permeability. However, the controlling factor(s) for the difference between the gas/Klinkenberg permeability and the liquid permeability is still unclear and further detailed investigations of the results of this study is proceeding. We expect that the numerical modelling and the discrepancies between measured and simulated pressure can be used to analyze and deduce the reasoning for the inconsistencies for the various plugs and enable us to conduct a more sound based estimation of the brine and Milli-Q permeability from the gas permeability of the plugs.

We recommend that the observed linear correlations between brine permeability and gas or Klinkenberg permeability for the Gassum and the Skagerrak Formations are included in future estimates of brine permeability of sandstone in areas where the mentioned formations constitute the geothermal reservoirs. It is also recommended that similar analysis are carried out for the other geothermal reservoirs i.e. the Bunter Sandstone and Haldager Sandstone Formations as well as for the Skagerrak and Gassum Formations in other parts of Denmark.

6. References

Al-Bulushi, I.R., Al-Maamari, R.S. and Wilson, O.B. (2012) Brine versus Klinkenberg corrected gas permeability correlation for Shuaiba carbonate formation. J. Pet. Sci. Eng. 92-93, 24-29.

Andreassen, K.A. and Fabricius, I.L. (2010) Biot critical frequency applied to description of failure and yield of highly porous chalk with different pore fluids. Geophysics 75, E205-E213.

Baraka-Lokmane, S. (2002) Hydraulic versus pneumatic measurements of fractured sandstone permeability. J. Pet. Sci. Eng. 36, 183-192.

Baraka-Lokmane, S., Main, I.G., Ngwenya, B.T., Elphick, S.C., Jones, C. and Hamilton, S.A. (2009) Correlation Between Microstructure and Flow Behavior in Porous Sandstones. Pet. Sci. Technol. 27, 511-529.

Bloomfield, J.P. and Williams, A.T. (1995) An empirical liquid permeability—gas permeability correlation for use in aquifer properties studies. Quarterly Journal of Engineering Geology and Hydrogeology 28, S143-S150.

Cardoso, O.R. and Balaban, R.d.C. (2015) Comparative study between Botucatu and Berea sandstone properties. Journal of South American Earth Sciences 62, 58-69.

Chen, M., Li, M., Wang, Y., Zhao, J.-Z. and Xiao, W.-L. (2016) The permeability of fontainebleau sandstone to gases and liquids. Pet. Sci. Technol. 34, 845-852.

Civan, F. (2015) Reservoir formation damage. Fundamentals, modeling, assessment, and mitigation, Third eddition ed. Gulf Professional Publisher, Elsevier, Burlington, MA.

Derjaguin, B.V. and Landau, L.D. (1941) Theory of the stability of strongly charged lyophobic sols and the adhesion of strongly charged particles in solutions of electrolytes. Acta Physicochim. USSR 14, 633-662.

Duan, Q. and Yang, X. (2014) Experimental studies on gas and water permeability of fault rocks from the rupture of the 2008 Wenchuan earthquake, China. Science China-Earth Sciences 57, 2825-2834.

Folk, R.L. (1966) A review of grain-size parameters. Sedimentology 6, 73-93.

Heid, J.G., McMahon, J.J., Nielsen, R.F. and Yuster, S.T. (1950) Study of the permeability of rocks to homogeneous fluids. American Petroleum Institute Drilling and production practice, 230-246.

Jones, F.O. and Owens, W.W. (1980) A LABORATORY STUDY OF LOW-PERMEABILITY GAS SANDS. Journal of Petroleum Technology 32, 1631-1640.

Khilar, K.C. and Fogler, H.S. (1984) THE EXISTENCE OF A CRITICAL SALT CONCENTRATION FOR PARTICLE RELEASE. J. Colloid Interface Sci. 101, 214-224.

Khilar, K.C., Vaidya, R.N. and Fogler, H.S. (1990) Colloidal-induced fines release in porous media. J. Pet. Sci. Eng. 4, 2313-2221.

Kia, S.F., Fogler, H.S. and Reed, M.G. (1987) EFFECT OF PH ON COLLOIDALLY INDUCED FINES MIGRATION. J. Colloid Interface Sci. 118, 158-168.

Klinkenberg, L.J. (1941) The permeability of porous meida to liquids and gases. American Petroleum Institute Drilling and production practice, 200-213.

Laier, T. (1982) Fluid analysis and scaling investigations of the Skagerrak transitional formation water of Thisted 2, DGU report.

Laier, T. (2008) Chemistry of Danish saline formation waters relevant for core fluid experiments – Fluid chemistry data for lab experiments related to CO_2 storage on deep aquifers. GEUS report 2008/48, Geological Survey of Denmark and Greenland, Copenhagen.

Loosveldt, H., Lafhaj, Z. and Skoczylas, F. (2002) Experimental study of gas and liquid permeability of a mortar. Cem. Concr. Res. 32, 1357-1363.

Luffel, D.L., Herrington, K.L. and Walls, J.D. (1993) Effect of Drying on Travis Peak Cores Containing Fibrous Illite. SPE Advanced Technology Series 1, 188-194.

Lund, J.W. and Boyd, T.L. (2016) Direct utilization of geothermal energy 2015 worldwide review. Geothermics 60, 66-93.

Mahesar, A., Memon, K.R., Memon, H.-U.-R. and Tunio, A. (2017) Comparison of Klinkenberg-Corrected Gas and Liquid Permeability in Kirthar Fold Belt Tight Gas Sands. Mehran University Research Journal of Engineering and Technology, Mehran
University of Engineering and Technology, Jamshoro, Pakistan 36, 957-964.

Nielsen, L.H. (2003) Late Triassic-Jurassic development of the Danish Basin and the Fennoscandian Border Zone, southern Scandinavia, in: Ineson, J.R., Surlyk, F. (Eds.), The Jurassic of Denmark and Greenland, Geological Survey of Denmark and Greenland Bulletin 1, pp. 459-526.

Olivarius, M. and Nielsen, L.H. (2016) Triassic paleogeography of the greater eastern Norwegian-Danish Basin: Constraints from provenance analysis of the Skagerrak Formation. Marine and Petroleum Geology 69, 168-182.

Parkhurst, D.L. and Appelo, C.A.J. (2013) Description of input and examples for PHREEQC version 3 - A computer program for speciation, batch-reaction, one-dimensional transport, and inverse geochemical calculations, U.S. Geological Survey Techniques and Methods.

Rosenbrand, E., Fabricius, I.L., Fisher, Q. and Grattoni, C. (2015a) Permeability in Rotliegend gas sandstones to gas and brine as predicted from NMR, mercury injection and image analysis. Marine and Petroleum Geology 64, 189-202.

Rosenbrand, E., Haugwitz, C., Jacobsen, P.S.M., Kjoller, C. and Fabricius, I.L. (2014) The effect of hot water injection on sandstone permeability. Geothermics 50, 155-166.

Rosenbrand, E., Kjoller, C., Riis, J.F., Kets, F. and Fabricius, I.L. (2015b) Different effects of temperature and salinity on permeability reduction by fines migration in Berea sandstone. Geothermics 53, 225-235.

Schembre, J.M. and Kovscek, A.R. (2005) Mechanism of formation damage at elevated temperature. J. Energy Resour. technol. Trans. ASME 127, 171-180.

Solymar, M., Fabricius, I.L. and Middleton, M. (2003) Flow characterization of glauconitic sandstones by integrated Dynamic Neutron Radiography and image analysis of backscattered electron micrographs. Petroleum Geoscience 9, 175-183.

Tanikawa, W. and Shimamoto, T. (2009) Correction to “comparison of Klinkenberg-corrected gas permeability and water permeability in sedimentary rocks”. International Journal of Rock Mechanics and Mining Sciences 46, 1394-1395.

Wang, F., Jiao, L., Lian, P. and Zeng, J. (2019) Apparent gas permeability, intrinsic permeability and liquid permeability of fractal porous media: Carbonate rock study with experiments and mathematical modelling. J. Pet. Sci. Eng. 173, 1304-1315.

Wang, J., Hu, H., Guan, W. and Li, H. (2015) Electrokinetic experimental study on saturated rock samples: zeta potential and surface conductance. Geophysical Journal International 201, 869-877.

Weibel, R., Olivarius, M., Friis, H., Kristensen, L., Hjuler, M.L., Kjoller, C., Pedersen, P.K., Boyce, A., Mathiesen, A. and Nielsen, L.H. (2017) Climatic influence on early and burial diagenesis in Triassic and Jurassic sandstones from the Norwegian – Danish Basin. The Depositional record 3, 60-91.

Wentworth, C.K. (1922) A scale of grade and class for clastic sediments. The journal of Geology 5, 377-392.

Appendix A

Overview of results

Gassum Formation

Sample id	Lab id	Well	Depth	Illite content[a)]	Kaolinite content[a)]	Grain size[a)]	Porosity	Gas perm	Klink perm	Brine perm	DW perm	Flow rate	Pore velocity	T_2 Brine	T_2 DW	MICP	BET
			m	%	%		%	mD	mD	mD	mD	ml/h	cm/h	ms	ms	um	m^2/g
Aa1-Ga3352.22A	14	Aars-1	3352.22	0	4	432	12.96	24.3	19.7	7.2	4.9			282	355	6	0.8
										6.6	4.5	6.2	10				
										7.0	4.8	15.5	25				
										7.3	4.9	28.0	45				
										6.7	4.5	6.2	10				
Aa1-Ga3353.05A	16	Aars-1	3353.05	2	15	412	16.09	187.8	157.1	86	81			447	631	na	na
										75	79	12	15				
										80	83	19	25				
										90	82	35	45				
										85	80	12	15				
Ve1-Ga2009.96C	8C	Vedsted-1	2009.96	0	7	261	25.91	298.9	264.9	148	51			224	251	12	1.1
										137	143	19	15				
										157	77	44	35				
										147	48	75	60				
										134	51	19	15				
Ve1-Ga2010.17B	9B	Vedsted-1	2010.17	5	3	246	27.77	557.2	501.5	342	34			251	398	12	1.0
										345	47	33	25				
										350	42	46	35				
										352	37	79	60				
										344	32	119	90				
										296	28	33	25				
Aa1-Ga3326.49B	13B	Aars-1	3326.49	12	0	649	12.82	2.65	2.32	0.8	0.4			16	10	2	3.1
										0.7	0.4	4.3	7				
										0.8	0.4	6.1	10				
										0.9	0.5	9.2	15				
										0.7	0.4	4.3	7				
Aa1-Ga3325.03B	11B	Aars-1	3325.03	7	0	660	12.72	5.56	4.85	2.4	2.0			224	398	2	1.5
										2.4	2.0	4.3	7				
										2.4	2.1	6.1	10				
										2.4	2.1	9.2	15				
										2.3	2.0	4.3	7				
Aa1-Ga3318.20A	20	Aars-1	3318.20	2	0	638	6.13	1.04	0.60	0.4	0.4			398	398		
										0.4	0.4	2.1	7				
										0.4	0.4	3.0	10				
										0.4	0.4	4.4	15				
										0.4	0.4	2.1	7				
Aa1-Ga3320.80A	21A	Aars-1	3320.80	7	1	869	14.61	44.2	40.6	1.4	1.1			398	11	6	2.7
										1.3	1.1	7.0	10				
										1.3	1.1	10.5	15				
										1.4	1.1	17.5	25				
										1.3	1.0	7.0	10				
Aa1-Ga3275.38A	22A	Aars-1	3275.38	0.2	7	971	13.63	151.1	118.6	65	53			562	251	16	0.2
										57	56	16	25				
										62	54	23	35				
										68	52	39	60				
										66	52	16	25				
Aa1-Ga3325.52A	12A	Aars-1	3325.52	7	0	660	9.81	0.75	0.49	0.1	0.1			16	14	1	3.1
										0.1	0.1	3.3	7				
										0.1	0.1	4.7	10				
										0.2	0.1	7.0	15				
										0.1	0.1	3.3	7				
Aa1-Ga3318.10A	10	Aars-1	3318.10	2	0	638	7.53	0.82	0.55	0.3	0.4			178	200	1	1.1
										0.3	0.3	2.5	7				
										0.3	0.4	3.6	10				
										0.4	0.4	5.4	15				
										0.3	0.4	2.5	7				

[a)] Estimate na: Not analysed

Skagerrak Formation

Sample id	Lab id	Well	Depth	Illite content[a)]	Kaolinite content[a)]	Grain size[a)]	Porosity	Gas perm	Klink perm	Brine perm	DW perm	Flow rate	Pore velocity	T_2 Brine	T_2 DW	MICP	BET
			m	%	%		%	mD	mD	mD	mD	ml/h	cm/h	ms	ms	um	m^2/g
Th2-Sk2761.63A	6	Thisted-2	2761.63	2	0	250	15.24	23.9	19.3	5.4	4.6			126	89	7	5.5
										5.0	4.6	5.1	7				
										5.3	4.6	10.9	15				
										5.6	4.7	18.1	25				
										5.3	4.5	5.1	7				
Fr2-Sk1051.00A	23	Frederikshavn-2	1051.00				8.62	0.33	0.16	b)	b)						
Th2-Sk2919.35B	4A	Thisted-2	2919.35	9	0	250	16.25	8.25	5.16	0.9	0.8			71	50	1	5.7
										0.7	0.7	7.7	10				
										0.8	0.8	11.5	15				
										1.0	0.8	19.2	25				
										0.9	0.8	7.7	10				
Mo1-Sk5034.24A	15	Mors-1	5034.24	4	0	250	5.23	1.68	1.33	0.1	0.1			14	10	2	5.3
										0.1	0.0	2.4	10				
										0.1	0.1	3.6	15				
										0.1	0.1	6.0	25				
										0.1	0.0	2.4	10				
Th2-Sk2923.05A	5	Thisted-2	2923.05	4	0	350	11.85	2.34	1.58	0.4	0.3			141	56	1	6.1
										0.4	0.3	5.6	10				
										0.4	0.3	8.4	15				
										0.5	0.3	14.0	25				
										0.4	0.3	5.6	10				
Mo1-Sk5089.57A	3	Mors-1	5089.57	7	0	325	5.80	3.19	2.78	0.3	0.2			16	20	2	5.2
										0.3	0.2	2.8	10				
										0.3	0.2	4.1	15				
										0.3	0.2	6.9	25				
										0.3	0.2	2.8	10				
Ve1-Sk2062.92B	7B	Vedsted-1	2062.92	2	5	325	26.46	437.5	393.5	85	44			282	89	12	0.9
										100	150	19	15				
										94	74	44	35				
										83	42	76	60				
										81	36	19	15				
Ga1-Sk3032.42A	1	Gassum-1	3032.42	22	0	175	6.55	0.28	0.04	0.004	0.002			16	35	0	3.4
										0.003	0.002	0.08	0.25				
										0.004	0.002	0.16	0.50				
										0.004	0.002	0.32	1.01				
										0.003	0.002	0.08	0.25				
Ga1-Sk3124.90A	2	Gassum-1	3124.90				6.19	0.25	0.04	c)	c)					0	2.8

[a)] Estimate [b)] Fluid perm was not possible, possibly due to smectite [c)] Test not carried out na: not analysed

Appendix B

Conventional core analysis (gas and klinkenberg permeability) results

Sample id	Lab id	Formation	Well	Depth	Diameter	Area	Length	Grain dens	Porosity	Gas perm	Klink perm
				m	mm	cm2	mm	g/cm3	%	mD	mD
Ve1-Ga2009.96A	8A	Gassum	Vedsted-1	2009.96	24.70	4.79	18.58	2.652	27.04	343.12	312.70
Ve1-Ga2009.96C	8C	Gassum	Vedsted-1	2009.96	24.78	4.82	21.20	2.649	25.91	298.86	264.88
Ve1-Ga2010.17B	9B	Gassum	Vedsted-1	2010.17	24.61	4.76	23.10	2.652	27.77	557.18	501.51
Ve1-Ga2010.17C	9C	Gassum	Vedsted-1	2010.17	24.54	4.73	16.85	2.648	27.27	370.44	323.91
Aa1-Ga3325.03A	11A	Gassum	Aars-1	3325.03	24.63	4.76	47.94	2.643	12.97	6.71	5.91
Aa1-Ga3325.03B	11B	Gassum	Aars-1	3325.03	24.70	4.79	48.33	2.643	12.72	5.56	4.85
Aa1-Ga3326.49A	13A	Gassum	Aars-1	3326.49	24.60	4.75	44.58	2.647	12.51	2.05	1.77
Aa1-Ga3326.49B	13B	Gassum	Aars-1	3326.49	24.65	4.77	47.00	2.648	12.82	2.65	2.32
Aa1-Ga3318.20A	20	Gassum	Aars-1	3318.20	24.74	4.81	51.15	2.660	6.13	1.04	0.60
Aa1-Ga3352.22A	14	Gassum	Aars-1	3352.22	24.71	4.80	49.36	2.644	12.96	24.29	19.71
Aa1-Ga3352.22B	14A	Gassum	Aars-1	3352.22	24.74	4.81	37.85	2.643	13.09	21.33	15.33
Aa1-Ga3353.05A	16	Gassum	Aars-1	3353.05	24.72	4.80	38.23	2.655	16.09	187.84	157.05
Aa1-Ga3320.80A	21A	Gassum	Aars-1	3320.80	24.68	4.78	31.77	2.638	14.61	44.23	40.58
Aa1-Ga3320.80B	21B	Gassum	Aars-1	3320.80	24.63	4.76	40.89	2.638	14.54	66.18	58.82
Aa1-Ga3275.38A	22A	Gassum	Aars-1	3275.38	24.63	4.76	42.25	2.664	13.63	151.06	118.57
Aa1-Ga3275.38B	22B	Gassum	Aars-1	3275.38	24.61	4.76	47.03	2.657	13.07	136.18	107.76
Aa1-Ga3318.10A	10	Gassum	Aars-1	3318.10	24.74	4.81	46.30	2.660	7.53	0.82	0.55
Aa1-Ga3318.10B	10A	Gassum	Aars-1	3318.10	24.75	4.81	34.75	2.662	7.37	0.62	0.41
Aa1-Ga3325.52A	12A	Gassum	Aars-1	3325.52	24.67	4.78	46.90	2.637	9.81	0.75	0.49
Aa1-Ga3325.52B	12B	Gassum	Aars-1	3325.52	24.71	4.80	36.58	2.636	9.08	0.61	0.45

Sample id	Lab id	Formation	Well	Depth	Diameter	Area	Length	Grain dens	Porosity	Gas perm	Klink perm
				m	mm	cm2	mm	g/cm3	%	mD	mD
Mo1-Sk5034.24A	15	Skagerrak	Mors-1	5034.24	24.20	4.60	35.48	2.704	5.23	1.68	1.33
Mo1-Sk5034.24B	15A	Skagerrak	Mors-1	5034.24	24.60	4.75	30.63	2.721	5.82	1.81	1.54
Mo1-Sk5089.57A	3	Skagerrak	Mors-1	5089.57	24.61	4.76	33.95	2.702	5.80	3.19	2.78
Mo1-Sk5089.57B	3A	Skagerrak	Mors-1	5089.57	24.62	4.76	21.06	2.690	5.70	4.72	3.70
Th2-Sk2919.35A	4	Skagerrak	Thisted-2	2919.35	24.32	4.65	39.11	2.697	16.35	9.69	6.03
Th2-Sk2919.35B	4A	Skagerrak	Thisted-2	2919.35	24.53	4.73	35.85	2.713	16.25	8.25	5.16
Th2-Sk2923.05A	5	Skagerrak	Thisted-2	2923.05	24.55	4.73	48.40	2.680	11.85	2.34	1.58
Th2-Sk2923.05B	5A	Skagerrak	Thisted-2	2923.05	24.45	4.70	24.05	2.671	13.02	2.42	1.70
Th2-Sk2761.63A	6	Skagerrak	Thisted-2	2761.63	24.60	4.75	45.85	2.658	15.24	23.87	19.26
Th2-Sk2761.63B	6A	Skagerrak	Thisted-2	2761.63	24.43	4.69	41.67	2.676	14.68	11.00	7.26
Fr2-Sk1051.00	23	Skagerrak	Frederikshavn-2	1051.00	24.62	4.76	55.38	2.620	8.62	0.32	0.16
Ga1-Sk3124.90A	2	Skagerrak	Gassum-1	3124.90	24.74	4.81	44.51	2.657	6.19	0.25	0.04
Ga1-Sk3124.90B	2A	Skagerrak	Gassum-1	3124.90	24.73	4.80	25.67	2.658	6.88	0.43	0.21
Ga1-Sk3032.42A	1	Skagerrak	Gassum-1	3032.42	24.85	4.85	28.58	2.646	6.55	0.28	0.04
Ga1-Sk3032.42B	1A	Skagerrak	Gassum-1	3032.42	24.85	4.85	26.25	2.646	6.10	0.26	0.09
Ve1-Sk2062.92A	7A	Skagerrak	Vedsted-1	2062.92	24.57	4.74	32.37	2.658	26.58	418.87	382.24
Ve1-Sk2062.92B	7B	Skagerrak	Vedsted-1	2062.92	24.61	4.76	35.30	2.658	26.46	437.47	393.51

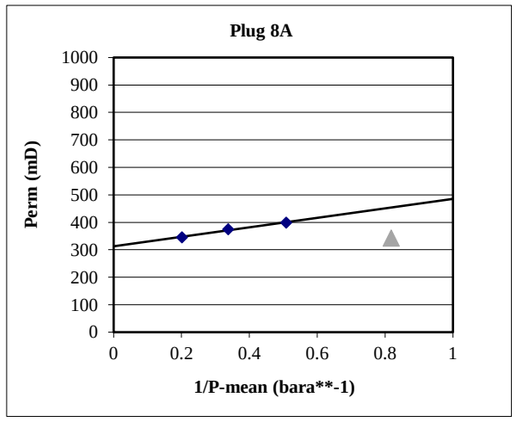
Plug 8A
Perm (mD)
1/P-mean (bara**-1)

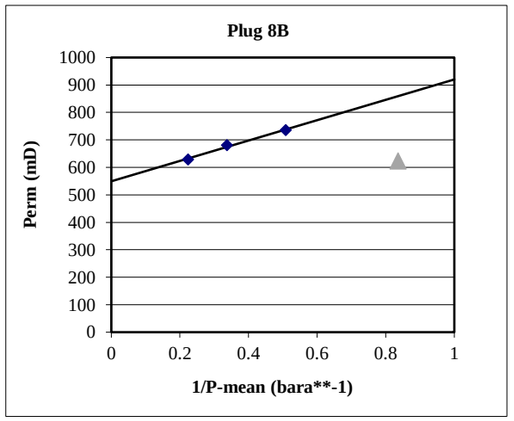
Plug 8B
Perm (mD)
1/P-mean (bara**-1)

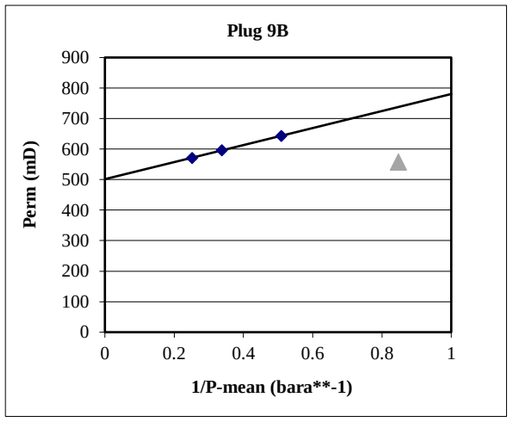
Plug 9B
Perm (mD)
1/P-mean (bara**-1)

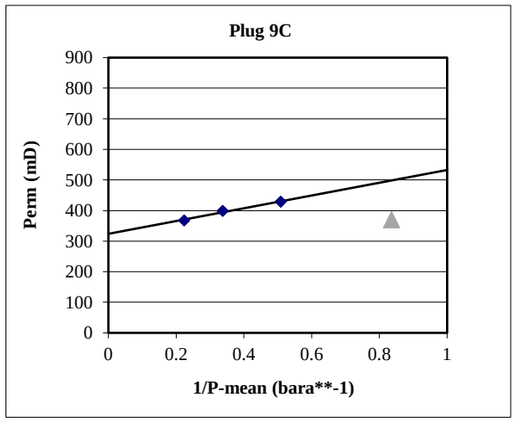
Plug 9C
Perm (mD)
1/P-mean (bara**-1)

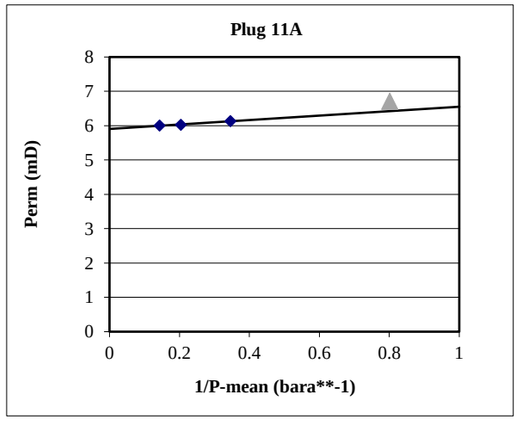
Plug 11A
Perm (mD)
1/P-mean (bara**-1)

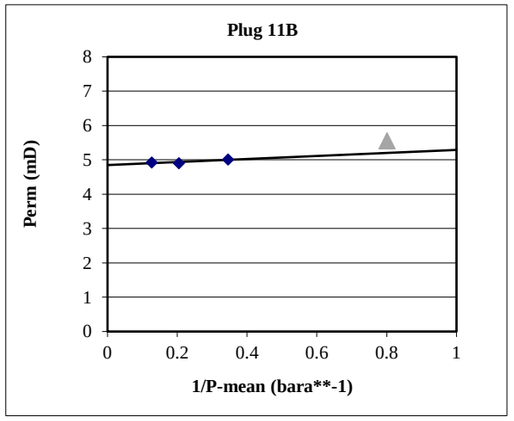
Plug 11B
Perm (mD)
1/P-mean (bara**-1)

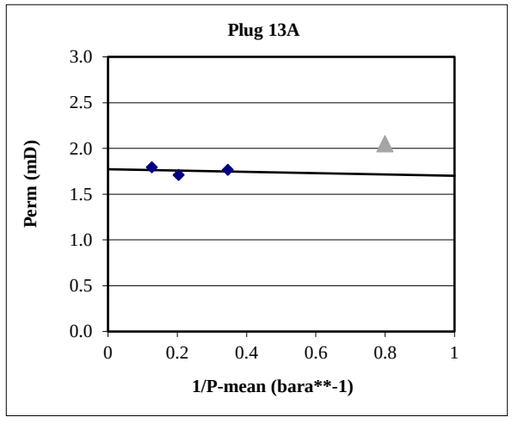
Plug 13A
Perm (mD)
1/P-mean (bara**-1)

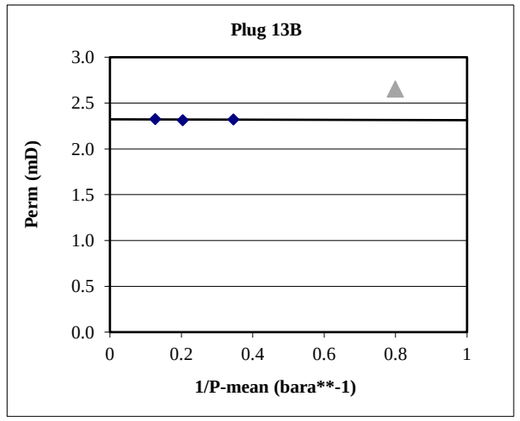
Plug 13B
Perm (mD)
1/P-mean (bara**-1)

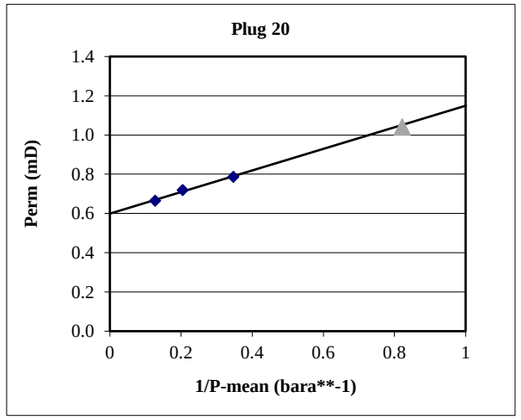
Plug 20
Perm (mD)
1/P-mean (bara**-1)

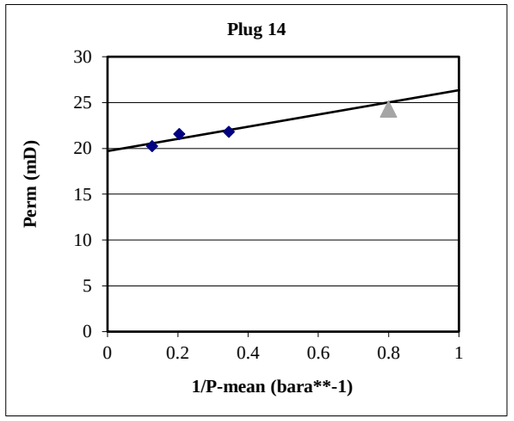
Plug 14
Perm (mD)
1/P-mean (bara**-1)

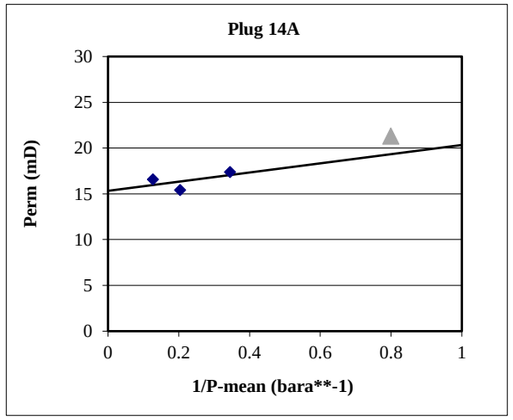
Plug 14A
Perm (mD)
1/P-mean (bara**-1)

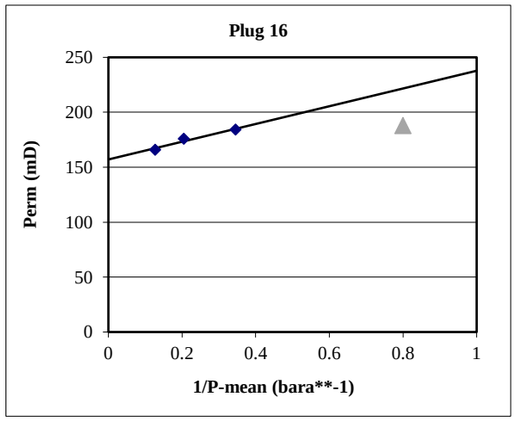
Plug 16
Perm (mD)
1/P-mean (bara**-1)

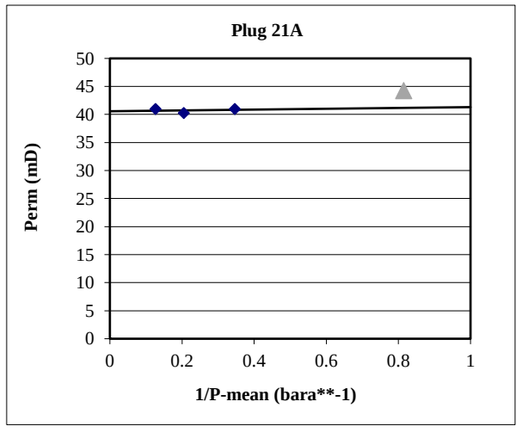
Plug 21A
Perm (mD)
1/P-mean (bara**-1)

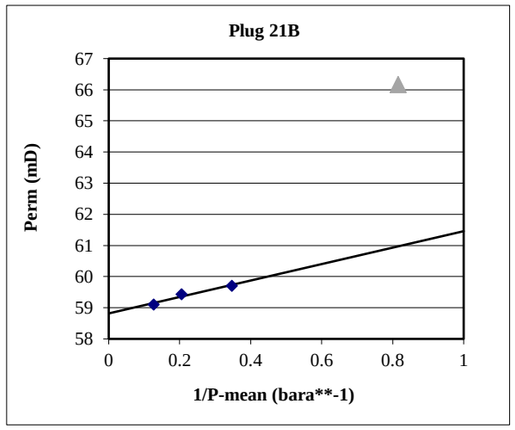
Plug 21B
Perm (mD)
1/P-mean (bara**-1)

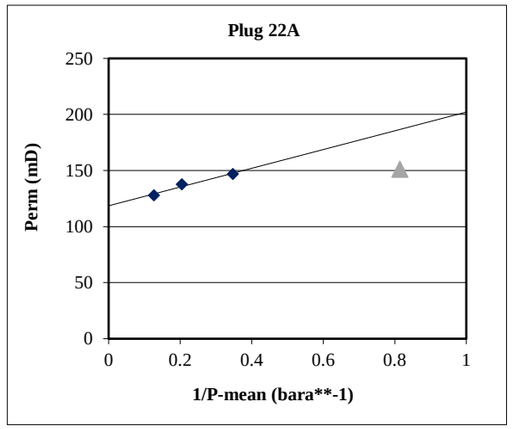
Plug 22A
Perm (mD)
1/P-mean (bara**-1)

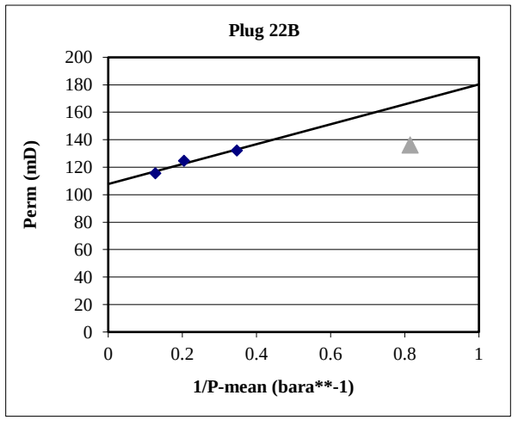
Plug 22B
Perm (mD)
1/P-mean (bara**-1)

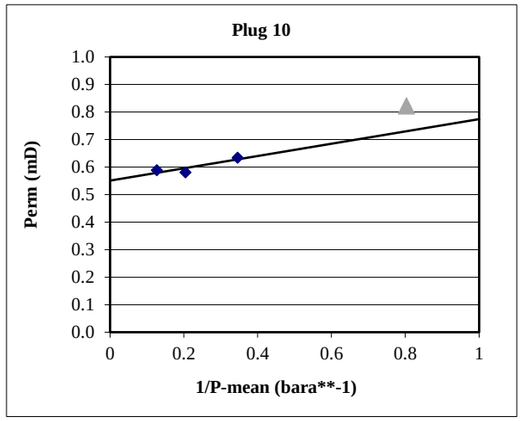
Plug 10
Perm (mD)
1/P-mean (bara**-1)

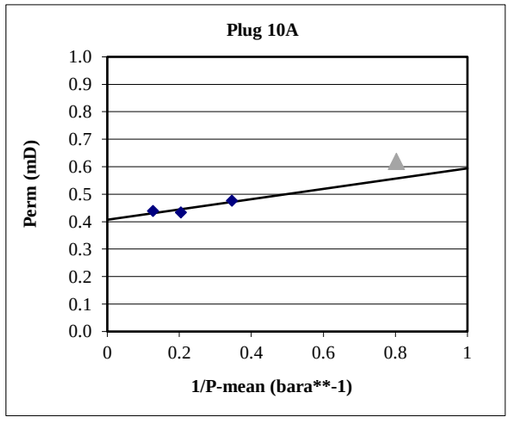
Plug 10A
Perm (mD)
1/P-mean (bara**-1)

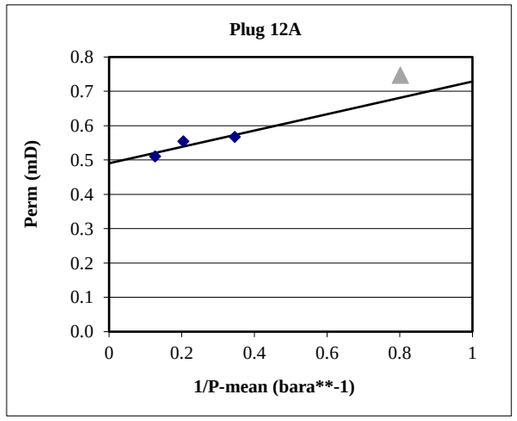
Plug 12A
Perm (mD)
1/P-mean (bara**-1)

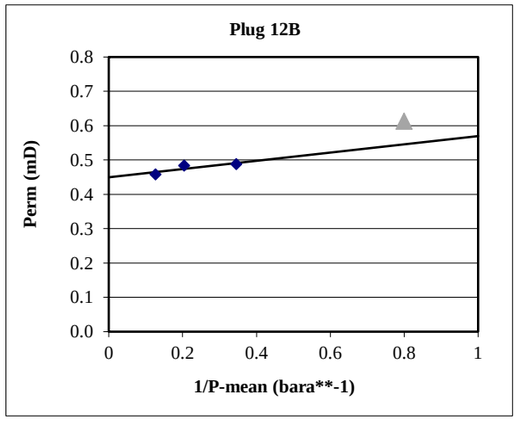
Plug 12B
Perm (mD)
1/P-mean (bara**-1)

Appendix C

Liquid permeability results

Plugs 8C and 9C: Similar grain size - Different clay type

Plug characteristics

Ve1-Ga2009.96C (Plug 8C)	Ve1-Ga2010.17B (Plug 9B)
	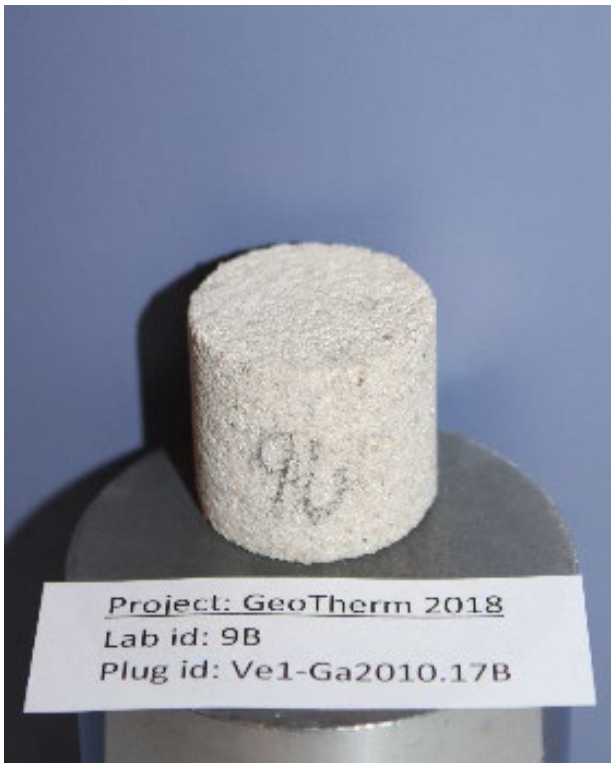
Formation: Gassum Well: Vedsted-1 Depth (m MD): 2009.96	Formation: Gassum Well: Vedsted-1 Depth (m MD): 2010.17B
Grain size (µm): 261 Clay type and content: 7% kaolinite	Grain size (µm): 246 Clay type and content: 3% kaolinite + 5% illite
Porosity (%): 25.91	Porosity (%): 27.77
Diameter (cm): 2.478 Length (cm): 2.120 Weight, dry (g): 19.32	Diameter (cm): 2.461 Length (cm): 2.310 Weight, dry (g): 20.65
Bulk volume (cm3): 9.84 Pore volume (cm3): 2.55	Bulk volume (cm3): 10.78 Pore volume (cm3): 2.99
Bulk density, dry (g/cm3): 1.963	Bulk density, dry (g/cm3): 1.915
Gas permeability (mD): 298.9 Klinkenberg permeability (mD): 264.9	Gas permeability (mD): 557.2 Klinkenberg permeability (mD): 501.5

Brine permeability

Ve1-Ga2009.96C (Plug 8C)

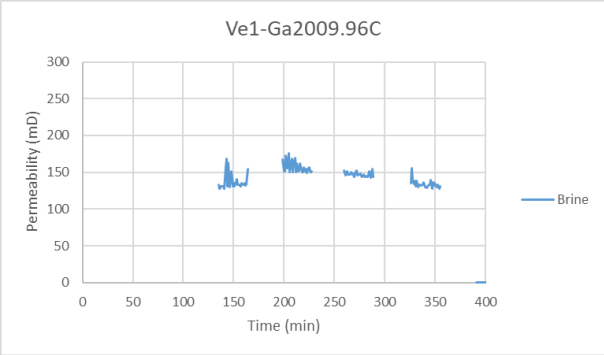

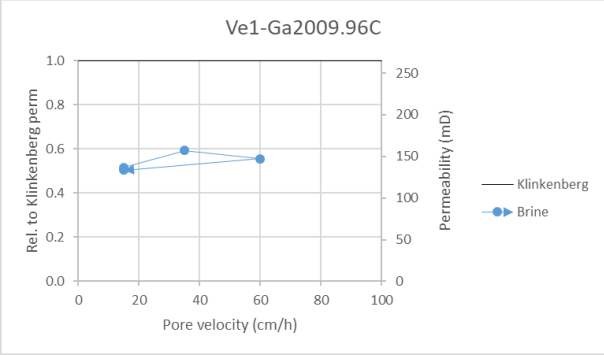

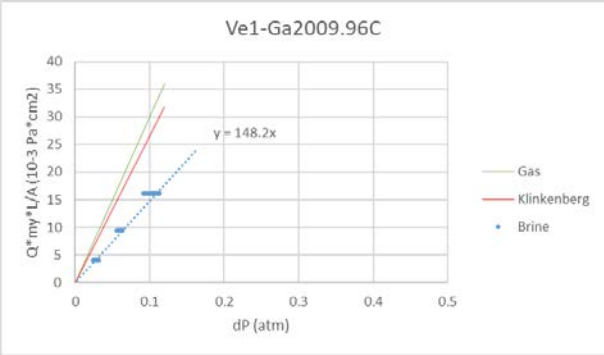

Brine viscosity (cP): 1.76
Weight, brine sat. (g): 22.39
Bulk density, brine sat. (g/cm3): 2.275

Pore velocity (cm/h)	Brine permeability (mD)
15	136.9
35	157.1
60	147.3
15	133.6
-	-
Best fit	148.2

Ve1-Ga2010.17B (Plug 9B)

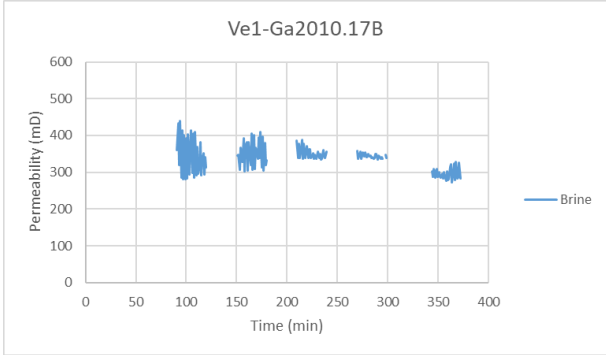

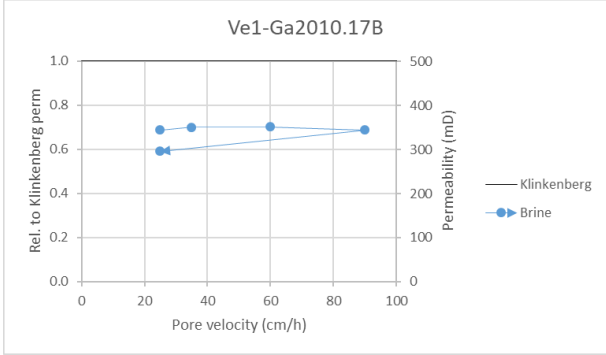

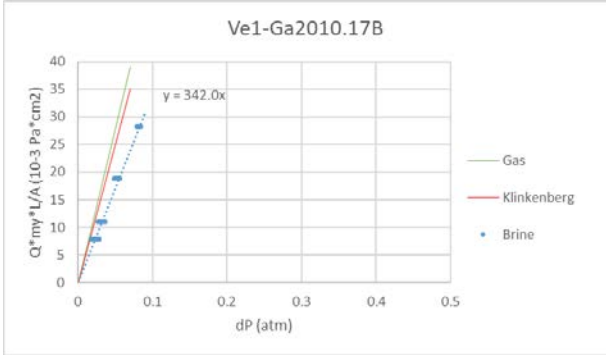

Brine viscosity (cP): 1.76
Weight, brine sat. (g): 24.25
Bulk density, brine sat. (g/cm3): 2.249

Pore velocity (cm/h)	Brine permeability (mD)
25	344.7
35	350.4
60	351.7
90	344.4
25	296.0
Best fit	342.0

DW permeability

Ve1-Ga2009.96C (Plug 8C)

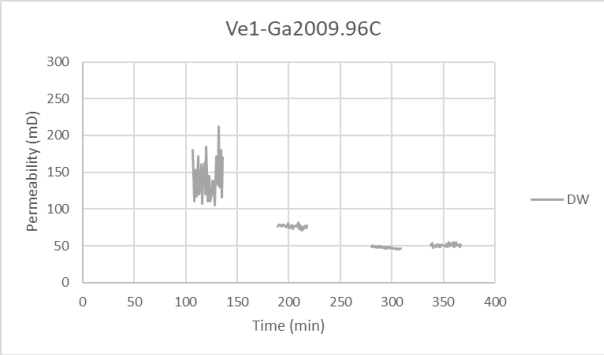

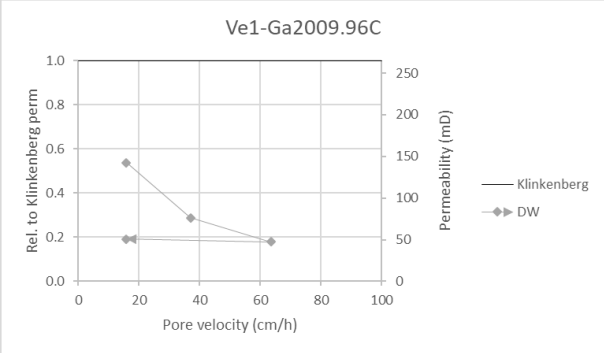

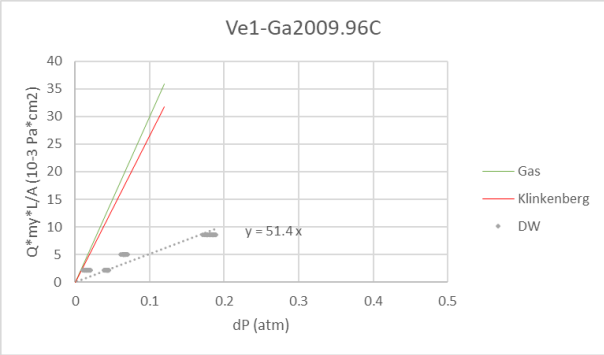

DW viscosity (cP): 0.89
Weight, DW sat. (g): 21.82
Bulk density, DW sat. (g/cm3): 2.217

Pore velocity (cm/h)	DW permeability (mD)
16	142.6
37	76.5
63	47.6
16	50.9
-	-
Best fit	51.4

Ve1-Ga2010.17B (Plug 9B)

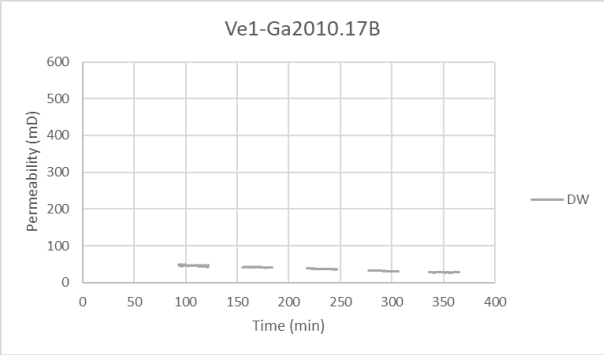

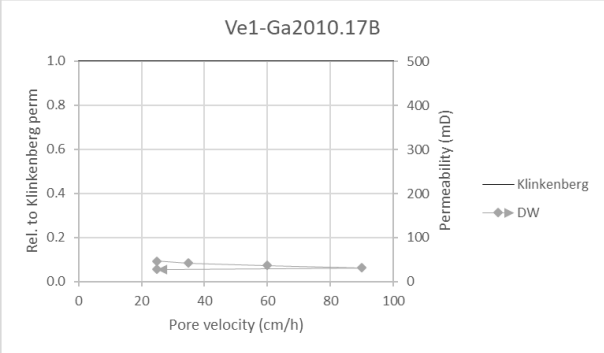

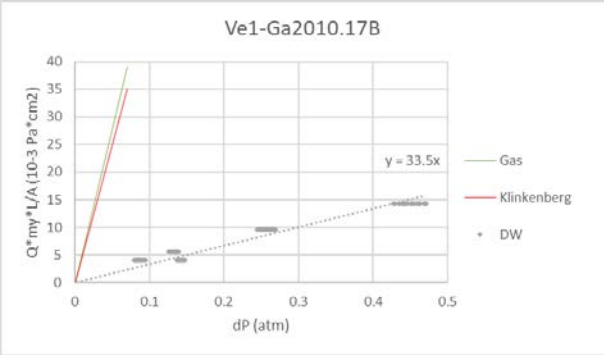

DW viscosity (cP): 0.89
Weight, DW sat. (g): 23.56
Bulk density, DW sat. (g/cm3): 2.185

Pore velocity (cm/h)	DW permeability (mD)
25	46.6
35	41.9
60	37.0
90	31.7
25	27.9
Best fit	33.5

Comparison between brine and DW measurements

Ve1-Ga2009.96C (Plug 8C)

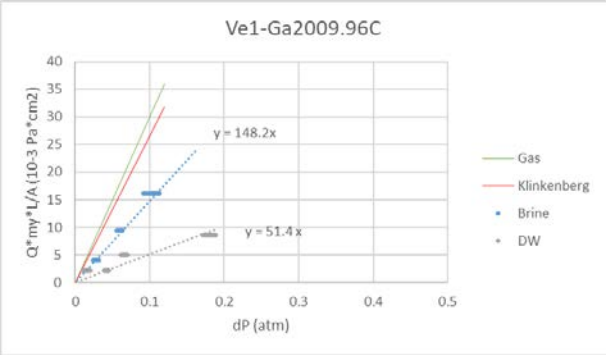

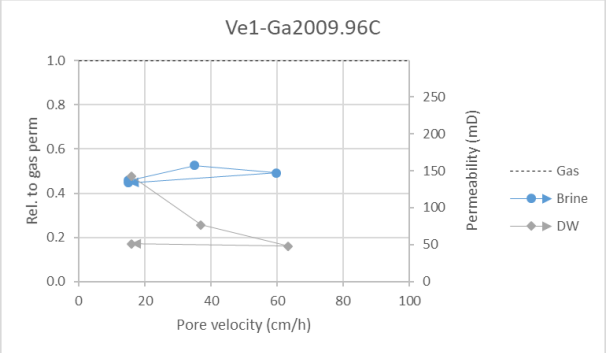

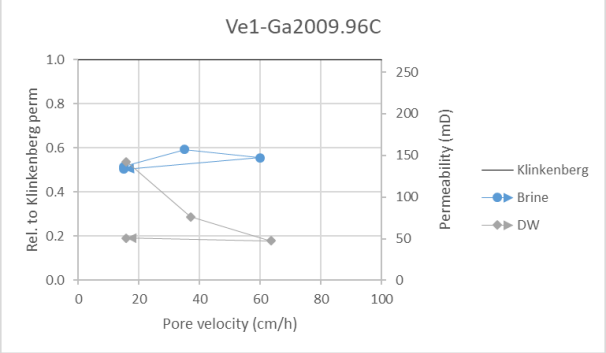

Ve1-Ga2010.17B (Plug 9B)

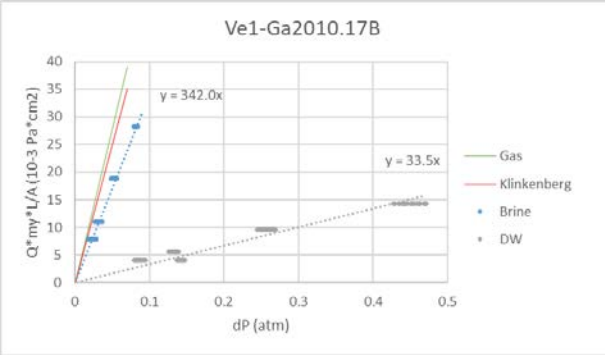

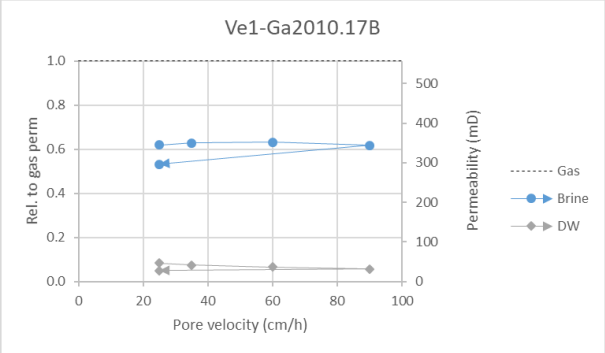

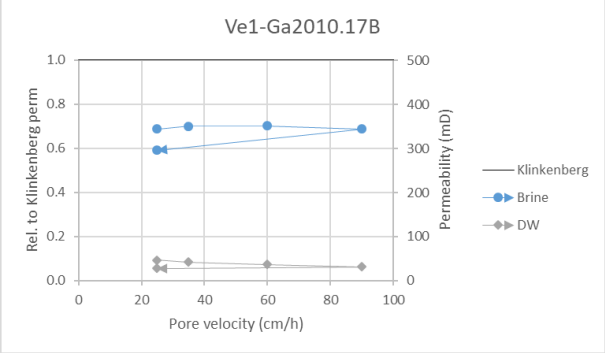

Plugs 11B, 13B, 10, 20: Similar grain size - Different illite content

Plug characteristics

Aa1-Ga3325.03B (Plug 11B)

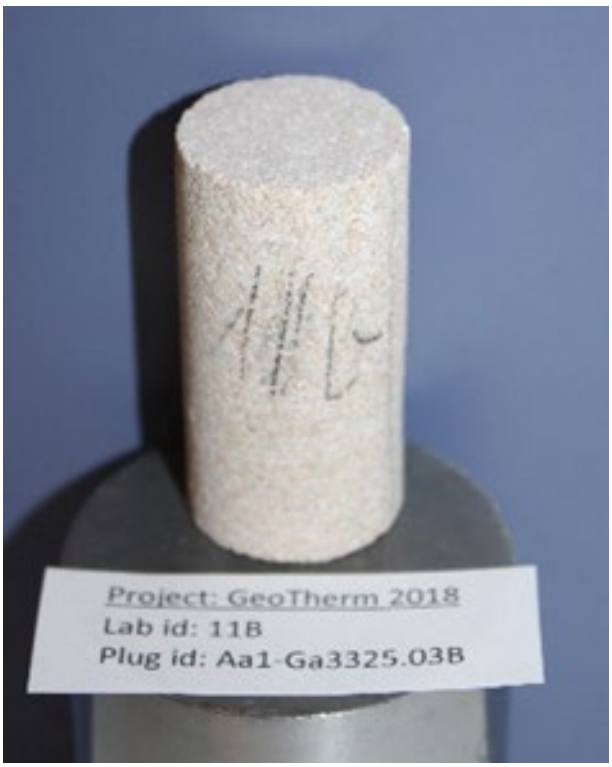

Formation: Gassum
Well: Aars-1
Depth (m MD): 3325.03

Grain size (µm):
Clay type and content: 7% illite

Porosity (%): 12.72

Diameter (cm): 2.470
Length (cm): 4.833
Weight, dry (g): 53.38

Bulk volume (cm3): 23.14
Pore volume (cm3): 2.94

Bulk density, dry (g/cm3): 2.307

Gas permeability (mD): 5.6
Klinkenberg permeability (mD): 4.9

Aa1-Ga3326.49B (Plug13B)

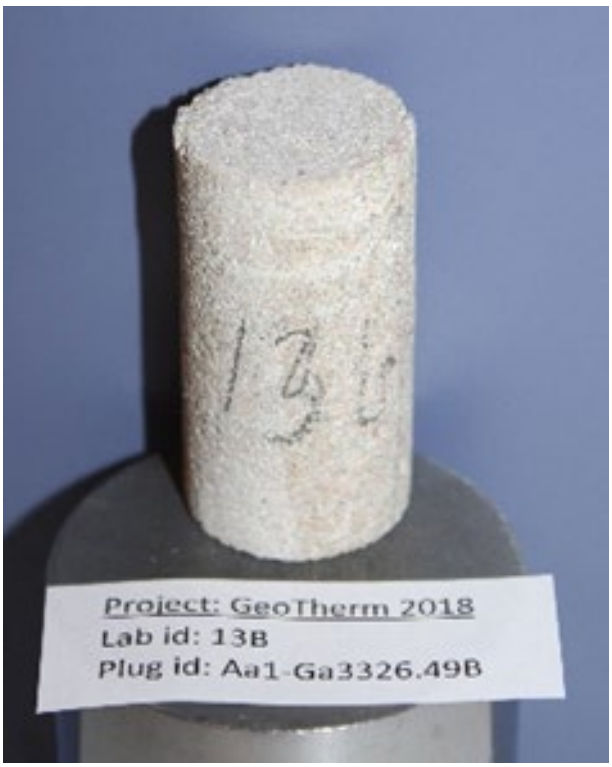

Formation: Gassum
Well: Aars-1
Depth (m MD): 3326.49

Grain size (µm):
Clay type and content: 12% illite

Porosity (%): 12.82

Diameter (cm): 2.465
Length (cm): 4.700
Weight, dry (g): 51.80

Bulk volume (cm3): 22.44
Pore volume (cm3): 2.88

Bulk density, dry (g/cm3): 2.309

Gas permeability (mD): 2.7
Klinkenberg permeability (mD): 2.3

Brine permeability

Aa1-Ga3325.03B (Plug 11B)

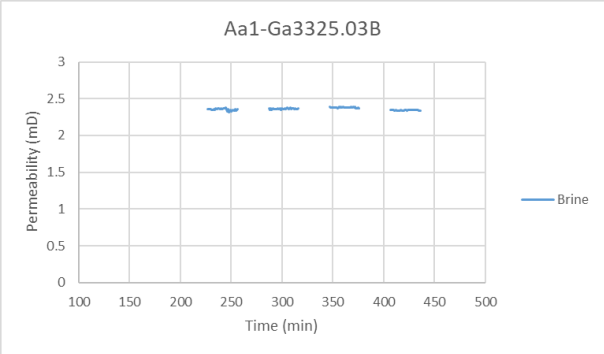

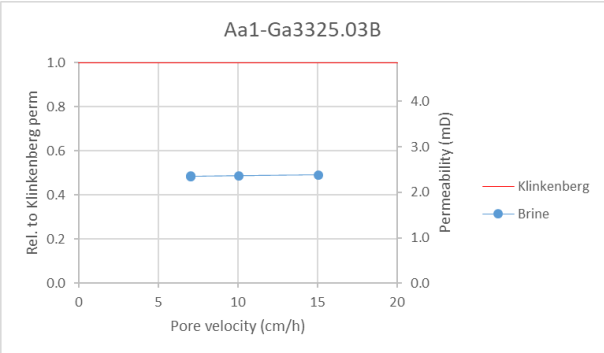

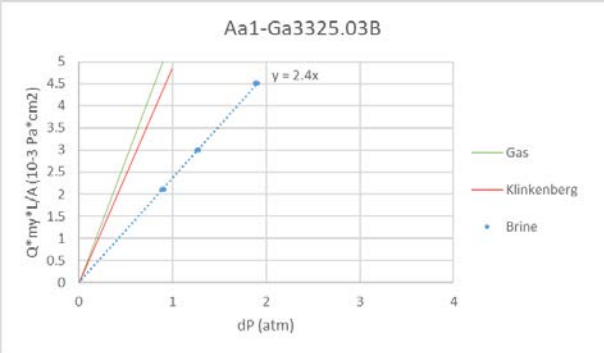

Brine viscosity (cP): 1.76
Weight, brine sat. (g): 56.90
Bulk density, brine sat. (g/cm3): 2.459

Pore velocity (cm/h)	Brine permeability (mD)
7	2.4
10	2.4
15	2.4
7	2.3
Best fit	2.4

Aa1-Ga3326.49B (Plug13B)

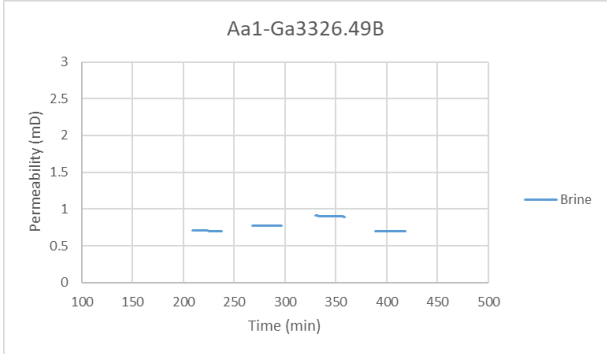

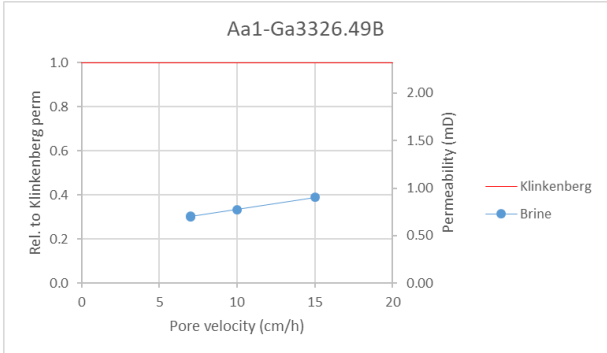

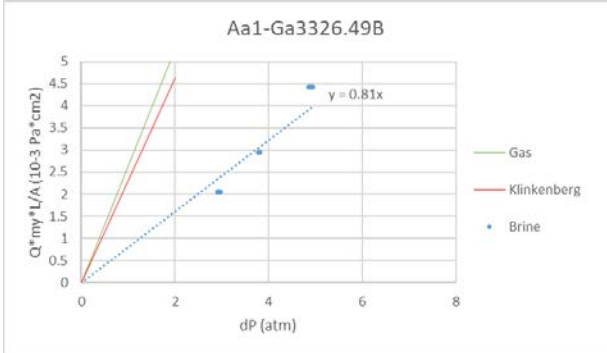

Brine viscosity (cP): 1.76
Weight, brine sat. (g): 55.30
Bulk density, brine sat. (g/cm3): 2.465

Pore velocity (cm/h)	Brine permeability (mD)
7	0.70
10	0.78
15	0.90
7	0.70
Best fit	0.81

DW permeability

Aa1-Ga3325.03B (Plug 11B)

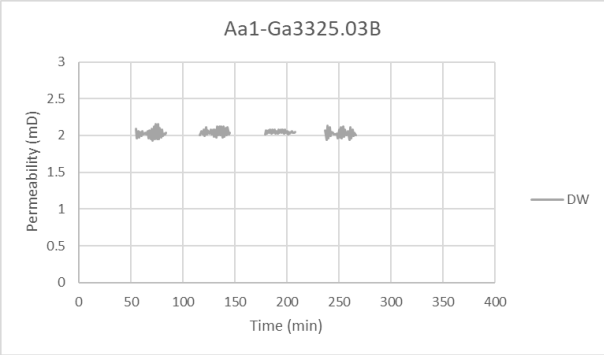

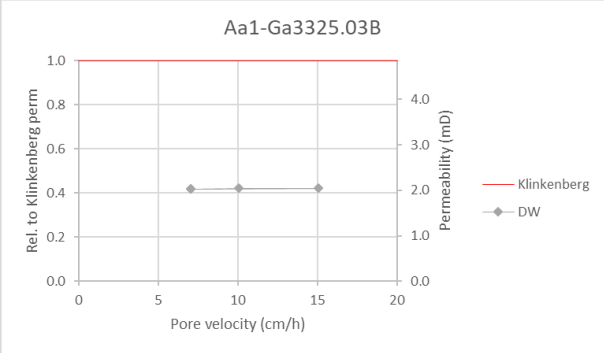

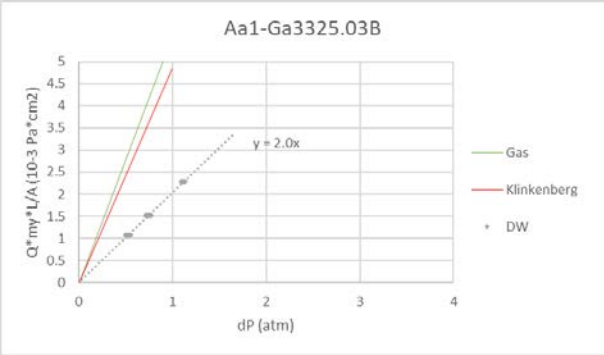

DW viscosity (cP): 0.89
Weight, DW sat. (g): 56.25
Bulk density, DW sat. (g/cm3): 2.431

Pore velocity (cm/h)	DW permeability (mD)
7	2.0
10	2.1
15	2.1
7	2.0
Best fit	2.0

Aa1-Ga3326.49B (Plug13B)

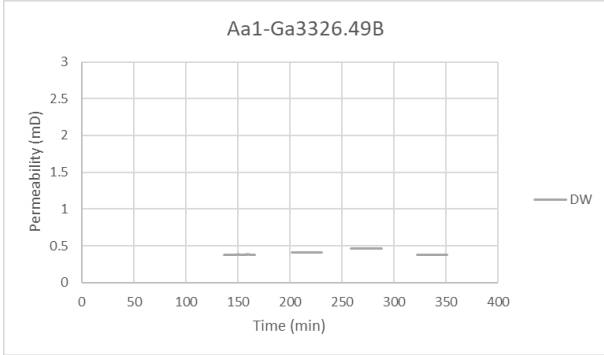

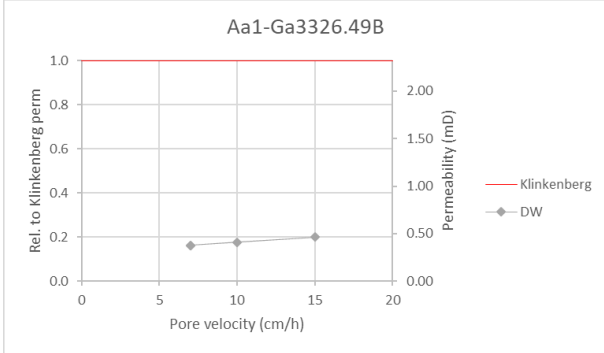

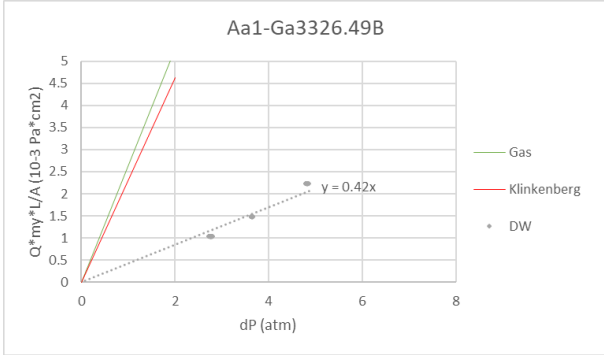

DW viscosity (cP): 0.89
Weight, DW sat. (g): 54.61
Bulk density, DW sat. (g/cm3): 2.434

Pore velocity (cm/h)	DW permeability (mD)
7	0.38
10	0.41
15	0.46
7	0.38
Best fit	0.42

Comparison

Aa1-Ga3325.03B (Plug 11B)

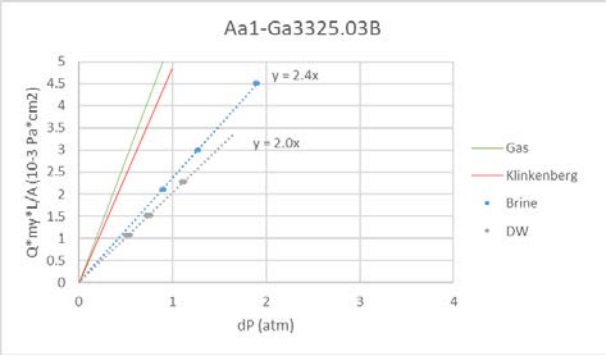

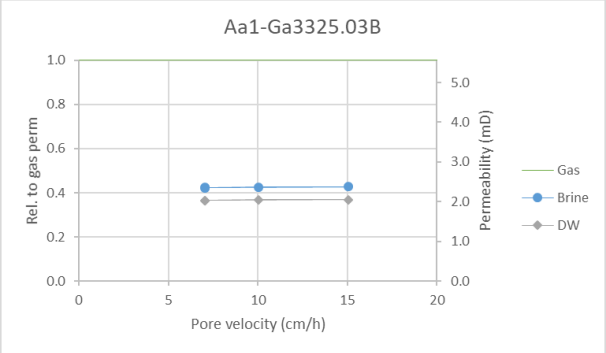

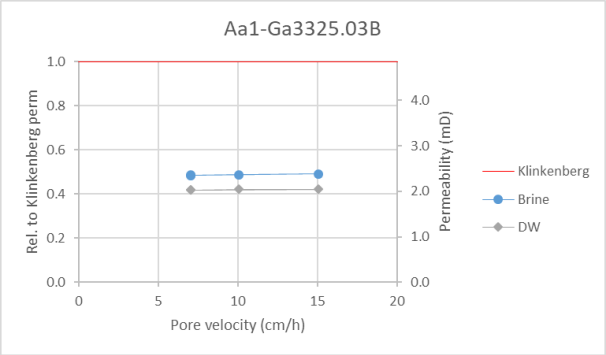

Aa1-Ga3326.49B (Plug13B)

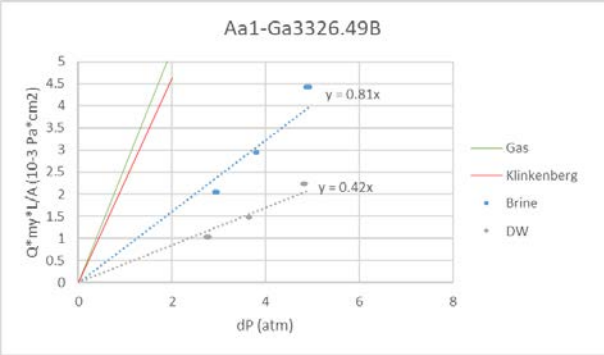

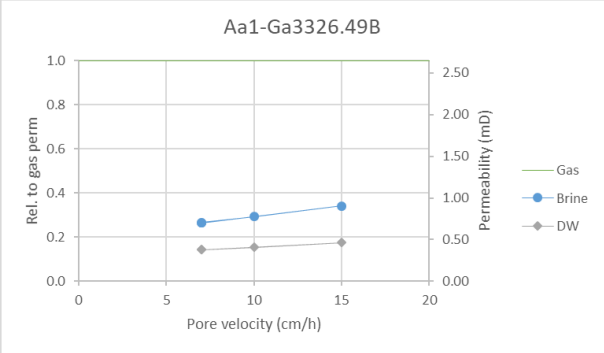

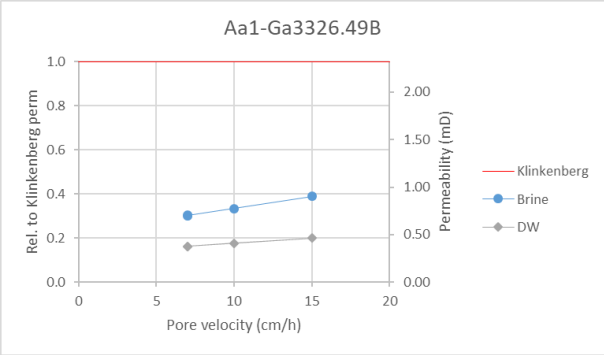

Plug characteristics

Aa1-Ga3318.20A (Plug 20)

Formation: Gassum
Well: Aars-1
Depth (m MD): 3318.20

Grain size (µm): 638
Clay type and content: 2% illite

Porosity (%): 6.13

Diameter (cm): 2.474
Length (cm): 5.115
Weight, dry (g): 61.57

Bulk volume (cm3): 24.66
Pore volume (cm3): 1.51

Bulk density, dry (g/cm3): 2.497

Gas permeability (mD): 1.0
Klinkenberg permeability (mD): 0.6

Aa1-Ga3318.10A (Plug 10)

Formation: Gassum
Well: Aars-1
Depth (m MD): 3318.10

Grain size (µm): 638
Clay type and content: 2% illite

Porosity (%): 7.53

Diameter (cm): 2.474
Length (cm): 4.630
Weight, dry (g): 55.49

Bulk volume (cm3): 22.56
Pore volume (cm3): 1.70

Bulk density, dry (g/cm3): 2.460

Gas permeability (mD): 0.8
Klinkenberg permeability (mD): 0.6

Brine permeability

Aa1-Ga3318.20A (Plug 20)

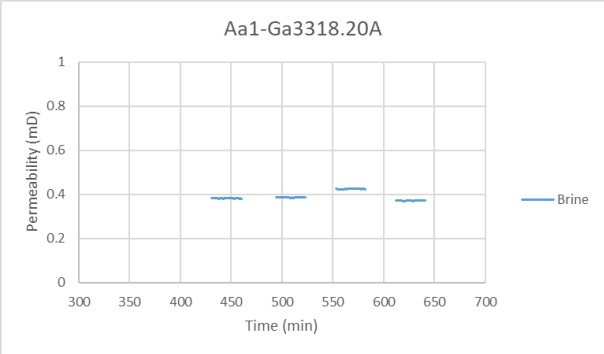

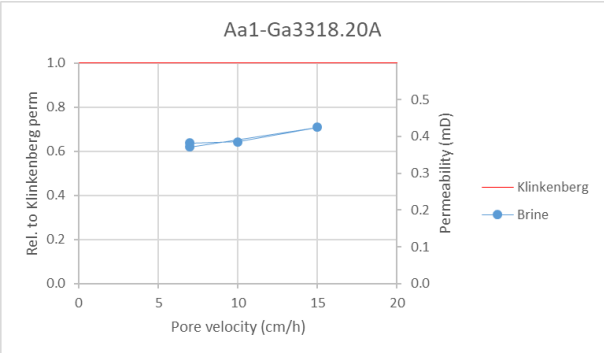

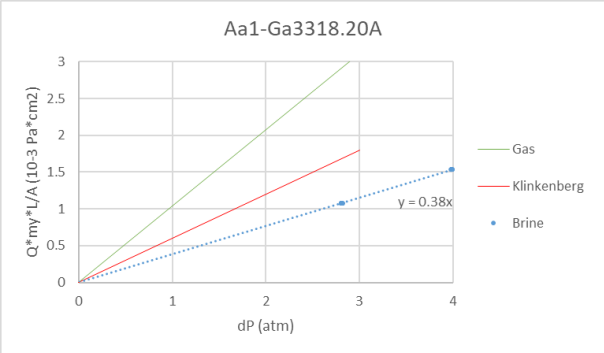

Brine viscosity (cP): 1.76
Weight, brine sat. (g): 63.39
Bulk density, brine sat. (g/cm3): 2.570

Pore velocity (cm/h)	Brine permeability (mD)
7	2.4
10	2.4
15	2.4
7	2.3
Best fit	2.4

Aa1-Ga3318.10A (Plug 10)

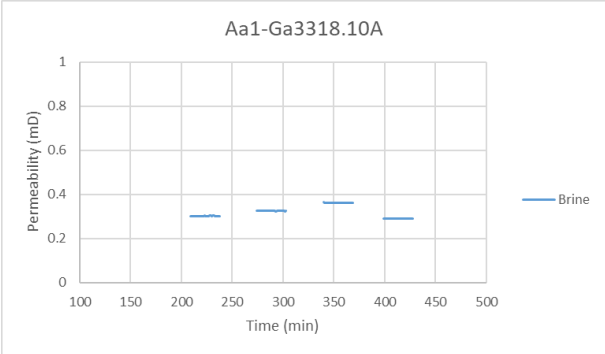

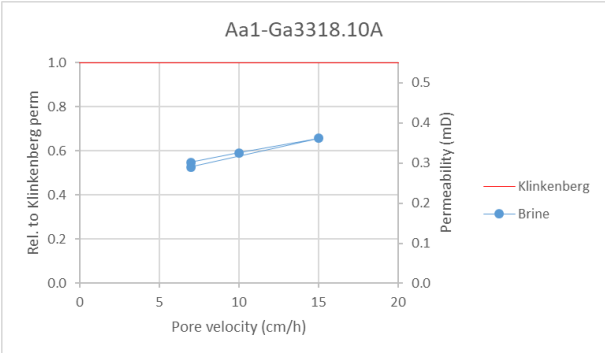

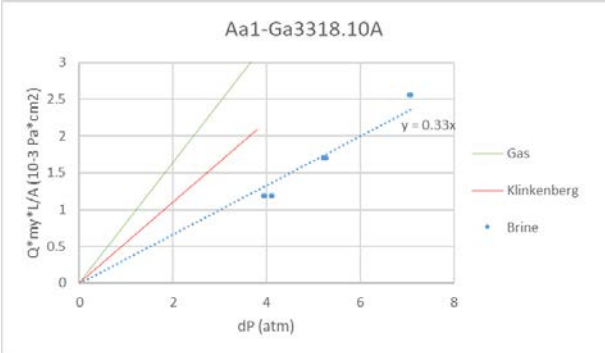

Brine viscosity (cP): 1.76
Weight, brine sat. (g): 57.52
Bulk density, brine sat. (g/cm3): 2.550

Pore velocity (cm/h)	Brine permeability (mD)
7	0.30
10	0.33
15	0.36
7	0.29
Best fit	0.33

DW permeability

Aa1-Ga3318.20A (Plug 20)

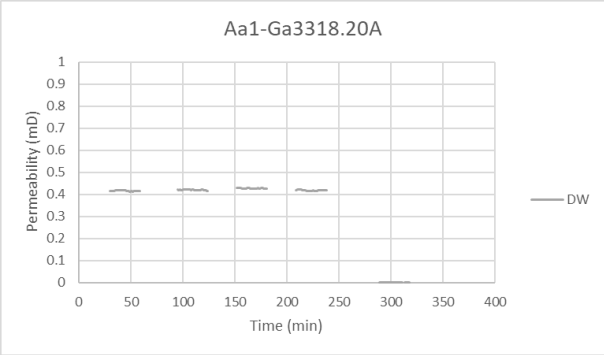

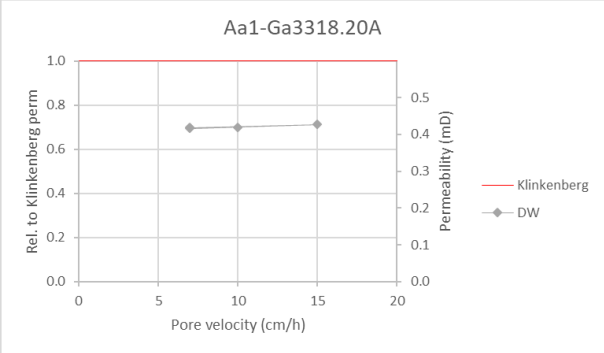

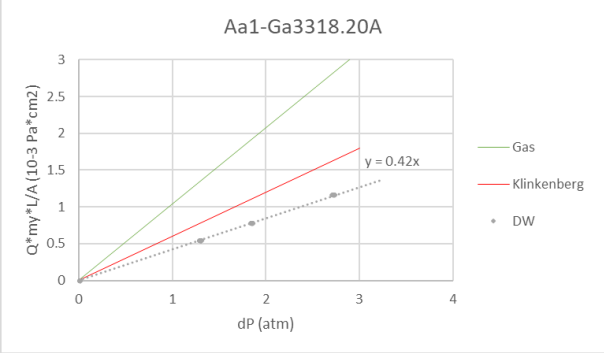

DW viscosity (cP): 0.89
Weight, DW sat. (g): 63.06
Bulk density, DW sat. (g/cm3): 2.557

Pore velocity (cm/h)	DW permeability (mD)
7	2.0
10	2.1
15	2.1
7	2.0
Best fit	2.0

Aa1-Ga3318.10A (Plug 10)

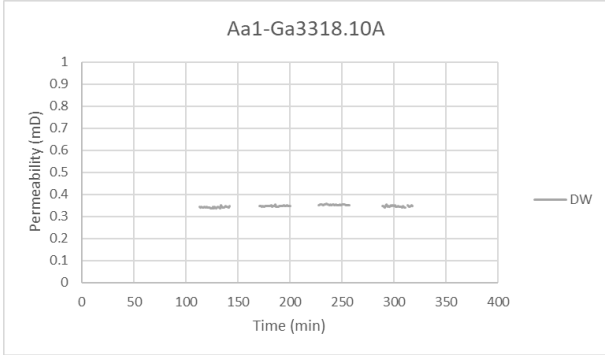

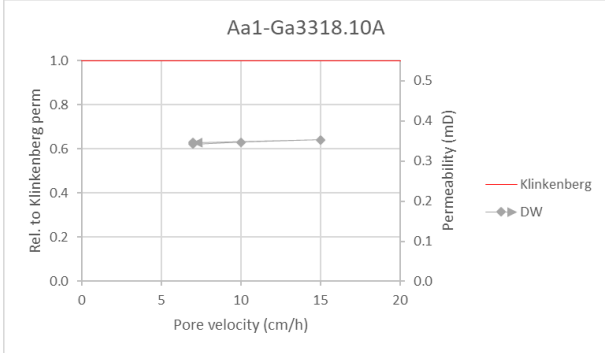

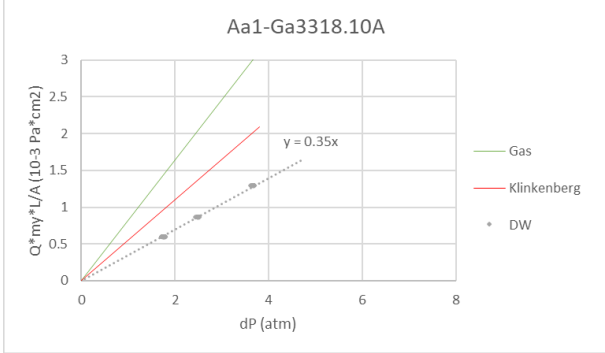

DW viscosity (cP): 0.89
Weight, DW sat. (g): 57.15
Bulk density, DW sat. (g/cm3): 2.533

Pore velocity (cm/h)	DW permeability (mD)
7	0.34
10	0.35
15	0.35
7	0.35
Best fit	0.35

Comparison

Aa1-Ga3318.20A (Plug 20)

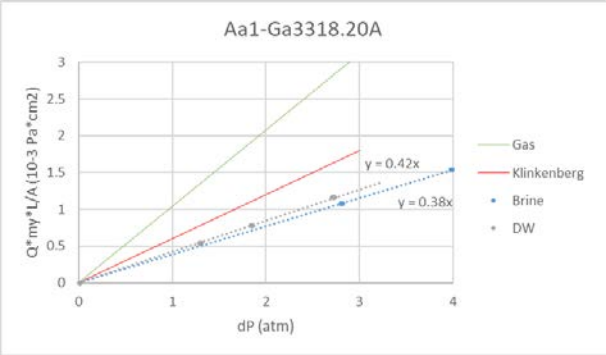

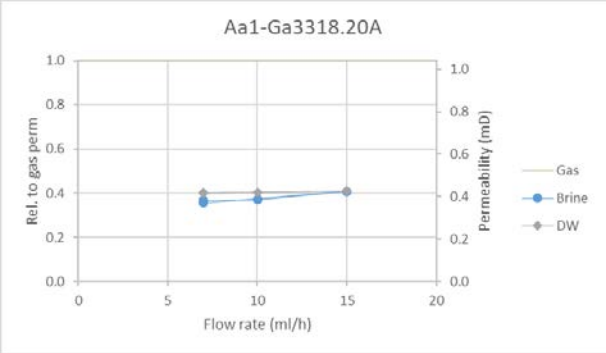

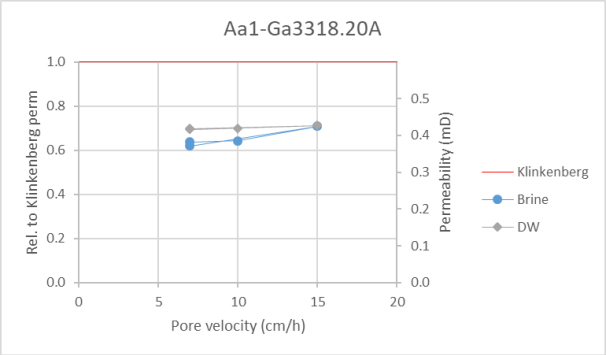

Aa1-Ga3318.10A (Plug 10)

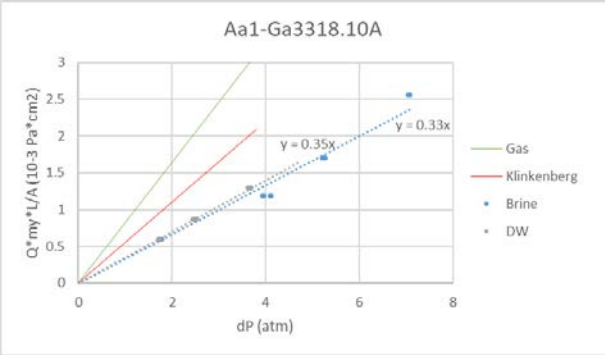

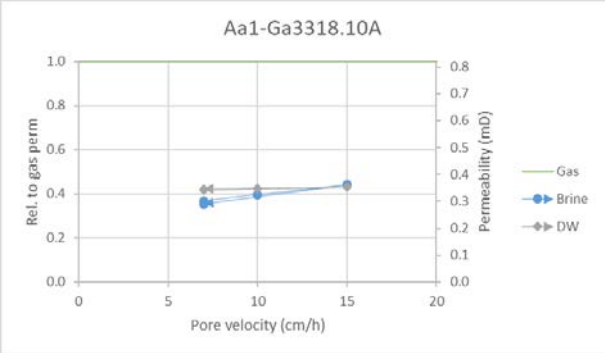

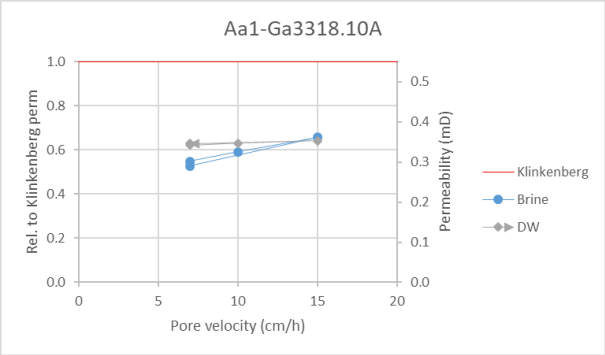

Plugs 14 and 16: Similar grain size - Different kaolinite

Plug characteristics

Aa1-Ga3352.22A (Plug 14)	Aa1-Ga3353.05A (Plug16)
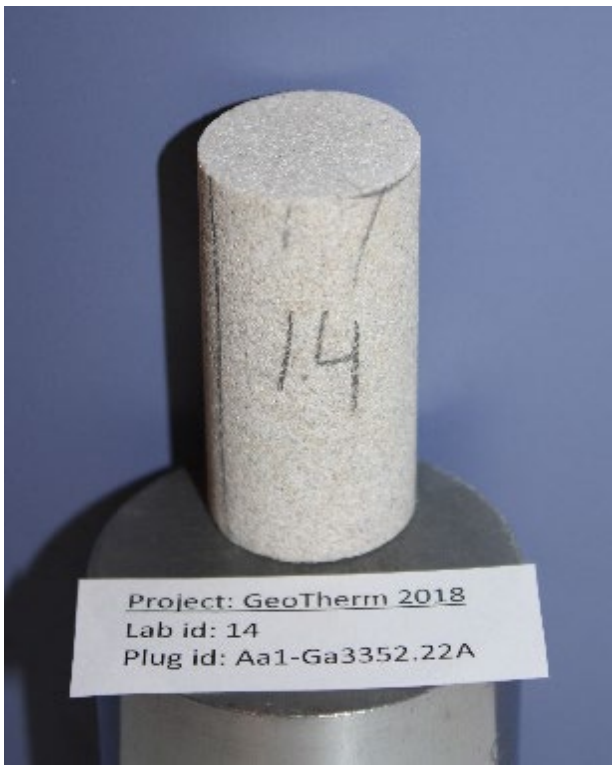	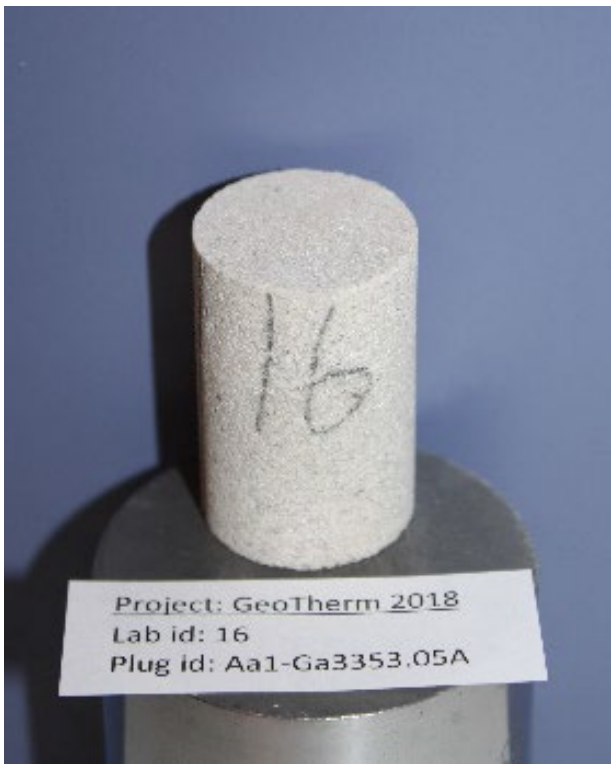
Formation: Gassum Well: Aars-1 Depth (m MD): 3352.22	Formation: Gassum Well: Aars-1 Depth (m MD): 3353.05
Grain size (µm): 432 Clay type and content: 4% kaolinite	Grain size (µm): 412 Clay type and content: 15% kaolinite and 2 % illite
Porosity (%): 13.0	Porosity (%): 16.1
Diameter (cm): 2.471 Length (cm): 4.936 Weight, dry (g): 55.00	Diameter (cm): 2.472 Length (cm): 3.823 Weight, dry (g): 41.26
Bulk volume (cm3): 23.90 Pore volume (cm3): 3.10	Bulk volume (cm3): 18.52 Pore volume (cm3): 2.98
Bulk density, dry (g/cm3): 2.301	Bulk density, dry (g/cm3): 2.228
Gas permeability (mD): 24.3 Klinkenberg permeability (mD): 19.7	Gas permeability (mD): 187.8 Klinkenberg permeability (mD): 157.1

Brine permeability

Aa1-Ga3352.22A (Plug 14)

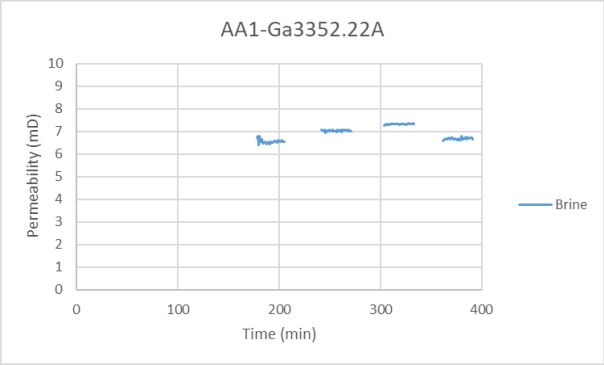

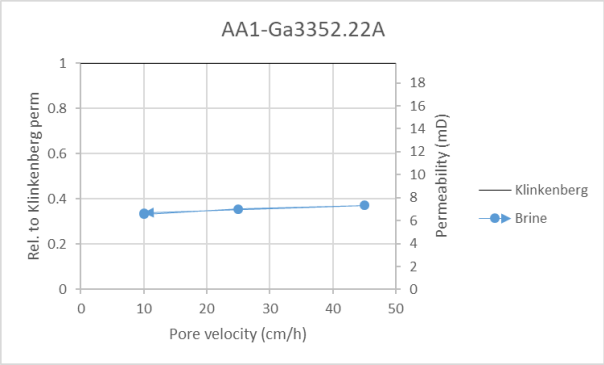

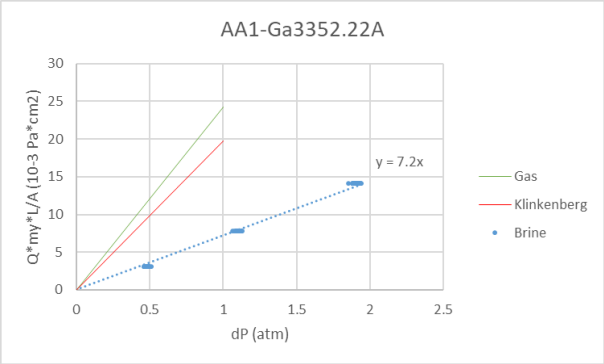

Brine viscosity (cP): 1.76
Weight, brine sat. (g): 58.79
Bulk density, brine sat. (g/cm3): 2.460

Pore velocity (cm/h)	Brine permeability (mD)
10	6.6
25	7.0
45	7.3
10	6.7
Best fit	7.2

Aa1-Ga3353.05A (Plug16)

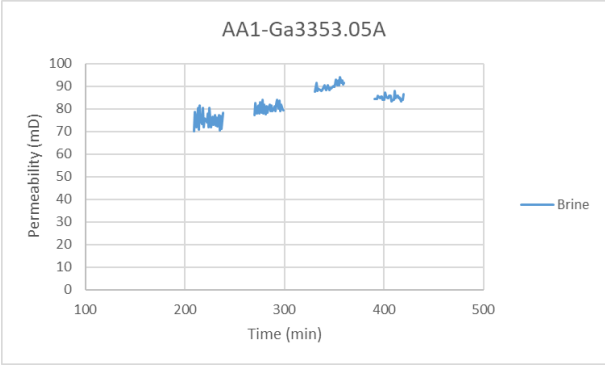

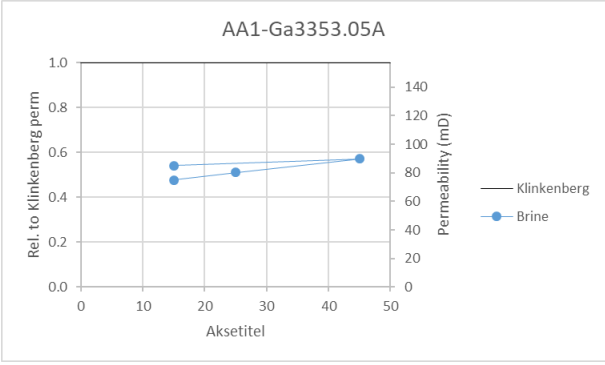

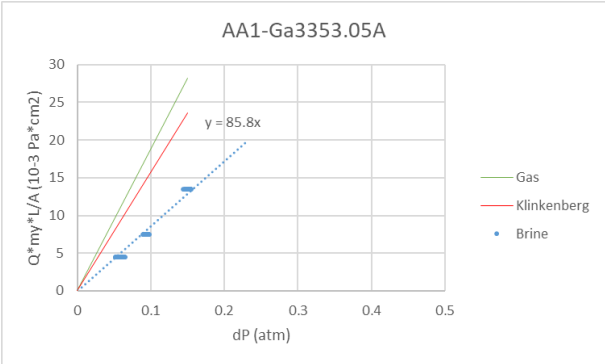

Brine viscosity (cP): 1.76
Weight, brine sat. (g): 44.89
Bulk density, brine sat. (g/cm3): 2.424

Pore velocity (cm/h)	Brine permeability (mD)
10	75.0
25	80.3
45	89.9
10	85.0
Best fit	85.8

DW permeability

Aa1-Ga3352.22A (Plug 14)

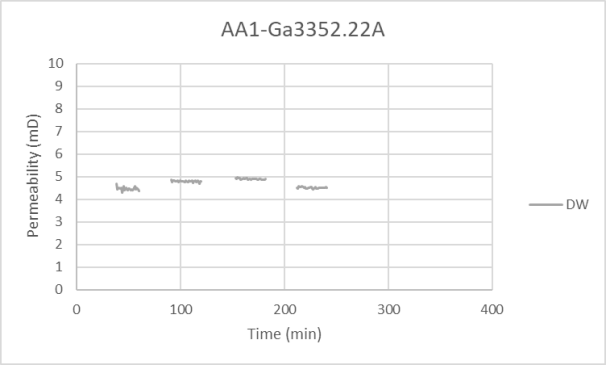

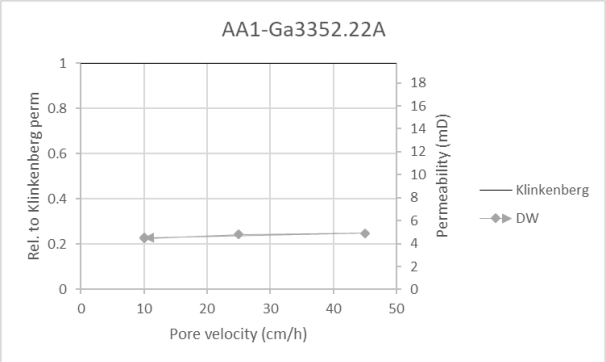

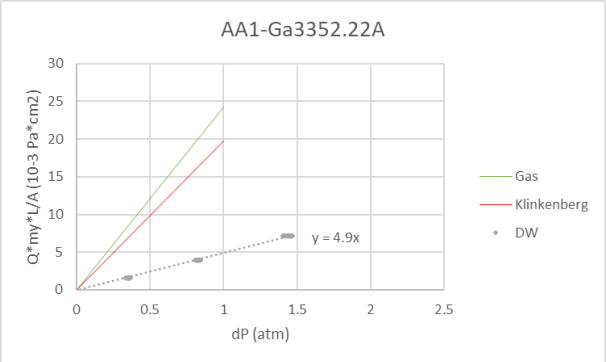

DW viscosity (cP): 0.89
Weight, DW sat. (g): 58.07
Bulk density, DW sat. (g/cm3): 2.430

Pore velocity (cm/h)	DW permeability (mD)
10	4.5
25	4.8
45	4.9
10	4.5
Best fit	4.9

Aa1-Ga3353.05A (Plug16)

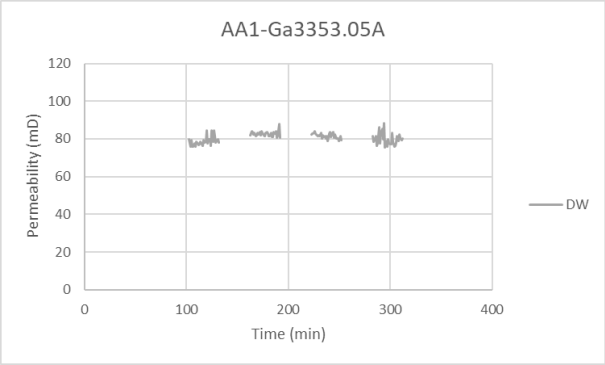

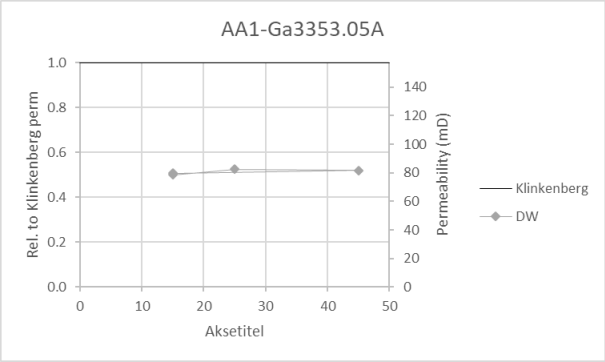

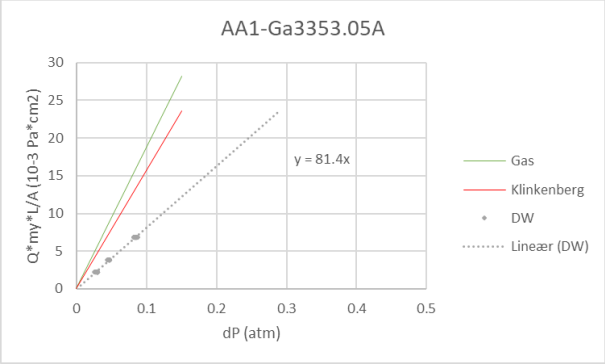

DW viscosity (cP): 0.89
Weight, DW sat. (g): 44.18
Bulk density, DW sat. (g/cm3): 2.386

Pore velocity (cm/h)	DW permeability (mD)
10	78.7
25	82.6
45	81.6
10	79.7
Best fit	81.4

Comparison

Aa1-Ga3352.22A (Plug 14)

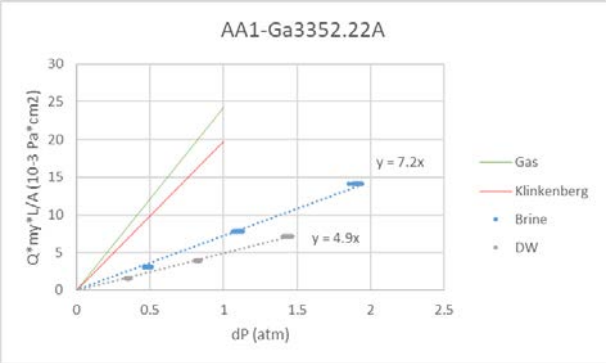

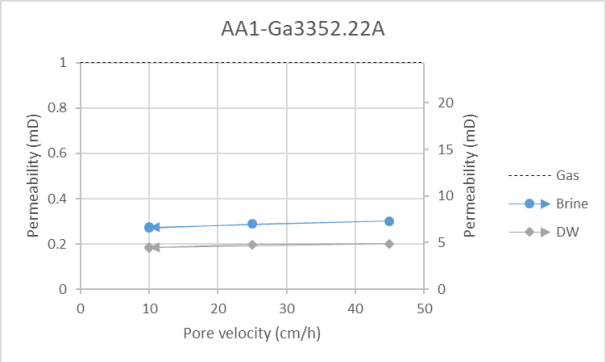

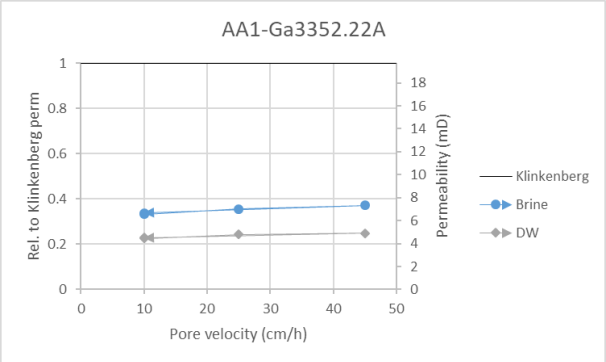

Aa1-Ga3353.05A (Plug16)

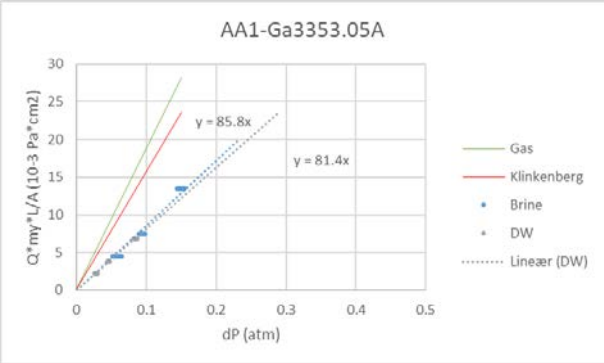

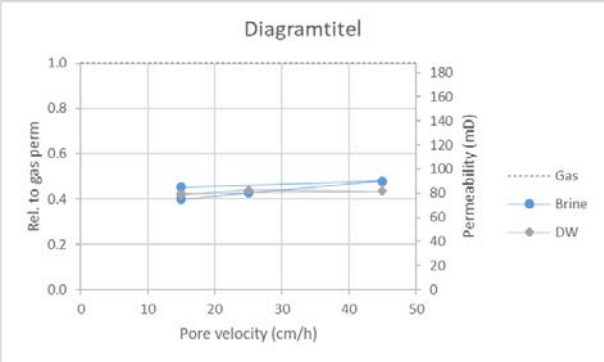

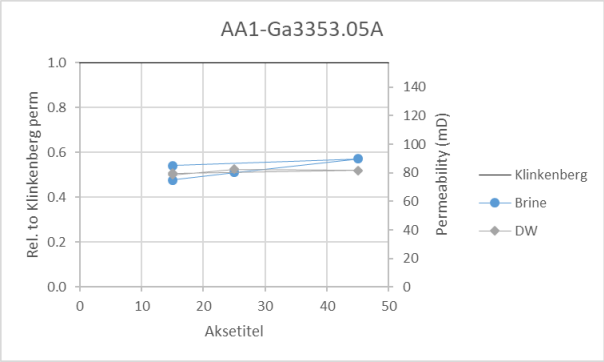

Plugs 21A, 22A and 12A: Similar grain size - Different clay type

Plug characteristics

Aa1-Ga3320.80A (Plug 21A)

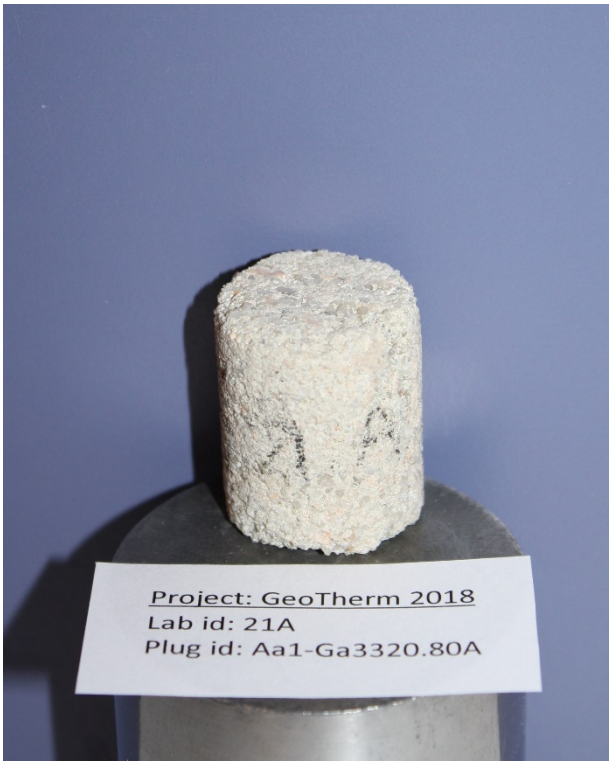

Formation: Gassum
Well: Aars-1
Depth (m MD): 3320.80

Grain size (µm): 869
Clay type and content: 7% illite and 1% kaolinite

Porosity (%): 14.61

Diameter (cm): 2.468
Length (cm): 3.177
Weight, dry (g): 31.78

Bulk volume (cm3): 14.11
Pore volume (cm3): 2.06

Bulk density, dry (g/cm3): 2.252

Gas permeability (mD): 44.23
Klinkenberg permeability (mD): 40.58

Aa1-Ga3275.38A (Plug 22A)

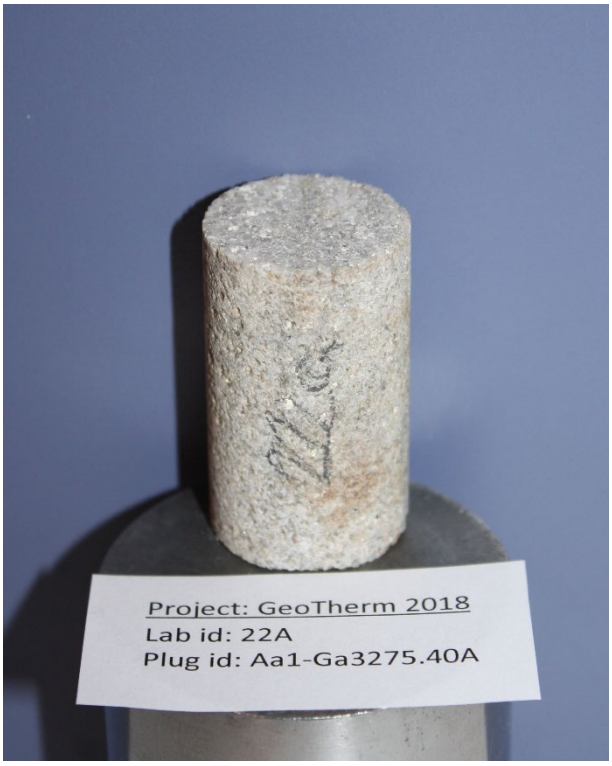

Formation: Gassum
Well: Aars-1
Depth (m MD): 3275.38

Grain size (µm): 971
Clay type and content: 7% kaolinite

Porosity (%): 13.63

Diameter (cm): 2.463
Length (cm): 4.225
Weight, dry (g): 46.32

Bulk volume (cm3): 20.14
Pore volume (cm3): 2.74

Bulk density, dry (g/cm3): 2.300

Gas permeability (mD): 151.1
Klinkenberg permeability (mD): 118.6

Brine permeability

Aa1-Ga3320.80A (Plug 21A)

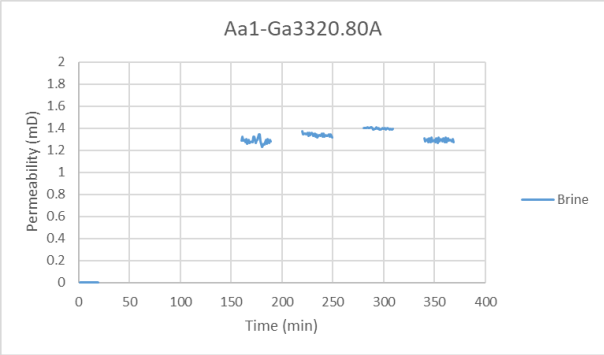

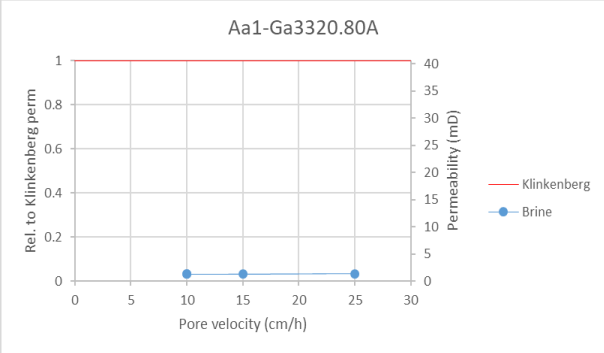

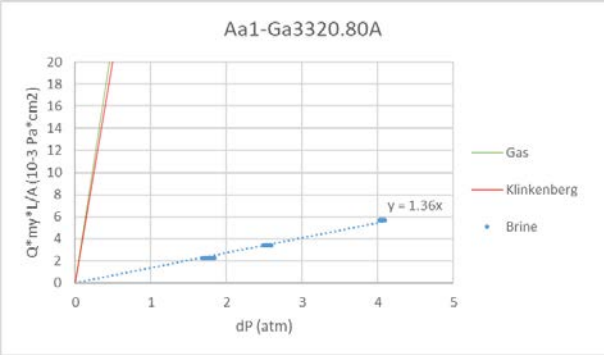

Brine viscosity (cP): 1.76
Weight, brine sat. (g): 34.30
Bulk density, brine sat. (g/cm3): 2.431

Pore velocity (cm/h)	Brine permeability (mD)
15	136.9
35	157.1
60	147.3
15	133.6
-	-
Best fit	148.2

Aa1-Ga3275.38A (Plug 22A)

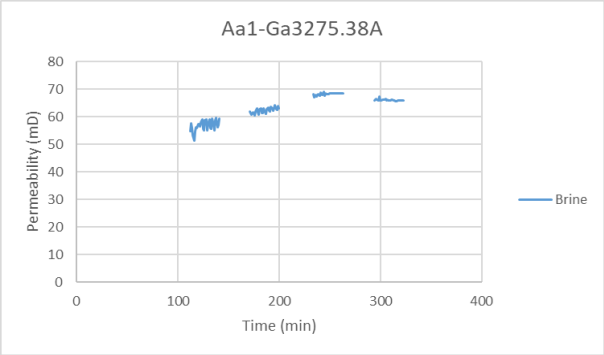

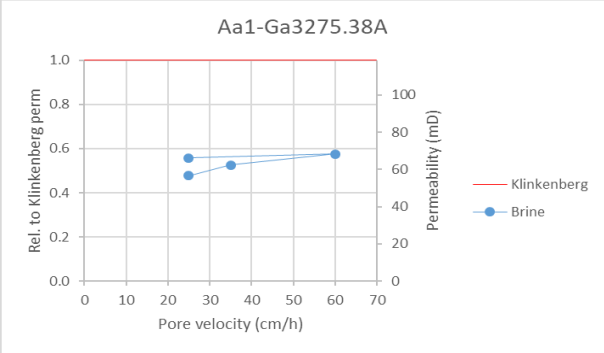

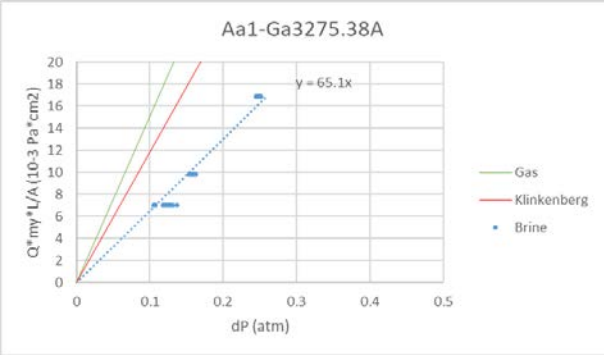

Brine viscosity (cP): 1.76
Weight, brine sat. (g): 49.69
Bulk density, brine sat. (g/cm3): 2.468

Pore velocity (cm/h)	Brine permeability (mD)
25	344.7
35	350.4
60	351.7
90	344.4
25	296.0
Best fit	342.0

DW permeability

Aa1-Ga3320.80A (Plug 21A)

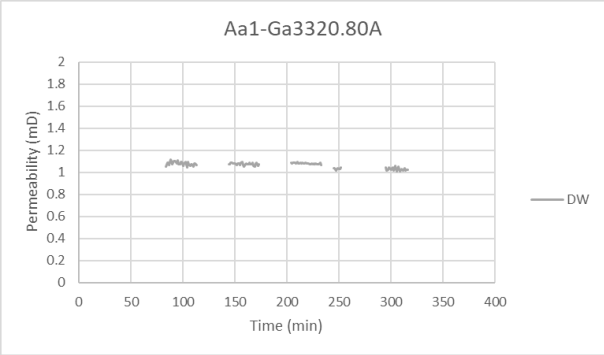

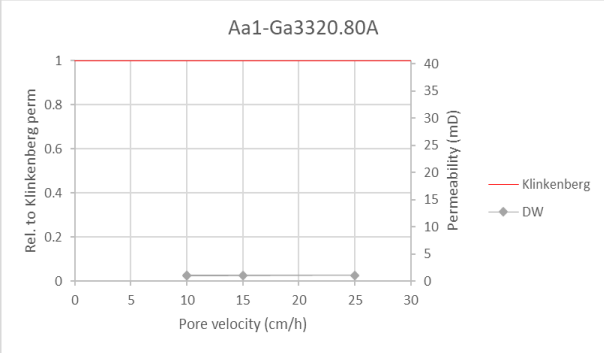

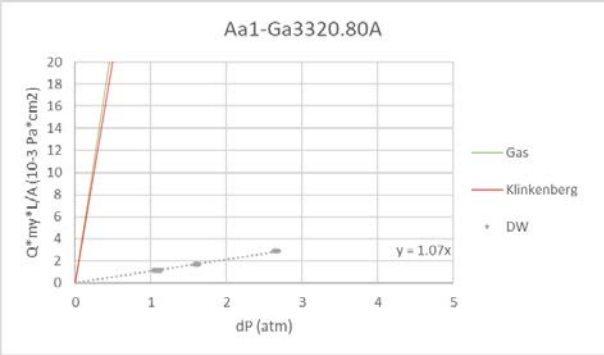

DW viscosity (cP): 0.89
Weight, DW sat. (g): 33.76
Bulk density, DW sat. (g/cm3): 2.393

Pore velocity (cm/h)	DW permeability (mD)
16	142.6
37	76.5
63	47.6
16	50.9
-	-
Best fit	51.4

Aa1-Ga3275.38A (Plug 22A)

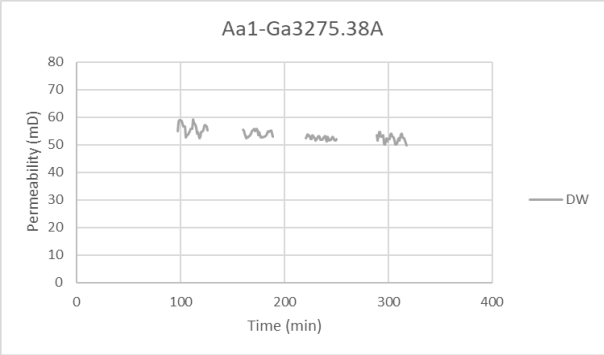

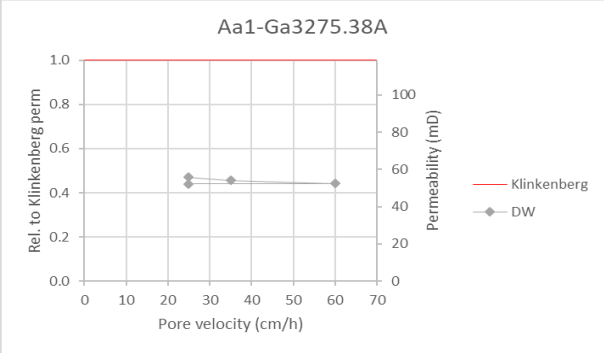

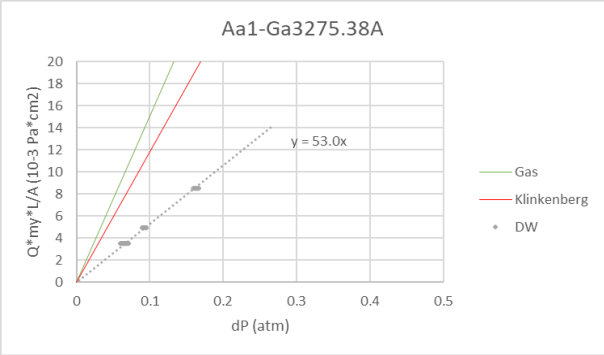

DW viscosity (cP): 0.89
Weight, DW sat. (g): 49.05
Bulk density, DW sat. (g/cm3): 2.436

Pore velocity (cm/h)	DW permeability (mD)
25	46.6
35	41.9
60	37.0
90	31.7
25	27.9
Best fit	33.5

Comparison between brine and DW measurements

Aa1-Ga3320.80A (Plug 21A)

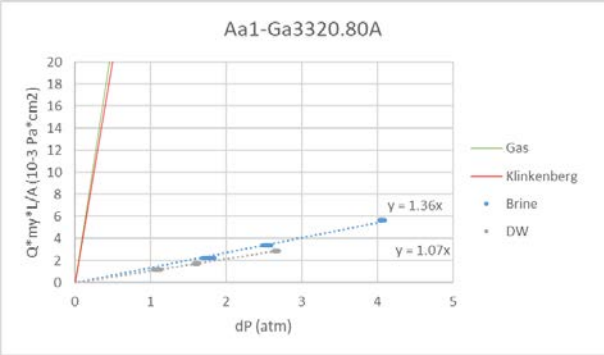

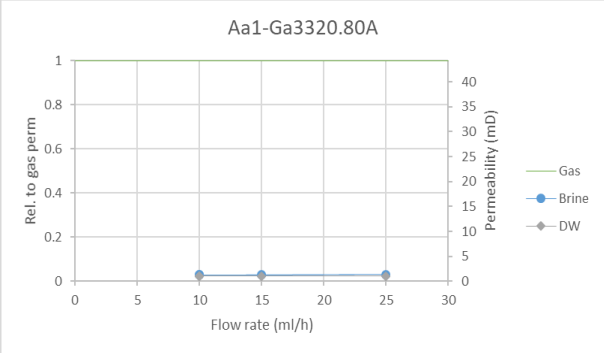

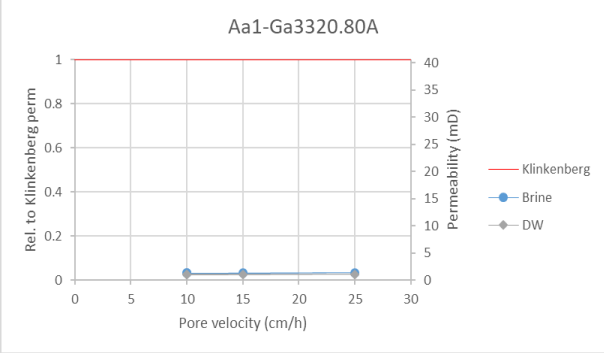

Aa1-Ga3275.38A (Plug 22A)

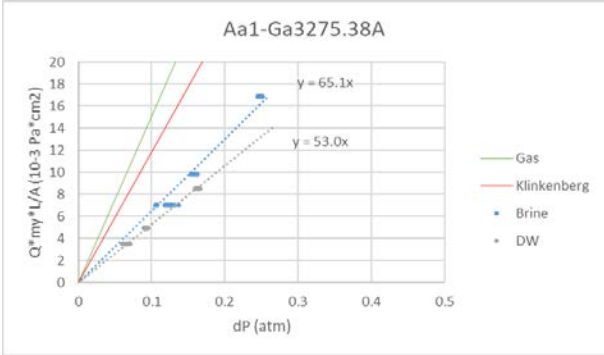

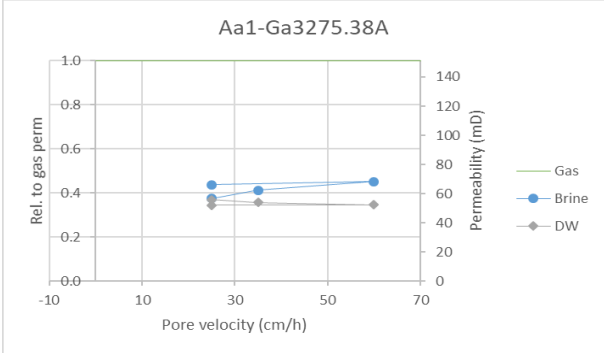

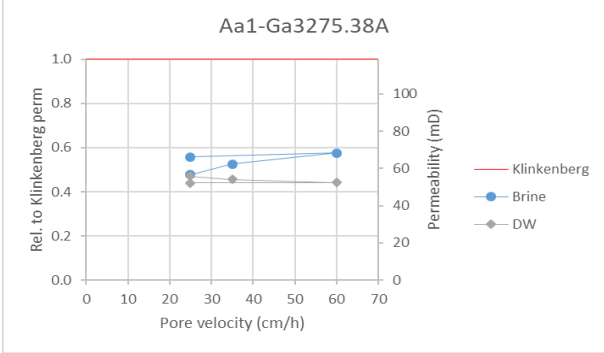

Plug characteristics

Aa1-Ga3325.52A (Plug 12A)

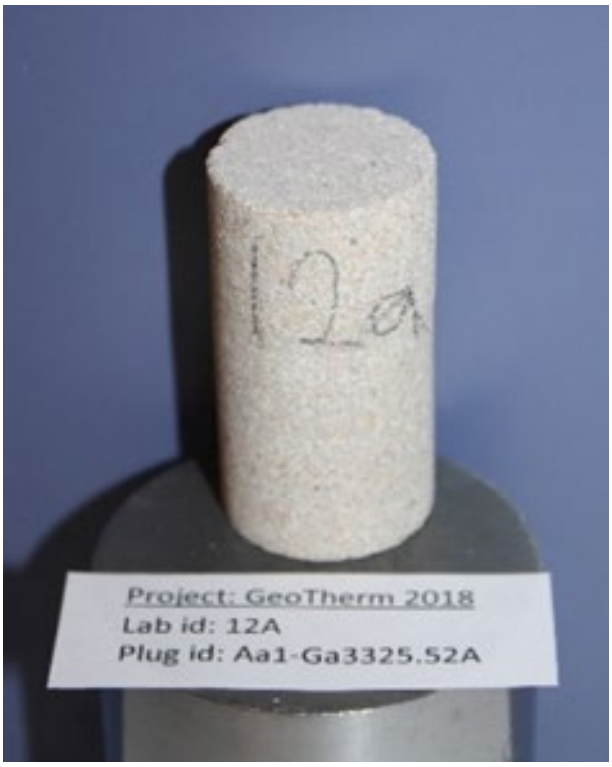

Formation: Gassum
Well: Aars-1
Depth (m MD): 3325.52

Grain size (µm): 660
Clay type and content: 7% illite

Porosity (%): 9.81

Diameter (cm): 2.467
Length (cm): 4.690
Weight, dry (g): 53.51

Bulk volume (cm3): 22.50
Pore volume (cm3): 2.21

Bulk density, dry (g/cm3): 2.378

Gas permeability (mD): 0.75
Klinkenberg permeability (mD): 0.49

Brine permeability

Aa1-Ga3325.52A (Plug 12A)

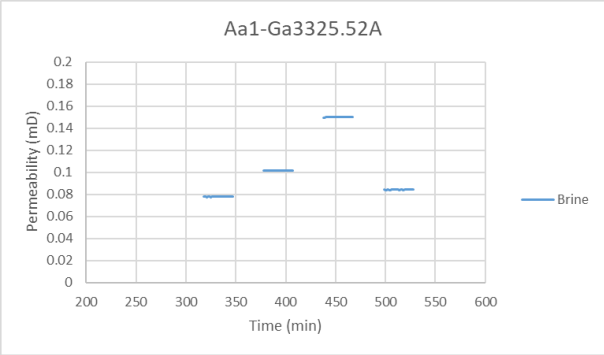

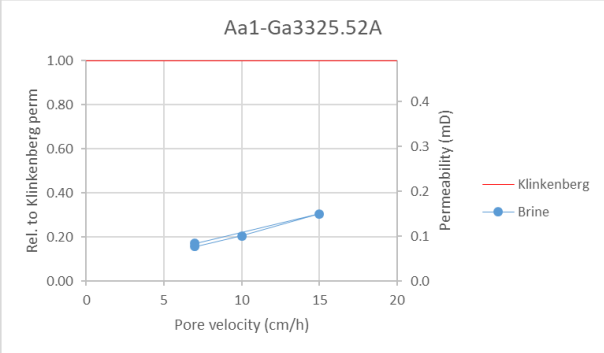

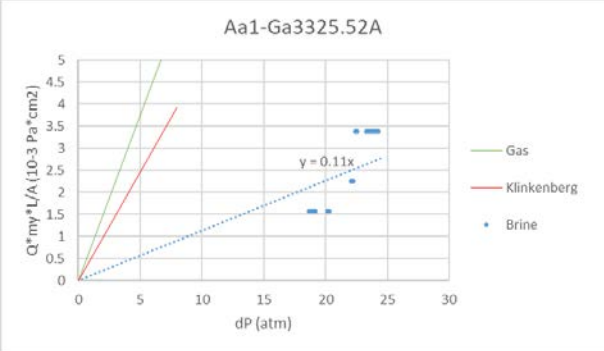

Brine viscosity (cP): 1.76
Weight, brine sat. (g): 56.17
Bulk density, brine sat. (g/cm3): 2.497

Pore velocity (cm/h)	Brine permeability (mD)
7.0	0.08
10.0	0.10
15.0	0.15
7.0	0.08
-	-
Best fit	0.11

DW permeability

Aa1-Ga3325.52A (Plug 12A)

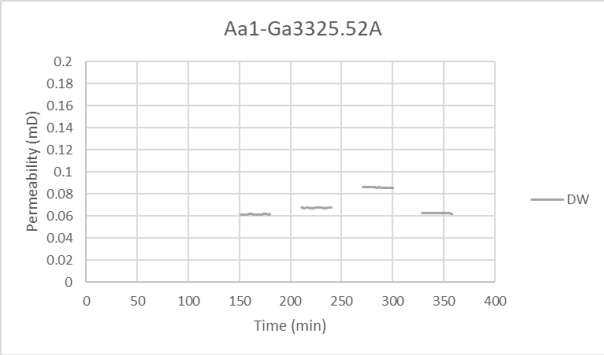

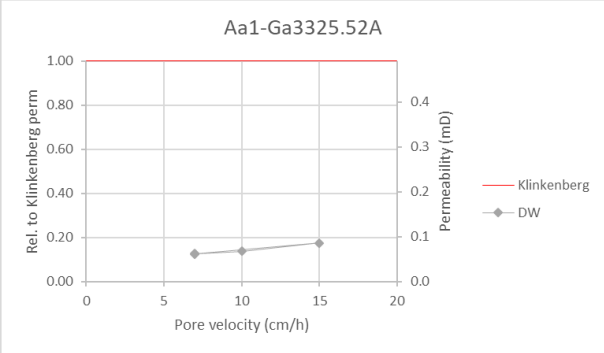

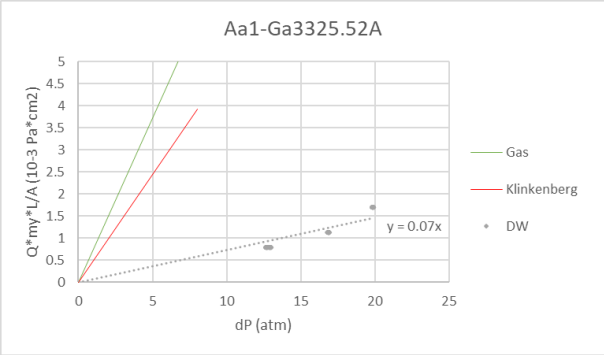

DW viscosity (cP): 0.89
Weight, DW sat. (g): 55.69
Bulk density, DW sat. (g/cm3): 2.475

Pore velocity (cm/h)	DW permeability (mD)
7.0	0.06
10.0	0.07
15.0	0.09
7.0	0.06
-	-
Best fit	0.07

Comparison between brine and DW measurements

Aa1-Ga3325.52A (Plug 12A)

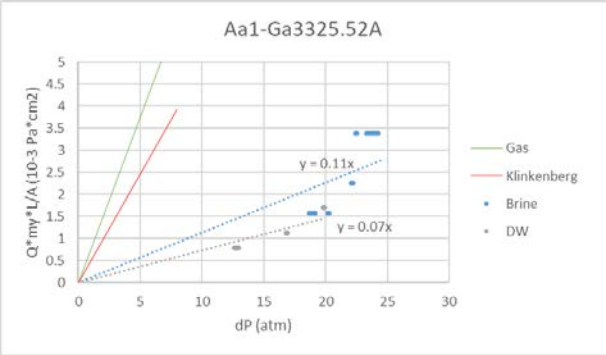

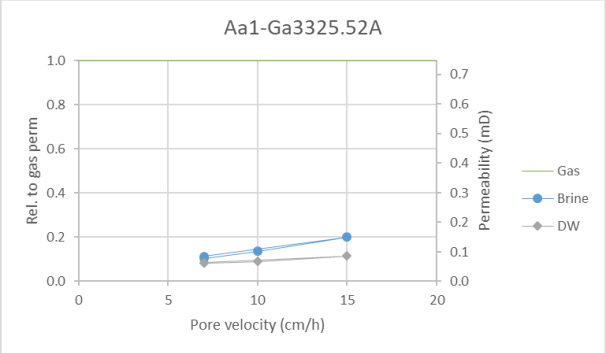

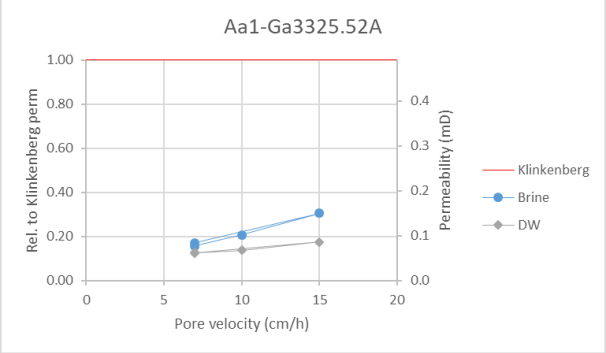

Plugs 4A and 15: Similar grain size - Different sorting

Plug characteristics

Th2-Sk2919.35B (Plug 4A)	Mo1-Sk5034.24A (Plug 15)
	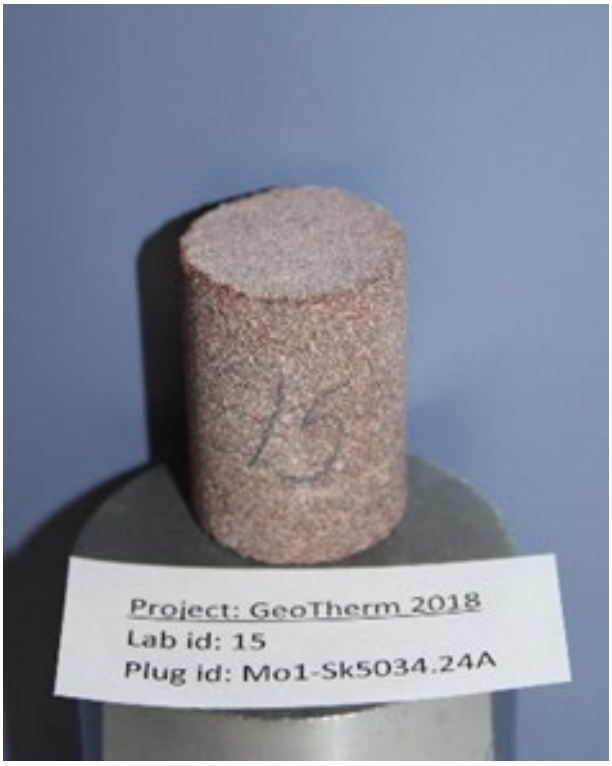
Formation: Skagerrak Well: Thisted-2 Depth (m MD): 2919.35	Formation: Skagerrak Well: Mors-1 Depth (m MD): 5034.24
Grain size (µm): 250 Clay type and content: 5-10% illite	Grain size (µm): 250 Clay type and content: 5-10% illite
Porosity (%): 16.25	Porosity (%): 5.23
Diameter (cm): 2.453 Length (cm): 3.585 Weight, dry (g): 38.71	Diameter (cm): 2.420 Length (cm): 3.548 Weight, dry (g): 43.80
Bulk volume (cm3): 17.04 Pore volume (cm3): 2.768	Bulk volume (cm3): 17.09 Pore volume (cm3): 0.894
Bulk density, dry (g/cm3): 2.285	Bulk density, dry (g/cm3): 2.684
Gas permeability (mD): 8.25 Klinkenberg permeability (mD): 5.16	Gas permeability (mD): 1.68 Klinkenberg permeability (mD): 1.33

Brine permeability

Th2-Sk2919.35B (Plug 4A)

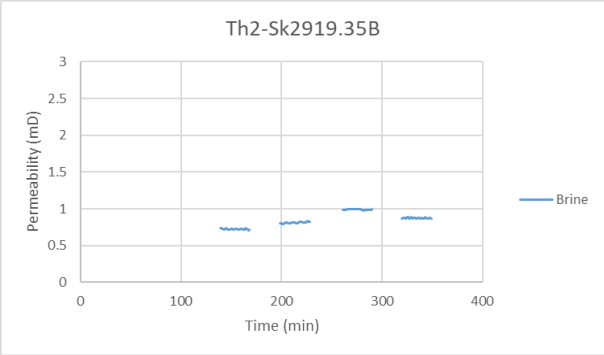

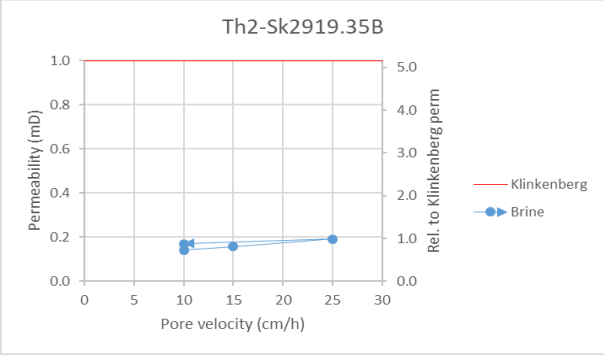

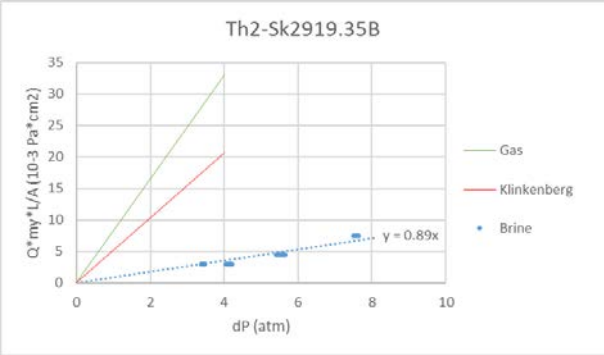

Brine viscosity (cP): 1.85
Weight, brine sat. (g): 42.11
Bulk density, brine sat. (g/cm3): 2.471

Pore velocity (cm/h)	Brine permeability (mD)
10	0.73
15	0.81
25	0.99
10	0.87
Best fit	0.89

Mo1-Sk5034.24A (Plug 15)

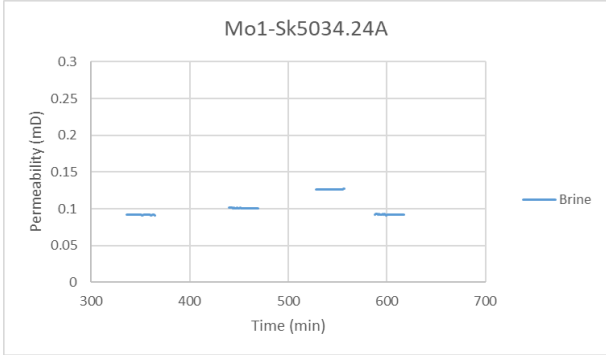

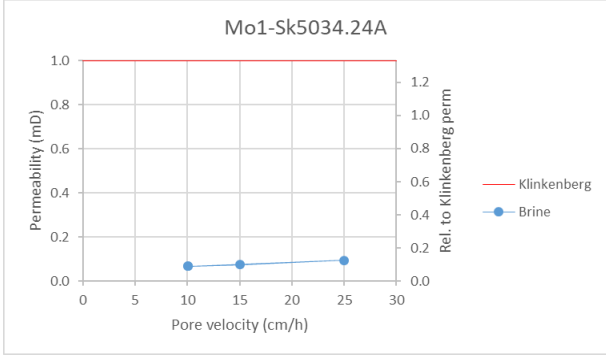

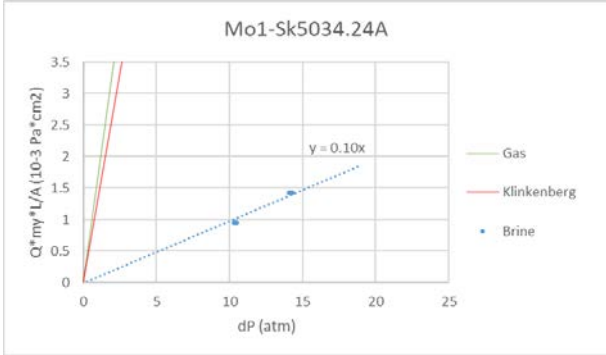

Brine viscosity (cP): 1.85
Weight, brine sat. (g): 44.93
Bulk density, brine sat. (g/cm3): 2.629

Pore velocity (cm/h)	Brine permeability (mD)
10	0.09
15	0.10
25	0.13
10	0.09
Best fit	0.10

DW permeability

Th2-Sk2919.35B (Plug 4A)

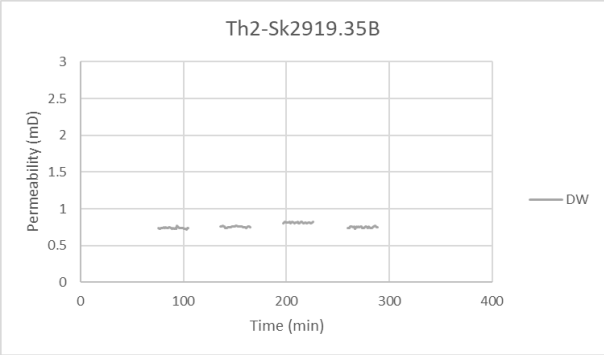

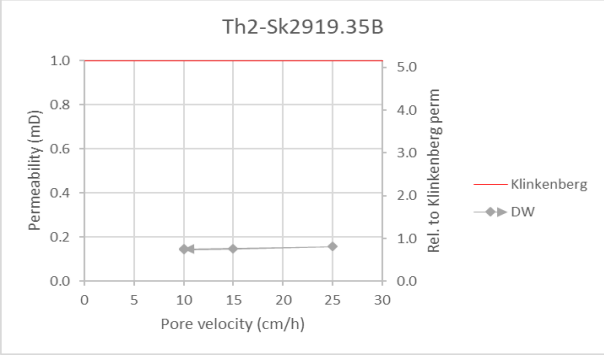

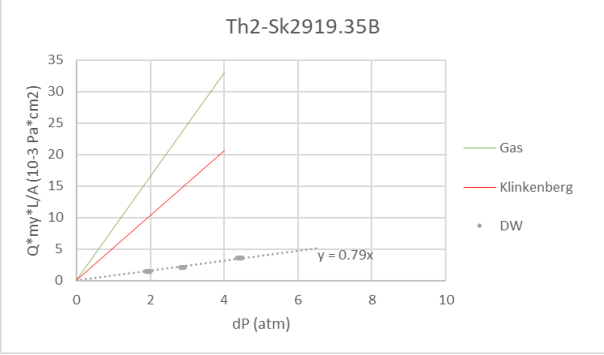

DW viscosity (cP): 0.89
Weight, DW sat. (g): 41.55
Bulk density, DW sat. (g/cm3): 2.438

Pore velocity (cm/h)	DW permeability (mD)
10	0.74
15	0.76
25	0.81
10	0.75
Best fit	0.79

Mo1-Sk5034.24A (Plug 15)

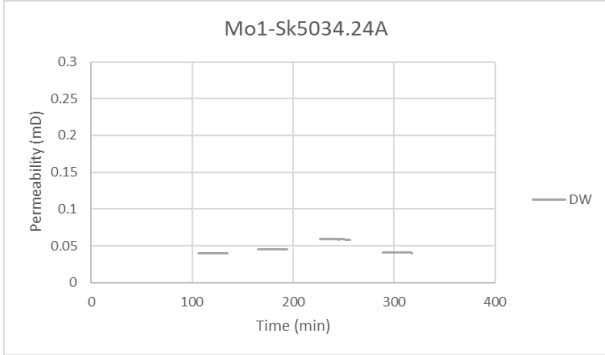

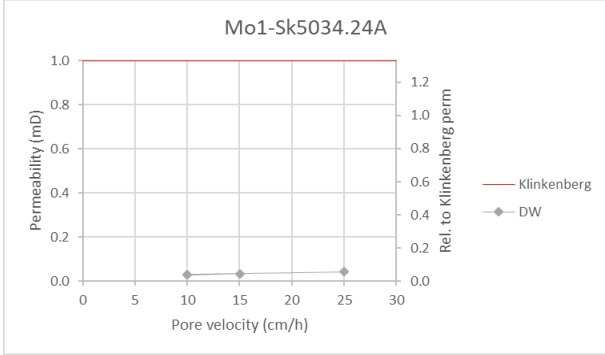

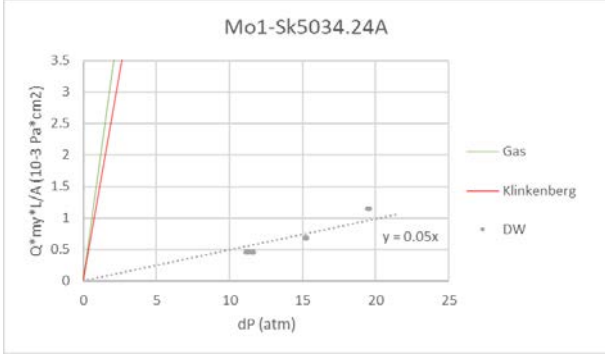

DW viscosity (cP): 0.89
Weight, DW sat. (g): 44.78
Bulk density, DW sat. (g/cm3): 2.620

Pore velocity (cm/h)	DW permeability (mD)
10	0.04
15	0.05
25	0.06
10	0.04
Best fit	0.05

Comparison between brine and DW measurements

Th2-Sk2919.35B (Plug 4A)

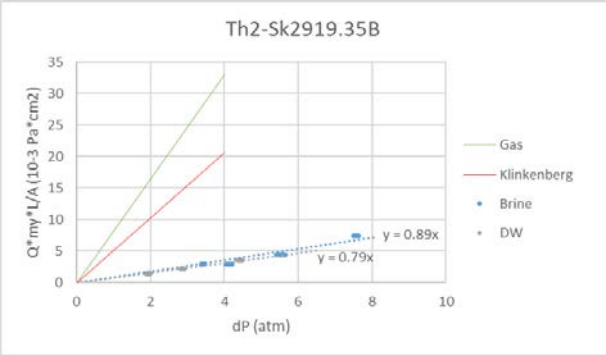

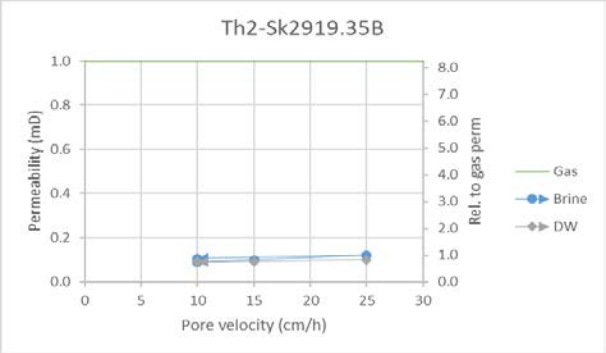

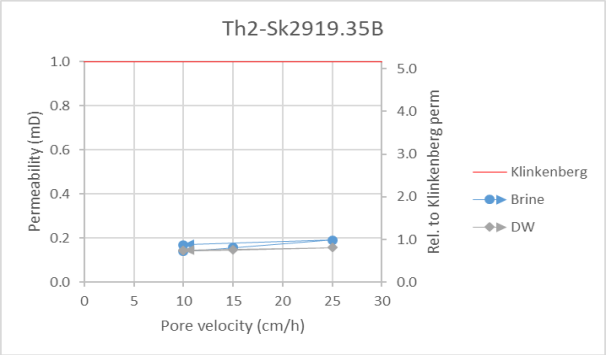

Mo1-Sk5034.24A (Plug 15)

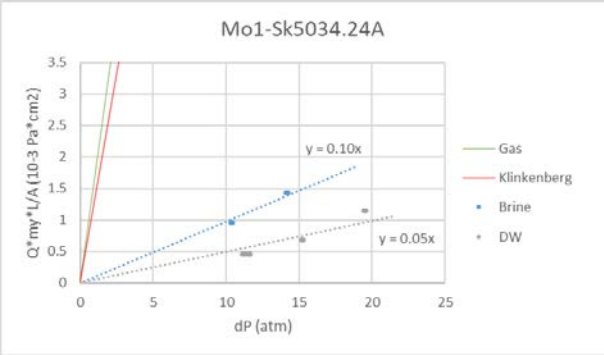

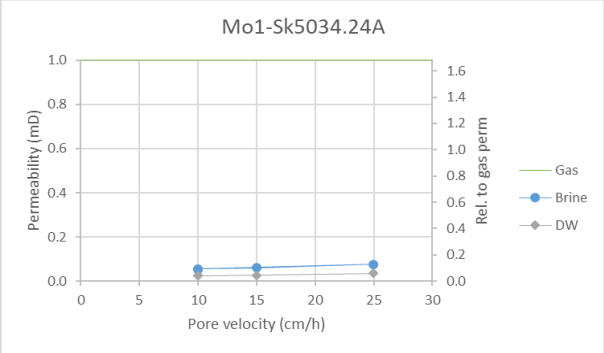

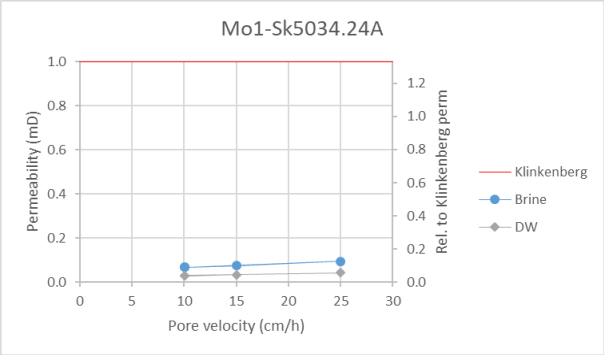

Plugs 5, 3 and 7B: Similar grain size - Different clay type, different porosity

Plug characteristics

Th2-Sk2923.05A (Plug 5)	Mo1-Sk5089.57A (Plug 3)
Formation: Skagerrak Well: Thisted-2 Depth (m MD): 2923.05	Formation: Skagerrak Well: Mors-1 Depth (m MD): 5089.57
Grain size (µm): 350 Clay type and content: 5-10% illite	Grain size (µm): 325 Clay type and content: 5-10% illite
Porosity (%): 11.85	Porosity (%): 5.80
Diameter (cm): 2.455 Length (cm): 4.840 Weight, dry (g): 54.67	Diameter (cm): 2.461 Length (cm): 3.395 Weight, dry (g): 40.48
Bulk volume (cm3): 23.14 Pore volume (cm3): 2.742	Bulk volume (cm3): 15.91 Pore volume (cm3): 0.923
Bulk density, dry (g/cm3): 2.363	Bulk density, dry (g/cm3): 2.544
Gas permeability (mD): 2.34 Klinkenberg permeability (mD): 1.58	Gas permeability (mD): 3.19 Klinkenberg permeability (mD): 2.78

Brine permeability

Th2-Sk2923.05A (Plug 5)

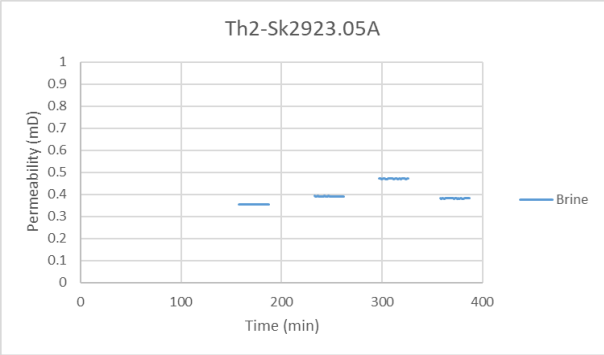

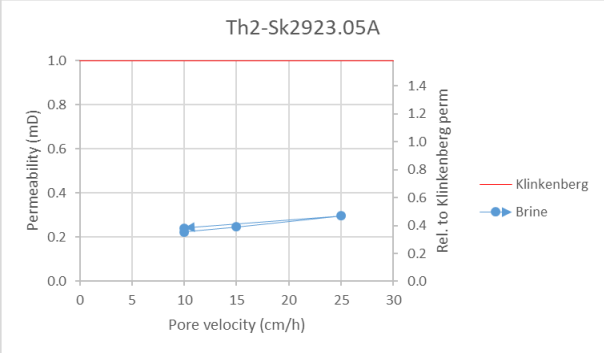

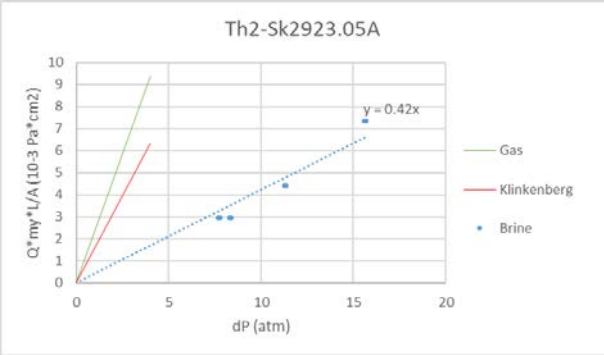

Brine viscosity (cP): 1.85
Weight, brine sat. (g): 58.05
Bulk density, brine sat. (g/cm3): 2.509

Pore velocity (cm/h)	Brine permeability (mD)
10	0.35
15	0.39
25	0.47
10	0.38
Best fit	0.42

Mo1-Sk5089.57A (Plug 3)

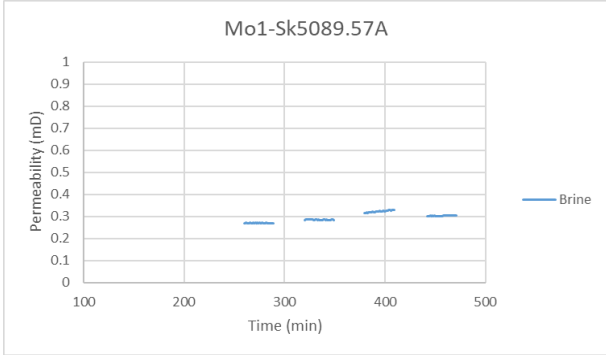

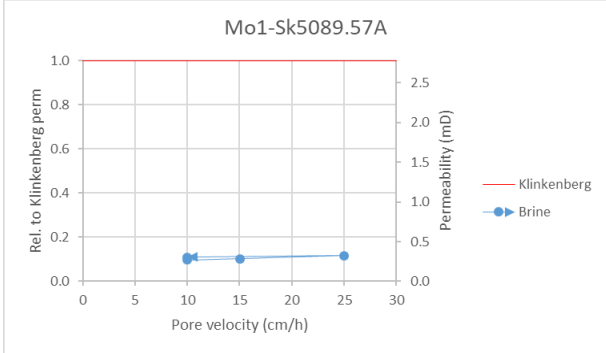

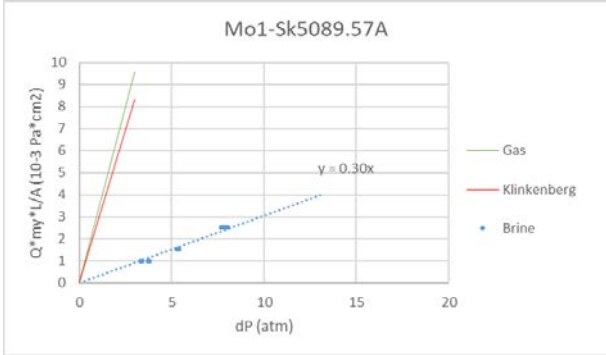

Brine viscosity (cP): 1.85
Weight, brine sat. (g): 41.63
Bulk density, brine sat. (g/cm3): 2.617

Pore velocity (cm/h)	Brine permeability (mD)
10	0.27
15	0.28
25	0.32
10	0.30
Best fit	0.30

DW permeability

Th2-Sk2923.05A (Plug 5)

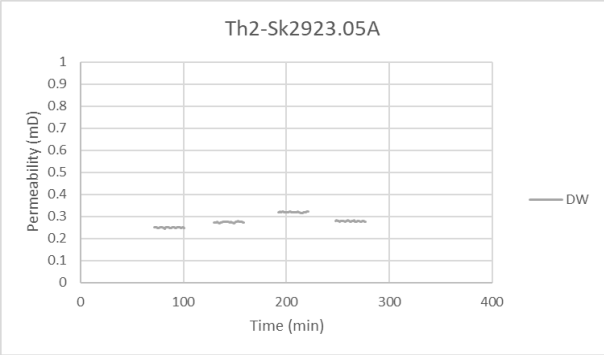

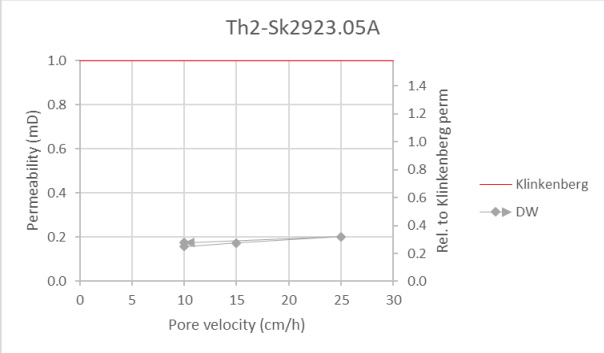

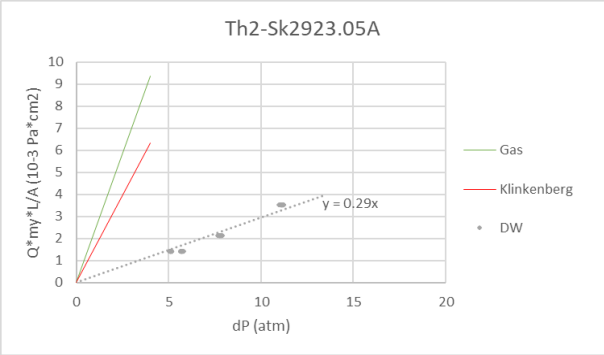

DW viscosity (cP): 0.89
Weight, DW sat. (g): 57.47
Bulk density, DW sat. (g/cm3): 2.484

Pore velocity (cm/h)	DW permeability (mD)
10	0.25
15	0.27
25	0.32
10	0.28
Best fit	0.29

Mo1-Sk5089.57A (Plug 3)

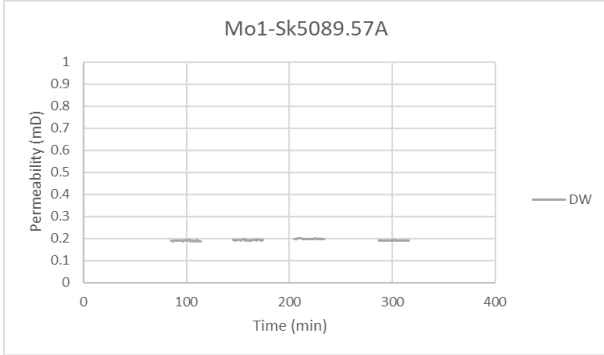

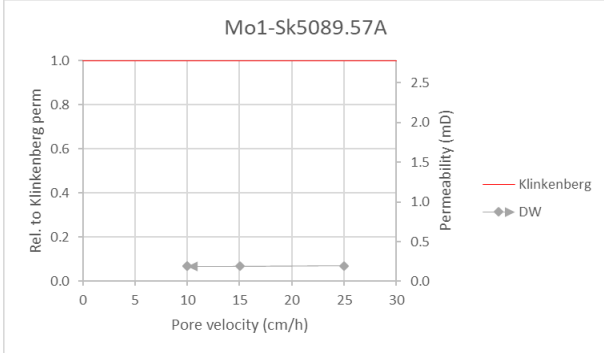

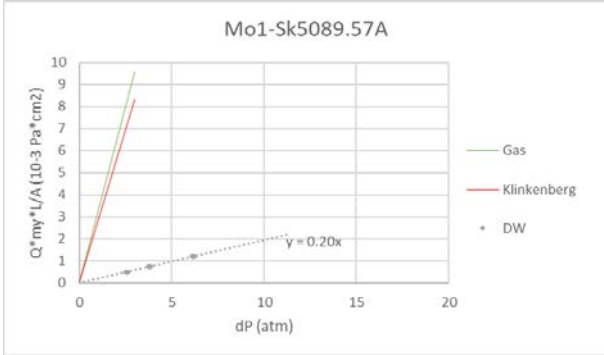

DW viscosity (cP): 0.89
Weight, DW sat. (g): 41.35
Bulk density, DW sat. (g/cm3): 2.599

Pore velocity (cm/h)	DW permeability (mD)
10	0.19
15	0.19
25	0.20
10	0.19
Best fit	0.20

Comparison between brine and DW measurements

Th2-Sk2923.05A (Plug 5)

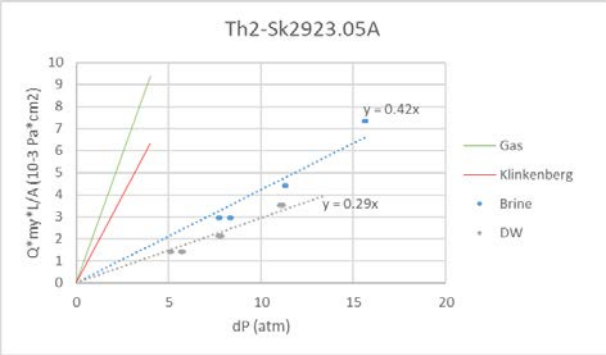

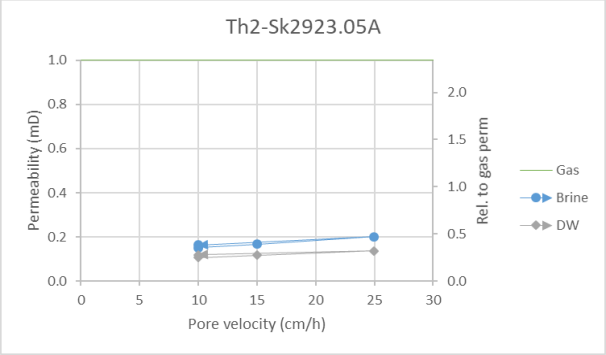

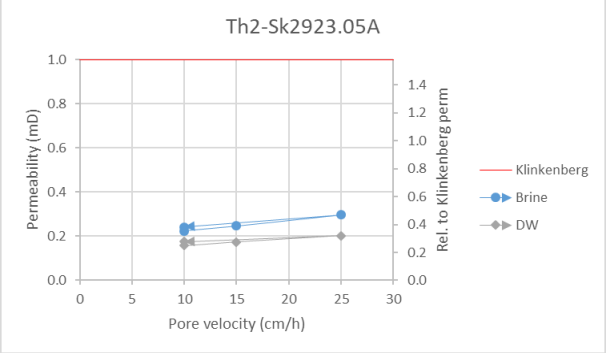

Mo1-Sk5089.57A (Plug 3)

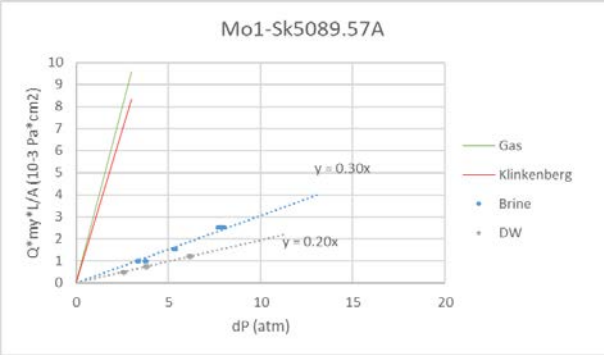

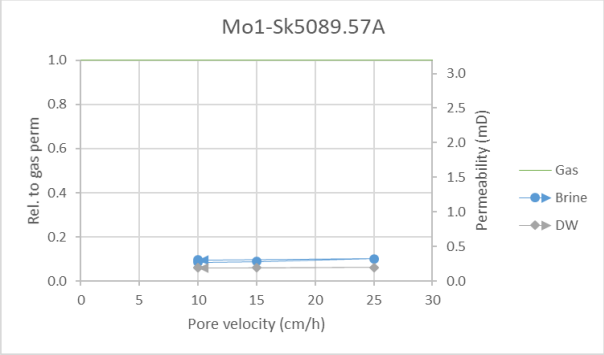

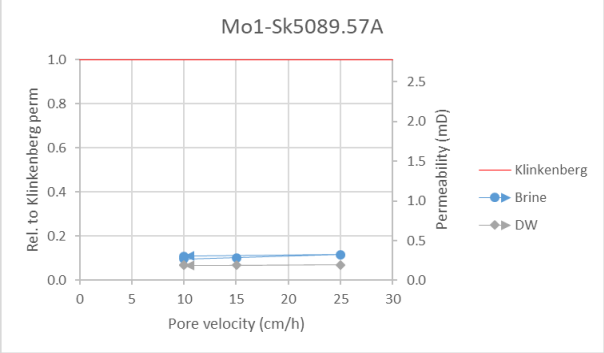

Plug characteristics

Ve1-Sk2062.92B (Plug 7B)

Formation: Skagerrak
Well: Vedsted-1
Depth (m MD): 2062.92

Grain size (µm): 325
Clay type and content: 5-10% kaolinite

Porosity (%): 26.46

Diameter (cm): 2.461
Length (cm): 3.530
Weight, dry (g): 32.47

Bulk volume (cm3): 16.61
Pore volume (cm3): 4.395

Bulk density, dry (g/cm3): 1.955

Gas permeability (mD): 437.5
Klinkenberg permeability (mD): 393.5

Brine permeability

Ve1-Sk2062.92B (Plug 7B)

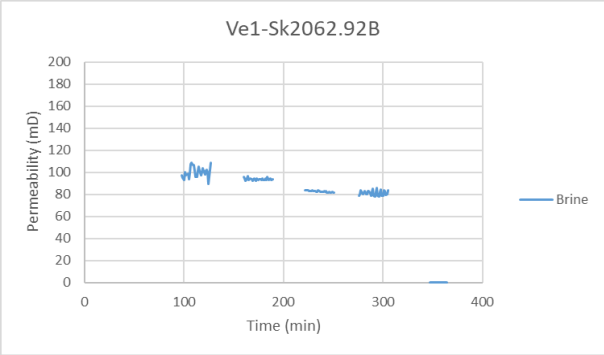

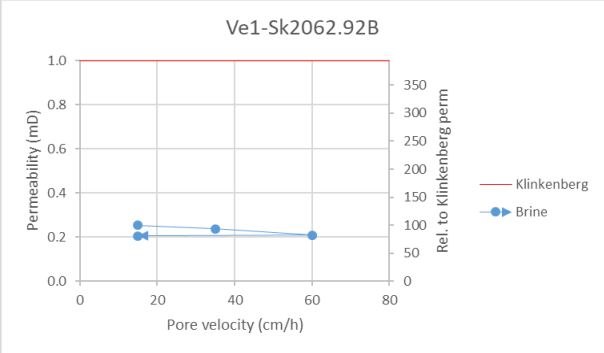

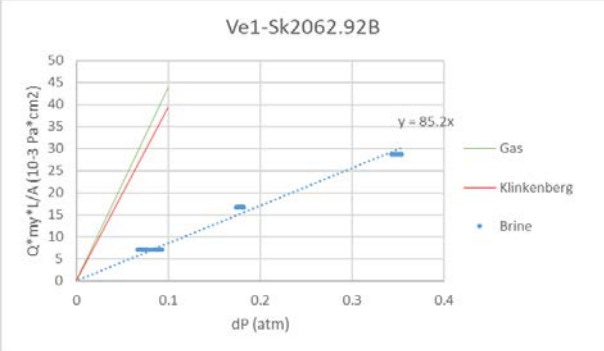

Brine viscosity (cP): 1.85
Weight, brine sat. (g): 37.77
Bulk density, brine sat. (g/cm3): 2.274

Pore velocity (cm/h)	Brine permeability (mD)
10	100.2
15	93.8
25	82.6
10	81.2
Best fit	85.2

DW permeability

Ve1-Sk2062.92B (Plug 7B)

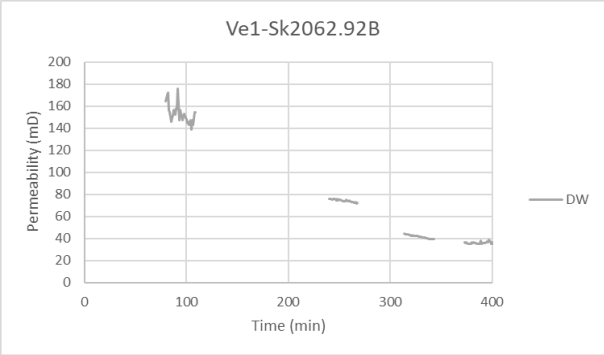

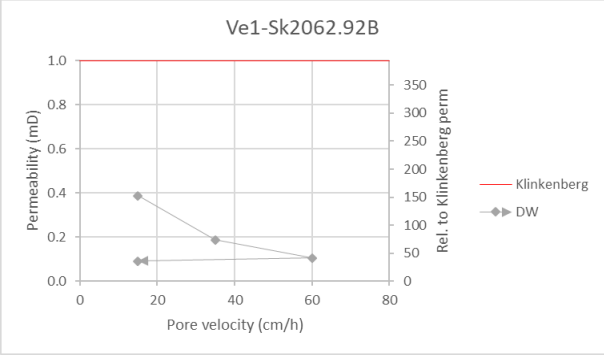

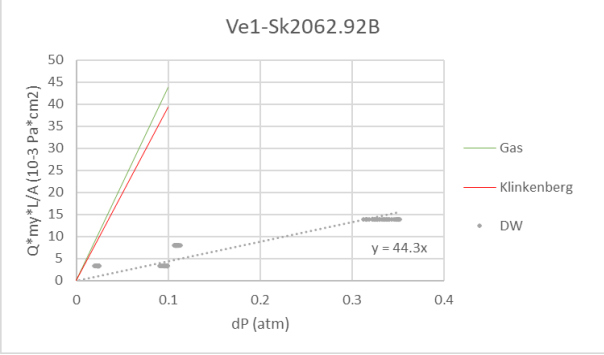

DW viscosity (cP): 0.89
Weight, DW sat. (g): 36.79
Bulk density, DW sat. (g/cm3): 2.215

Pore velocity (cm/h)	DW permeability (mD)
10	152.6
15	74.3
25	41.6
10	36.0
Best fit	44.3

Comparison between brine and DW measurements

Ve1-Sk2062.92B (Plug 7B)

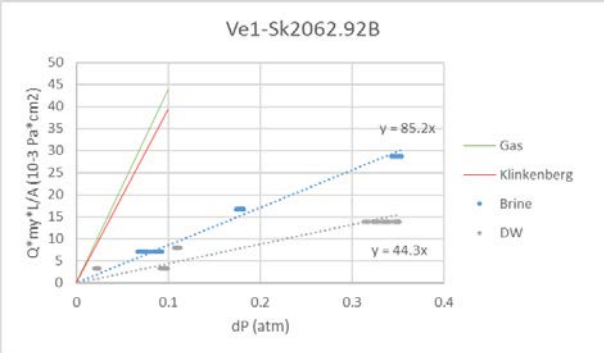

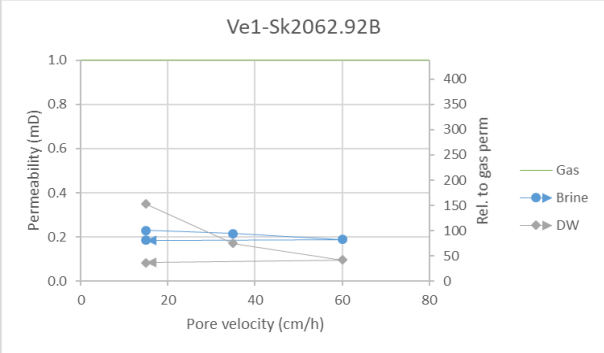

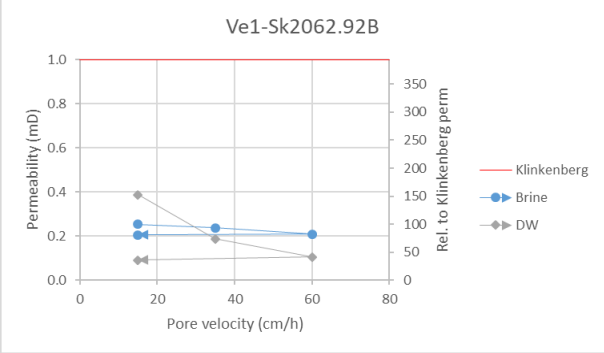

Plug 6: Only sample with mixed-layer ordered smectite/chlorite

Plug characteristics

Th2-Sk2761.63A (Plug 6)

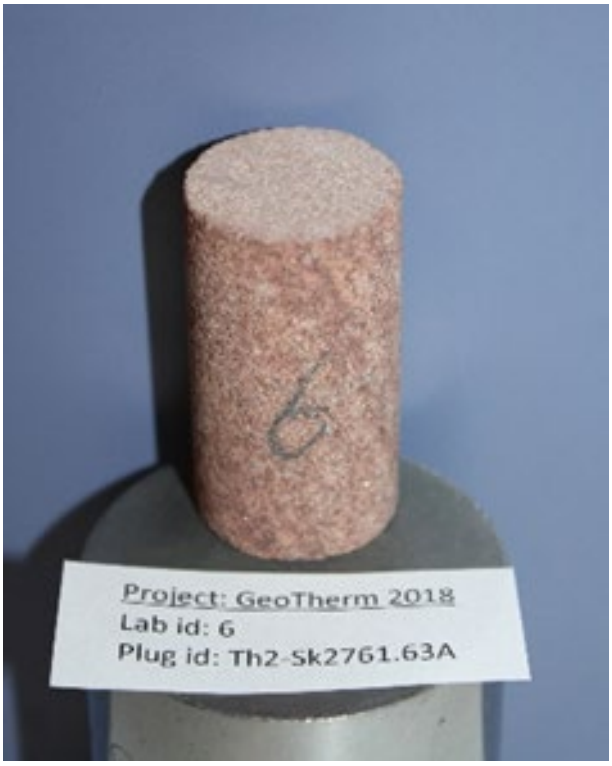

Formation: Skagerrak
Well: Thisted-2
Depth (m MD): 2761.63

Grain size (µm): 250
Clay type and content: 5-10% smectite/chlorite

Porosity (%): 15.24

Diameter (cm): 2.460
Length (cm): 4.585
Weight, dry (g): 49.63

Bulk volume (cm3): 22.03
Pore volume (cm3): 3.357

Bulk density, dry (g/cm3): 2.253

Gas permeability (mD): 23.87
Klinkenberg permeability (mD): 19.26

Brine permeability

Th2-Sk2761.63A (Plug 6)

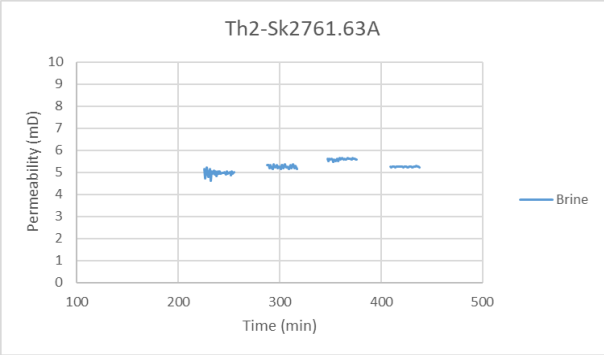

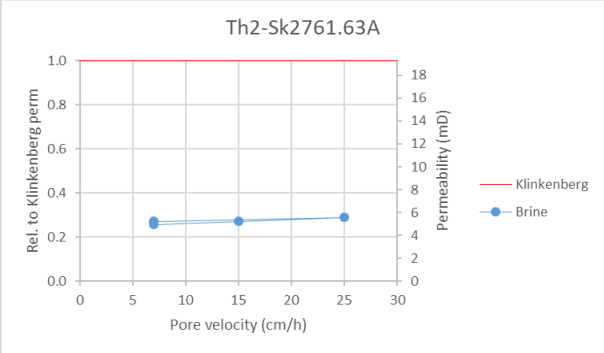

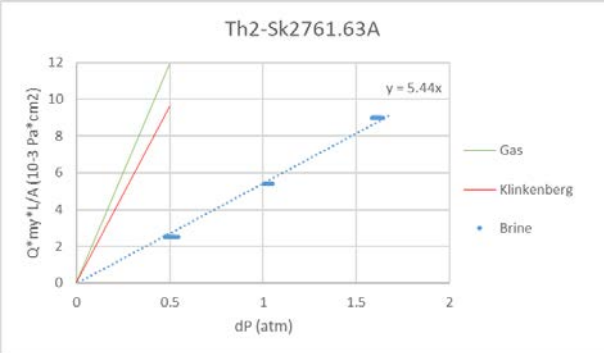

Brine viscosity (cP): 1.85
Weight, brine sat. (g): 42.11
Bulk density, brine sat. (g/cm3): 2.471

Pore velocity (cm/h)	Brine permeability (mD)
7	4.97
15	5.25
25	5.59
7	5.25
Best fit	5.44

DW permeability

Th2-Sk2761.63A (Plug 6)

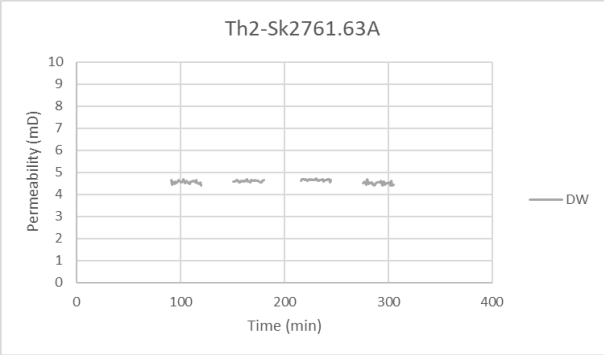

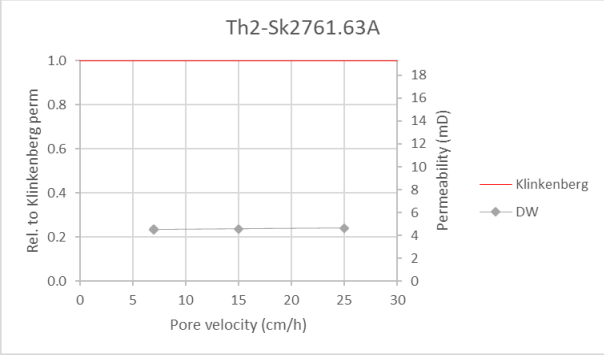

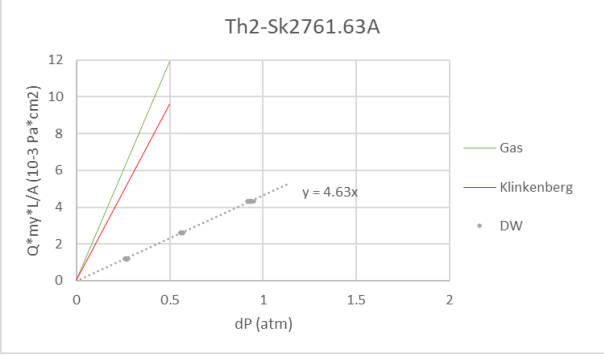

DW viscosity (cP): 0.89
Weight, DW sat. (g): 33.76
Bulk density, DW sat. (g/cm3): 2.393

Pore velocity (cm/h)	DW permeability (mD)
10	4.56
15	4.60
25	4.65
10	4.51
Best fit	4.63

Comparison between brine and DW measurements

Th2-Sk2761.63A (Plug 6)

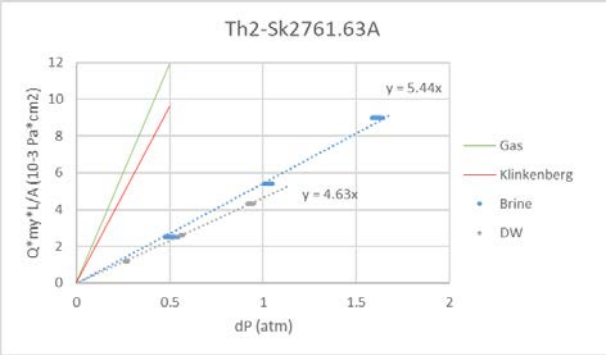

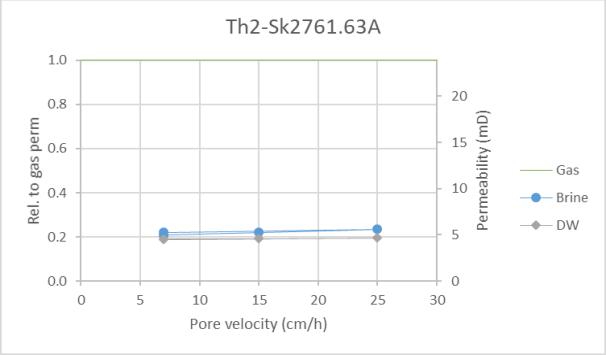

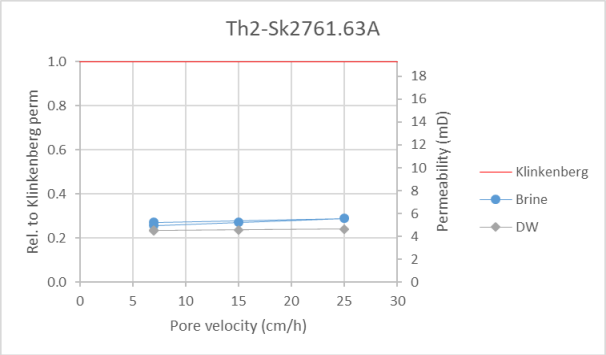

Plug 1: Very low permeability

Plug characteristics

Ga1-Sk3032.42A (Plug 1)	
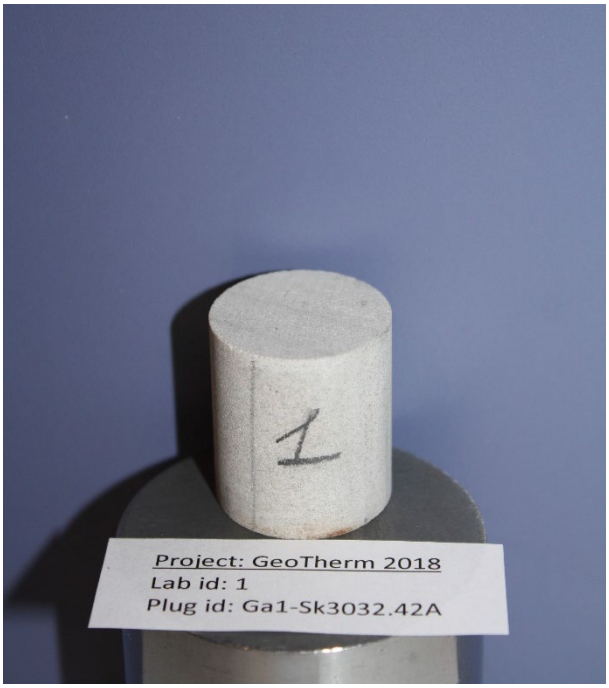 Formation: Skagerrak Well: Gassum-1 Depth (m MD): 3032.42 Grain size (µm): 175 Clay type and content: 22% illite Porosity (%): 6.55 Diameter (cm): 2.485 Length (cm): 2.858 Weight, dry (g): 34.23 Bulk volume (cm3): 13.85 Pore volume (cm3): 0.907 Bulk density, dry (g/cm3): 2.469 Gas permeability (mD): 0.28 Klinkenberg permeability (mD): 0.04	

Brine permeability

Ga1-Sk3032.42A (Plug 1)

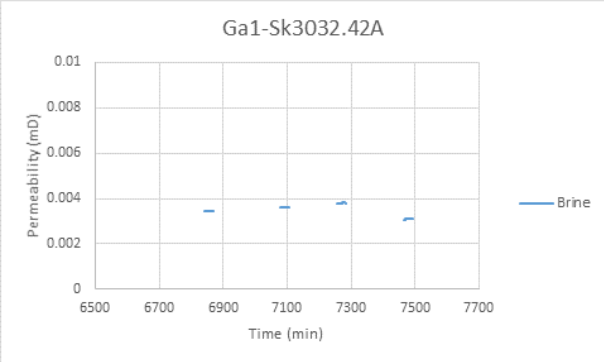

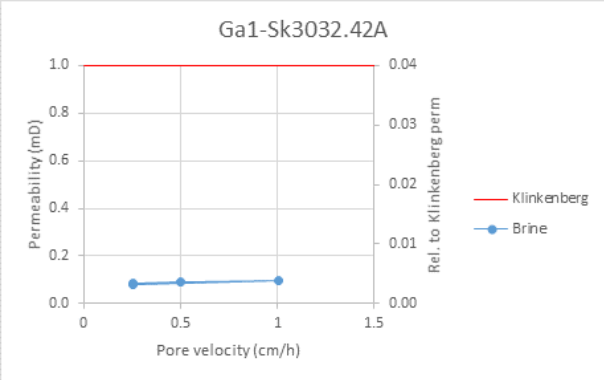

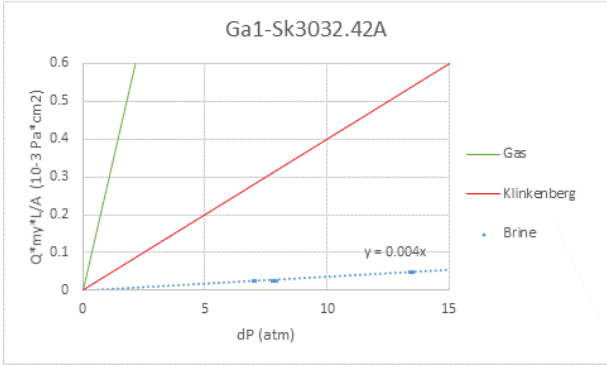

Brine viscosity (cP): 1.76
Weight, brine sat. (g): 35.29
Bulk density, brine sat. (g/cm3): 2.549

Pore velocity (cm/h)	Brine permeability (mD)
0.25	0.003
0.50	0.004
1.01	0.004
0.25	0.003
-	-
Best fit	0.004

DW permeability

Ga1-Sk3032.42A (Plug 1)

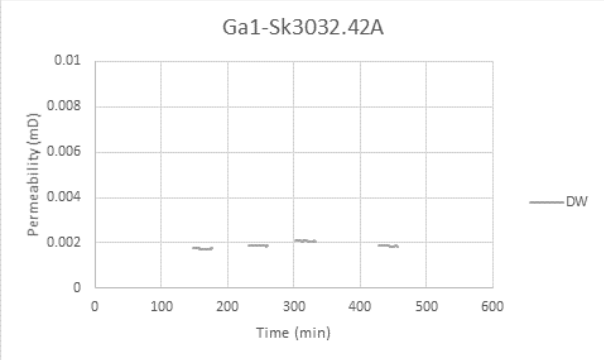

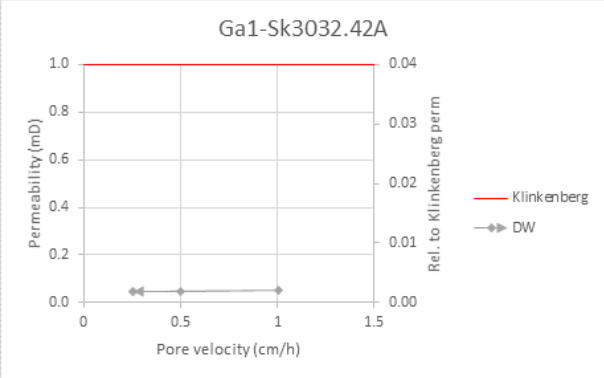

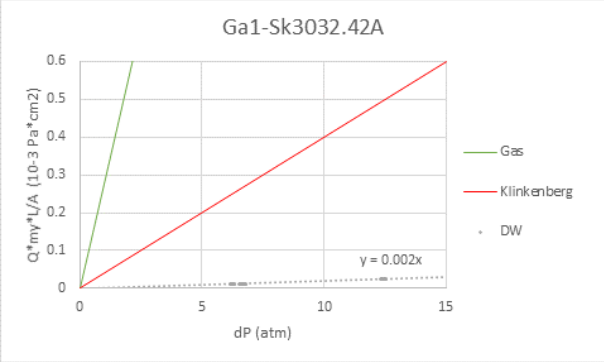

DW viscosity (cP): 0.89
Weight, DW sat. (g): 35.09
Bulk density, DW sat. (g/cm3): 2.534

Pore velocity (cm/h)	DW permeability (mD)
0.25	0.002
0.50	0.002
1.01	0.002
0.25	0.002
-	-
Best fit	0.002

Comparison between brine and DW measurements

Ga1-Sk3032.42A (Plug 1)

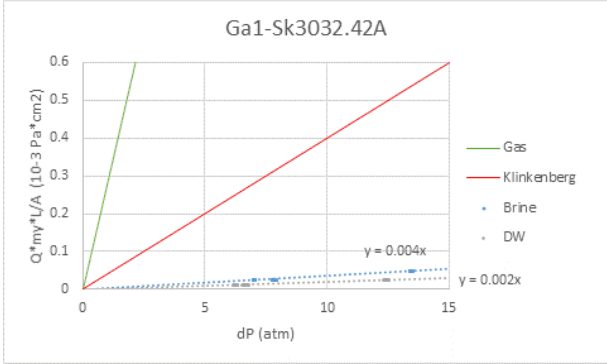

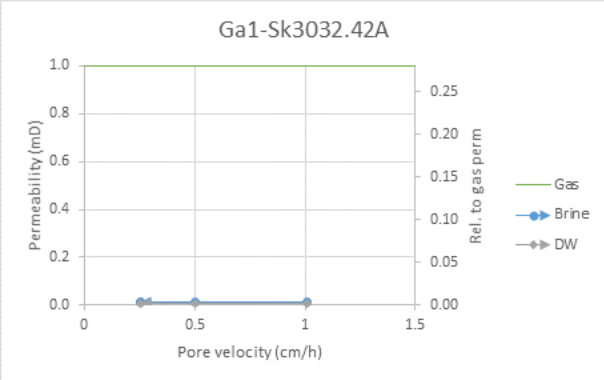

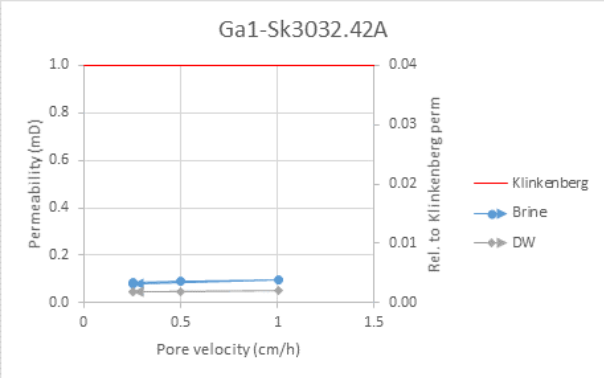

Appendix D

NMR results

Plug 14

T_2 NMR

Project	John-for-H.H.	**Helium Porosity**	0.0 p.u.
Sample	Aa1-Ga3352.22A	**Confining Stress**	0.00 MPa
Well	Gassum-lab14Brine	**Gas Permeability**	0.000000 mD
Sample Depth	0.0ft	**Brine Permeability**	0.000000 mD
Legal Location / Block		**Bulk Volume**	23.983 ml

Total NMR Porosity	12.7 p.u.	**T_2 Log Mean**	108.668 ms
Sample State	Undefined	**SNR**	85.82
Date Preformed	2019/07/02 02:59 PM	**NSA**	32
Calibration	6.3300E-5 ml/m.u.		

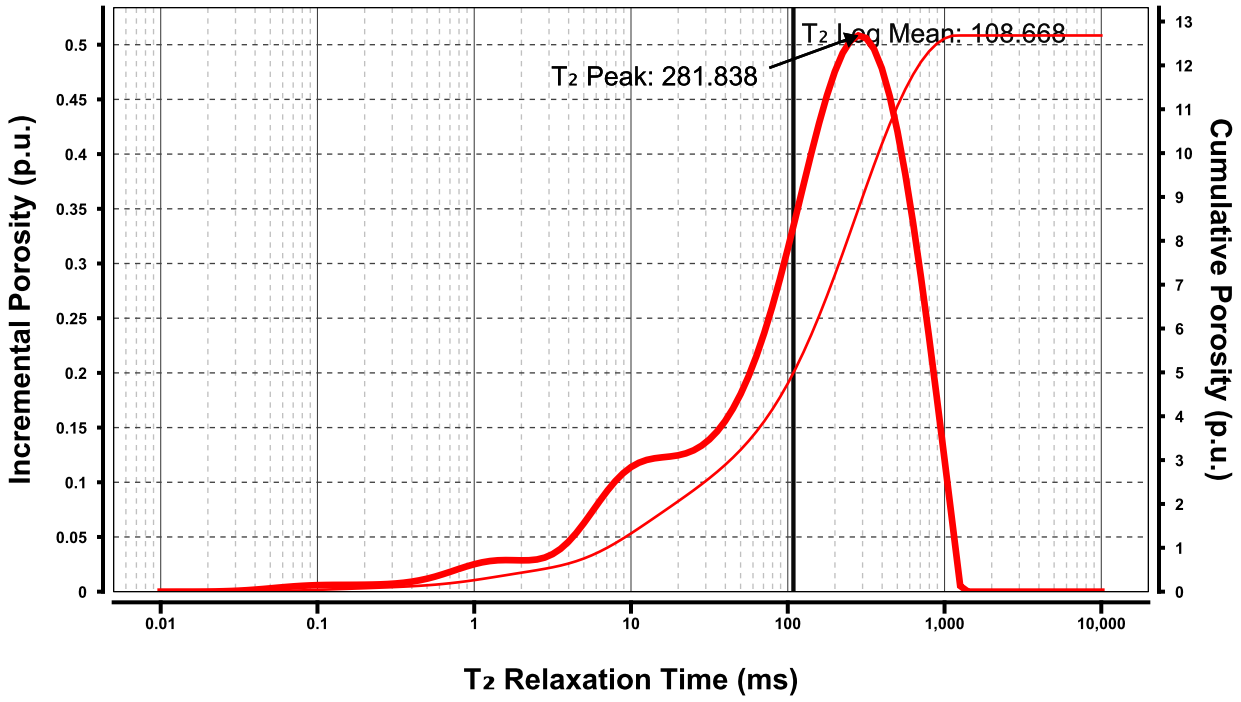

Plug 16

T_2 NMR

Project	John-for-H.H.	**Helium Porosity**	0.0 p.u.
Sample	Aa1-Ga3353.05A	**Confining Stress**	0.00 MPa
Well	Gassum-lab16Brine	**Gas Permeability**	0.000000 mD
Sample Depth	0.0ft	**Brine Permeability**	0.000000 mD
Legal Location / Block		**Bulk Volume**	18.602 ml

Total NMR Porosity	14.9 p.u.	**T_2 Log Mean**	220.479 ms
Sample State	Undefined	**SNR**	77.02
Date Preformed	2019/07/02 03:40 PM	**NSA**	32
Calibration	6.3300E-5 ml/m.u.		

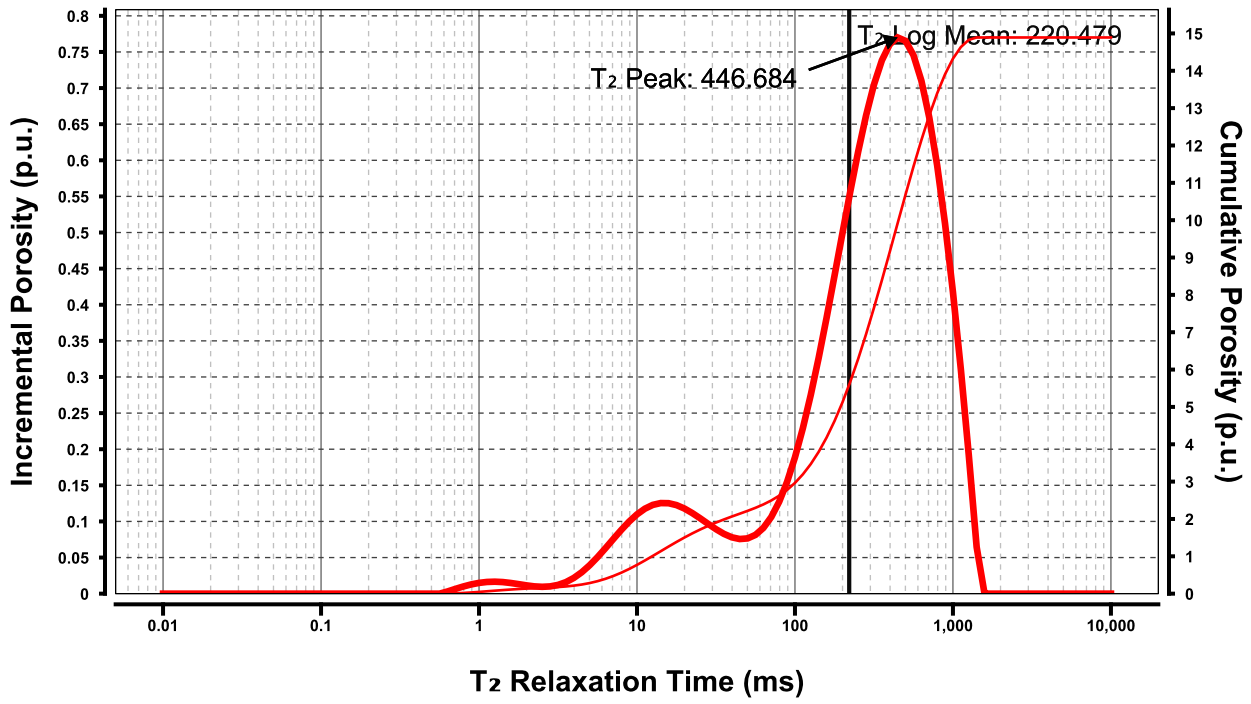

Plug 8C brine

T_2 NMR

Project	John-for-H.H.	**Helium Porosity**	0.0 p.u.
Sample	Ve1-Ga2009.96C	**Confining Stress**	0.00 MPa
Well	Gassum-Lab8CBrine	**Gas Permeability**	0.000000 mD
Sample Depth	0.0ft	**Brine Permeability**	0.000000 mD
Legal Location / Block		**Bulk Volume**	10.282 ml

Total NMR Porosity	23.7 p.u.	**T_2 Log Mean**	102.048 ms
Sample State	Undefined	**SNR**	67.26
Date Preformed	2019/07/02 04:18 PM	**NSA**	32
Calibration	6.3300E-5 ml/m.u.		

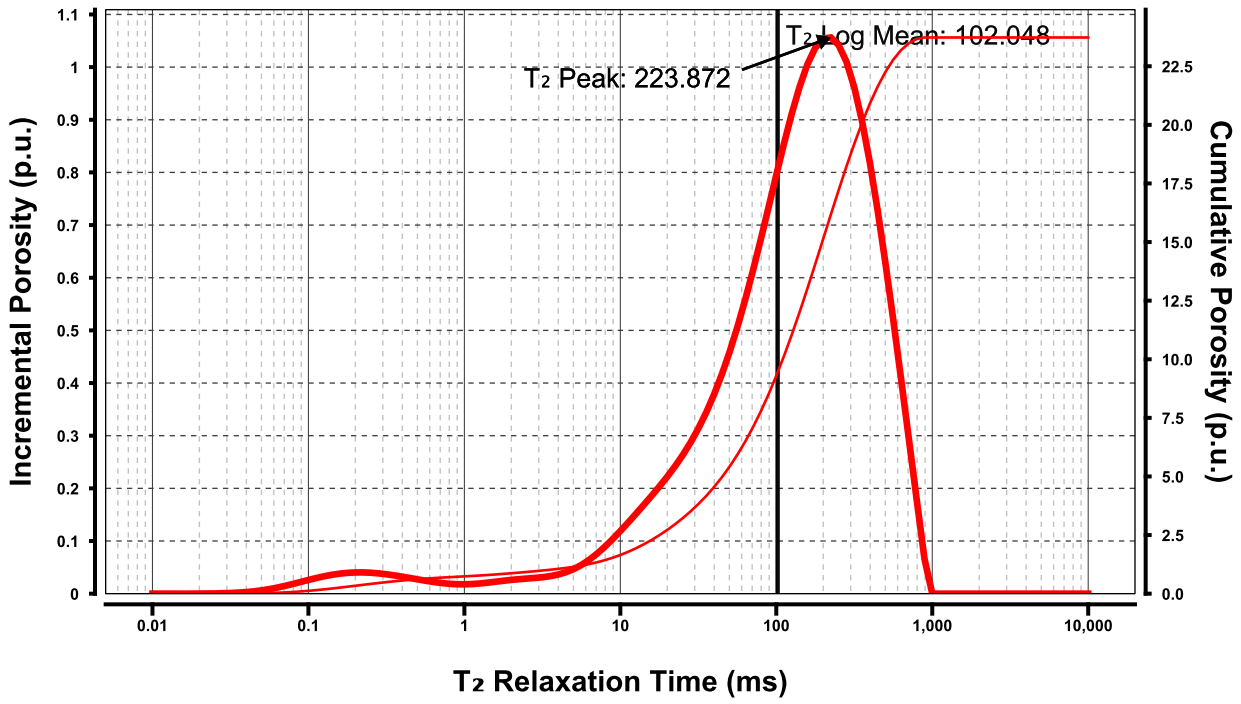

Plug 9B Brine

T_2 NMR

Project	John-for-H.H.	**Helium Porosity**	0.0 p.u.
Sample	Ve1-Ga2010.17B	**Confining Stress**	0.00 MPa
Well	Gassum-Lab9B-Brine	**Gas Permeability**	0.000000 mD
Sample Depth	0.0ft	**Brine Permeability**	0.000000 mD
Legal Location / Block		**Bulk Volume**	11.162 ml

Total NMR Porosity	25.5 p.u.	**T_2 Log Mean**	142.300 ms
Sample State	Undefined	**SNR**	80.10
Date Preformed	2019/07/05 09:54 AM	**NSA**	32
Calibration	6.3300E-5 ml/m.u.		

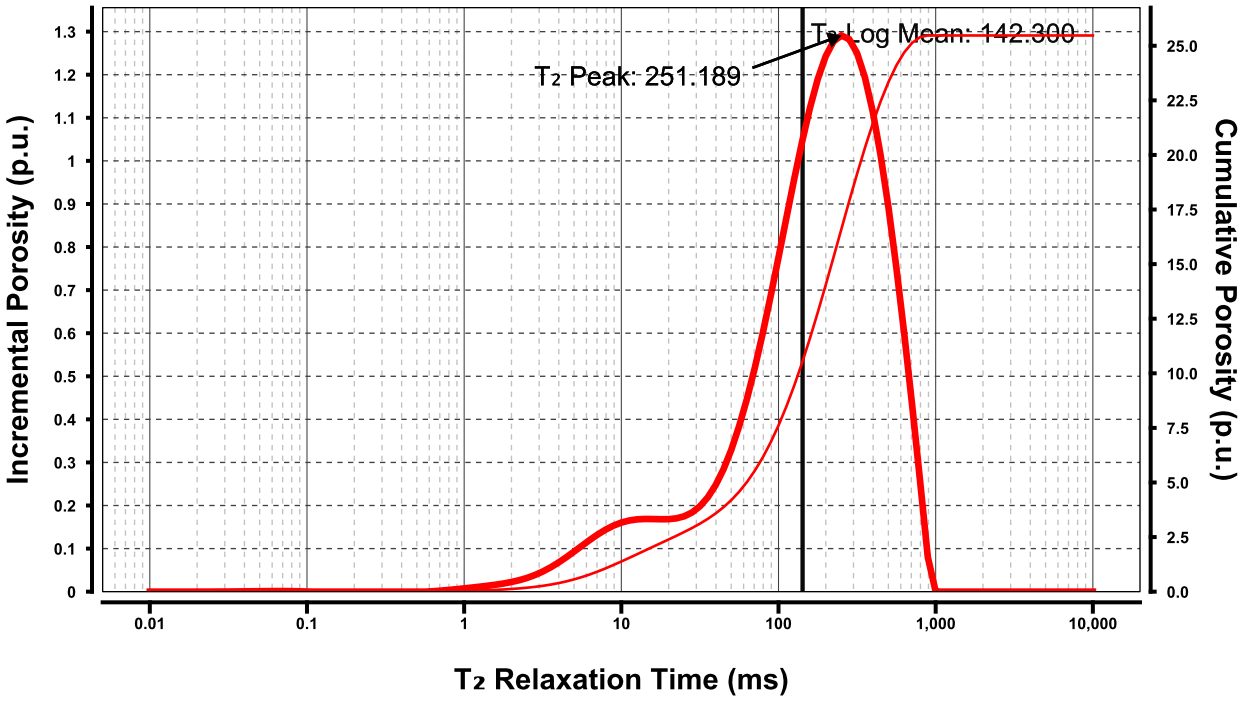

Plug 13B Brine

T_2 NMR

Project	John-for-H.H.	**Helium Porosity**	0.0 p.u.
Sample	Aa1-Ga3326.49B	**Confining Stress**	0.00 MPa
Well	GassumLab13B	**Gas Permeability**	0.000000 mD
Sample Depth	0.0ft	**Brine Permeability**	0.000000 mD
Legal Location / Block		**Bulk Volume**	22.703 ml

Total NMR Porosity	12.4 p.u.	**T_2 Log Mean**	28.744 ms
Sample State	Undefined	**SNR**	79.20
Date Preformed	2019/07/05 10:47 AM	**NSA**	32
Calibration	6.3300E-5 ml/m.u.		

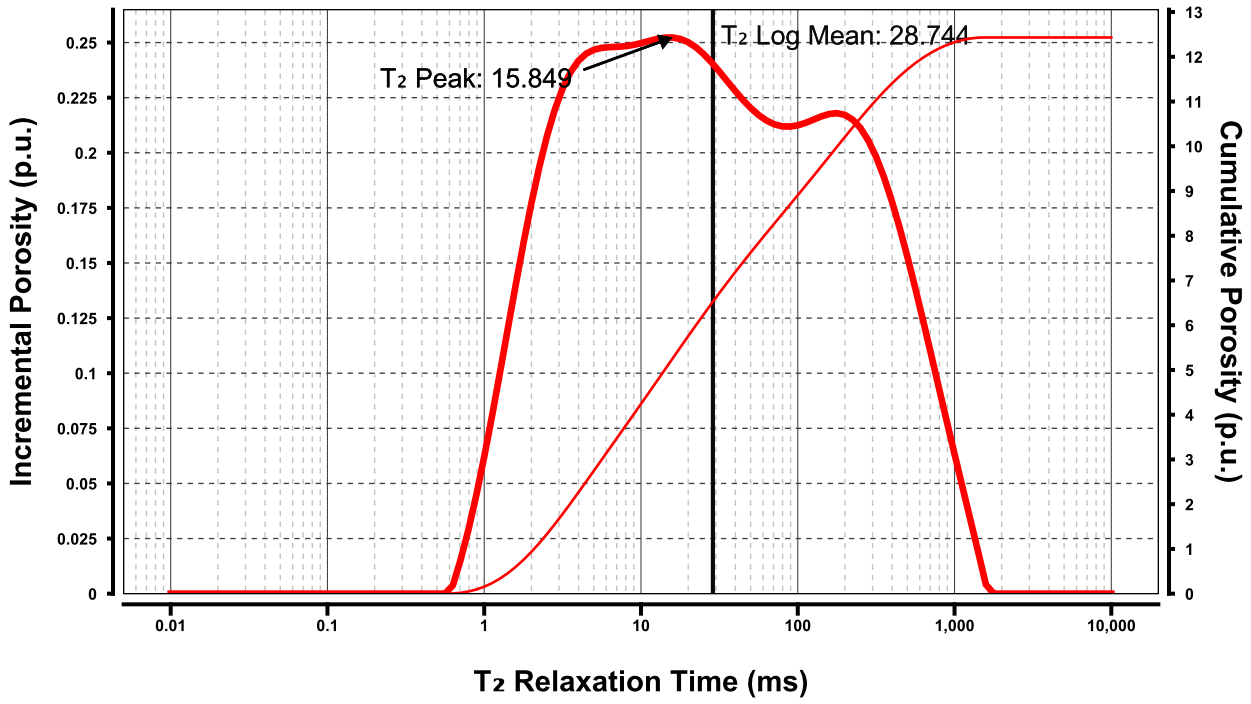

Plug 11B Brine

T_2 NMR

Project	John-for-H.H.	**Helium Porosity**	0.0 p.u.
Sample	Aa1-Ga3325.03B	**Confining Stress**	0.00 MPa
Well	GsssumLab11B	**Gas Permeability**	0.000000 mD
Sample Depth	0.0ft	**Brine Permeability**	0.000000 mD
Legal Location / Block		**Bulk Volume**	23.192 ml

Total NMR Porosity	12.2 p.u.	**T_2 Log Mean**	70.871 ms
Sample State	Undefined	**SNR**	78.35
Date Preformed	2019/07/05 11:27 AM	**NSA**	32
Calibration	6.3300E-5 ml/m.u.		

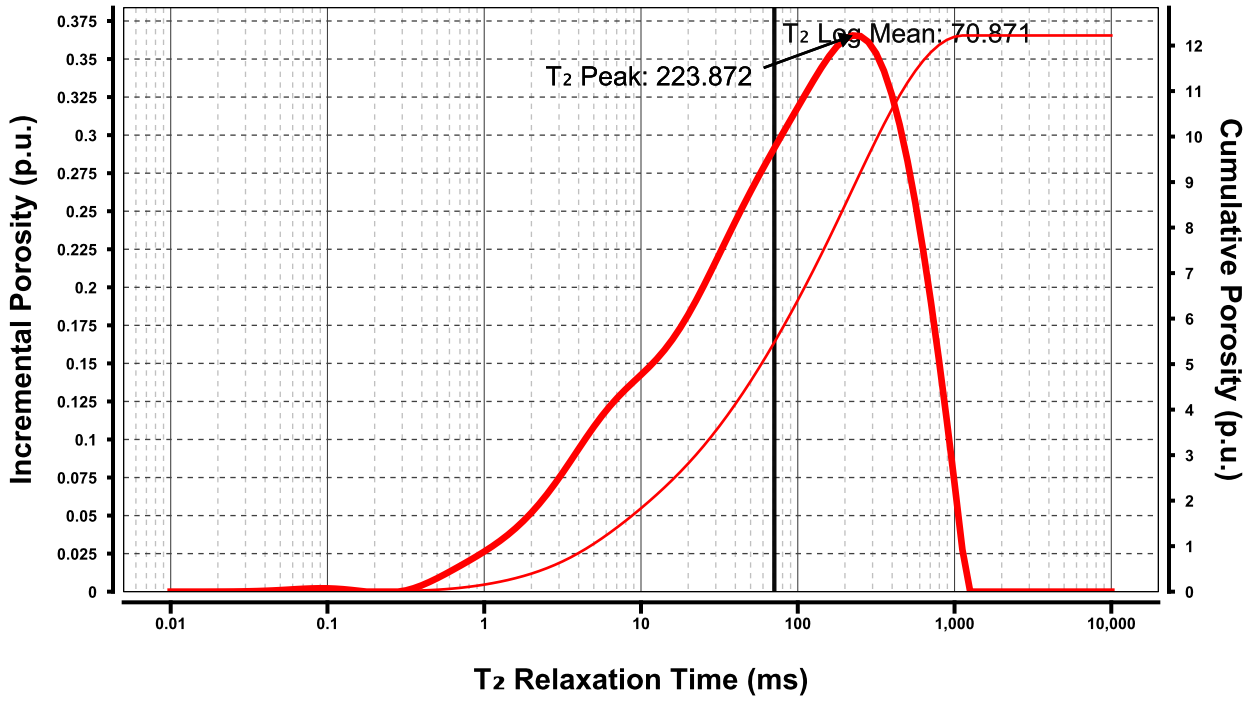

Plug 20 Brine

T_2 NMR

Project	John-for-H.H.	**Helium Porosity**	0.0 p.u.
Sample	Aa1-Ga3318.20A	**Confining Stress**	0.00 MPa
Well	GassumLab20Brine	**Gas Permeability**	0.000000 mD
Sample Depth	0.0ft	**Brine Permeability**	0.000000 mD
Legal Location / Block		**Bulk Volume**	24.684 ml

Total NMR Porosity	6.2 p.u.	**T_2 Log Mean**	136.788 ms
Sample State	Undefined	**SNR**	43.89
Date Preformed	2019/07/05 12:08 PM	**NSA**	32
Calibration	6.3300E-5 ml/m.u.		

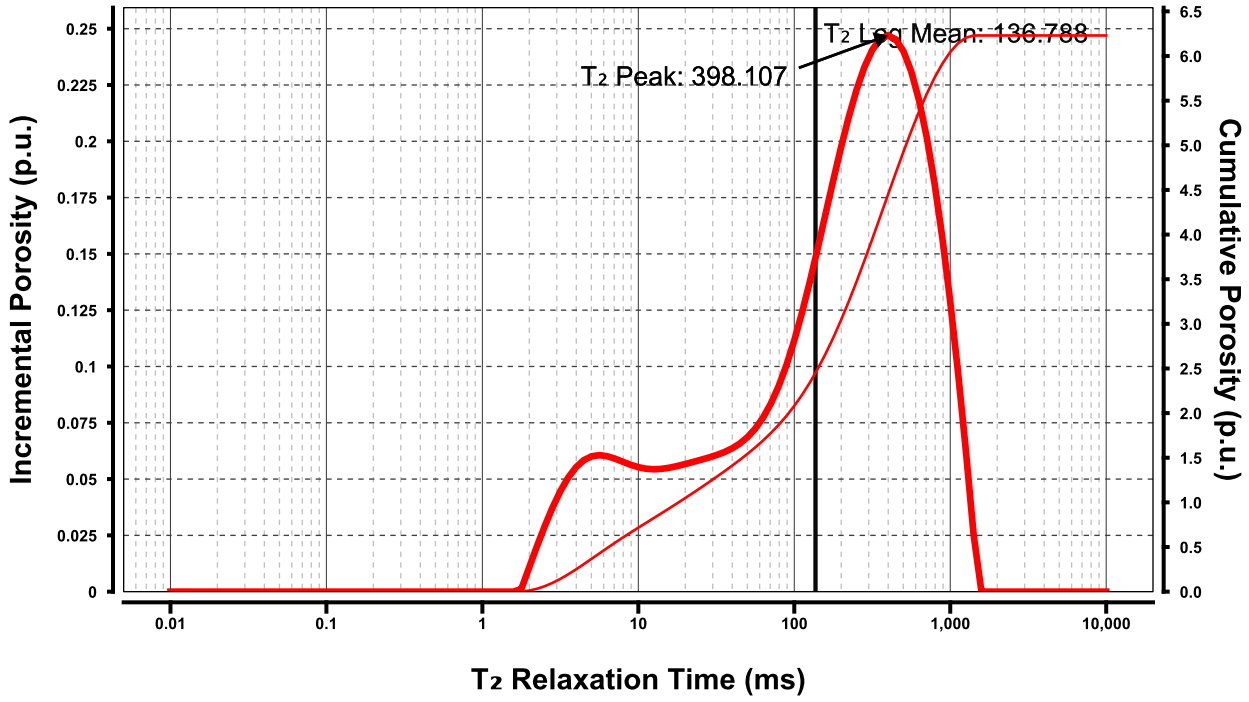

Plug 21A Brine

T_2 NMR

Project	John-for-H.H.	**Helium Porosity**	0.0 p.u.
Sample	Aa1-Ga3320.80A	**Confining Stress**	0.00 MPa
Well	Gassumlab21ABrime	**Gas Permeability**	0.000000 mD
Sample Depth	0.0ft	**Brine Permeability**	0.000000 mD
Legal Location / Block		**Bulk Volume**	15.189 ml

Total NMR Porosity	13.6 p.u.	**T_2 Log Mean**	51.936 ms
Sample State	Undefined	**SNR**	54.14
Date Preformed	2019/07/05 01:10 PM	**NSA**	32
Calibration	6.3300E-5 ml/m.u.		

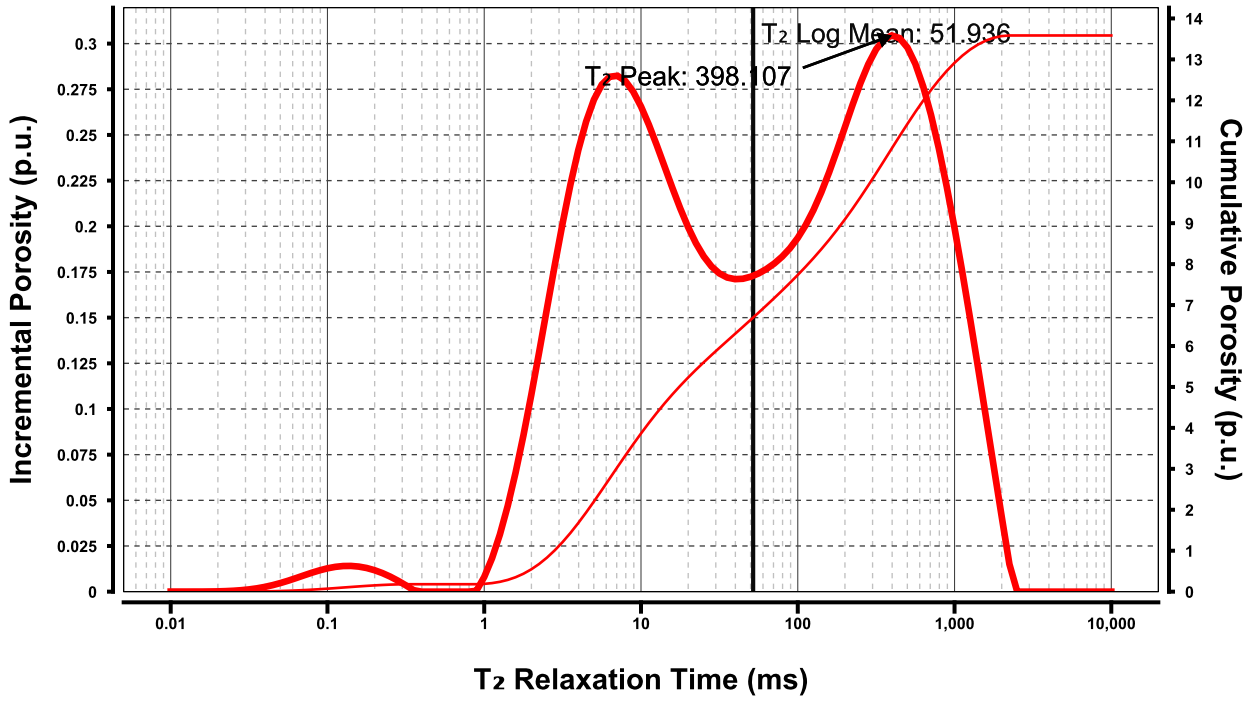

Plug 22A Brine

T_2 NMR

Project	John-for-H.H.	**Helium Porosity**	0.0 p.u.
Sample	Aa1-Ga3275.38A	**Confining Stress**	0.00 MPa
Well	GassumLab22A	**Gas Permeability**	0.000000 mD
Sample Depth	0.0ft	**Brine Permeability**	0.000000 mD
Legal Location / Block		**Bulk Volume**	20.433 ml

Total NMR Porosity	13.6 p.u.	**T_2 Log Mean**	247.158 ms
Sample State	Undefined	**SNR**	76.62
Date Preformed	2019/07/05 01:44 PM	**NSA**	32
Calibration	6.3300E-5 ml/m.u.		

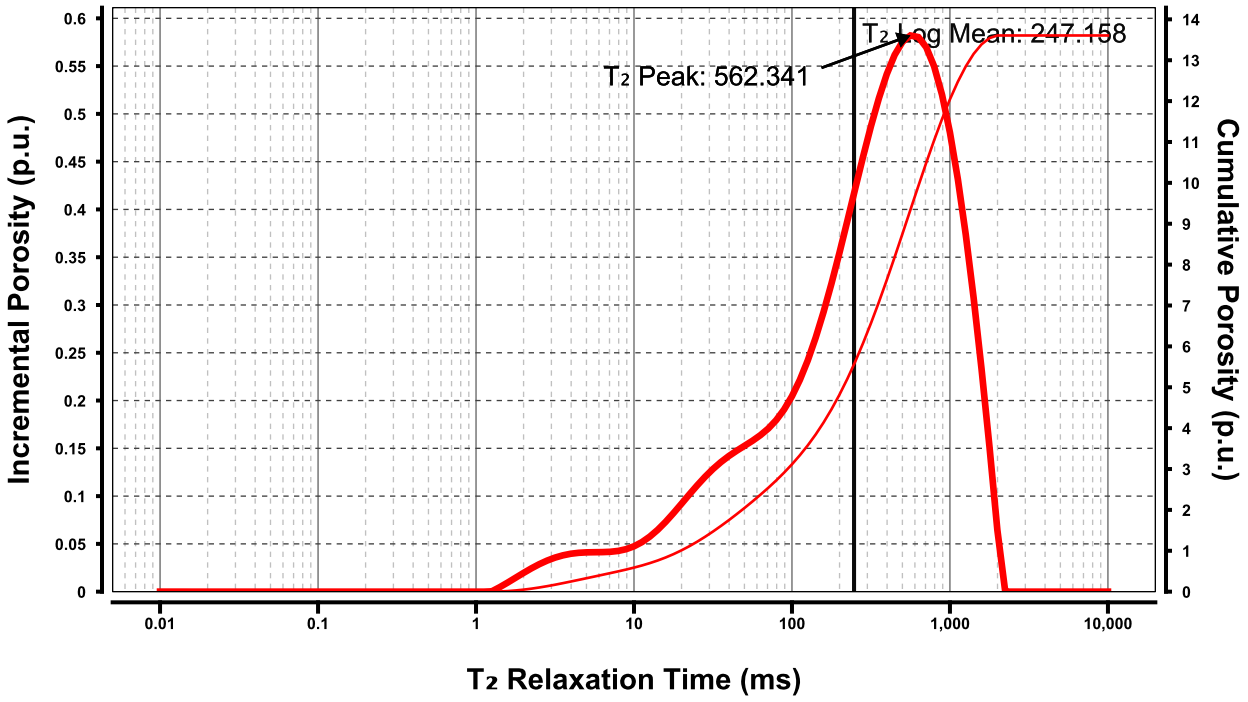

Plug 12A Brine

T_2 NMR

Project	John-for-H.H.	**Helium Porosity**	0.0 p.u.
Sample	Aa1-Ga3325.52A	**Confining Stress**	0.00 MPa
Well	Gassum	**Gas Permeability**	0.000000 mD
Sample Depth	0.0ft	**Brine Permeability**	0.000000 mD
Legal Location / Block		**Bulk Volume**	22.747 ml

Total NMR Porosity	9.9 p.u.	**T_2 Log Mean**	25.492 ms
Sample State	Undefined	**SNR**	57.51
Date Preformed	2019/07/30 01:20 PM	**NSA**	32
Calibration	6.3300E-5 ml/m.u.		

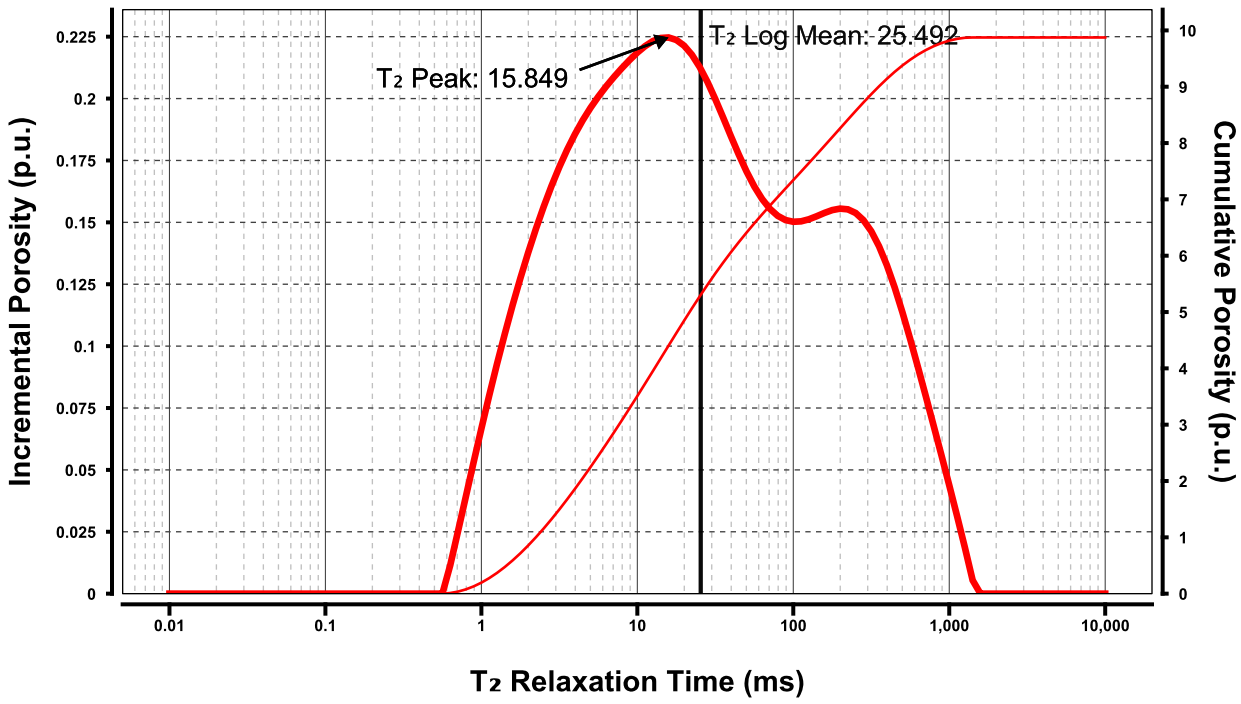

Plug 10 Brine

T_2 NMR

Project	John-for-H.H.	**Helium Porosity**	0.0 p.u.
Sample	Aa1-Ga3318.10A	**Confining Stress**	0.00 MPa
Well	GassumLab10Brine	**Gas Permeability**	0.000000 mD
Sample Depth	0.0ft	**Brine Permeability**	0.000000 mD
Legal Location / Block		**Bulk Volume**	22.734 ml

Total NMR Porosity	7.7 p.u.	**T_2 Log Mean**	70.464 ms
Sample State	Undefined	**SNR**	46.57
Date Preformed	2019/07/05 03:22 PM	**NSA**	32
Calibration	6.3300E-5 ml/m.u.		

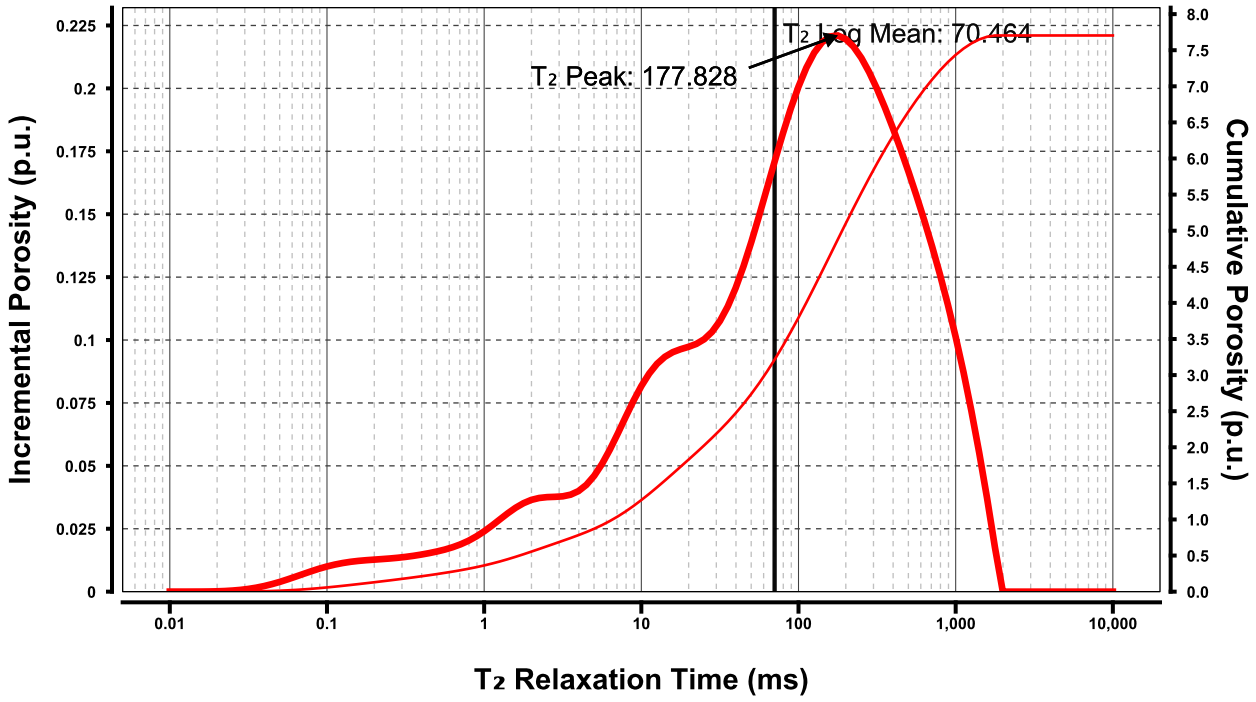

Plug 6 Brine
T_2 NMR

Project	John-for-H.H.	**Helium Porosity**	0.0 p.u.
Sample	Th2-Sk2761.63A	**Confining Stress**	0.00 MPa
Well	Skagerrak	**Gas Permeability**	0.000000 mD
Sample Depth	0.0ft	**Brine Permeability**	0.000000 mD
Legal Location / Block		**Bulk Volume**	22.400 ml

Total NMR Porosity	15.1 p.u.	**T_2 Log Mean**	34.393 ms
Sample State	Undefined	**SNR**	94.35
Date Preformed	2019/07/02 08:45 AM	**NSA**	32
Calibration	6.3300E-5 ml/m.u.		

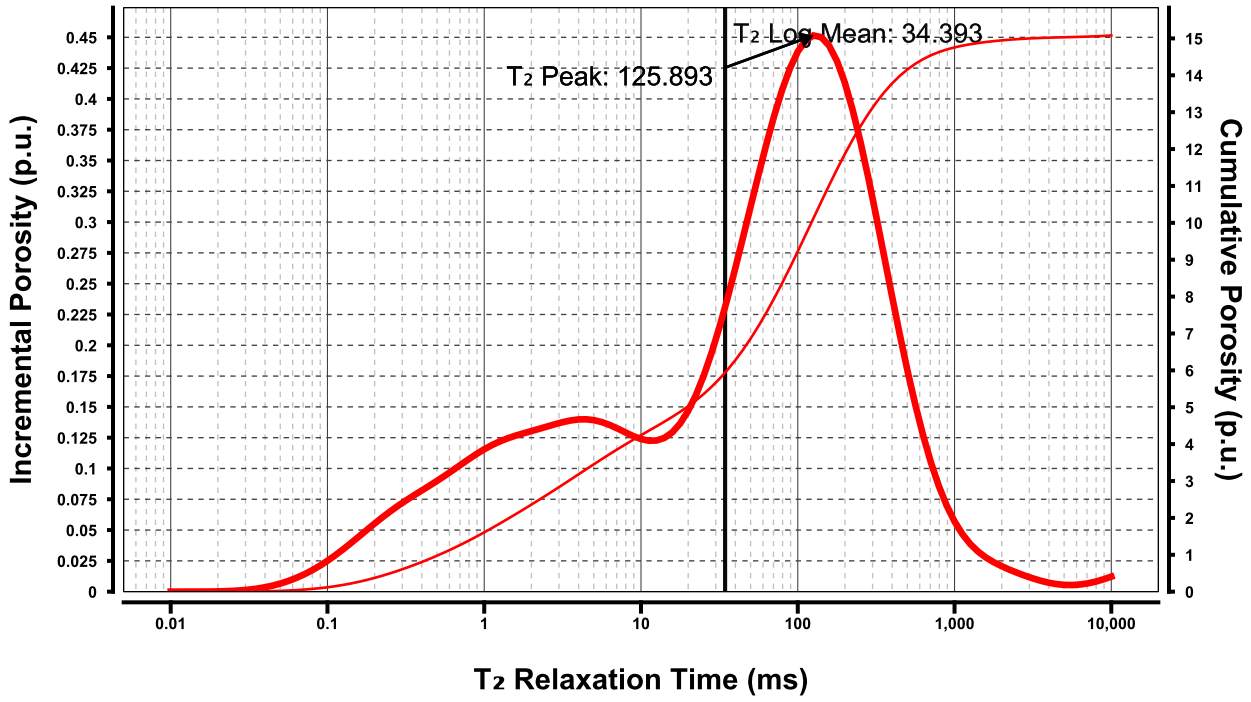

Plug 4A Brine

T_2 NMR

Project	John-for-H.H.	**Helium Porosity**	0.0 p.u.
Sample	Th2-Sk2919.35B	**Confining Stress**	0.00 MPa
Well	Skagerrak	**Gas Permeability**	0.000000 mD
Sample Depth	0.0ft	**Brine Permeability**	0.000000 mD
Legal Location / Block		**Bulk Volume**	17.579 ml

Total NMR Porosity	17.3 p.u.	**T_2 Log Mean**	12.520 ms
Sample State	Undefined	**SNR**	82.62
Date Preformed	2019/07/30 08:57 AM	**NSA**	32
Calibration	6.3300E-5 ml/m.u.		

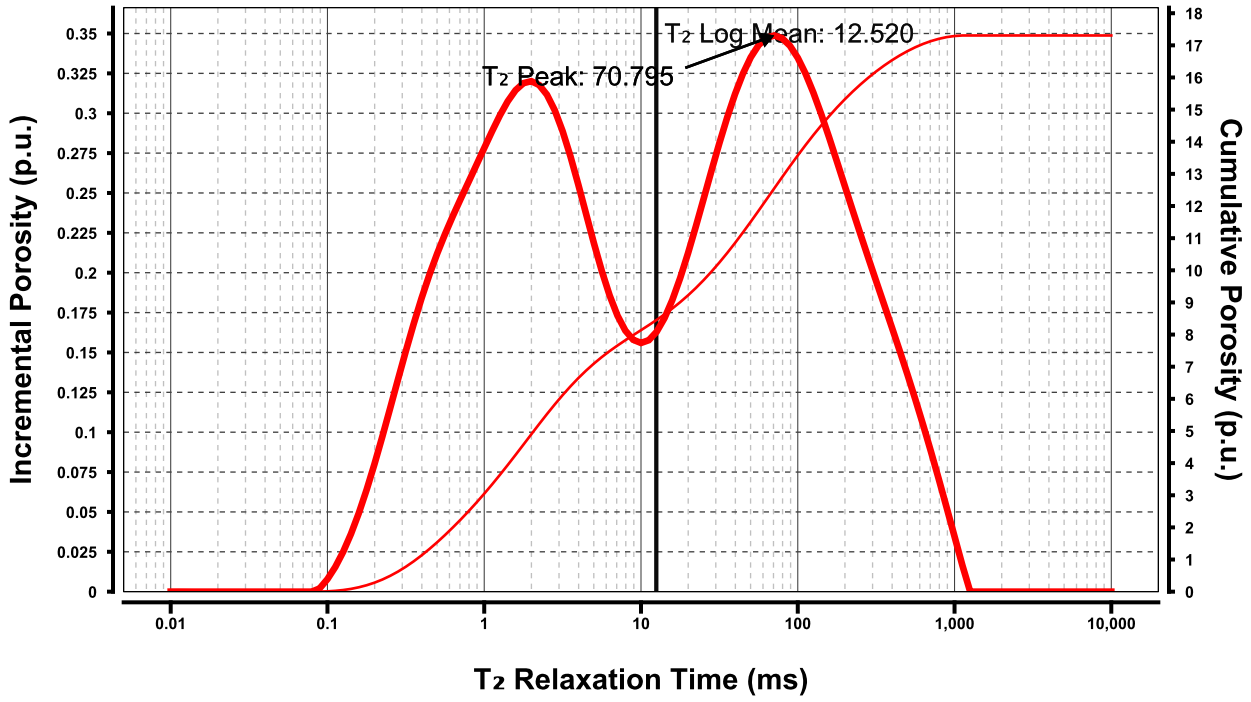

Plug 15 Brine

T_2 NMR

Project	John-for-H.H.	**Helium Porosity**	0.0 p.u.
Sample	Mo1-Sk5034.24A	**Confining Stress**	0.00 MPa
Well	Skagerrak	**Gas Permeability**	0.000000 mD
Sample Depth	0.0ft	**Brine Permeability**	0.000000 mD
Legal Location / Block		**Bulk Volume**	17.336 ml

Total NMR Porosity	8.4 p.u.	**T_2 Log Mean**	6.858 ms
Sample State	Undefined	**SNR**	38.39
Date Preformed	2019/07/30 09:42 AM	**NSA**	32
Calibration	6.3300E-5 ml/m.u.		

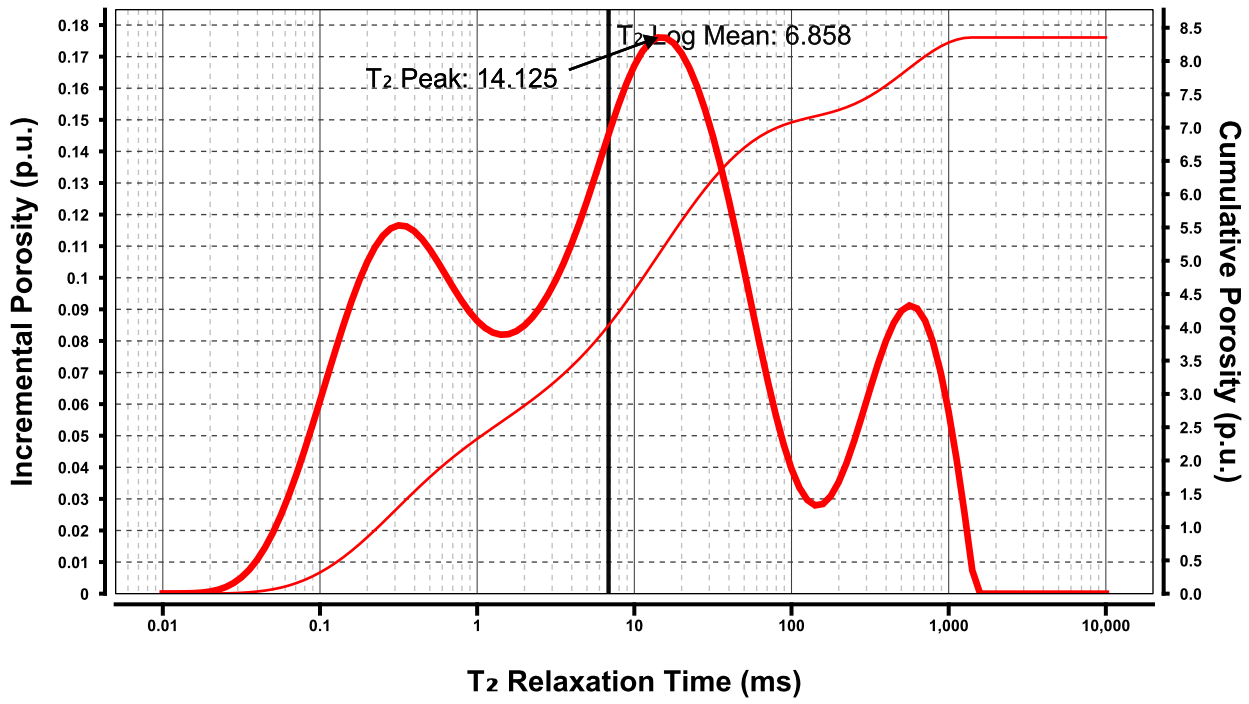

Plug 3 Brine
T_2 NMR

Project	John-for-H.H.	**Helium Porosity**	0.0 p.u.
Sample	Th2-Sk2923.05A	**Confining Stress**	0.00 MPa
Well	Skagerrak Lab5Brine	**Gas Permeability**	0.000000 mD
Sample Depth	0.0ft	**Brine Permeability**	0.000000 mD
Legal Location / Block		**Bulk Volume**	23.617 ml

Total NMR Porosity	13.2 p.u.	**T_2 Log Mean**	11.950 ms
Sample State	Undefined	**SNR**	82.33
Date Preformed	2019/07/02 11:28 AM	**NSA**	32
Calibration	6.3300E-5 ml/m.u.		

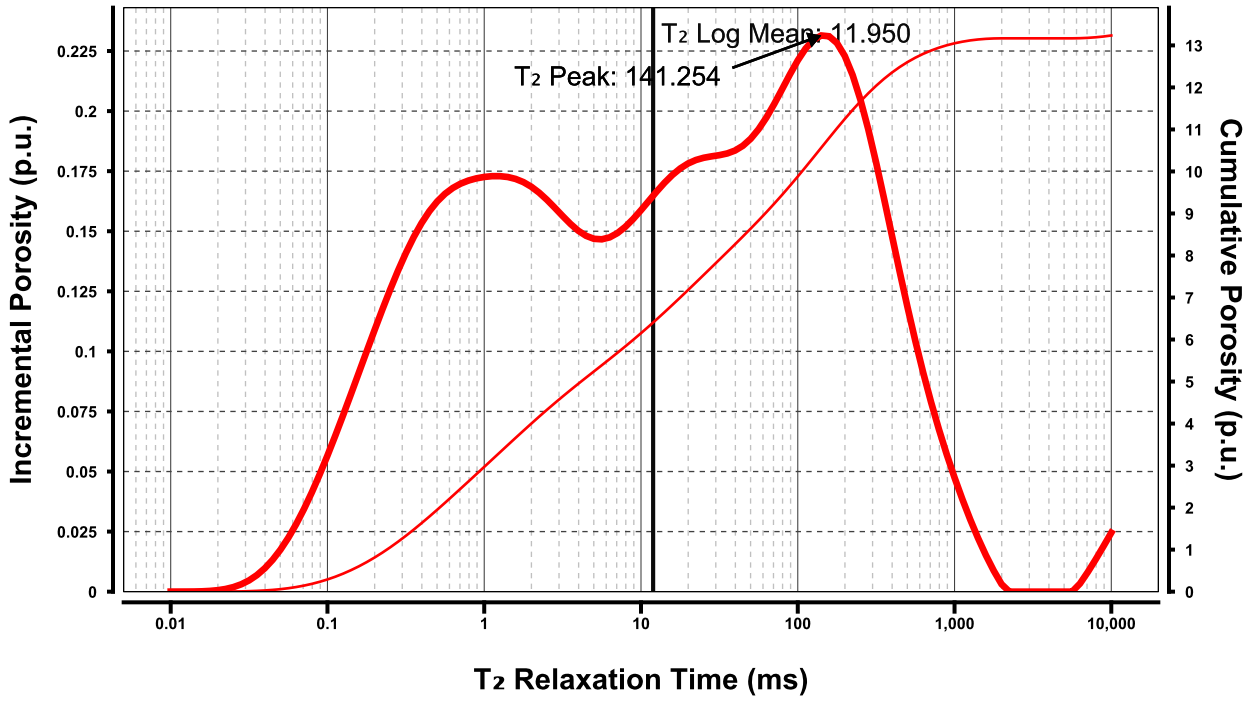

Plug 3 Brine

T_2 NMR

Project	John-for-H.H.	**Helium Porosity**	0.0 p.u.
Sample	Mo-Sk5089.57A	**Confining Stress**	0.00 MPa
Well	Skagerrak	**Gas Permeability**	0.000000 mD
Sample Depth	0.0ft	**Brine Permeability**	0.000000 mD
Legal Location / Block		**Bulk Volume**	16.339 ml

Total NMR Porosity	8.0 p.u.	**T_2 Log Mean**	15.833 ms
Sample State	Undefined	**SNR**	34.63
Date Preformed	2019/07/30 10:23 AM	**NSA**	32
Calibration	6.3300E-5 ml/m.u.		

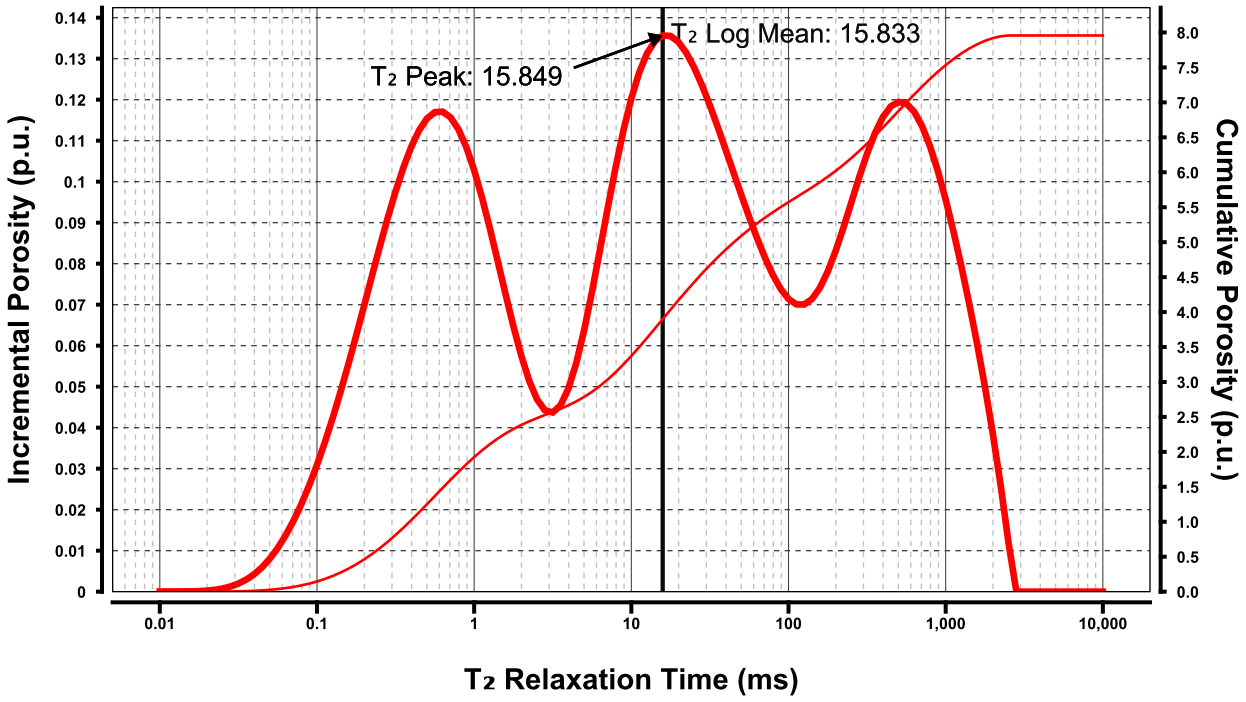

Plug 7B Brine

T_2 NMR

Project	John-for-H.H.	**Helium Porosity**	0.0 p.u.
Sample	Ve1-Sk2062.92B	**Confining Stress**	0.00 MPa
Well	Skagerrak-lab7BBrine	**Gas Permeability**	0.000000 mD
Sample Depth	0.0ft	**Brine Permeability**	0.000000 mD
Legal Location / Block		**Bulk Volume**	17.169 ml

Total NMR Porosity	23.6 p.u.	**T_2 Log Mean**	143.180 ms
Sample State	Undefined	**SNR**	113.00
Date Preformed	2019/07/02 01:22 PM	**NSA**	32
Calibration	6.3300E-5 ml/m.u.		

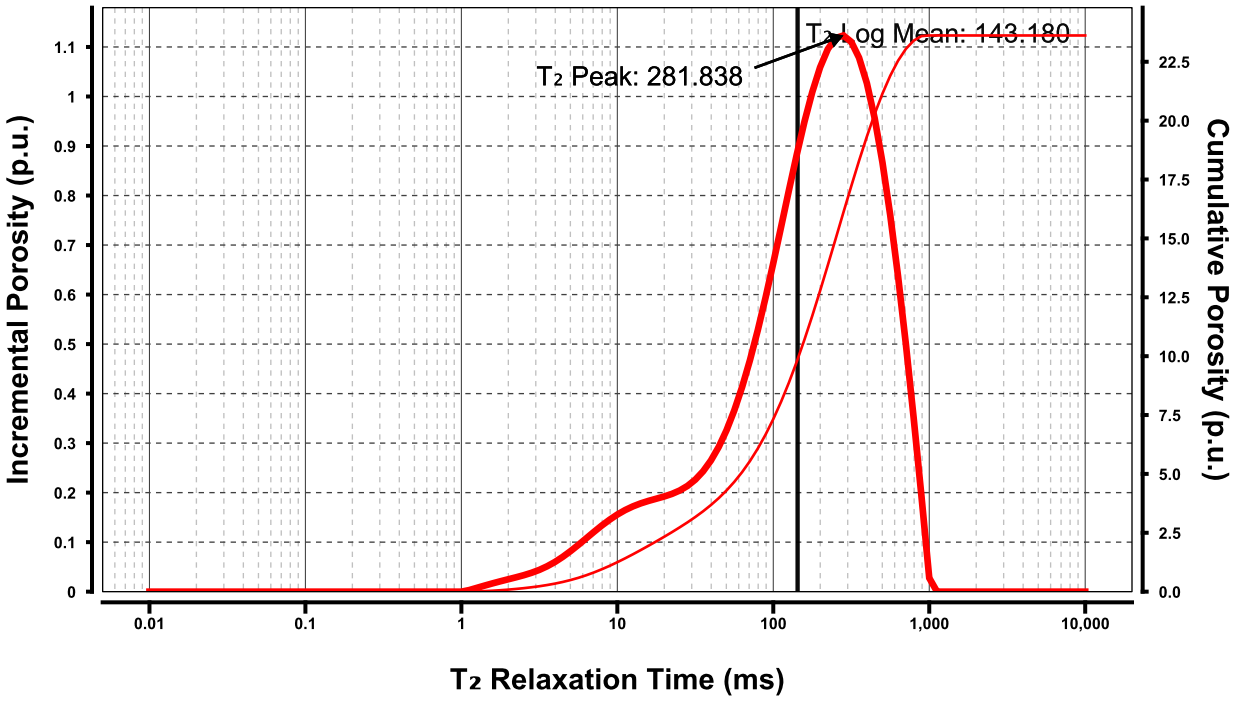

Plug 1 Brine

T_2 NMR

Project	John-for-H.H.	**Helium Porosity**	0.0 p.u.
Sample	Aa1-Ga3325.52A	**Confining Stress**	0.00 MPa
Well	Gassum	**Gas Permeability**	0.000000 mD
Sample Depth	0.0ft	**Brine Permeability**	0.000000 mD
Legal Location / Block		**Bulk Volume**	22.747 ml

Total NMR Porosity	9.9 p.u.	**T_2 Log Mean**	25.492 ms
Sample State	Undefined	**SNR**	57.51
Date Preformed	2019/07/30 01:20 PM	**NSA**	32
Calibration	6.3300E-5 ml/m.u.		

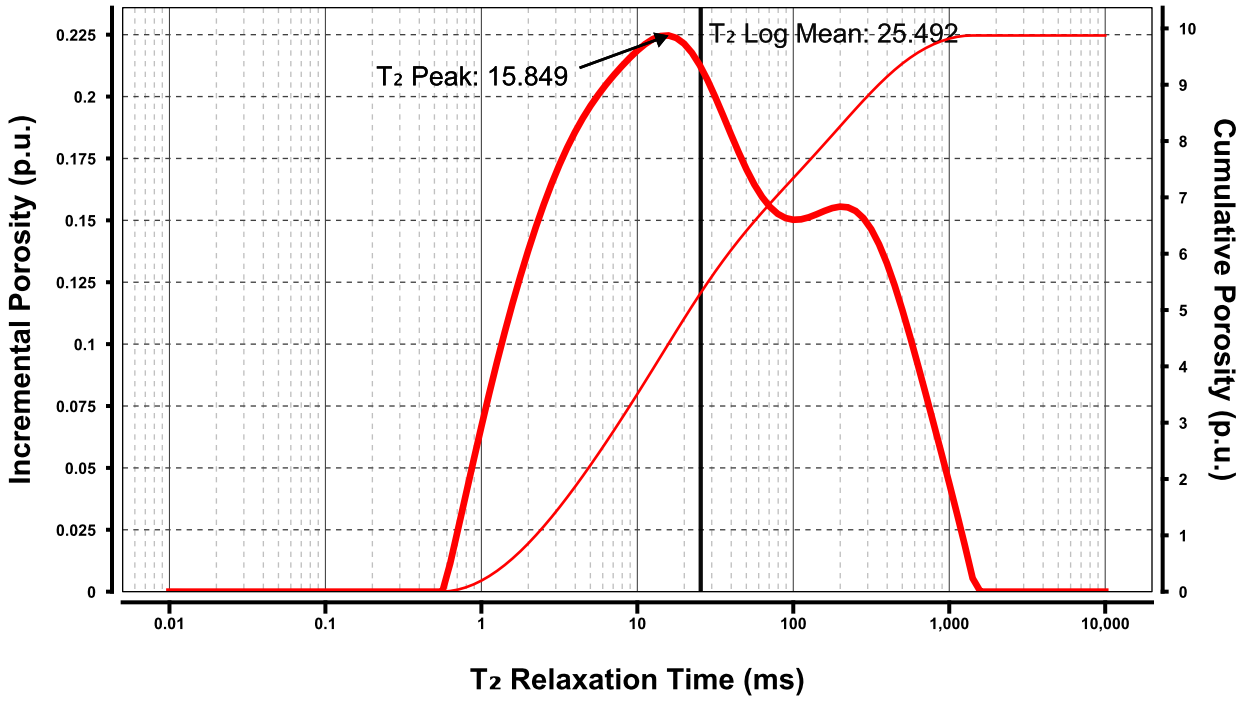

Plug 14 Distilled water

T_2 NMR

Project	John-for-H.H.	**Helium Porosity**	0.0 p.u.
Sample	Aa1-Ga335	**Confining Stress**	0.00 MPa
Well	Gassum	**Gas Permeability**	0.000000 mD
Sample Depth	0.0ft	**Brine Permeability**	0.000000 mD
Legal Location / Block		**Bulk Volume**	23.983 ml

Total NMR Porosity	13.5 p.u.	**T_2 Log Mean**	130.194 ms
Sample State	Undefined	**SNR**	86.88
Date Preformed	2019/05/21 09:05 AM	**NSA**	32
Calibration	6.3300E-5 ml/m.u.		

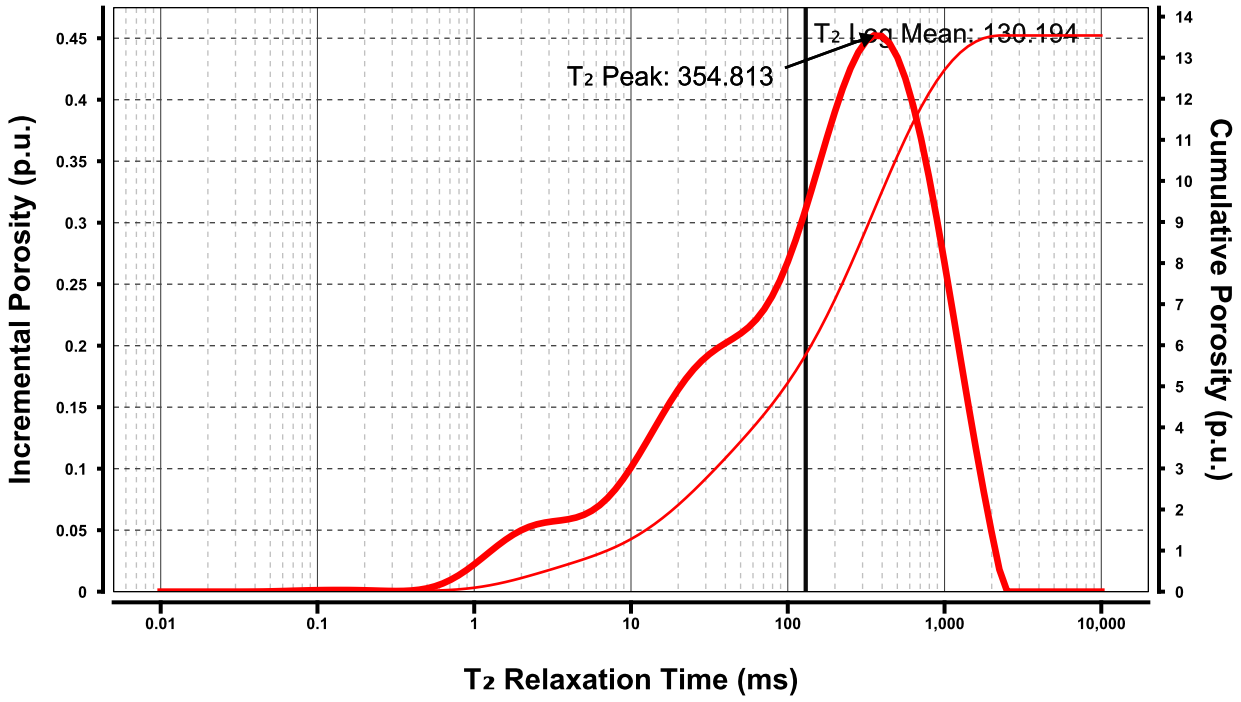

Plug 16 Distilled water

T_2 NMR

Project	John-for-H.H.	**Helium Porosity**	0.0 p.u.
Sample	Aa1-Ga335Lab16	**Confining Stress**	0.00 MPa
Well	Gassum	**Gas Permeability**	0.000000 mD
Sample Depth	0.0ft	**Brine Permeability**	0.000000 mD
Legal Location / Block		**Bulk Volume**	18.602 ml

Total NMR Porosity	16.7 p.u.	**T_2 Log Mean**	270.983 ms
Sample State	Undefined	**SNR**	89.30
Date Preformed	2019/05/21 12:11 PM	**NSA**	32
Calibration	6.3300E-5 ml/m.u.		

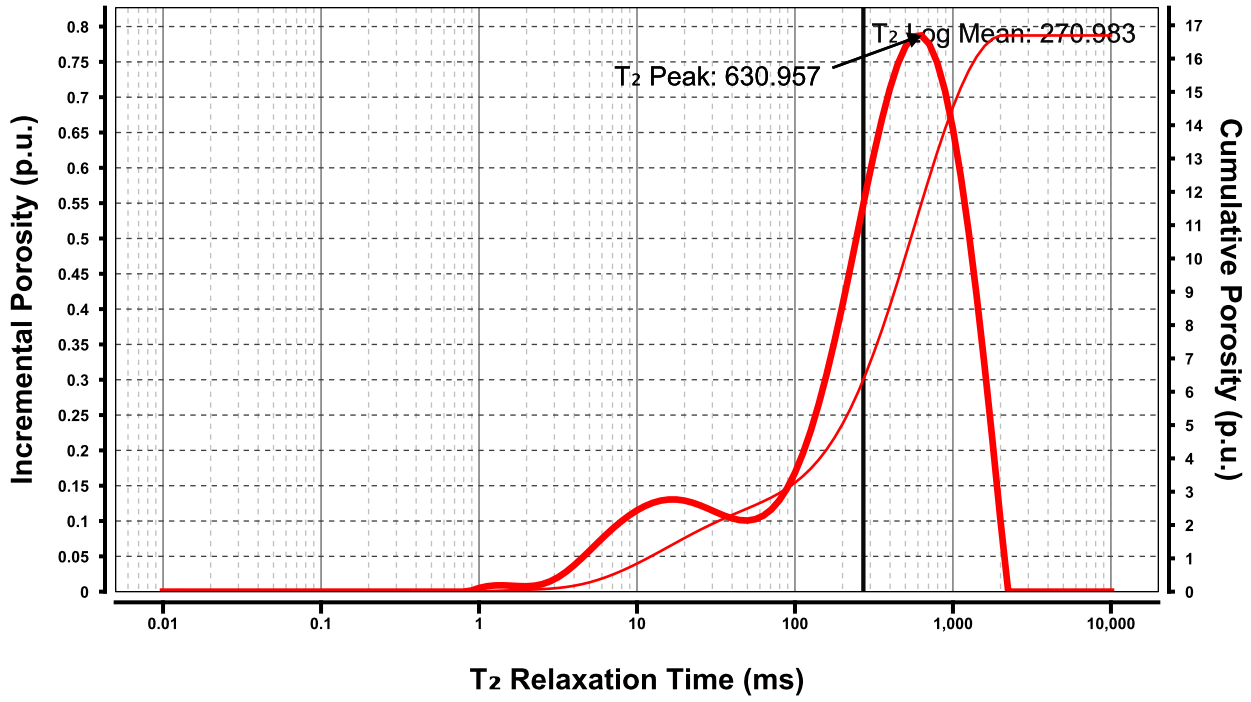

Plug 8 Distilled water

T_2 NMR

Project	John-for-H.H.	**Helium Porosity**	0.0 p.u.
Sample	Ve1-Ga200	**Confining Stress**	0.00 MPa
Well	Gassum	**Gas Permeability**	0.000000 mD
Sample Depth	0.0ft	**Brine Permeability**	0.000000 mD
Legal Location / Block		**Bulk Volume**	10.282 ml

Total NMR Porosity	24.7 p.u.	**T_2 Log Mean**	120.638 ms
Sample State	Undefined	**SNR**	71.26
Date Preformed	2019/05/21 01:45 PM	**NSA**	32
Calibration	6.3300E-5 ml/m.u.		

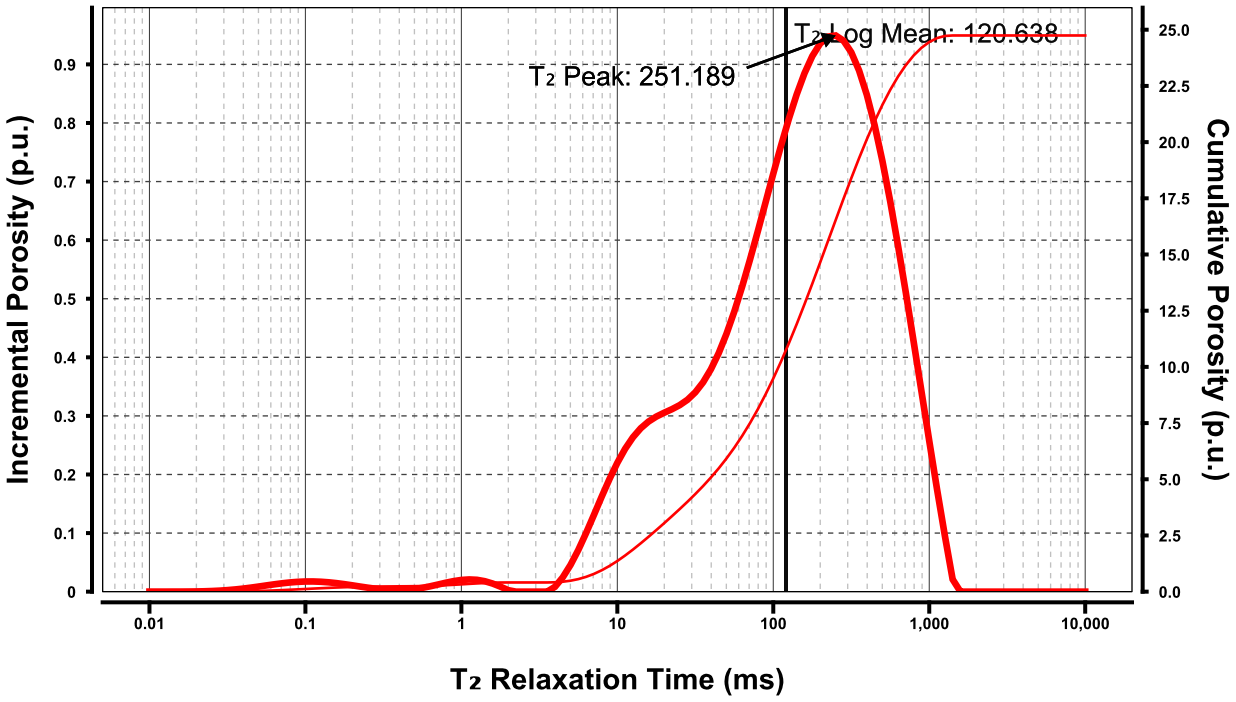

Plug 9B Distilled water

T_2 NMR

Project	John-for-H.H.	**Helium Porosity**	0.0 p.u.
Sample	Ve1-Ga201	**Confining Stress**	0.00 MPa
Well	Gassum	**Gas Permeability**	0.000000 mD
Sample Depth	0.0ft	**Brine Permeability**	0.000000 mD
Legal Location / Block		**Bulk Volume**	11.162 ml

Total NMR Porosity	27.3 p.u.	**T_2 Log Mean**	145.229 ms
Sample State	Undefined	**SNR**	84.50
Date Preformed	2019/05/21 02:35 PM	**NSA**	32
Calibration	6.3300E-5 ml/m.u.		

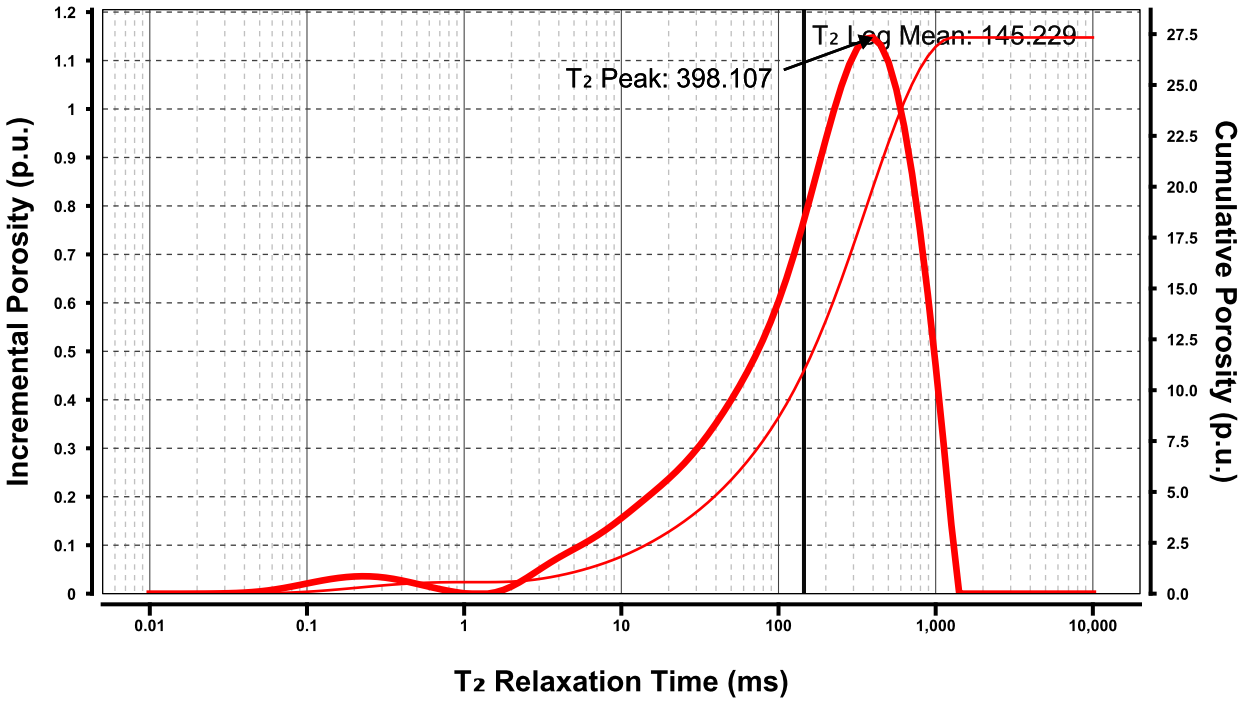

Plug 13B Distilled water

T_2 NMR

Project	John-for-H.H.	**Helium Porosity**	0.0 p.u.
Sample	Aa1-Ga332	**Confining Stress**	0.00 MPa
Well	Gassum	**Gas Permeability**	0.000000 mD
Sample Depth	0.0ft	**Brine Permeability**	0.000000 mD
Legal Location / Block		**Bulk Volume**	22.703 ml

Total NMR Porosity	14.6 p.u.	**T_2 Log Mean**	24.305 ms
Sample State	Undefined	**SNR**	94.57
Date Preformed	2019/05/24 08:41 AM	**NSA**	32
Calibration	6.3300E-5 ml/m.u.		

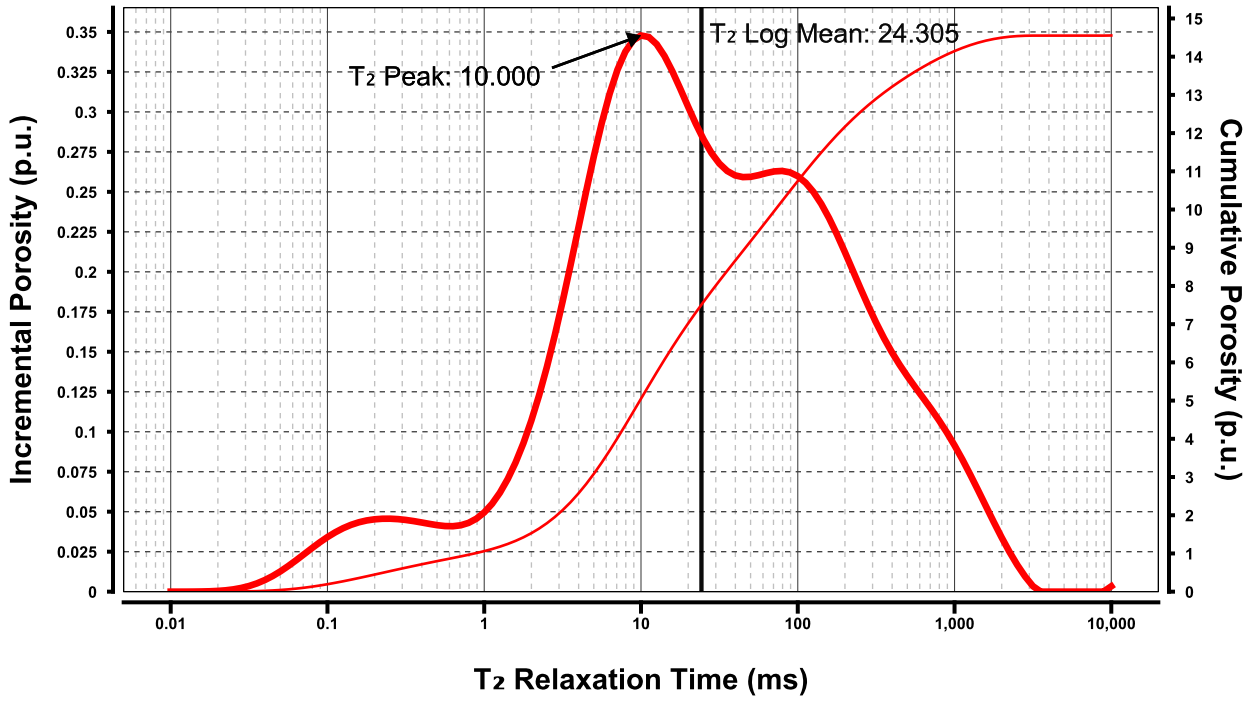

Plug 11B Distilled water

T_2 NMR

Project	John-for-H.H.	**Helium Porosity**	0.0 p.u.
Sample	Aa1-Ga331	**Confining Stress**	0.00 MPa
Well	Gassum	**Gas Permeability**	0.000000 mD
Sample Depth	0.0ft	**Brine Permeability**	0.000000 mD
Legal Location / Block		**Bulk Volume**	24.684 ml

Total NMR Porosity	6.9 p.u.	**T_2 Log Mean**	155.369 ms
Sample State	Undefined	**SNR**	46.41
Date Preformed	2019/05/24 11:14 AM	**NSA**	32
Calibration	6.3300E-5 ml/m.u.		

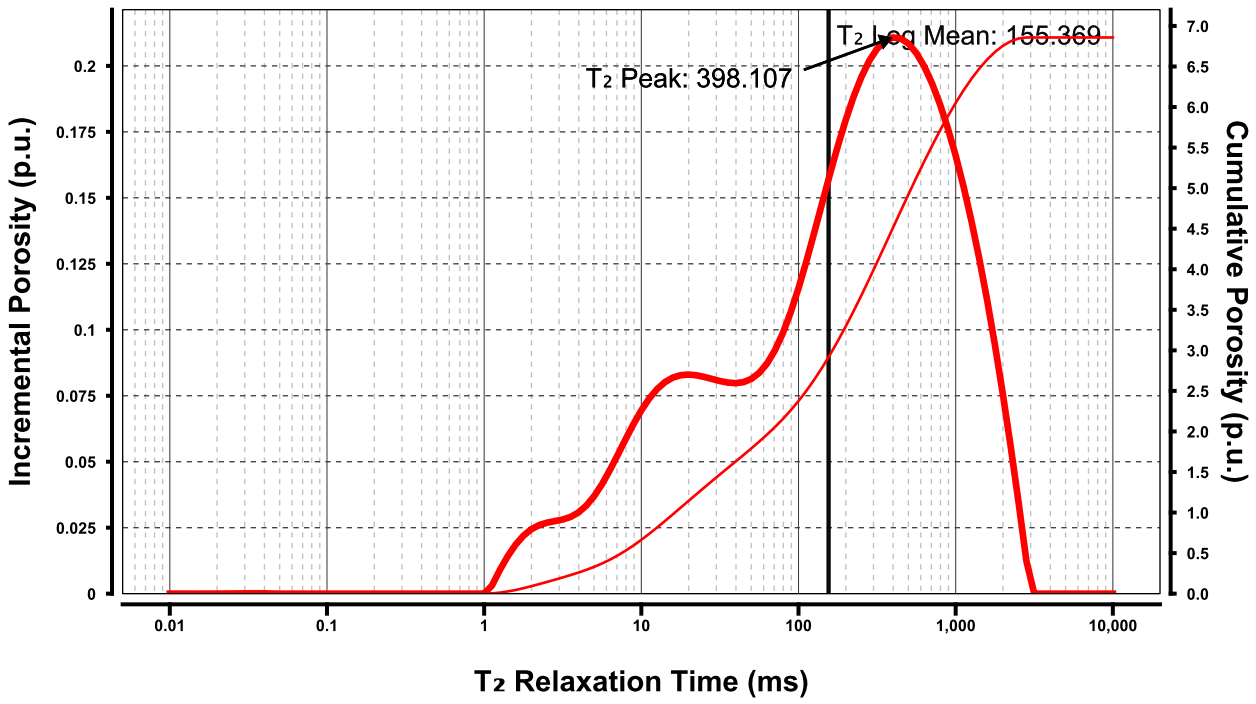

Plug 20 Distilled water

T_2 NMR

Project	John-for-H.H.	**Helium Porosity**	0.0 p.u.
Sample	Aa1-Ga331	**Confining Stress**	0.00 MPa
Well	Gassum	**Gas Permeability**	0.000000 mD
Sample Depth	0.0ft	**Brine Permeability**	0.000000 mD
Legal Location / Block		**Bulk Volume**	24.684 ml

Total NMR Porosity	6.9 p.u.	**T_2 Log Mean**	155.369 ms
Sample State	Undefined	**SNR**	46.41
Date Preformed	2019/05/24 11:14 AM	**NSA**	32
Calibration	6.3300E-5 ml/m.u.		

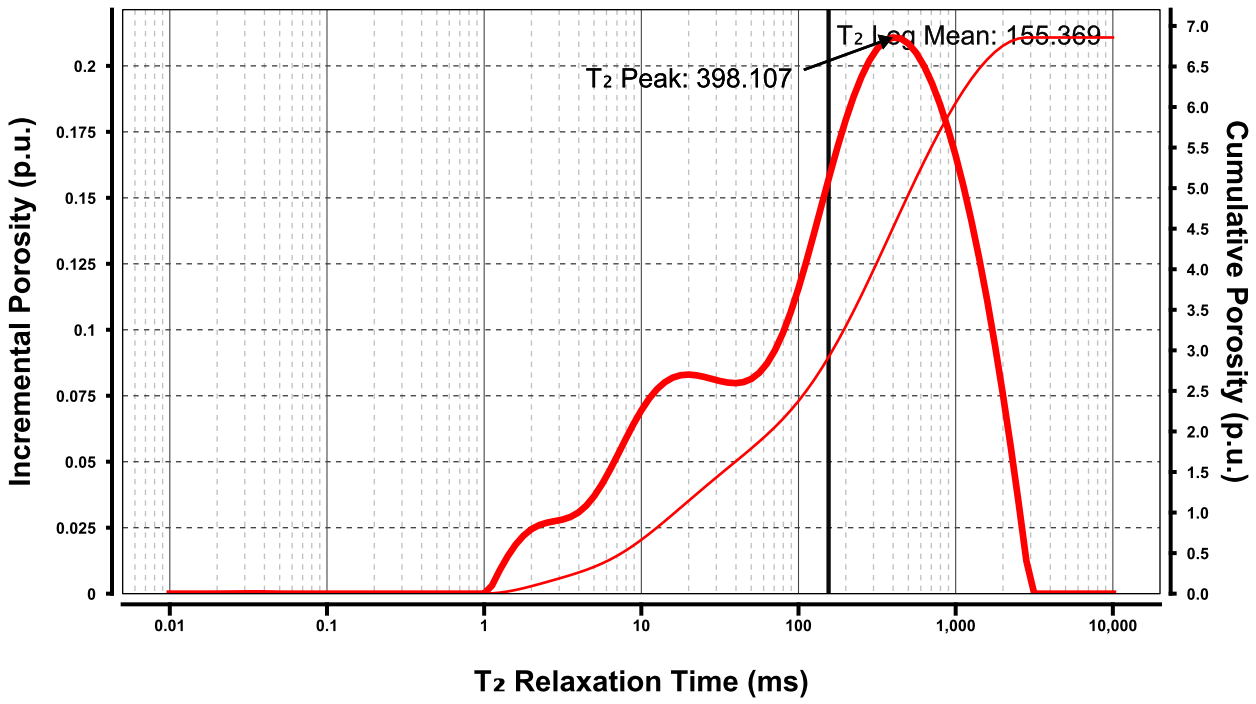

Plug 21A Distilled water

T_2 NMR

Project	John-for-H.H.	**Helium Porosity**	0.0 p.u.
Sample	Aa1-Ga332Lab21A	**Confining Stress**	0.00 MPa
Well	Gassum	**Gas Permeability**	0.000000 mD
Sample Depth	0.0ft	**Brine Permeability**	0.000000 mD
Legal Location / Block		**Bulk Volume**	15.189 ml

Total NMR Porosity	13.8 p.u.	**T_2 Log Mean**	47.237 ms
Sample State	Undefined	**SNR**	59.70
Date Preformed	2019/05/24 11:56 AM	**NSA**	32
Calibration	6.3300E-5 ml/m.u.		

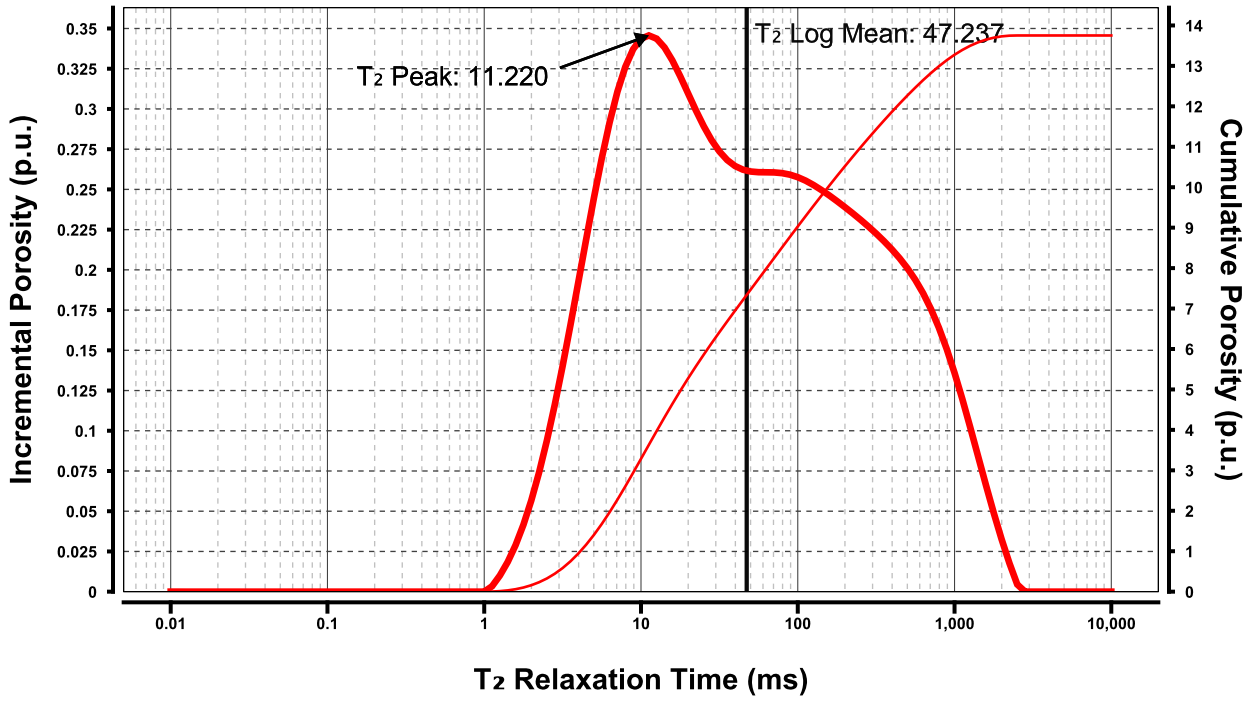

Plug 22A Distilled water
T_2 NMR

Project	John-for-H.H.	**Helium Porosity**	0.0 p.u.
Sample	Aa1-Ga327	**Confining Stress**	0.00 MPa
Well	Gassum	**Gas Permeability**	0.000000 mD
Sample Depth	0.0ft	**Brine Permeability**	0.000000 mD
Legal Location / Block		**Bulk Volume**	20.433 ml

Total NMR Porosity	14.6 p.u.	**T_2 Log Mean**	132.247 ms
Sample State	Undefined	**SNR**	80.48
Date Preformed	2019/05/24 01:27 PM	**NSA**	32
Calibration	6.3300E-5 ml/m.u.		

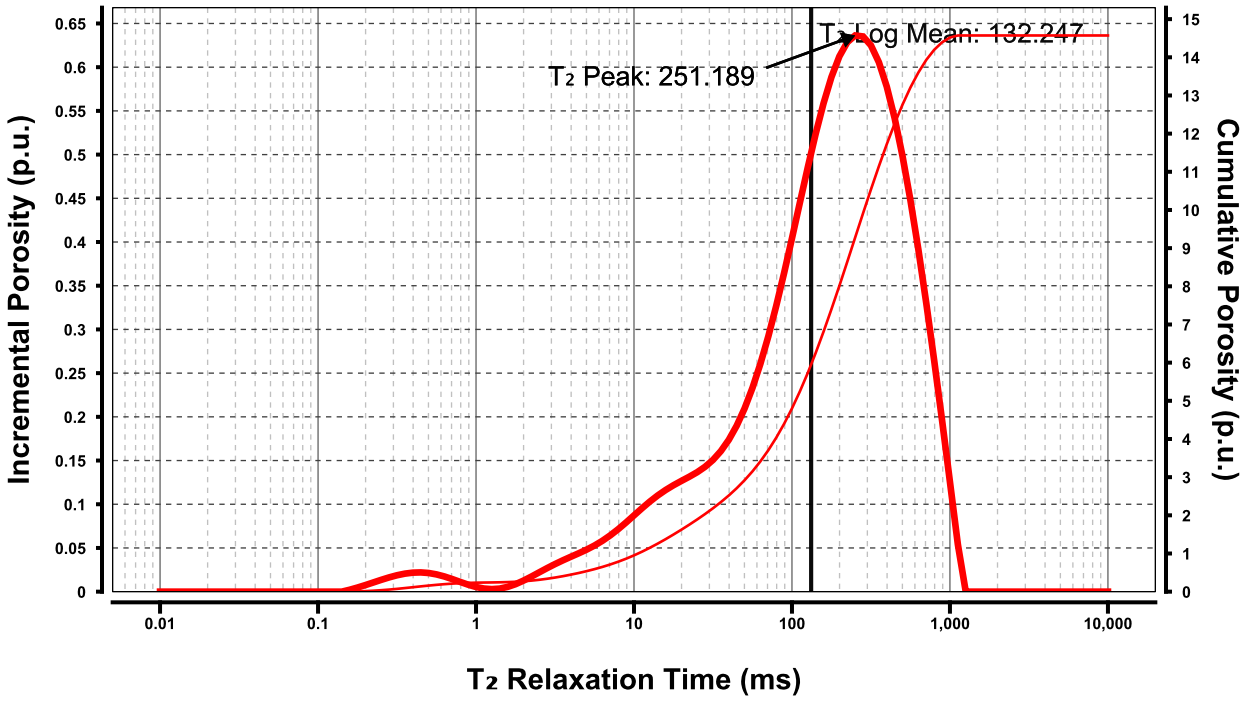

Plug 12A Distilled water

T_2 NMR

Project	John-for-H.H.	**Helium Porosity**	0.0 p.u.
Sample	Aa1-Ga332Lab12A	**Confining Stress**	0.00 MPa
Well	Gassum	**Gas Permeability**	0.000000 mD
Sample Depth	0.0ft	**Brine Permeability**	0.000000 mD
Legal Location / Block		**Bulk Volume**	22.747 ml

Total NMR Porosity	11.1 p.u.	**T_2 Log Mean**	29.575 ms
Sample State	Undefined	**SNR**	68.45
Date Preformed	2019/05/24 03:34 PM	**NSA**	32
Calibration	6.3300E-5 ml/m.u.		

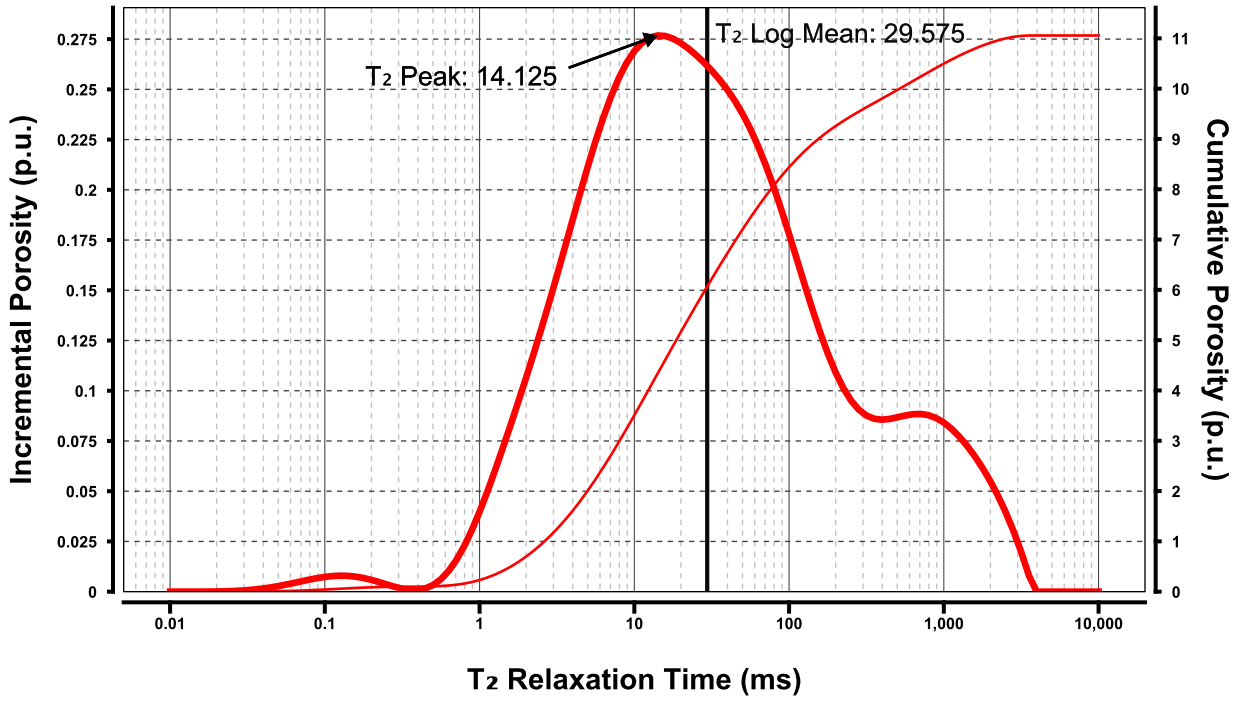

Plug 12 Distilled water

T_2 NMR

Project	John-for-H.H.	**Helium Porosity**	0.0 p.u.
Sample	Aa1-Ga331Lab10	**Confining Stress**	0.00 MPa
Well	Gassum	**Gas Permeability**	0.000000 mD
Sample Depth	0.0ft	**Brine Permeability**	0.000000 mD
Legal Location / Block		**Bulk Volume**	22.734 ml

Total NMR Porosity	8.2 p.u.	**T_2 Log Mean**	72.875 ms
Sample State	Undefined	**SNR**	51.57
Date Preformed	2019/05/24 02:50 PM	**NSA**	32
Calibration	6.3300E-5 ml/m.u.		

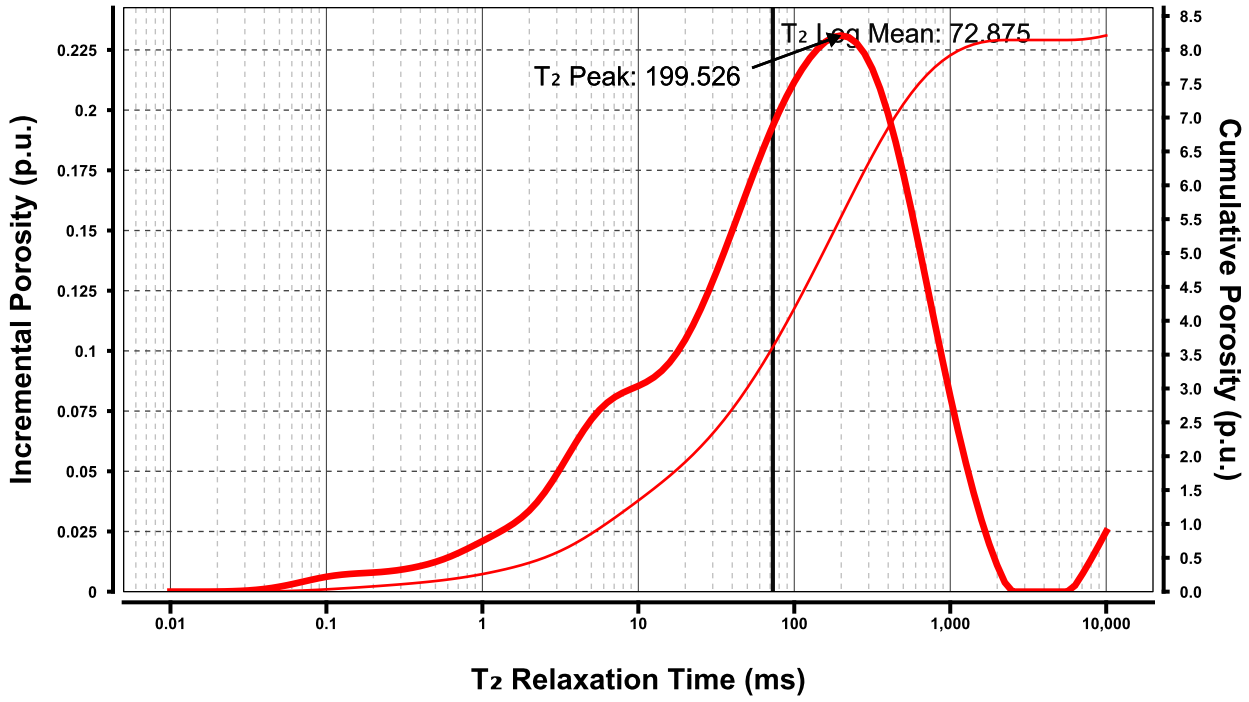

Plug 6 Distilled water
T_2 NMR

Project	John-for-H.H.	**Helium Porosity**	0.0 p.u.
Sample	Th2-Sk2761	**Confining Stress**	0.00 MPa
Well	Skagerrak	**Gas Permeability**	0.000000 mD
Sample Depth	0.0ft	**Brine Permeability**	0.000000 mD
Legal Location / Block		**Bulk Volume**	22.400 ml

Total NMR Porosity	16.9 p.u.	**T_2 Log Mean**	31.620 ms
Sample State	Undefined	**SNR**	101.94
Date Preformed	2019/05/14 08:48 AM	**NSA**	32
Calibration	6.3300E-5 ml/m.u.		

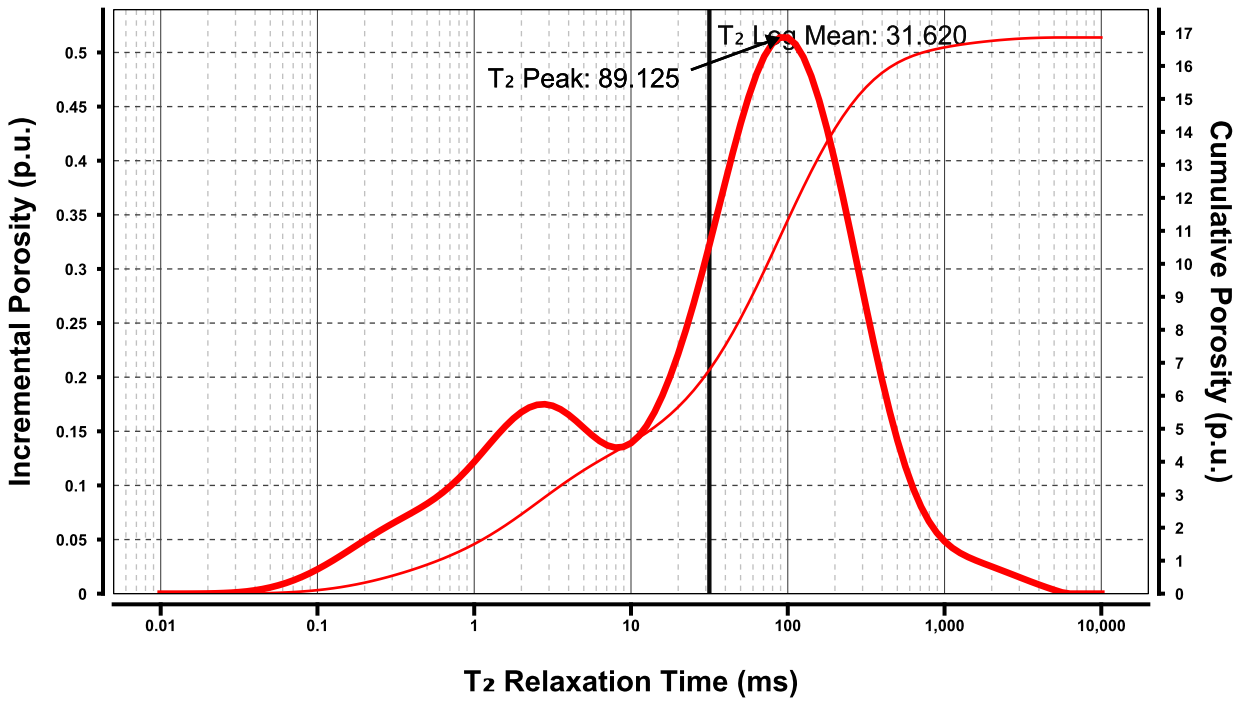

Plug 4A Distilled water

T_2 NMR

Project	John-for-H.H.	**Helium Porosity**	0.0 p.u.
Sample	Th-2Sk2919	**Confining Stress**	0.00 MPa
Well	Skagerrak	**Gas Permeability**	0.000000 mD
Sample Depth	0.0ft	**Brine Permeability**	0.000000 mD
Legal Location / Block		**Bulk Volume**	17.671 ml

Total NMR Porosity	19.0 p.u.	**T_2 Log Mean**	13.174 ms
Sample State	Undefined	**SNR**	93.11
Date Preformed	2019/05/07 03:18 PM	**NSA**	32
Calibration	6.3300E-5 ml/m.u.		

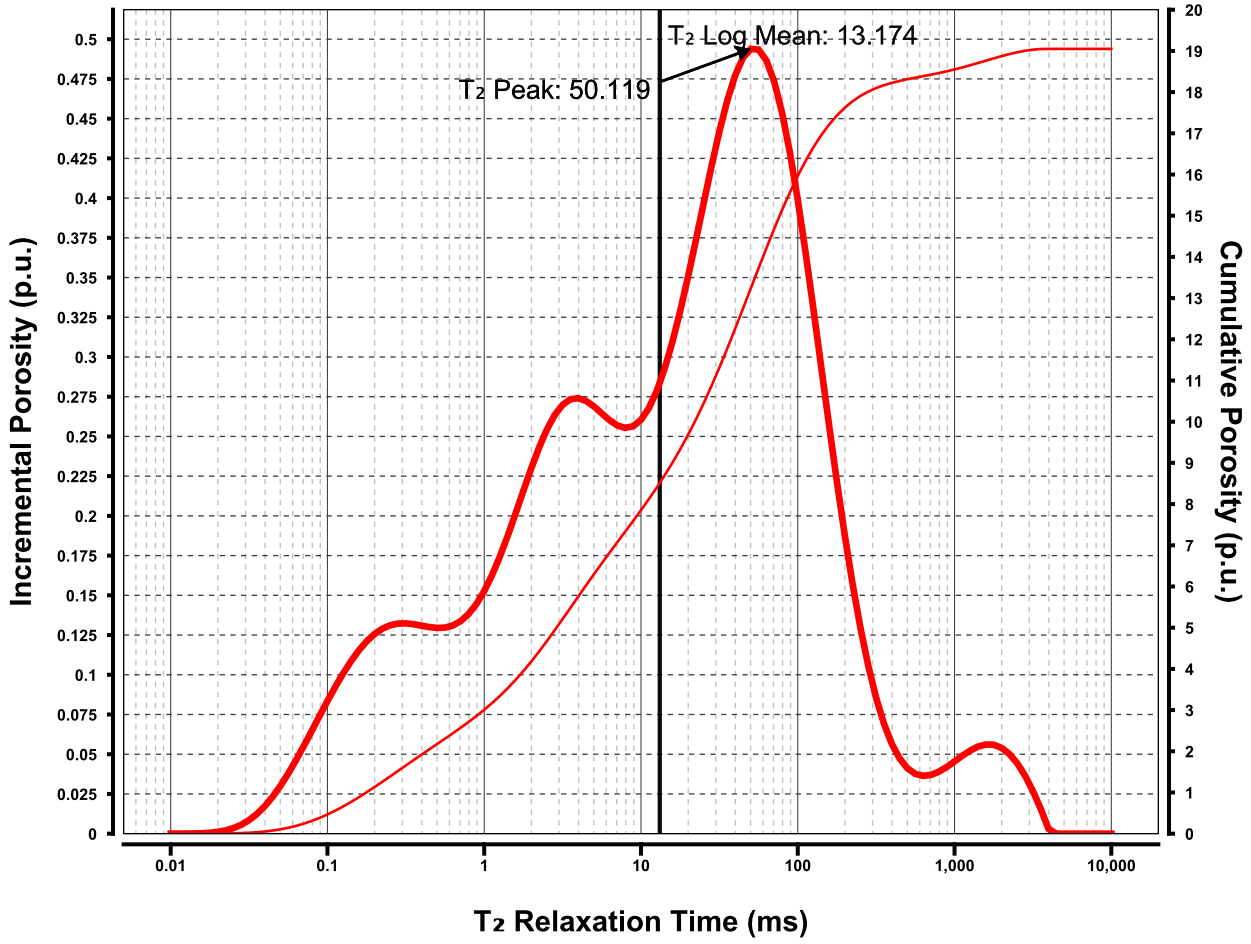

Plug 15 Distilled water
T_2 NMR

Project	John-for-H.H.	**Helium Porosity**	0.0 p.u.
Sample	Mo1-Sk503	**Confining Stress**	0.00 MPa
Well	Skagerrak	**Gas Permeability**	0.000000 mD
Sample Depth	0.0ft	**Brine Permeability**	0.000000 mD
Legal Location / Block		**Bulk Volume**	17.671 ml

Total NMR Porosity	9.3 p.u.	**T_2 Log Mean**	4.466 ms
Sample State	Undefined	**SNR**	42.20
Date Preformed	2019/05/10 11:03 AM	**NSA**	32
Calibration	6.3300E-5 ml/m.u.		

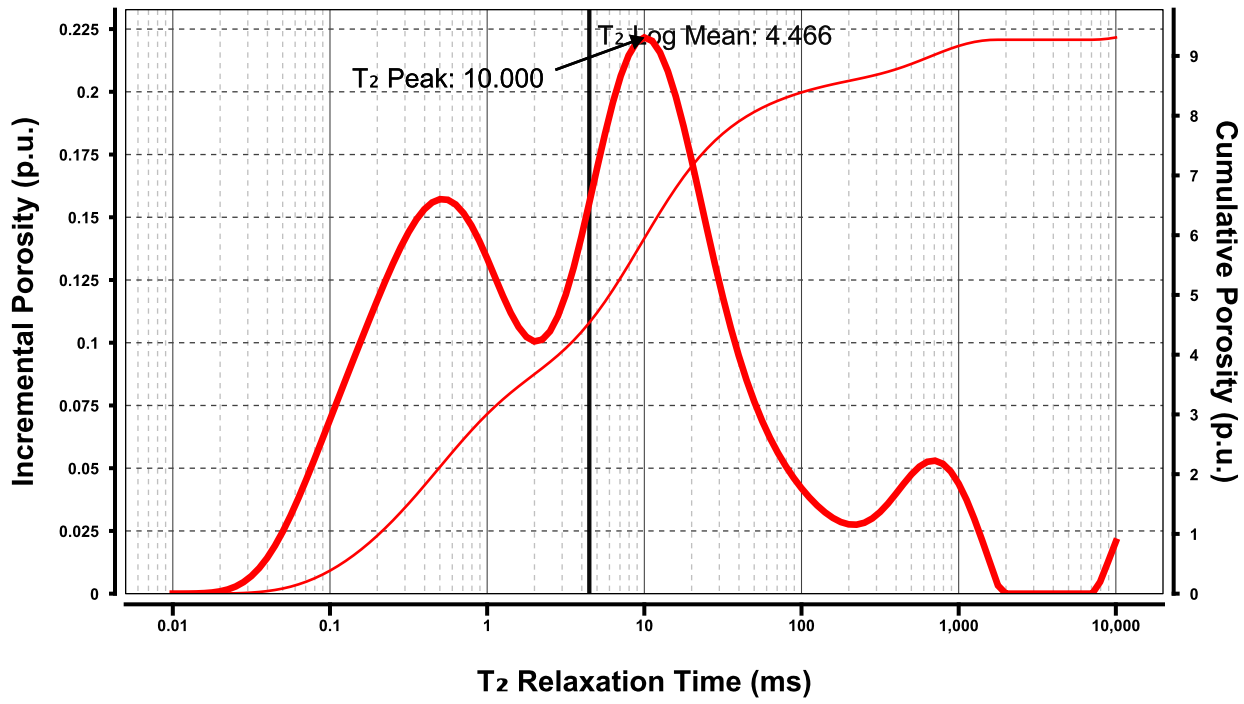

Plug 5 Distilled water

T_2 NMR

Project	John-for-H.H.	**Helium Porosity**	0.0 p.u.
Sample	Hh2-Sk2923	**Confining Stress**	0.00 MPa
Well	Skagerrak	**Gas Permeability**	0.000000 mD
Sample Depth	0.0ft	**Brine Permeability**	0.000000 mD
Legal Location / Block		**Bulk Volume**	23.617 ml

Total NMR Porosity	14.3 p.u.	**T_2 Log Mean**	12.241 ms
Sample State	Undefined	**SNR**	89.02
Date Preformed	2019/05/14 09:38 AM	**NSA**	32
Calibration	6.3300E-5 ml/m.u.		

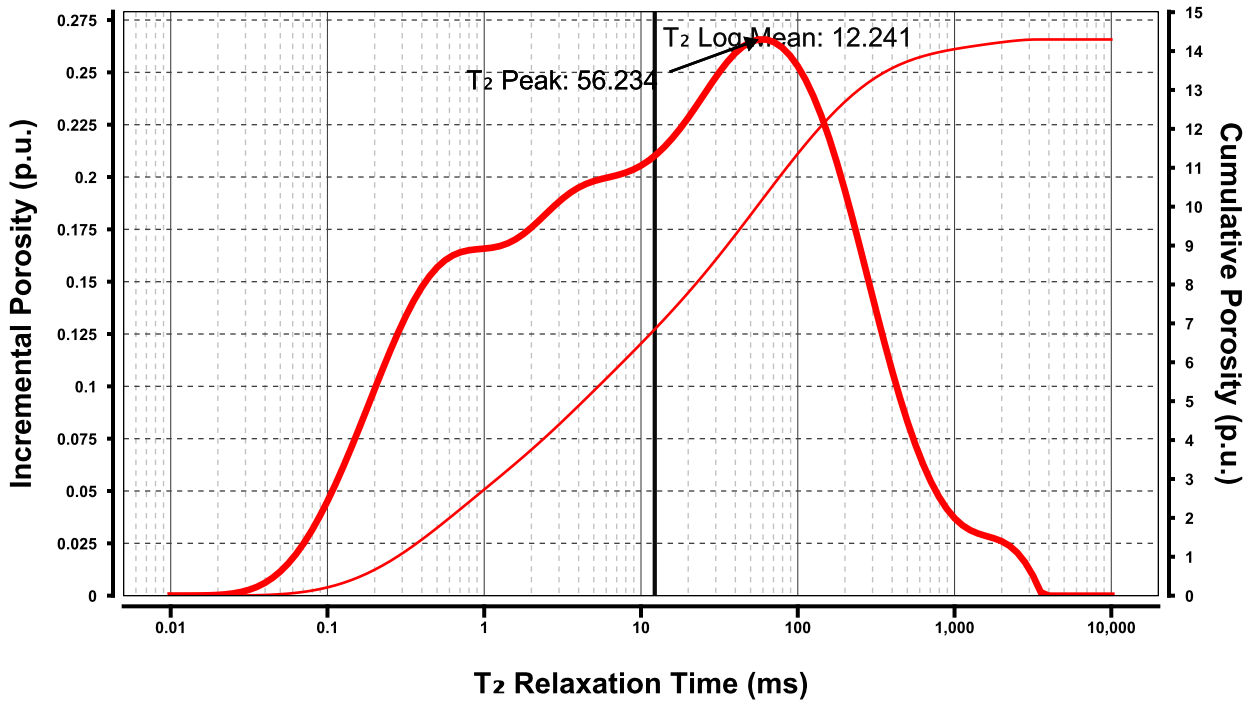

Plug 3 Distilled water

T_2 NMR

Project	John-for-H.H.	**Helium Porosity**	0.0 p.u.
Sample	Mo1-Sk508	**Confining Stress**	0.00 MPa
Well	Skagerrak	**Gas Permeability**	0.000000 mD
Sample Depth	0.0ft	**Brine Permeability**	0.000000 mD
Legal Location / Block		**Bulk Volume**	16.339 ml

Total NMR Porosity	7.7 p.u.	**T_2 Log Mean**	4.769 ms
Sample State	Undefined	**SNR**	34.95
Date Preformed	2019/05/14 10:32 AM	**NSA**	32
Calibration	6.3300E-5 ml/m.u.		

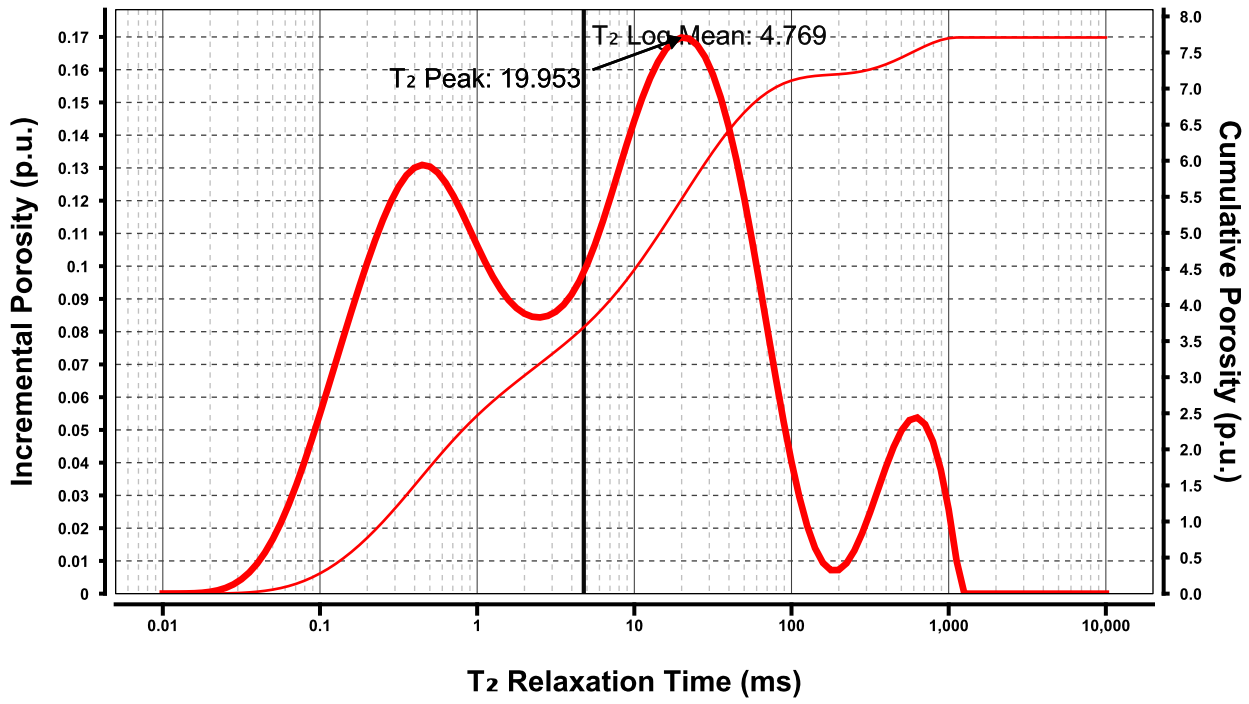

Plug 7B Distilled water
T_2 NMR

Project	John-for-H.H.	**Helium Porosity**	0.0 p.u.
Sample	Th2-Sk2761	**Confining Stress**	0.00 MPa
Well	Skagerrak	**Gas Permeability**	0.000000 mD
Sample Depth	0.0ft	**Brine Permeability**	0.000000 mD
Legal Location / Block		**Bulk Volume**	22.400 ml

Total NMR Porosity	16.9 p.u.	**T_2 Log Mean**	31.620 ms
Sample State	Undefined	**SNR**	101.94
Date Preformed	2019/05/14 08:48 AM	**NSA**	32
Calibration	6.3300E-5 ml/m.u.		

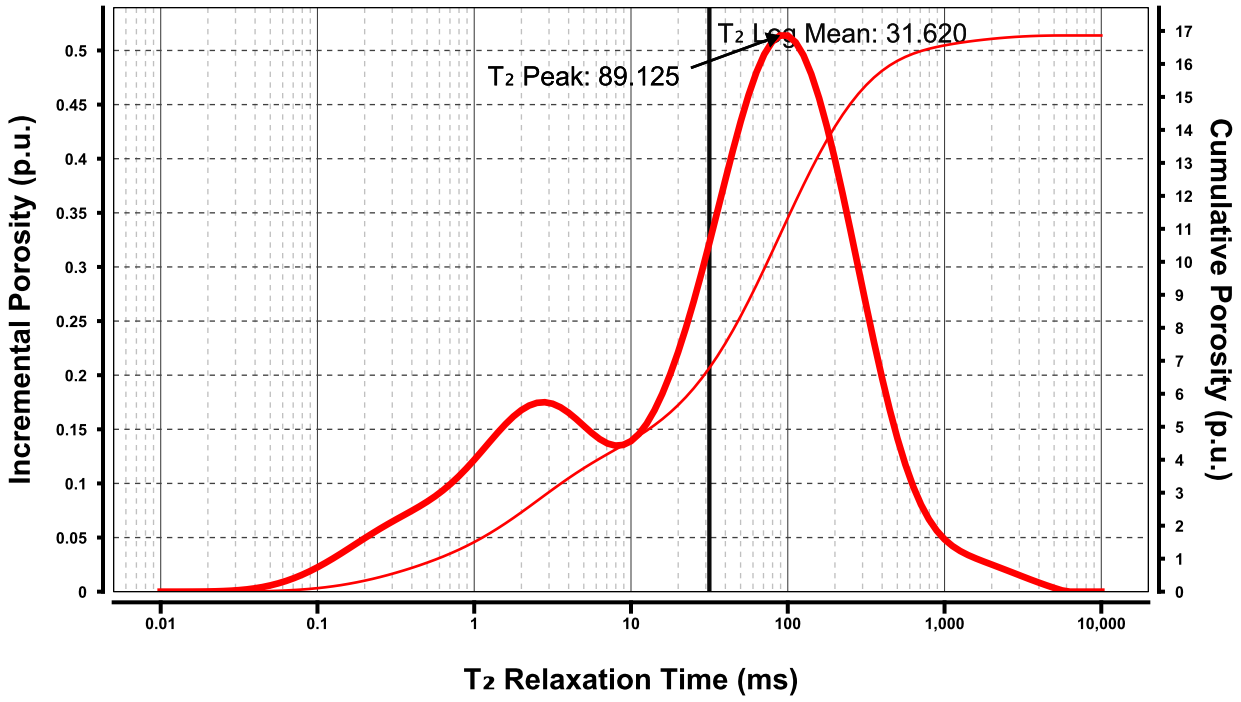

Plug 1 Distilled water

T_2 NMR

Project	John-for-H.H.	**Helium Porosity**	0.0 p.u.
Sample	Ga1-Sk303?	**Confining Stress**	0.00 MPa
Well	Skagerrak	**Gas Permeability**	0.000000 mD
Sample Depth	0.0ft	**Brine Permeability**	0.000000 mD
Legal Location / Block		**Bulk Volume**	13.903 ml

Total NMR Porosity	7.4 p.u.	**T_2 Log Mean**	11.809 ms
Sample State	Undefined	**SNR**	28.43
Date Preformed	2019/05/14 12:06 PM	**NSA**	32
Calibration	6.3300E-5 ml/m.u.		

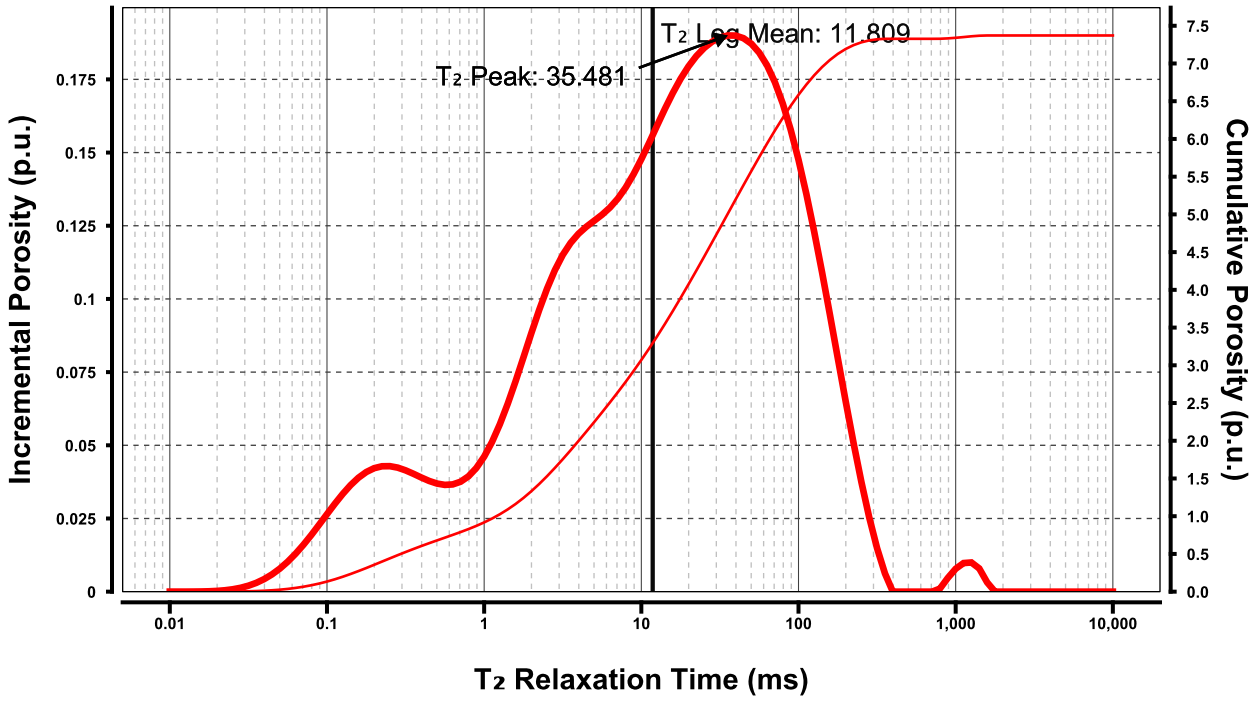

Appendix E

MICP results

Gassum formation

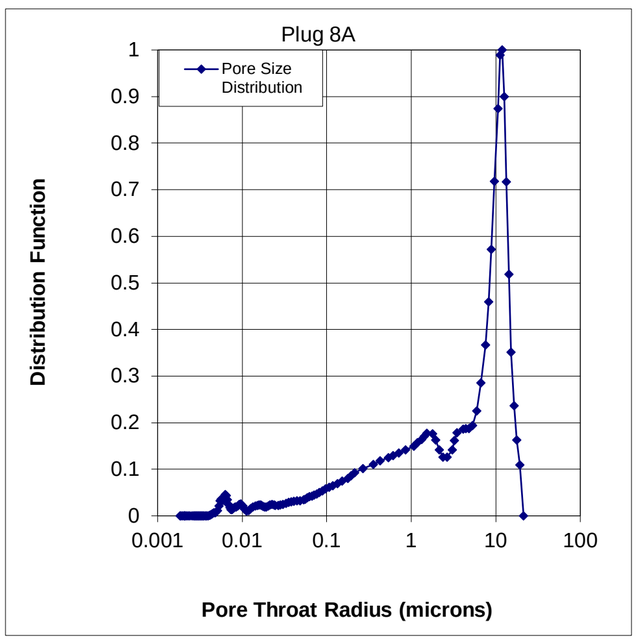

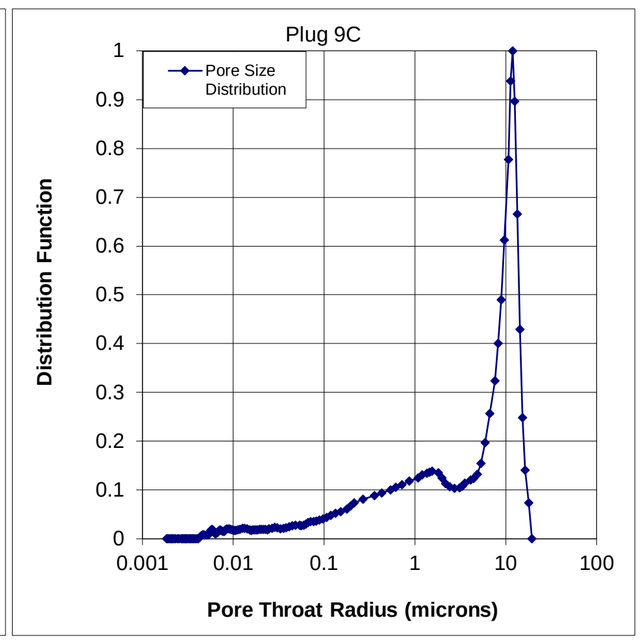

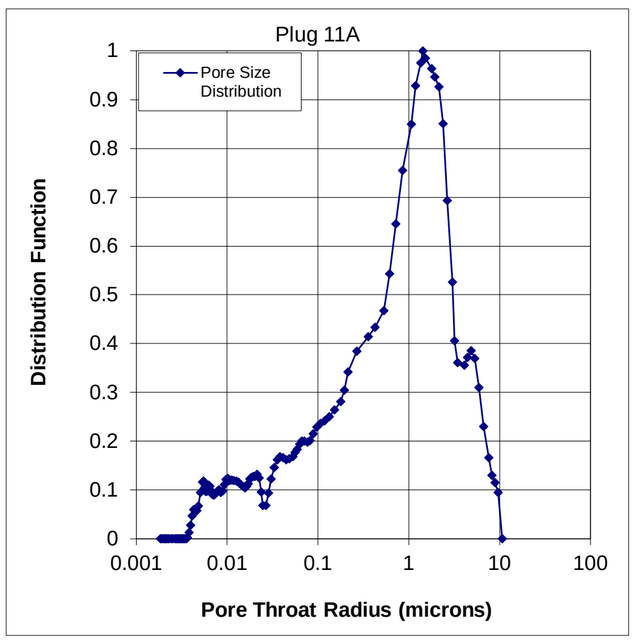

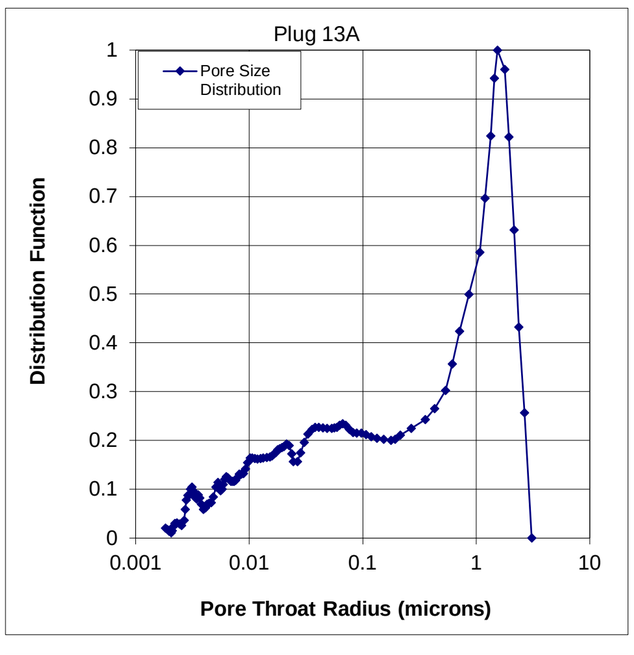

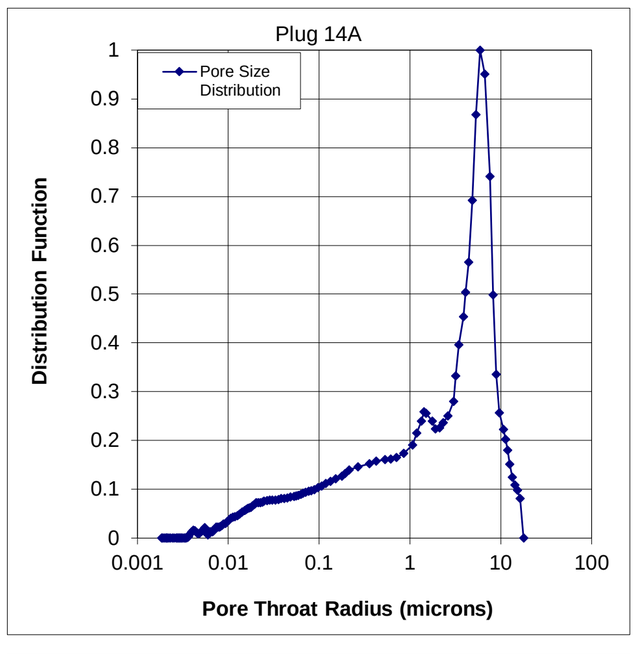

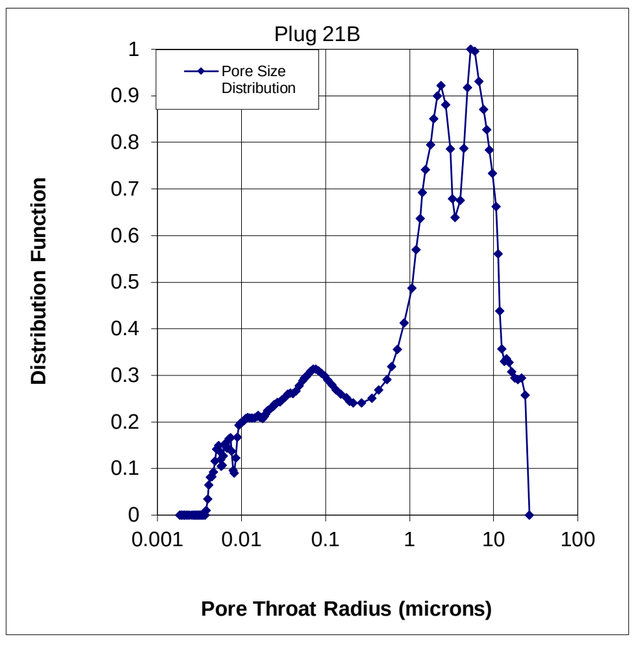

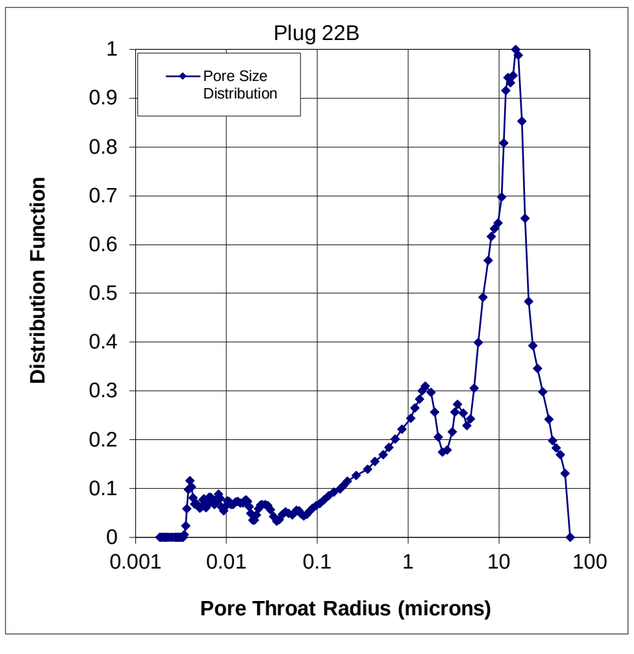

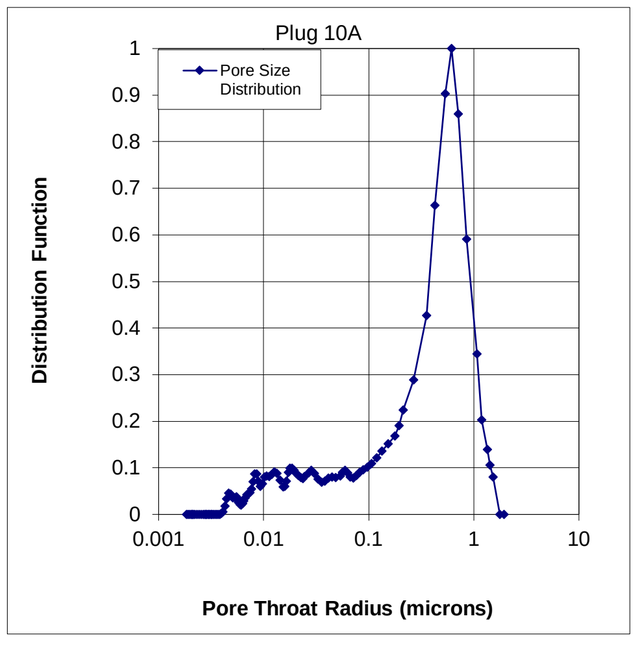

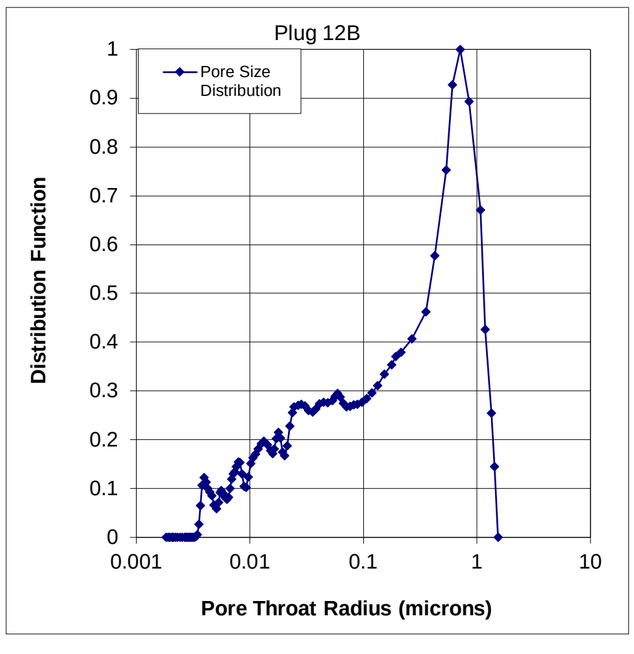

Skagerrak formation

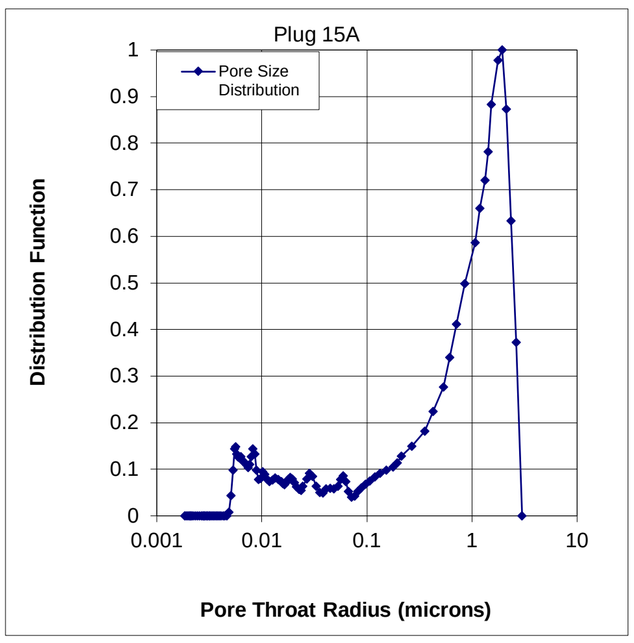

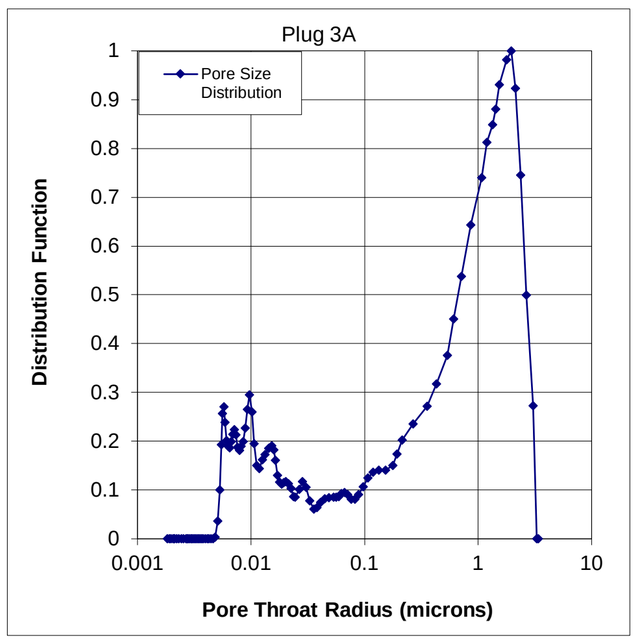

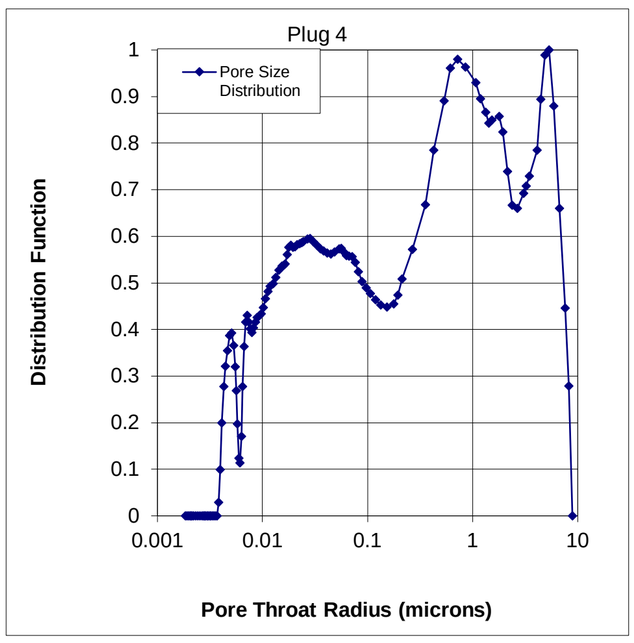

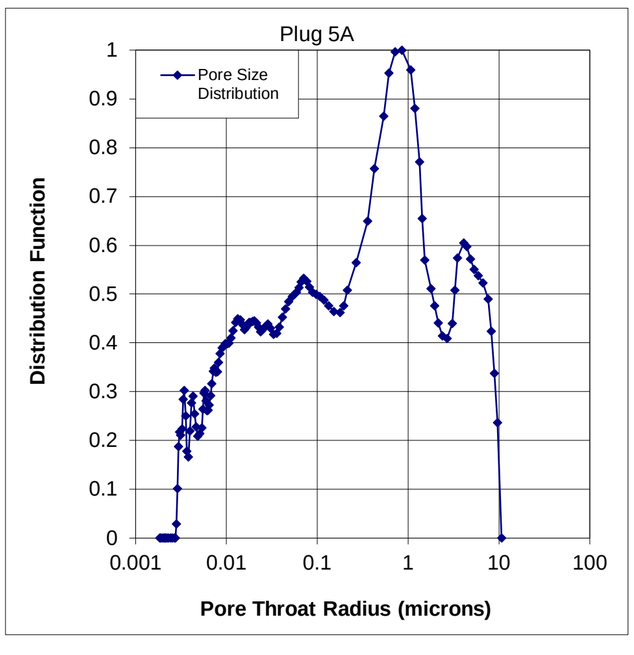

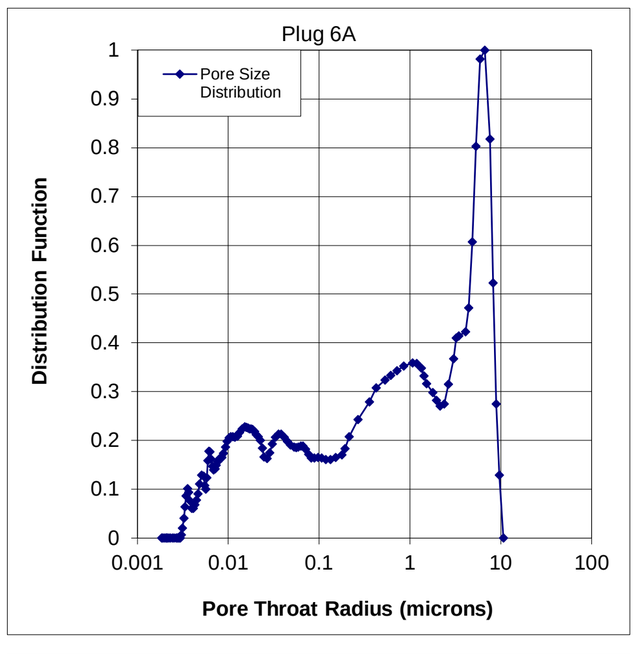

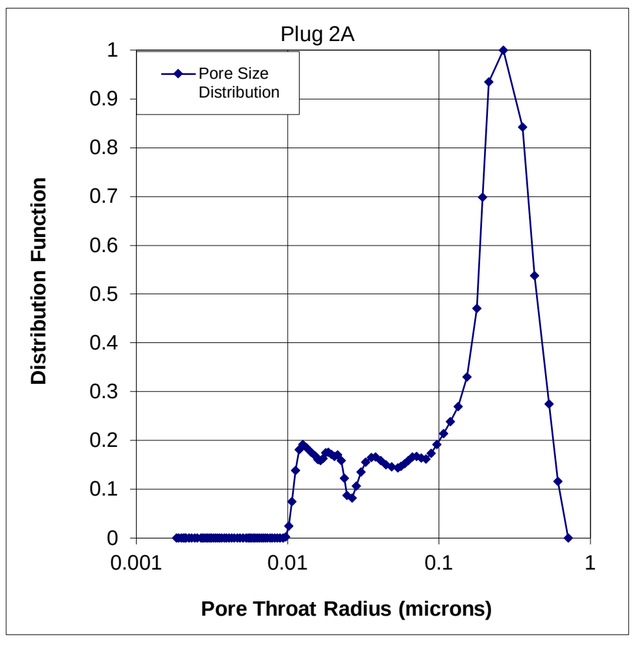

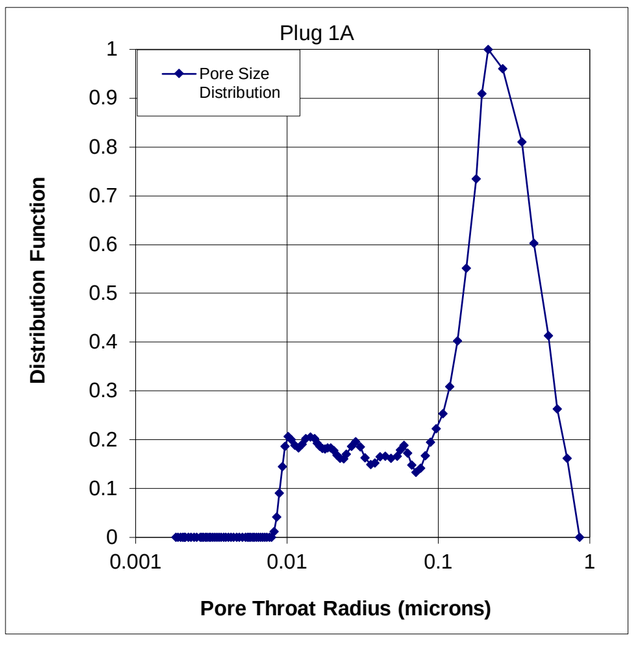

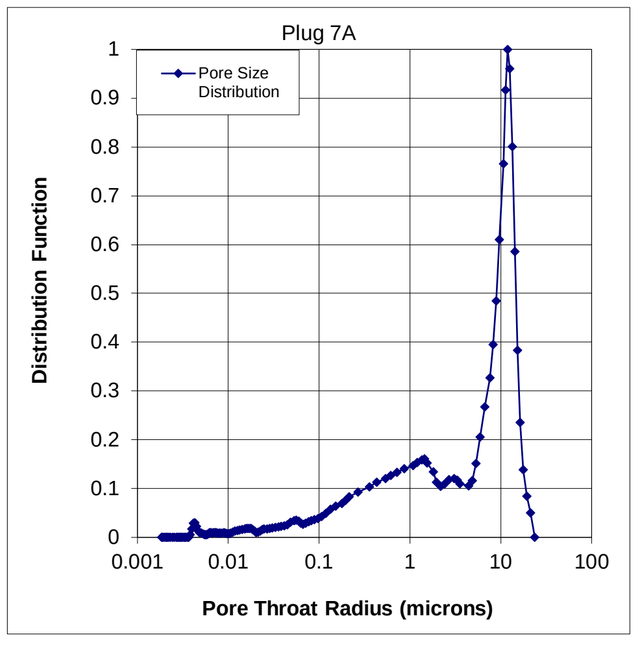

Appendix F

BET results

Plug 8A

Quantachrome® ASiQwin™- Automated Gas Sorption Data Acquisition and Reduction
© 1994-2016, Quantachrome Instruments
version 5.0

Analysis Report
Operator: JCTR Date:2019/08/16 Operator: JCTR Date:2019/08/30
Sample ID: Hanne 8A Filename: 190816-03.qps
Sample Desc: Comment: _6 Point BET
Sample Weight: 3.4271 g Instrument: Autosorb iQ Station 1
Approx. Outgas Time:3.1 hrs Final Outgas Temp.:60 °C Extended info: Available
Analysis gas: Nitrogen Non-ideality: 6.58e-05 1/Torr CellType: 9mm
Analysis Time: 0:15 hr:min Bath temp.: 77.35 K
Analysis Mode: Standard VoidVol Remeasure:off
VoidVol. Mode: He Measure Cold Zone V: 4.34912 cc Warm Zone V: 7.27308 cc
Data Reduction Parameters
Thermal Transpiration: onEff. mol. diameter (D): 3.54 ÅEff. cell stem diam. (d): 4.0000 mm

Adsorbate modelNitrogen Temperature 77.350K
Molec. Wt.: 28.013 Cross Section: 16.200 Å² Liquid Density: 0.806 g/cc

Relative Pressure P/Po	Volume @ STP cc/g	1 / [W((Po/P) - 1)] 1/g
4.98355e-02	0.2061	2.0359e+02
1.02405e-01	0.2408	3.7906e+02
1.52624e-01	0.2699	5.3396e+02
2.02686e-01	0.2981	6.8221e+02
2.52613e-01	0.3274	8.2612e+02
3.02437e-01	0.3577	9.6969e+02

BET summary
Slope = 3017.071 1/g
Intercept = 6.478e+01 1/g
Correlation coefficient, r = 0.999592
C constant= 47.573

Surface Area = 1.130 m²/g

Plug 9C

Quantachrome® ASiQwin™- Automated Gas Sorption Data Acquisition and Reduction
© 1994-2016, Quantachrome Instruments
version 5.0

Analysis Report
Operator: JCTR Date:2019/08/19 Operator: JCTR Date:2019/08/30
Sample ID: Hanne 9C Filename: 190819-02.qps
Sample Desc: Comment: _6 Point BET
Sample Weight: 2.7547 g Instrument: Autosorb iQ Station 1
Approx. Outgas Time:3.1 hrs Final Outgas Temp.:60 °C Extended info: Available
Analysis gas: Nitrogen Non-ideality: 6.58e-05 1/Torr CellType: 9mm
Analysis Time: 0:19 hr:min Bath temp.: 77.35 K
Analysis Mode: Standard VoidVol Remeasure:off
VoidVol. Mode: He Measure Cold Zone V: 4.9351 cc Warm Zone V: 7.32006 cc
Data Reduction Parameters
Thermal Transpiration: onEff. mol. diameter (D): 3.54 ÅEff. cell stem diam. (d): 4.0000 mm

Adsorbate modelNitrogen Temperature 77.350K
Molec. Wt.: 28.013 Cross Section: 16.200 Å² Liquid Density: 0.806 g/cc

Relative Pressure P/Po	Volume @ STP cc/g	1 / [W((Po/P) - 1)] 1/g
5.27506e-02	0.1628	2.7363e+02
1.02913e-01	0.1939	4.7329e+02
1.53380e-01	0.2219	6.5323e+02
2.03133e-01	0.2492	8.1852e+02
2.53591e-01	0.2769	9.8188e+02
3.03056e-01	0.3043	1.1434e+03

BET summary
Slope = 3445.071 1/g
Intercept = 1.103e+02 1/g
Correlation coefficient, r = 0.999219
C constant= 32.234

Surface Area = 0.980 m²/g

Plug 11A

Quantachrome® ASiQwin™- Automated Gas Sorption Data Acquisition and Reduction
© 1994-2016, Quantachrome Instruments
version 5.0

Analysis Report
Operator: JCTR Date:2019/08/20 Operator: JCTR Date:2019/08/30
Sample ID: Hanne 11A Filename: 190820-01.qps
Sample Desc: Comment: _6 Point BET
Sample Weight: 3.9543 g Instrument: Autosorb iQ Station 1
Approx. Outgas Time:3.1 hrs Final Outgas Temp.:60 °C Extended info: Available
Analysis gas: Nitrogen Non-ideality: 6.58e-05 1/Torr CellType: 9mm
Analysis Time: 0:19 hr:min Bath temp.: 77.35 K
Analysis Mode: Standard VoidVol Remeasure:off
VoidVol. Mode: He Measure Cold Zone V: 4.39656 cc Warm Zone V: 7.36788 cc
Data Reduction Parameters
Thermal Transpiration: onEff. mol. diameter (D): 3.54 ÅEff. cell stem diam. (d): 4.0000 mm

Adsorbate modelNitrogen Temperature 77.350K
Molec. Wt.: 28.013 Cross Section: 16.200 Å² Liquid Density: 0.806 g/cc

Relative Pressure P/Po	Volume @ STP cc/g	1 / [W((Po/P) - 1)] 1/g
4.85240e-02	0.2791	1.4619e+02
1.01063e-01	0.3208	2.8040e+02
1.51919e-01	0.3565	4.0198e+02
2.01899e-01	0.3914	5.1708e+02
2.54518e-01	0.4318	6.3265e+02
3.01184e-01	0.4689	7.3550e+02

BET summary
Slope = 2322.664 1/g
Intercept = 4.231e+01 1/g
Correlation coefficient, r = 0.999566
C constant= 55.895

Surface Area = 1.473 m²/g

Plug 13A

Quantachrome® ASiQwin™- Automated Gas Sorption Data Acquisition and Reduction
© 1994-2016, Quantachrome Instruments
version 5.0

Analysis Report
Operator: JCTR Date:2019/08/19 Operator: JCTR Date:2019/08/30
Sample ID: Hanne 13A Filename: 190819-01.qps
Sample Desc: Comment: _6 Point BET
Sample Weight: 4.9174 g Instrument: Autosorb iQ Station 1
Approx. Outgas Time:3.1 hrs Final Outgas Temp.:60 °C Extended info: Available
Analysis gas: Nitrogen Non-ideality: 6.58e-05 1/Torr CellType: 9mm
Analysis Time: 0:18 hr:min Bath temp.: 77.35 K
Analysis Mode: Standard VoidVol Remeasure:off
VoidVol. Mode: He Measure Cold Zone V: 4.06296 cc Warm Zone V: 7.31225 cc
Data Reduction Parameters
Thermal Transpiration: onEff. mol. diameter (D): 3.54 ÅEff. cell stem diam. (d): 4.0000 mm

Adsorbate modelNitrogen Temperature 77.350K
Molec. Wt.: 28.013 Cross Section: 16.200 Å² Liquid Density: 0.806 g/cc

Relative Pressure P/Po	Volume @ STP cc/g	1 / [W((Po/P) - 1)] 1/g
4.60972e-02	0.6071	6.3690e+01
1.02988e-01	0.7036	1.3057e+02
1.46952e-01	0.7688	1.7929e+02
1.96165e-01	0.8403	2.3236e+02
2.53438e-01	0.9290	2.9238e+02
2.96324e-01	0.9973	3.3783e+02

BET summary
Slope = 1090.112 1/g
Intercept = 1.671e+01 1/g
Correlation coefficient, r = 0.999749
C constant= 66.238

Surface Area = 3.146 m²/g

Plug 14A

Quantachrome® ASiQwin™- Automated Gas Sorption Data Acquisition and Reduction
© 1994-2016, Quantachrome Instruments
version 5.0

Analysis Report
Operator: JCTR Date:2019/08/16 Operator: JCTR Date:2019/08/30
Sample ID: hanne 14A Filename: 190816-02.qps
Sample Desc: Comment: _6 Point BET
Sample Weight: 5.5717 g Instrument: Autosorb iQ Station 1
Approx. Outgas Time:3.1 hrs Final Outgas Temp.:60 °C Extended info: Available
Analysis gas: Nitrogen Non-ideality: 6.58e-05 1/Torr CellType: 9mm
Analysis Time: 0:15 hr:min Bath temp.: 77.35 K
Analysis Mode: Standard VoidVol Remeasure:off
VoidVol. Mode: He Measure Cold Zone V: 3.84693 cc Warm Zone V: 7.33488 cc
Data Reduction Parameters
Thermal Transpiration: onEff. mol. diameter (D): 3.54 ÅEff. cell stem diam. (d): 4.0000 mm

Adsorbate modelNitrogen Temperature 77.350K
Molec. Wt.: 28.013 Cross Section: 16.200 Å² Liquid Density: 0.806 g/cc

Relative Pressure P/Po	Volume @ STP cc/g	1 / [W((Po/P) - 1)] 1/g
4.83974e-02	0.1627	2.5016e+02
1.02144e-01	0.1857	4.9014e+02
1.52508e-01	0.2053	7.0145e+02
2.02537e-01	0.2250	9.0323e+02
2.52040e-01	0.2465	1.0936e+03
3.01747e-01	0.2699	1.2810e+03

BET summary
Slope = 4058.624 1/g
Intercept = 7.000e+01 1/g
Correlation coefficient, r = 0.999480
C constant= 58.980

Surface Area = 0.844 m²/g

Plug 21B

Quantachrome® ASiQwin™- Automated Gas Sorption Data Acquisition and Reduction
© 1994-2016, Quantachrome Instruments
version 5.0

Analysis Report
Operator: JCTR Date:2019/08/20 Operator: JCTR Date:2019/08/30
Sample ID: Hanne 21B Filename: 190820-02.qps
Sample Desc: Comment: _6 Point BET
Sample Weight: 4.5176 g Instrument: Autosorb iQ Station 1
Approx. Outgas Time:3.1 hrs Final Outgas Temp.:60 °C Extended info: Available
Analysis gas: Nitrogen Non-ideality: 6.58e-05 1/Torr CellType: 9mm
Analysis Time: 0:18 hr:min Bath temp.: 77.35 K
Analysis Mode: Standard VoidVol Remeasure:off
VoidVol. Mode: He Measure Cold Zone V: 4.26784 cc Warm Zone V: 7.33177 cc
Data Reduction Parameters
Thermal Transpiration: onEff. mol. diameter (D): 3.54 ÅEff. cell stem diam. (d): 4.0000 mm

Adsorbate modelNitrogen Temperature 77.350K
Molec. Wt.: 28.013 Cross Section: 16.200 Å² Liquid Density: 0.806 g/cc

Relative Pressure P/Po	Volume @ STP cc/g	1 / [W((Po/P) - 1)] 1/g
4.61883e-02	0.5159	7.5104e+01
9.77317e-02	0.5876	1.4750e+02
1.48120e-01	0.6494	2.1423e+02
1.98372e-01	0.7106	2.7862e+02
2.47806e-01	0.7754	3.3996e+02
2.97585e-01	0.8438	4.0172e+02

BET summary
Slope = 1294.635 1/g
Intercept = 1.936e+01 1/g
Correlation coefficient, r = 0.999709
C constant= 67.878

Surface Area = 2.650 m²/g

Plug 22B

Quantachrome® ASiQwin™- Automated Gas Sorption Data Acquisition and Reduction
© 1994-2016, Quantachrome Instruments
version 5.0

Analysis Report
Operator: JCTR Date:2019/08/21 Operator: JCTR Date:2019/08/30
Sample ID: Hanne 22B Filename: 190821-01.qps
Sample Desc: Comment: _6 Point BET
Sample Weight: 5.3718 g Instrument: Autosorb iQ Station 1
Approx. Outgas Time:3.1 hrs Final Outgas Temp.:60 °C Extended info: Available
Analysis gas: Nitrogen Non-ideality: 6.58e-05 1/Torr CellType: 9mm
Analysis Time: 0:16 hr:min Bath temp.: 77.35 K
Analysis Mode: Standard VoidVol Remeasure:off
VoidVol. Mode: He Measure Cold Zone V: 3.61221 cc Warm Zone V: 7.26797 cc
Data Reduction Parameters
Thermal Transpiration: onEff. mol. diameter (D): 3.54 ÅEff. cell stem diam. (d): 4.0000 mm

Adsorbate modelNitrogen Temperature 77.350K
Molec. Wt.: 28.013 Cross Section: 16.200 Å² Liquid Density: 0.806 g/cc

Relative Pressure P/Po	Volume @ STP cc/g	1 / [W((Po/P) - 1)] 1/g
5.06745e-02	0.0336	1.2730e+03
1.04581e-01	0.0419	2.2313e+03
1.54569e-01	0.0480	3.0495e+03
2.04649e-01	0.0538	3.8251e+03
2.54637e-01	0.0594	4.6004e+03
3.04583e-01	0.0658	5.3244e+03

BET summary
Slope = 15906.491 1/g
Intercept = 5.375e+02 1/g
Correlation coefficient, r = 0.999413
C constant= 30.594

Surface Area = 0.212 m²/g

Plug 10A

Quantachrome® ASiQwin™- Automated Gas Sorption Data Acquisition and Reduction
© 1994-2016, Quantachrome Instruments
version 5.0

Analysis Report
Operator: JCTR Date:2019/08/21 Operator: JCTR Date:2019/08/30
Sample ID: Hanne 10A Filename: 190821-03.qps
Sample Desc: Comment: _6 Point BET
Sample Weight: 4.8704 g Instrument: Autosorb iQ Station 1
Approx. Outgas Time:3.1 hrs Final Outgas Temp.:60 °C Extended info: Available
Analysis gas: Nitrogen Non-ideality: 6.58e-05 1/Torr CellType: 9mm
Analysis Time: 0:15 hr:min Bath temp.: 77.35 K
Analysis Mode: Standard VoidVol Remeasure:off
VoidVol. Mode: He Measure Cold Zone V: 4.14584 cc Warm Zone V: 7.30542 cc
Data Reduction Parameters
Thermal Transpiration: onEff. mol. diameter (D): 3.54 ÅEff. cell stem diam. (d): 4.0000 mm

Adsorbate modelNitrogen Temperature 77.350K
Molec. Wt.: 28.013 Cross Section: 16.200 Å² Liquid Density: 0.806 g/cc

Relative Pressure P/Po	Volume @ STP cc/g	1 / [W((Po/P) - 1)] 1/g
4.65025e-02	0.2128	1.8341e+02
1.01440e-01	0.2448	3.6898e+02
1.51966e-01	0.2708	5.2947e+02
2.01837e-01	0.2970	6.8115e+02
2.51683e-01	0.3250	8.2794e+02
3.01313e-01	0.3548	9.7263e+02

BET summary
Slope = 3086.379 1/g
Intercept = 5.137e+01 1/g
Correlation coefficient, r = 0.999583
C constant= 61.076

Surface Area = 1.110 m²/g

Plug 12B

Quantachrome® ASiQwin™- Automated Gas Sorption Data Acquisition and Reduction
© 1994-2016, Quantachrome Instruments
version 5.0

Analysis Report
Operator: JCTR Date:2019/08/21 Operator: JCTR Date:2019/08/30
Sample ID: Hanne 12B Filename: 190821-02.qps
Sample Desc: Comment: _6 Point BET
Sample Weight: 4.9333 g Instrument: Autosorb iQ Station 1
Approx. Outgas Time:3.1 hrs Final Outgas Temp.:60 °C Extended info: Available
Analysis gas: Nitrogen Non-ideality: 6.58e-05 1/Torr CellType: 9mm
Analysis Time: 0:20 hr:min Bath temp.: 77.35 K
Analysis Mode: Standard VoidVol Remeasure:off
VoidVol. Mode: He Measure Cold Zone V: 4.011 cc Warm Zone V: 7.34817 cc
Data Reduction Parameters
Thermal Transpiration: onEff. mol. diameter (D): 3.54 ÅEff. cell stem diam. (d): 4.0000 mm

Adsorbate modelNitrogen Temperature 77.350K
Molec. Wt.: 28.013 Cross Section: 16.200 Å² Liquid Density: 0.806 g/cc

Relative Pressure P/Po	Volume @ STP cc/g	1 / [W((Po/P) - 1)] 1/g
4.90171e-02	0.6056	6.8102e+01
9.65815e-02	0.6824	1.2535e+02
1.46590e-01	0.7533	1.8244e+02
1.96418e-01	0.8223	2.3784e+02
2.46752e-01	0.8967	2.9230e+02
3.03465e-01	0.9840	3.5426e+02

BET summary
Slope = 1120.548 1/g
Intercept = 1.604e+01 1/g
Correlation coefficient, r = 0.999821
C constant= 70.863

Surface Area = 3.064 m²/g

Plug 15A

Quantachrome® ASiQwin™- Automated Gas Sorption Data Acquisition and Reduction
© 1994-2016, Quantachrome Instruments
version 5.0

Analysis Report
Operator: JCTR Date:2019/08/01 Operator: JCTR Date:2019/08/30
Sample ID: Hanne 15A Filename: 190801-01.qps
Sample Desc: Comment: _6 Point BET
Sample Weight: 4.088 g Instrument: Autosorb iQ Station 1
Approx. Outgas Time:1.1 hrs Final Outgas Temp.:350 °C Extended info: Available
Analysis gas: Nitrogen Non-ideality: 6.58e-05 1/Torr CellType: 9mm
Analysis Time: 0:25 hr:min Bath temp.: 77.35 K
Analysis Mode: Standard VoidVol Remeasure:off
VoidVol. Mode: He Measure Cold Zone V: 4.19542 cc Warm Zone V: 7.23271 cc
Data Reduction Parameters
Thermal Transpiration: onEff. mol. diameter (D): 3.54 ÅEff. cell stem diam. (d): 4.0000 mm

Adsorbate modelNitrogen Temperature 77.350K
Molec. Wt.: 28.013 Cross Section: 16.200 Å² Liquid Density: 0.806 g/cc

Relative Pressure P/Po	Volume @ STP cc/g	1 / [W((Po/P) - 1)] 1/g
5.17601e-02	1.1584	3.7703e+01
1.01566e-01	1.2879	7.0233e+01
1.52920e-01	1.4014	1.0307e+02
1.96126e-01	1.4889	1.3111e+02
2.52464e-01	1.6063	1.6822e+02
3.03344e-01	1.7147	2.0318e+02

BET summary
Slope = 655.482 1/g
Intercept = 3.317e+00 1/g
Correlation coefficient, r = 0.999933
C constant= 198.622

Surface Area = 5.286 m²/g

Plug 3A

Quantachrome® ASiQwin™- Automated Gas Sorption Data
Acquisition and Reduction
© 1994-2016, Quantachrome Instruments
version 5.0

Analysis Report
Operator: JCTR Date:2019/08/02 Operator: JCTR Date:2019/08/30
Sample ID: Hanne 3A Filename: 190802-02.qps
Sample Desc: Comment: _6 Point BET
Sample Weight: 4.0322 g Instrument: Autosorb iQ Station 1
Approx. Outgas Time:1.1 hrs Final Outgas Temp.:350 °C Extended info: Available
Analysis gas: Nitrogen Non-ideality: 6.58e-05 1/Torr CellType: 9mm
Analysis Time: 0:41 hr:min Bath temp.: 77.35 K
Analysis Mode: Standard VoidVol Remeasure:off
VoidVol. Mode: He Measure Cold Zone V: 4.40776 cc Warm Zone V: 7.35245 cc
Data Reduction Parameters
Thermal Transpiration: onEff. mol. diameter (D): 3.54 ÅEff. cell stem diam. (d): 4.0000 mm

Adsorbate modelNitrogen Temperature 77.350K
Molec. Wt.: 28.013 Cross Section: 16.200 Å² Liquid Density: 0.806 g/cc

Relative Pressure P/Po	Volume @ STP cc/g	1 / [W((Po/P) - 1)] 1/g
5.04944e-02	1.1256	3.7803e+01
1.00585e-01	1.2614	7.0936e+01
1.52916e-01	1.3772	1.0488e+02
1.96265e-01	1.4634	1.3351e+02
2.53266e-01	1.5781	1.7196e+02
2.96787e-01	1.6614	2.0326e+02

BET summary
Slope = 668.719 1/g
Intercept = 3.331e+00 1/g
Correlation coefficient, r = 0.999872
C constant= 201.786

Surface Area = 5.182 m²/g

Plug 4

Quantachrome® ASiQwin™- Automated Gas Sorption Data
Acquisition and Reduction
© 1994-2016, Quantachrome Instruments
version 5.0

Analysis Report
Operator: JCTR Date:2019/07/30 Operator: JCTR Date:2019/08/30
Sample ID: Hanne 4 Filename: 190730-02.qps
Sample Desc: Comment: _6 Point BET
Sample Weight: 2.4649 g Instrument: Autosorb iQ Station 1
Approx. Outgas Time:1.1 hrs Final Outgas Temp.:350 °C Extended info: Available
Analysis gas: Nitrogen Non-ideality: 6.58e-05 1/Torr CellType: 9mm
Analysis Time: 0:19 hr:min Bath temp.: 77.35 K
Analysis Mode: Standard VoidVol Remeasure:off
VoidVol. Mode: He Measure Cold Zone V: 5.09517 cc Warm Zone V: 7.24698 cc
Data Reduction Parameters
Thermal Transpiration: onEff. mol. diameter (D): 3.54 ÅEff. cell stem diam. (d): 4.0000 mm

Adsorbate modelNitrogen Temperature 77.350K
Molec. Wt.: 28.013 Cross Section: 16.200 Å² Liquid Density: 0.806 g/cc

Relative Pressure P/Po	Volume @ STP cc/g	1 / [W((Po/P) - 1)] 1/g
4.89181e-02	1.1224	3.6665e+01
9.61031e-02	1.2701	6.6979e+01
1.47029e-01	1.4061	9.8082e+01
1.97225e-01	1.5343	1.2812e+02
2.47008e-01	1.6669	1.5745e+02
2.96657e-01	1.8019	1.8728e+02

BET summary
Slope = 605.448 1/g
Intercept = 8.198e+00 1/g
Correlation coefficient, r = 0.999904
C constant= 74.854

Surface Area = 5.675 m²/g

Plug 5A

Quantachrome® ASiQwin™- Automated Gas Sorption Data
Acquisition and Reduction
© 1994-2016, Quantachrome Instruments
version 5.0

Analysis Report
Operator: JCTR Date:2019/08/02 Operator: JCTR Date:2019/08/30
Sample ID: Hanne 5A Filename: 190802-01.qps
Sample Desc: Comment: _6 Point BET
Sample Weight: 2.985 g Instrument: Autosorb iQ Station 1
Approx. Outgas Time:1.1 hrs Final Outgas Temp.:350 °C Extended info: Available
Analysis gas: Nitrogen Non-ideality: 6.58e-05 1/Torr CellType: 9mm
Analysis Time: 0:25 hr:min Bath temp.: 77.35 K
Analysis Mode: Standard VoidVol Remeasure:off
VoidVol. Mode: He Measure Cold Zone V: 4.79985 cc Warm Zone V: 7.38742 cc
Data Reduction Parameters
Thermal Transpiration: onEff. mol. diameter (D): 3.54 ÅEff. cell stem diam. (d): 4.0000 mm

Adsorbate modelNitrogen Temperature 77.350K
Molec. Wt.: 28.013 Cross Section: 16.200 Å² Liquid Density: 0.806 g/cc

Relative Pressure P/Po	Volume @ STP cc/g	1 / [W((Po/P) - 1)] 1/g
4.92032e-02	1.2131	3.4130e+01
1.02218e-01	1.3884	6.5612e+01
1.53567e-01	1.5387	9.4341e+01
1.96500e-01	1.6543	1.1828e+02
2.52663e-01	1.8107	1.4939e+02
2.96525e-01	1.9344	1.7435e+02

BET summary
Slope = 564.167 1/g
Intercept = 7.225e+00 1/g
Correlation coefficient, r = 0.999938
C constant= 79.084

Surface Area = 6.095 m²/g

Plug 6A

Quantachrome® ASiQwin™- Automated Gas Sorption Data
Acquisition and Reduction
© 1994-2016, Quantachrome Instruments
version 5.0

Analysis Report
Operator: JCTR Date:2019/07/30 Operator: JCTR Date:2019/08/30
Sample ID: Hanne 6A Filename: 190730-01.qps
Sample Desc: Comment: _6 Point BET
Sample Weight: 1.4684 g Instrument: Autosorb iQ Station 1
Approx. Outgas Time:1.1 hrs Final Outgas Temp.:350 °C Extended info: Available
Analysis gas: Nitrogen Non-ideality: 6.58e-05 1/Torr CellType: 9mm
Analysis Time: 0:18 hr:min Bath temp.: 77.35 K
Analysis Mode: Standard VoidVol Remeasure:off
VoidVol. Mode: He Measure Cold Zone V: 5.41121 cc Warm Zone V: 7.38467 cc
Data Reduction Parameters
Thermal Transpiration: onEff. mol. diameter (D): 3.54 ÅEff. cell stem diam. (d): 4.0000 mm

Adsorbate modelNitrogen Temperature 77.350K
Molec. Wt.: 28.013 Cross Section: 16.200 Å² Liquid Density: 0.806 g/cc

Relative Pressure P/Po	Volume @ STP cc/g	1 / [W((Po/P) - 1)] 1/g
4.97488e-02	1.0473	3.9998e+01
9.95447e-02	1.2019	7.3591e+01
1.50122e-01	1.3405	1.0544e+02
2.00080e-01	1.4733	1.3583e+02
2.50124e-01	1.6061	1.6617e+02
2.99993e-01	1.7384	1.9725e+02

BET summary
Slope = 624.332 1/g
Intercept = 1.050e+01 1/g
Correlation coefficient, r = 0.999839
C constant= 60.486

Surface Area = 5.486 m²/g

Plug 2A

Quantachrome® ASiQwin™- Automated Gas Sorption Data
Acquisition and Reduction
© 1994-2016, Quantachrome Instruments
version 5.0

Analysis Report
Operator: JCTR Date:2019/08/16 Operator: JCTR Date:2019/08/30
Sample ID: Hanne 2A Filename: 190816-01.qps
Sample Desc: Comment: _6 Point BET
Sample Weight: 4.6011 g Instrument: Autosorb iQ Station 1
Approx. Outgas Time:3.1 hrs Final Outgas Temp.:60 °C Extended info: Available
Analysis gas: Nitrogen Non-ideality: 6.58e-05 1/Torr CellType: 9mm
Analysis Time: 0:20 hr:min Bath temp.: 77.35 K
Analysis Mode: Standard VoidVol Remeasure:off
VoidVol. Mode: He Measure Cold Zone V: 4.12445 cc Warm Zone V: 7.39515 cc
Data Reduction Parameters
Thermal Transpiration: onEff. mol. diameter (D): 3.54 ÅEff. cell stem diam. (d): 4.0000 mm

Adsorbate modelNitrogen Temperature 77.350K
Molec. Wt.: 28.013 Cross Section: 16.200 Å² Liquid Density: 0.806 g/cc

Relative Pressure P/Po	Volume @ STP cc/g	1 / [W((Po/P) - 1)] 1/g
4.72411e-02	0.5084	7.8034e+01
9.61993e-02	0.5888	1.4465e+02
1.47512e-01	0.6624	2.0902e+02
1.96929e-01	0.7316	2.6818e+02
2.47237e-01	0.8040	3.2683e+02
2.96644e-01	0.8757	3.8533e+02

BET summary
Slope = 1224.422 1/g
Intercept = 2.479e+01 1/g
Correlation coefficient, r = 0.999610
C constant= 50.395

Surface Area = 2.788 m²/g

Plug 1A

Quantachrome® ASiQwin™- Automated Gas Sorption Data
Acquisition and Reduction
© 1994-2016, Quantachrome Instruments
version 5.0

Analysis Report
Operator: JCTR Date:2019/08/15 Operator: JCTR Date:2019/08/30
Sample ID: Hanne 1A Filename: 190815-01.qps
Sample Desc: Comment: _6 Point BET
Sample Weight: 4.6636 g Instrument: Autosorb iQ Station 1
Approx. Outgas Time:3.1 hrs Final Outgas Temp.:60 °C Extended info: Available
Analysis gas: Nitrogen Non-ideality: 6.58e-05 1/Torr CellType: 9mm
Analysis Time: 0:19 hr:min Bath temp.: 77.35 K
Analysis Mode: Standard VoidVol Remeasure:off
VoidVol. Mode: He Measure Cold Zone V: 4.24346 cc Warm Zone V: 7.2795 cc

Data Reduction Parameters
Thermal Transpiration: onEff. mol. diameter (D): 3.54 ÅEff. cell stem diam. (d): 4.0000 mm

Adsorbate modelNitrogen Temperature 77.350K
Molec. Wt.: 28.013 Cross Section: 16.200 Å² Liquid Density: 0.806 g/cc

Relative Pressure P/Po	Volume @ STP cc/g	1 / [W((Po/P) - 1)] 1/g
5.25875e-02	0.6826	6.5065e+01
9.61797e-02	0.7593	1.1214e+02
1.53773e-01	0.8492	1.7121e+02
1.97219e-01	0.9149	2.1485e+02
2.53574e-01	1.0057	2.7028e+02
2.96562e-01	1.0758	3.1356e+02

BET summary
Slope = 1014.329 1/g
Intercept = 1.369e+01 1/g
Correlation coefficient, r = 0.999893
C constant= 75.075

Surface Area = 3.388 m²/g

Plug 7A

Quantachrome® ASiQwin™- Automated Gas Sorption Data
Acquisition and Reduction
© 1994-2016, Quantachrome Instruments
version 5.0

Analysis Report
Operator: JCTR Date:2019/08/13 Operator: JCTR Date:2019/08/30
Sample ID: hanne 7A Filename: 190813-01.qps
Sample Desc: Comment: _6 Point BET
Sample Weight: 2.9888 g Instrument: Autosorb iQ Station 1
Approx. Outgas Time:1.1 hrs Final Outgas Temp.:350 °C Extended info: Available
Analysis gas: Nitrogen Non-ideality: 6.58e-05 1/Torr CellType: 9mm
Analysis Time: 0:15 hr:min Bath temp.: 77.35 K
Analysis Mode: Standard VoidVol Remeasure:off
VoidVol. Mode: He Measure Cold Zone V: 5.01515 cc Warm Zone V: 7.1864 cc
Data Reduction Parameters
Thermal Transpiration: onEff. mol. diameter (D): 3.54 ÅEff. cell stem diam. (d): 4.0000 mm

Adsorbate modelNitrogen Temperature 77.350K
Molec. Wt.: 28.013 Cross Section: 16.200 Å² Liquid Density: 0.806 g/cc

Relative Pressure P/Po	Volume @ STP cc/g	1 / [W((Po/P) - 1)] 1/g
5.40728e-02	0.1603	2.8534e+02
1.03110e-01	0.1866	4.9302e+02
1.53165e-01	0.2098	6.8980e+02
2.03106e-01	0.2318	8.7986e+02
2.53359e-01	0.2537	1.0704e+03
3.02989e-01	0.2758	1.2613e+03

BET summary
Slope = 3896.992 1/g
Intercept = 8.510e+01 1/g
Correlation coefficient, r = 0.999815
C constant= 46.791

Surface Area = 0.875 m²/g

Appendix G

Water chemistry

Concentration of major ions in the effluent from the liquid permeability measurement

Brine

Plug	Formation	Cl mg/l	SO4 mg/l	Na mg/l	K mg/l	Ca mg/l	Mg mg/l
8C	Gassum	178101	205	71176	1874	32462	2354
9B	Gassum	177386	210	72177	1954	33127	2339
10	Gassum	173581	199	71872	1923	32717	2218
11B	Gassum	169264	193	69651	1868	31557	2136
12A	Gassum	159794	200	64100	1677	29548	2002
13B	Gassum	179616	224	70728	1870	32142	2176
14	Gassum	183911	215	72566	1949	33084	2319
16	Gassum	180355	211	70806	1894	32447	2249
20	Gassum	171042	204	67755	1757	30558	2136
21A	Gassum	173920	204	69406	1858	31634	2141
22A	Gassum	179990	255	70983	1881	32468	2259
1	Skagerrak	173492	220	56610	3026	34718	7637
3	Skagerrak	176848	230	56487	3085	34589	7565
4A	Skagerrak	181679	232	58590	3062	35777	7984
5	Skagerrak	182895	223	57242	3067	35048	7683
6	Skagerrak	185778	239	59798	3093	36766	7978
7B	Skagerrak	178062	219	59170	3063	36217	7888
15	Skagerrak	183135	236	57959	3042	35680	7762
Gassum brine		172923	250	70000	1800	32700	2300
Skagerrak brine		177697	270	57000	3000	36000	8100

Distilled water

Plug	Formation	Cl mg/l	SO4 mg/l	Na mg/l	K mg/l	Ca mg/l	Mg mg/l
8C	Gassum	92	0.329	35.1	0.69	16.8	0.442
9B	Gassum	34	0.209	11.4	0.331	5.62	0.145
10	Gassum	3315	5.25	1328	42.1	645	45.9
11B	Gassum	1673	5.69	711	26.0	328	23.5
12A-2	Gassum	1559	6.28	609	25.8	352	21.8
13B	Gassum	204	3.85	87.5	6.37	39.7	3.03
14	Gassum	193	1.08	29.6	1.46	17.6	1.27
16	Gassum	3871	5.99	1588	40.4	864	52.6
20	Gassum	591	1.23	238	5.65	114	8.31
21A-	Gassum	473	1.24	191	5.47	91.4	6.16
22A	Gassum	319	4.35	124	3.28	61.0	4.06
1	Skagerrak	2338	3.07	738	36.0	473	100
3	Skagerrak	1474	2.27	471	59.0	309	71.6
4A	Skagerrak	583	9.22	180	17.0	122	26.7
5	Skagerrak	1241	90.0	439	32.6	282	58.4
6	Skagerrak	968	128	351	52.6	251	43.1
7B	Skagerrak	299	0.654	100	6.42	61.2	12.6
15	Skagerrak	830	1.90	261	52.7	153	36.5

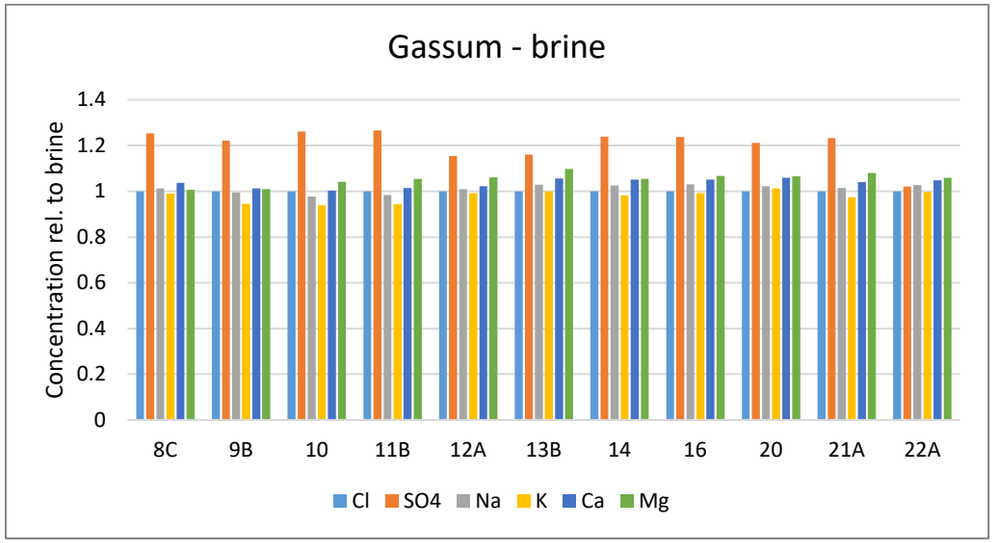
Gassum - brine
Concentration rel. to brine
1.4
1.2
1
0.8
0.6
0.4
0.2
0
8C
9B
10
11B
12A
13B
14
16
20
21A
22A
Cl
SO4
Na
K
Ca
Mg

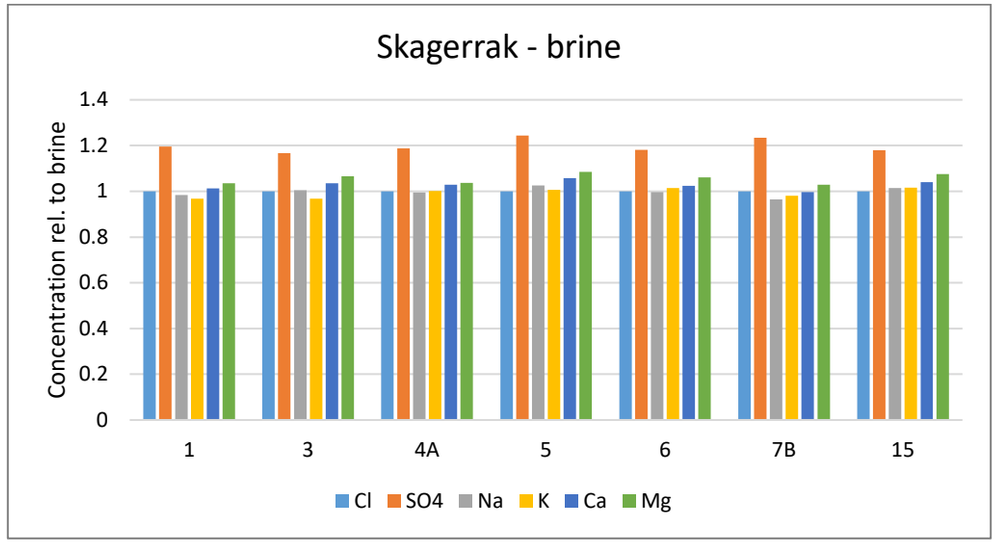
Skagerrak - brine
Concentration rel. to brine
1.4
1.2
1
0.8
0.6
0.4
0.2
0
1
3
4A
5
6
7B
15
Cl
SO4
Na
K
Ca
Mg

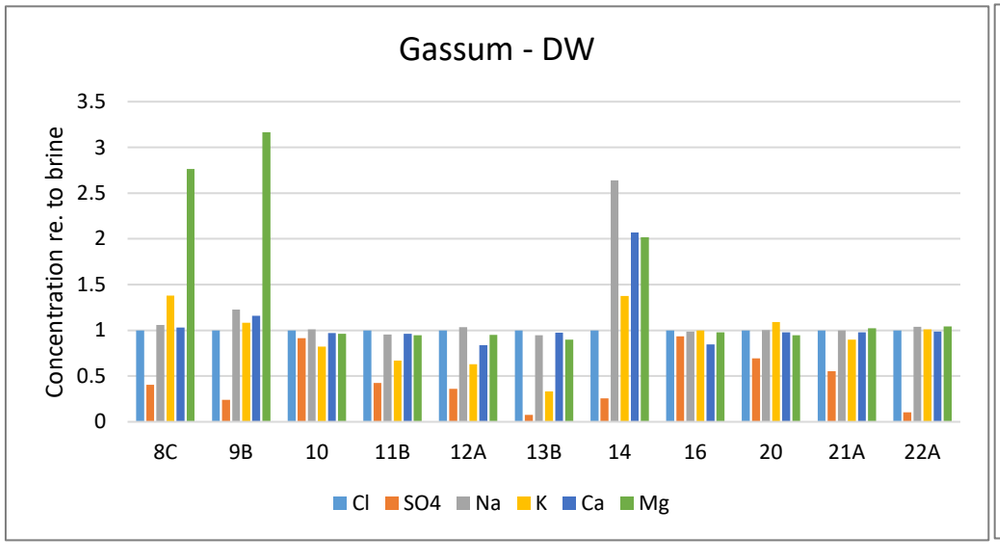
Gassum - DW
Concentration re. to brine
3.5
3
2.5
2
1.5
1
0.5
0
8C
9B
10
11B
12A
13B
14
16
20
21A
22A
Cl
SO4
Na
K
Ca
Mg

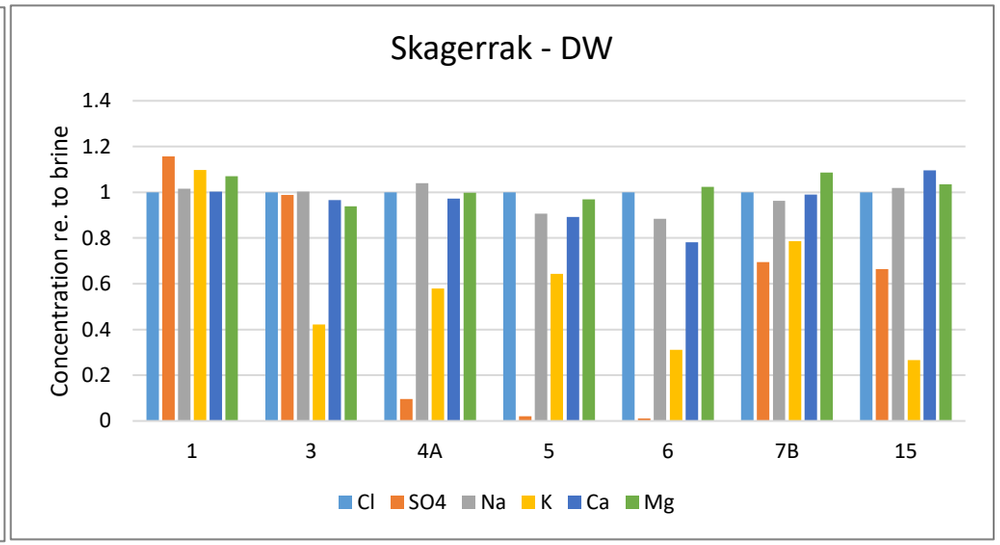
Skagerrak - DW
Concentration re. to brine
1.4
1.2
1
0.8
0.6
0.4
0.2
0
1
3
4A
5
6
7B
15
Cl
SO4
Na
K
Ca
Mg

Appendix H

Mineralogical overview

Aa1-Ga3352.22A plug 14

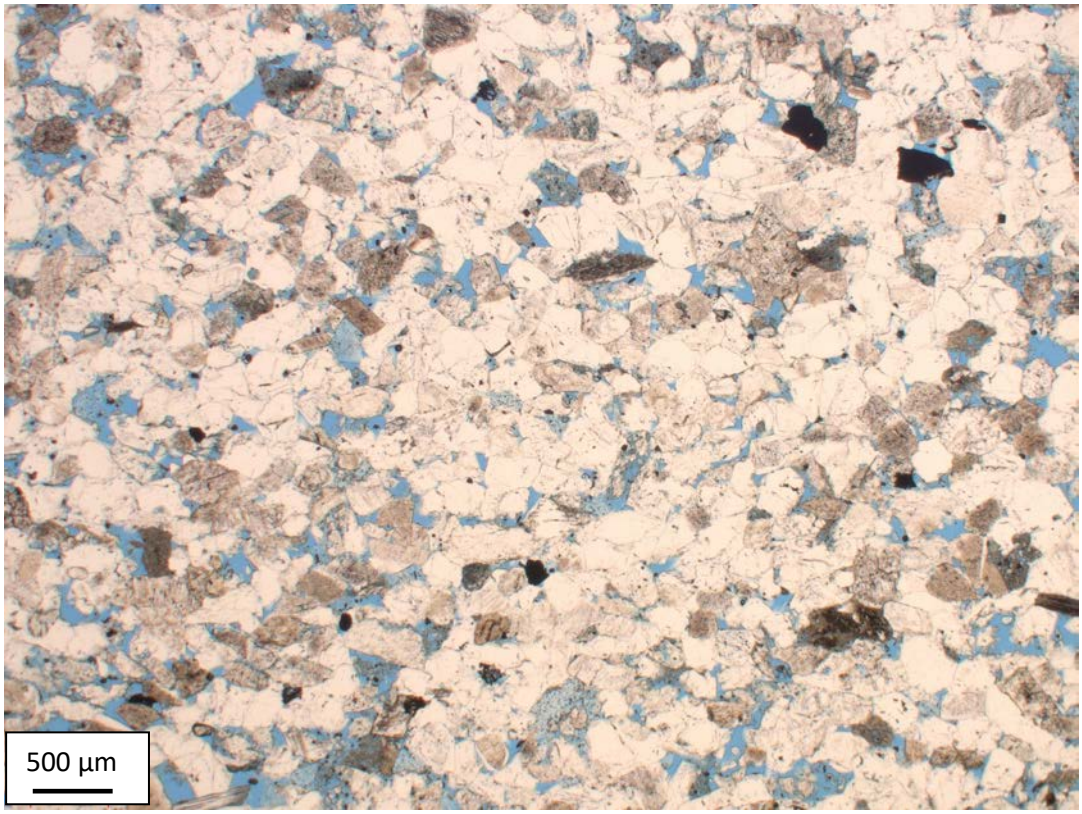

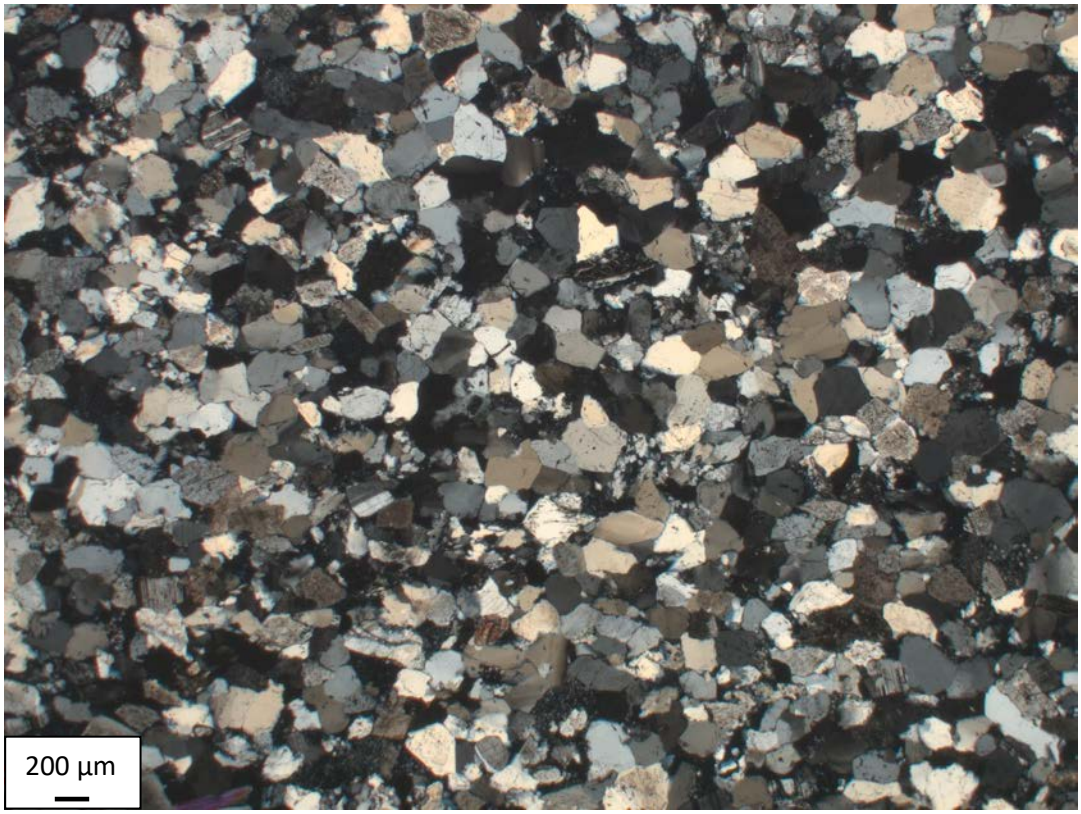

Aa1-Ga3353.05A plug 16

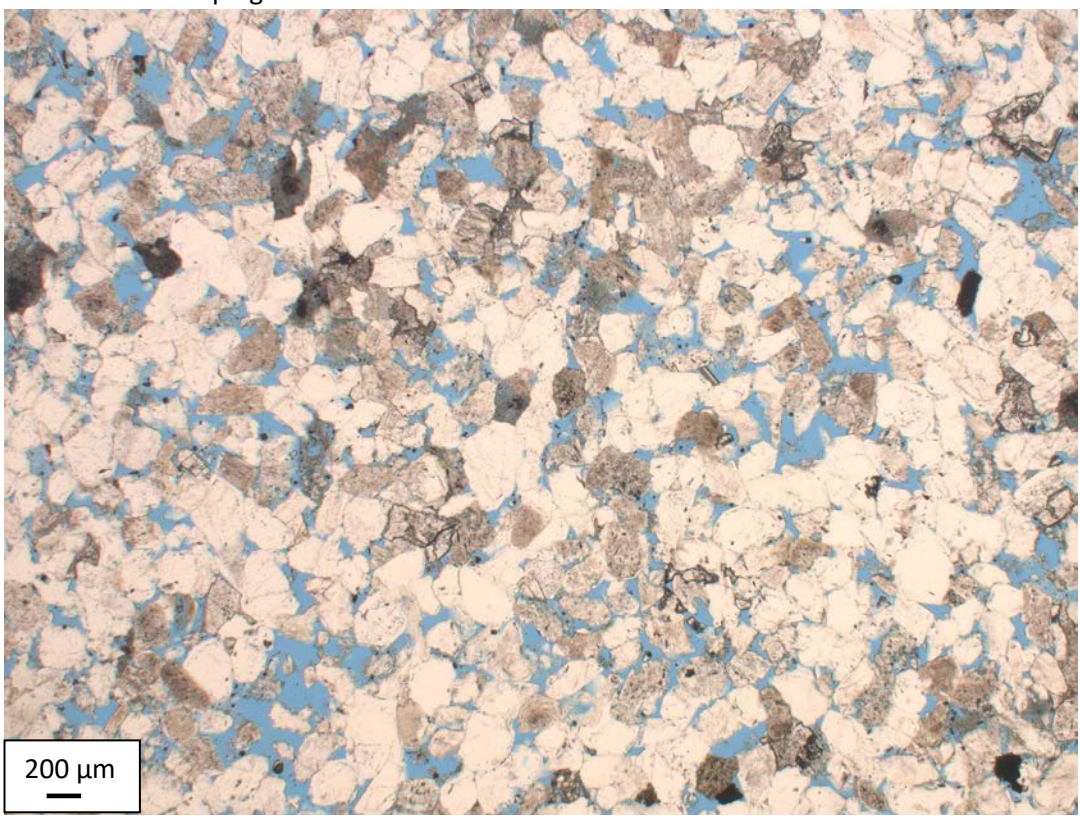

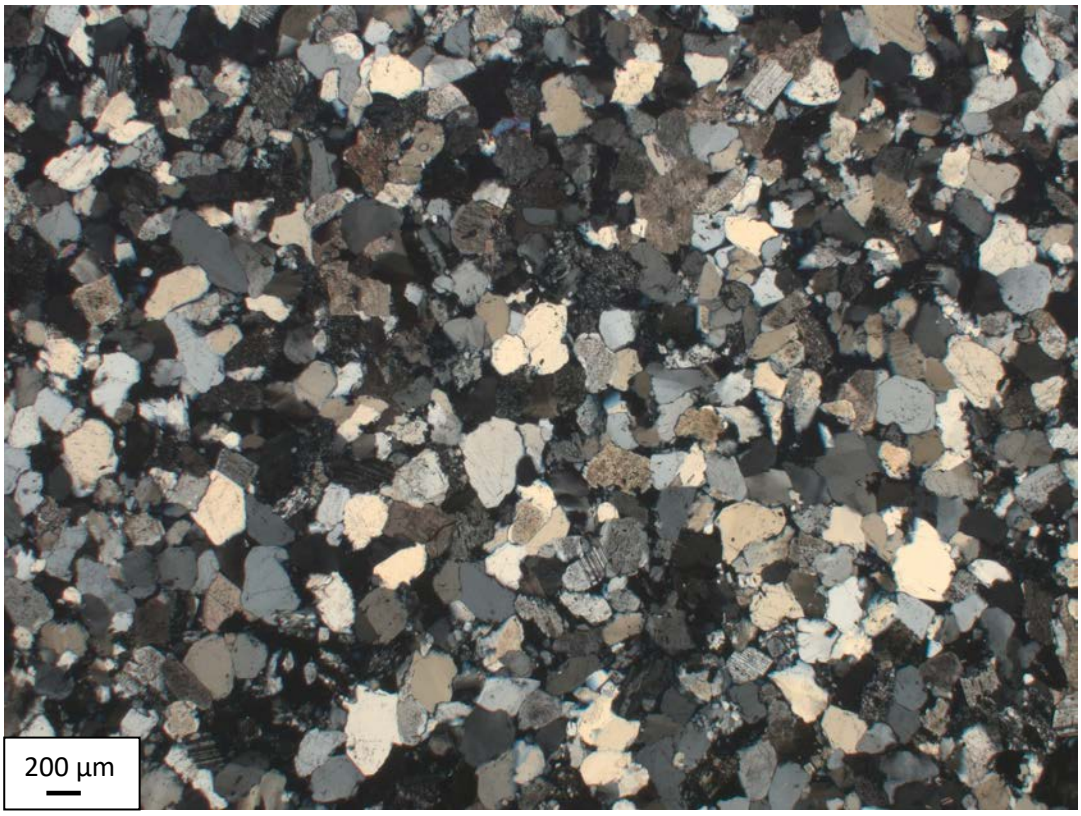

Ve1-Ga2009.96C plug 8C

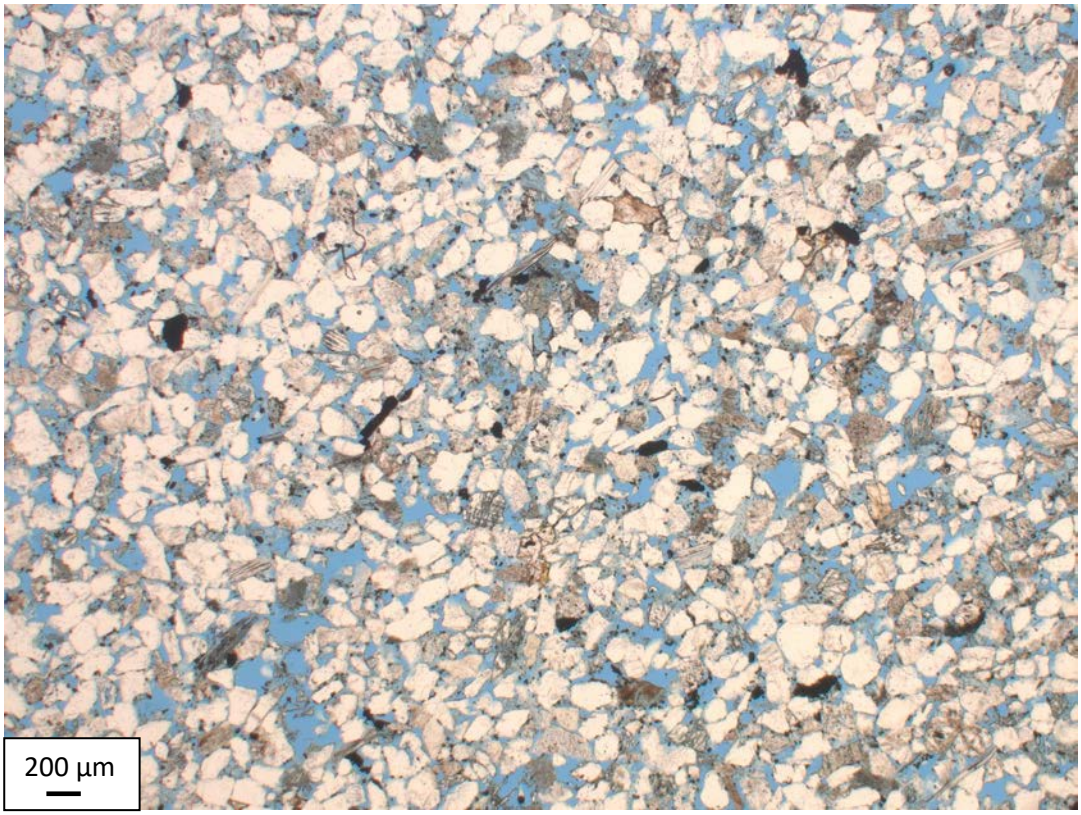

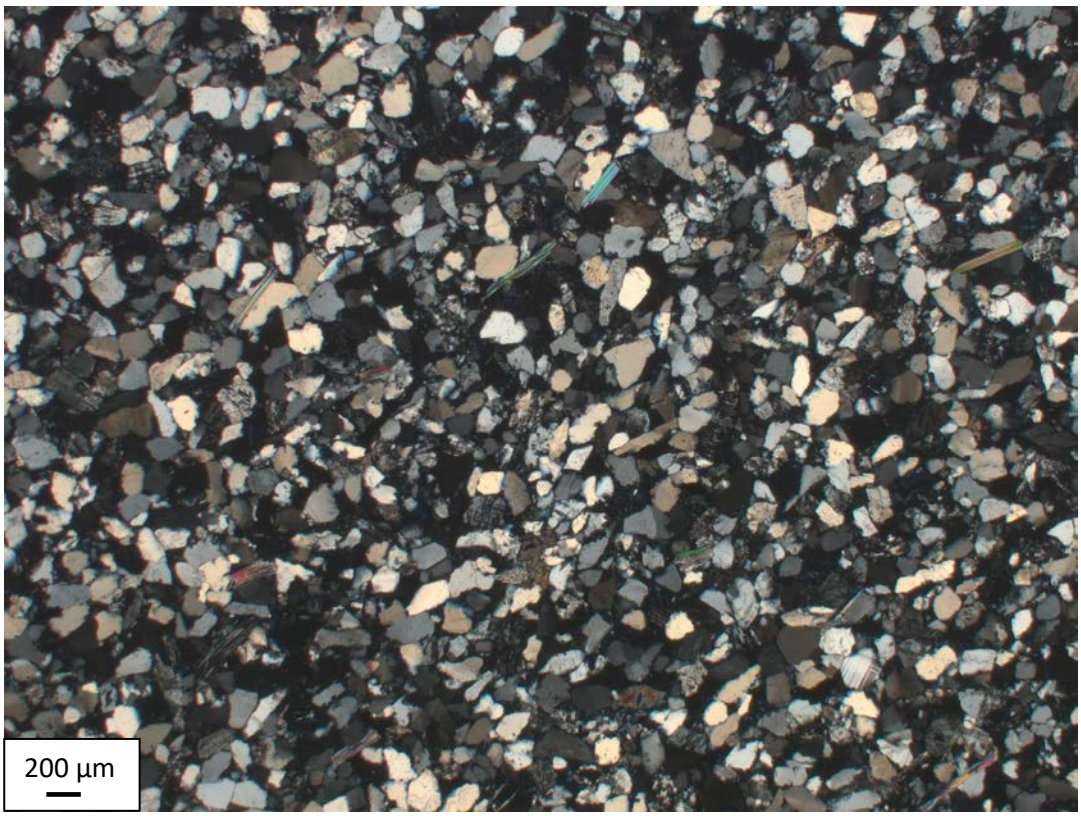

Aa1-Ga3326.49b Plug 13B

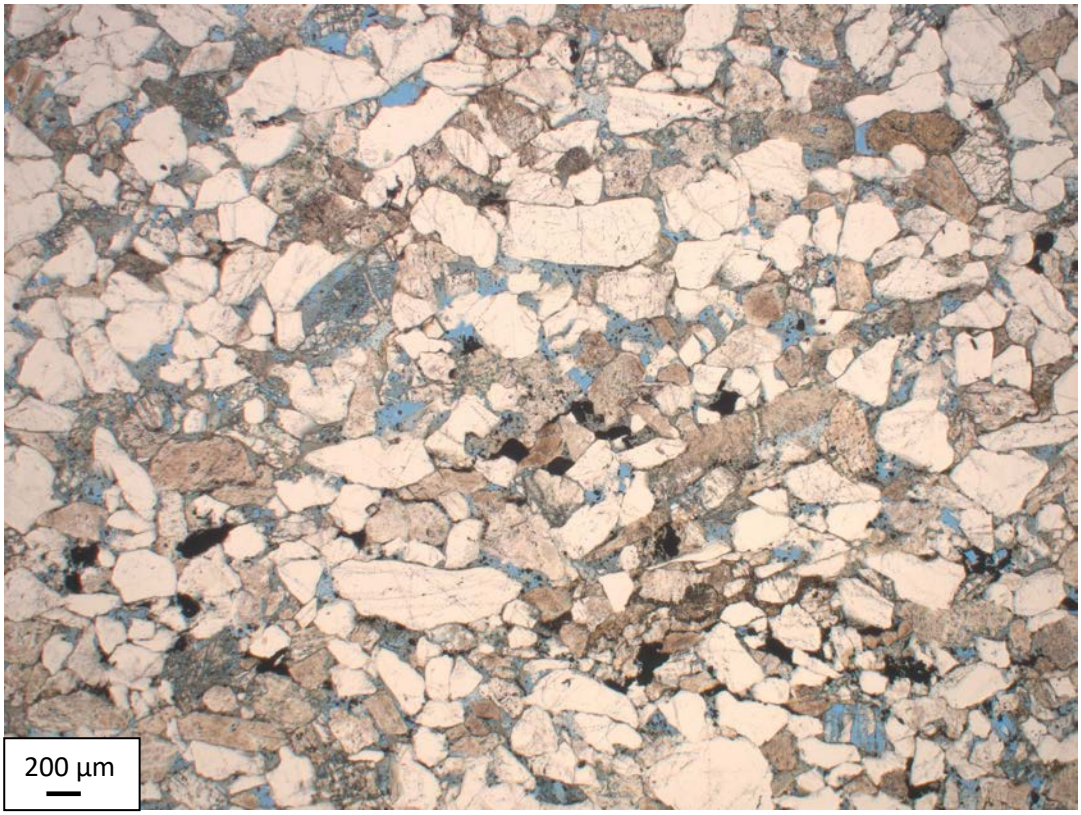

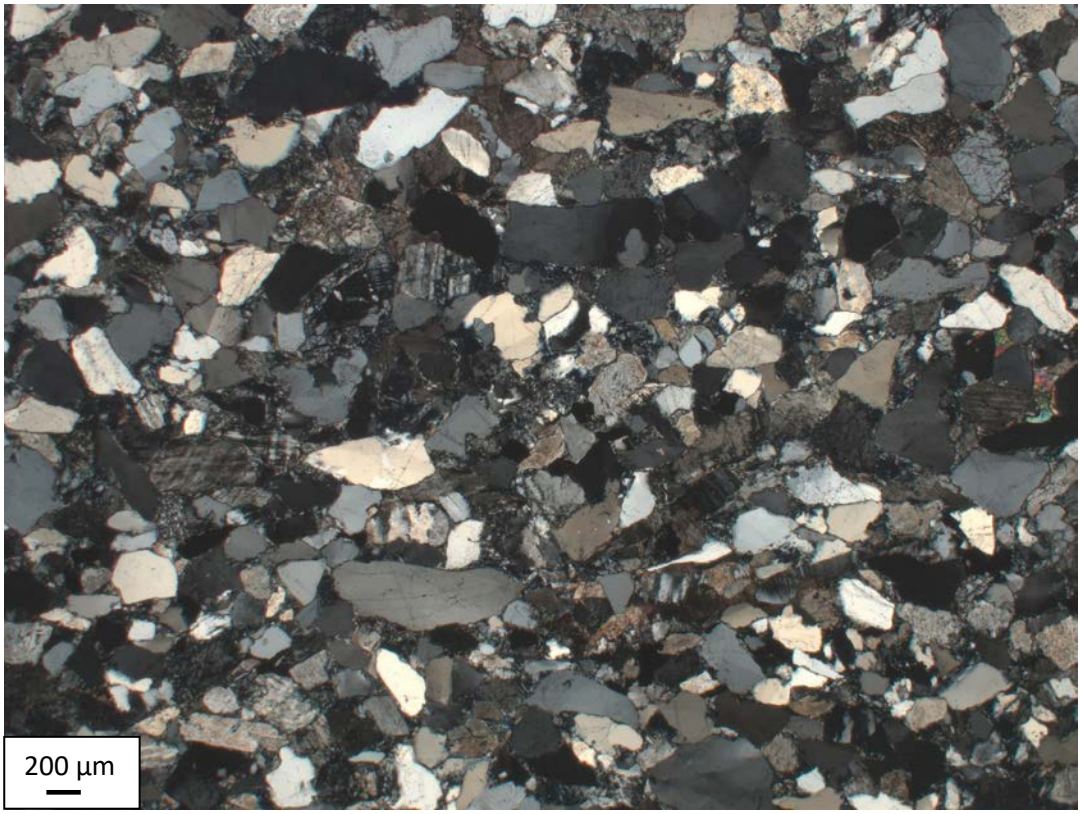

Aa1-Ga3325.03B Plug 11B

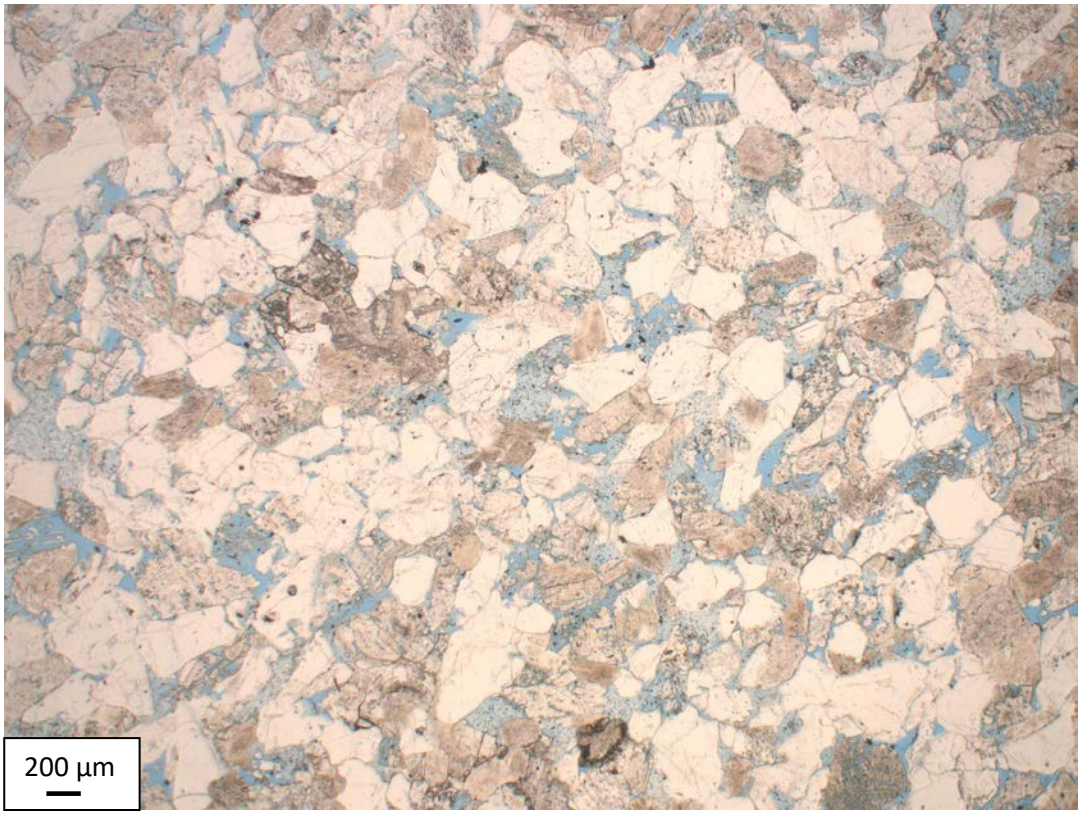

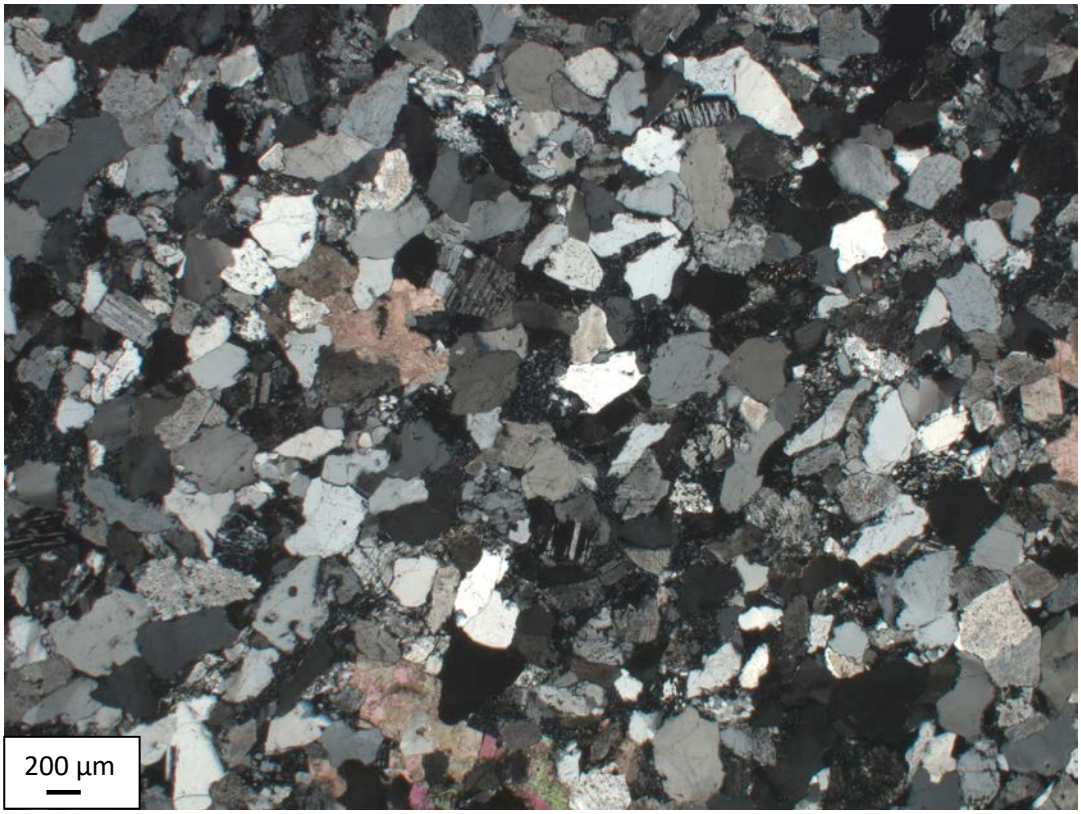

Aa1-Ga3318.20A Plug 20

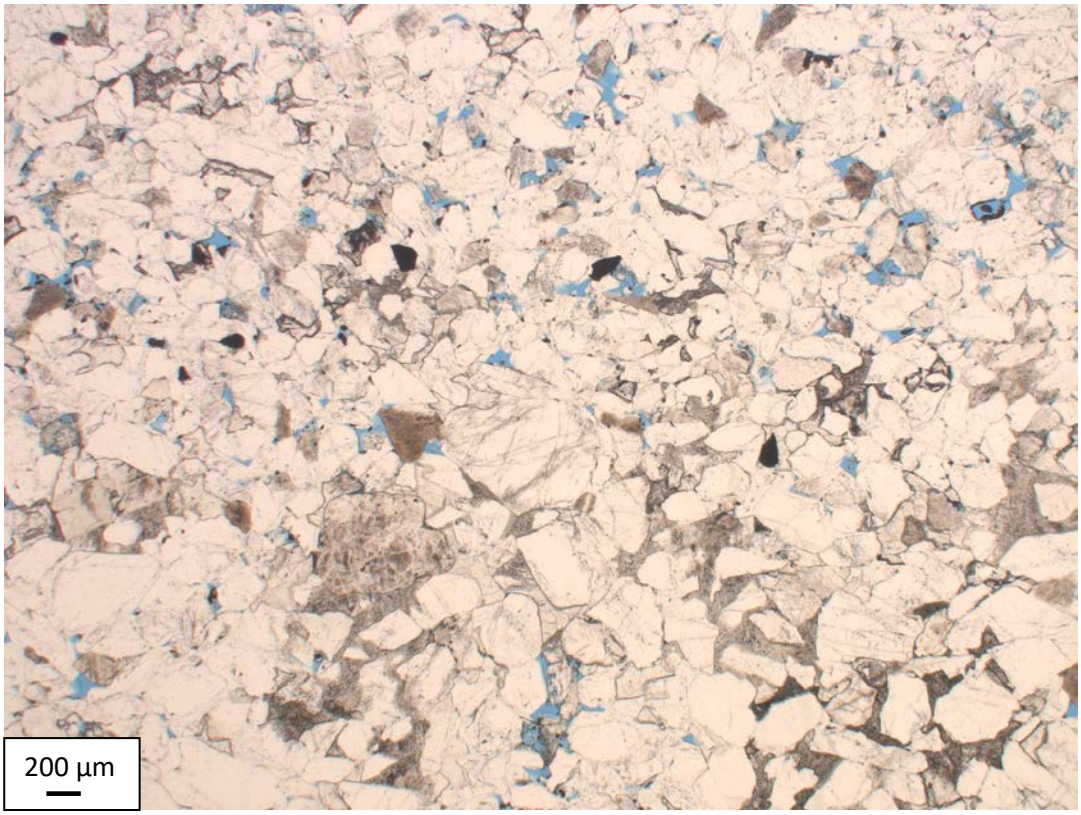

Aa1-Ga3320.80A Plug 21A

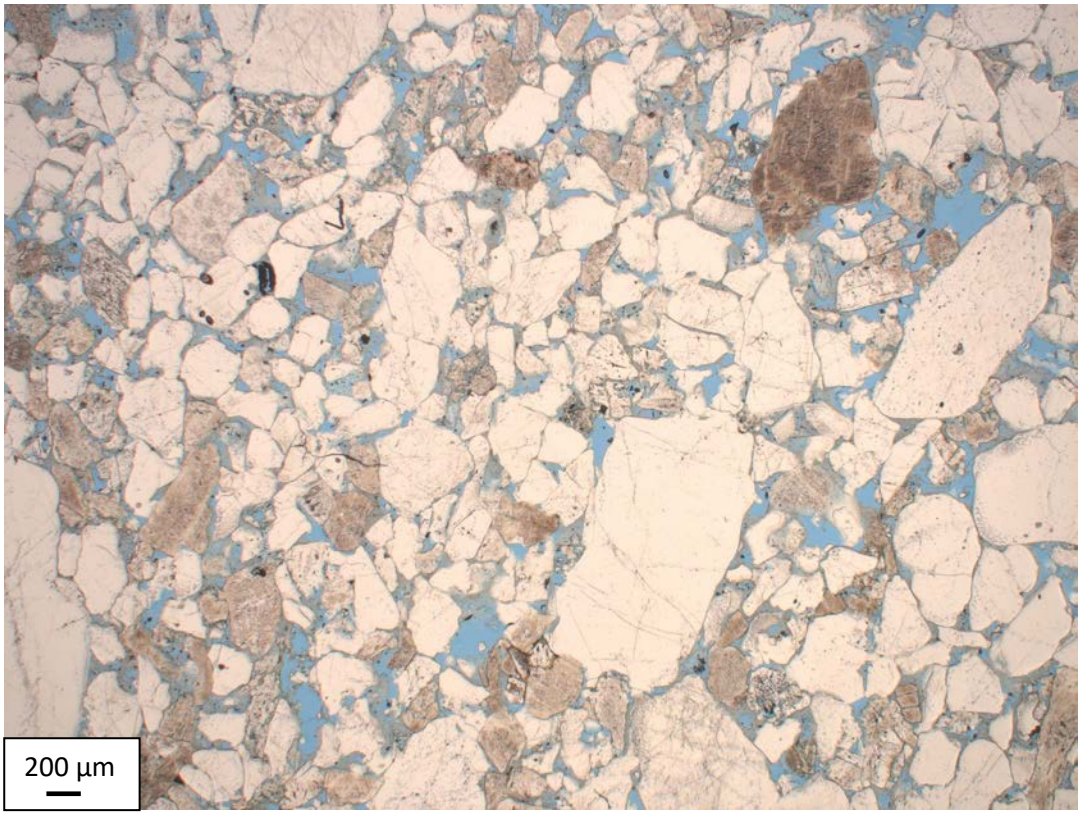

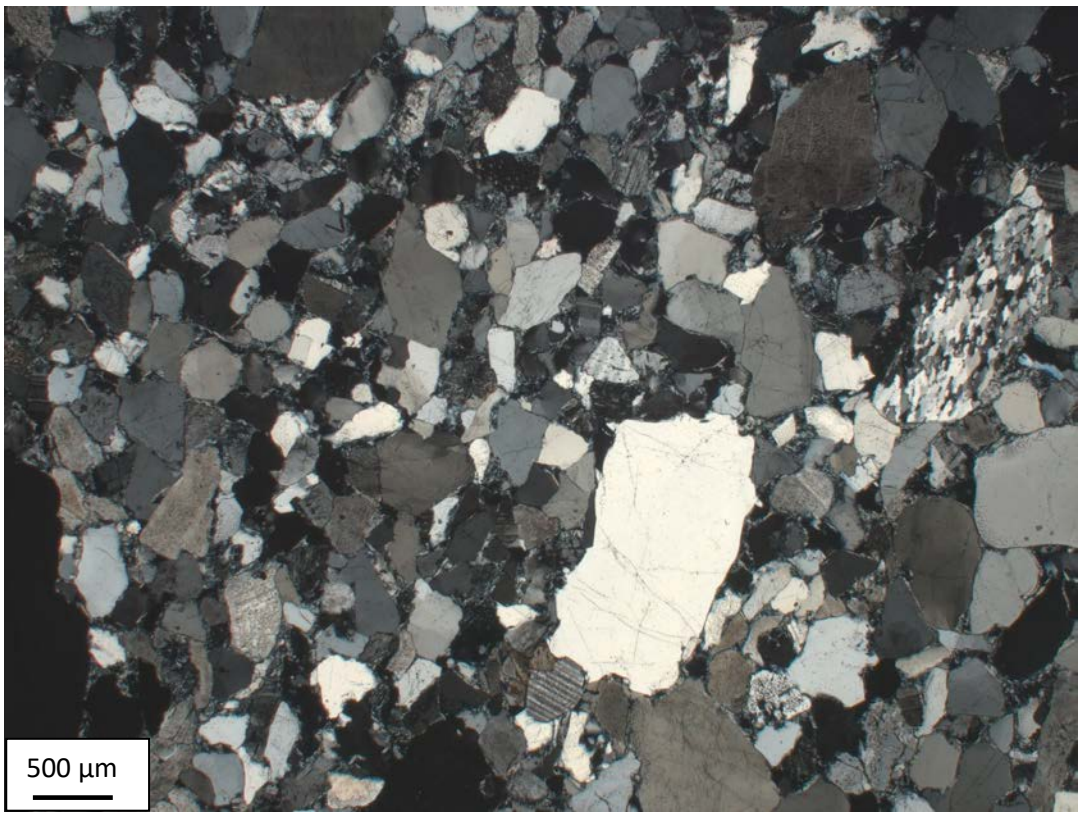

Aa1-Ga3275.38A Plug 22A

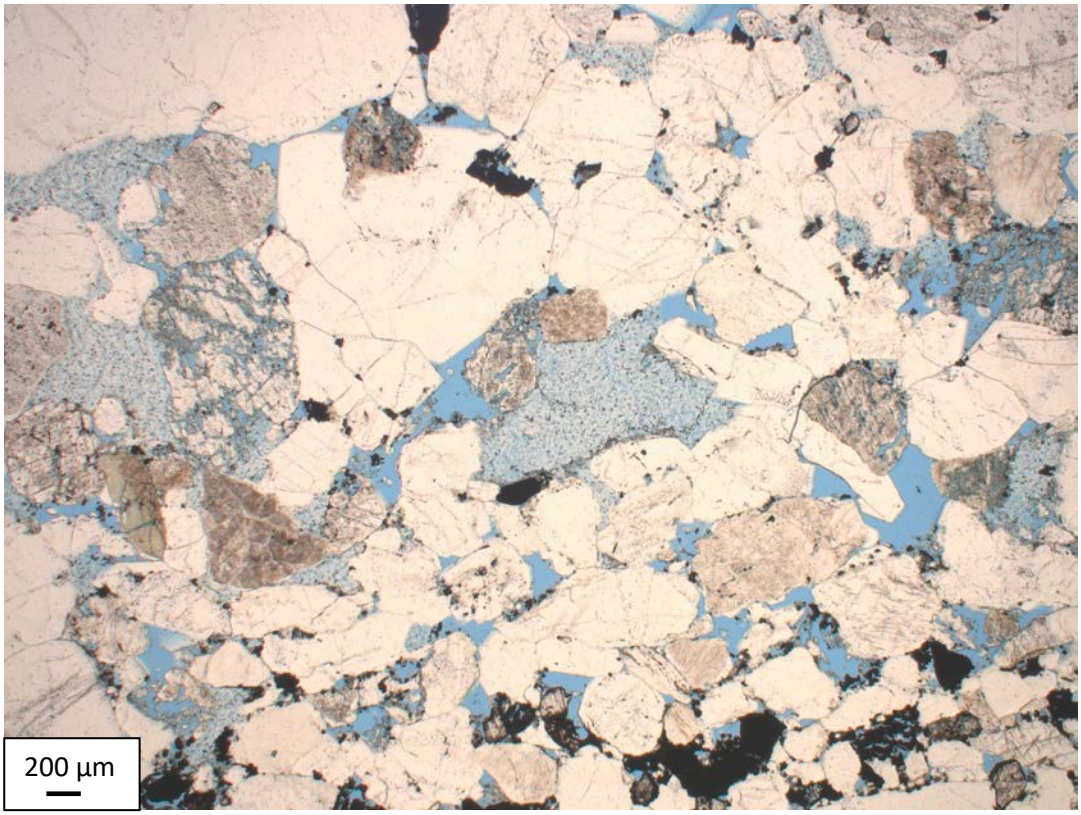

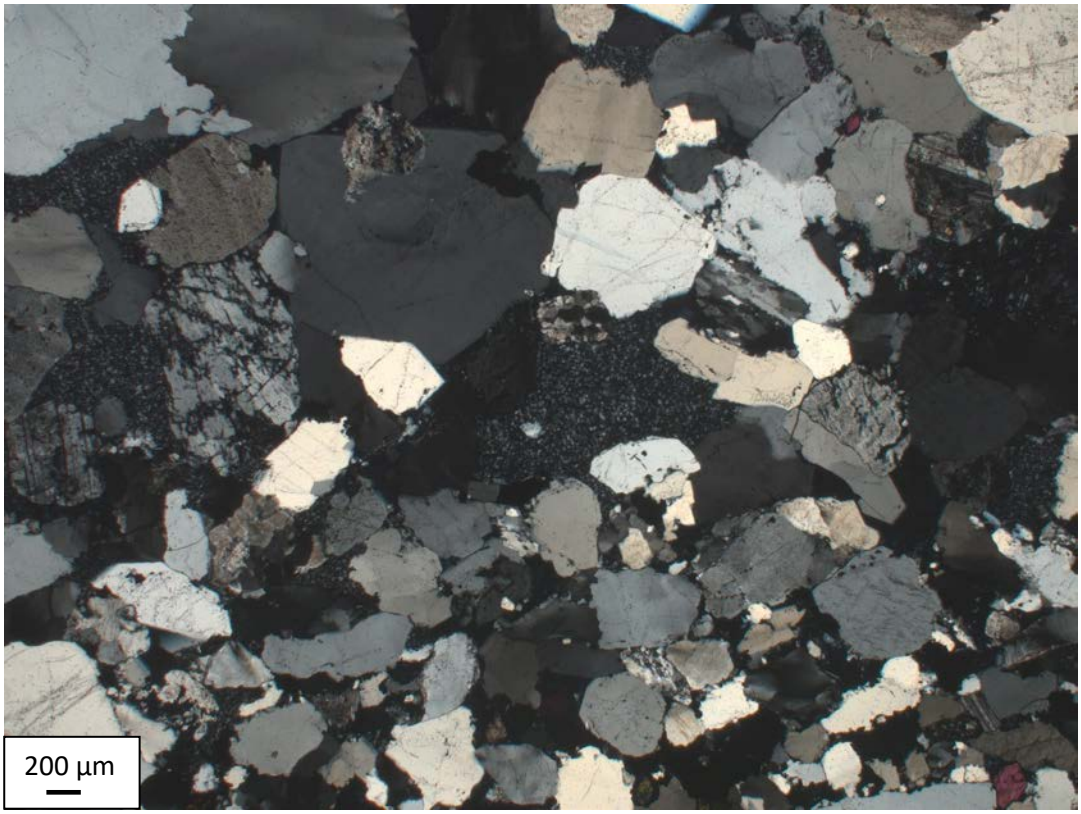

Aa1-Ga3325.52A Plug 12A

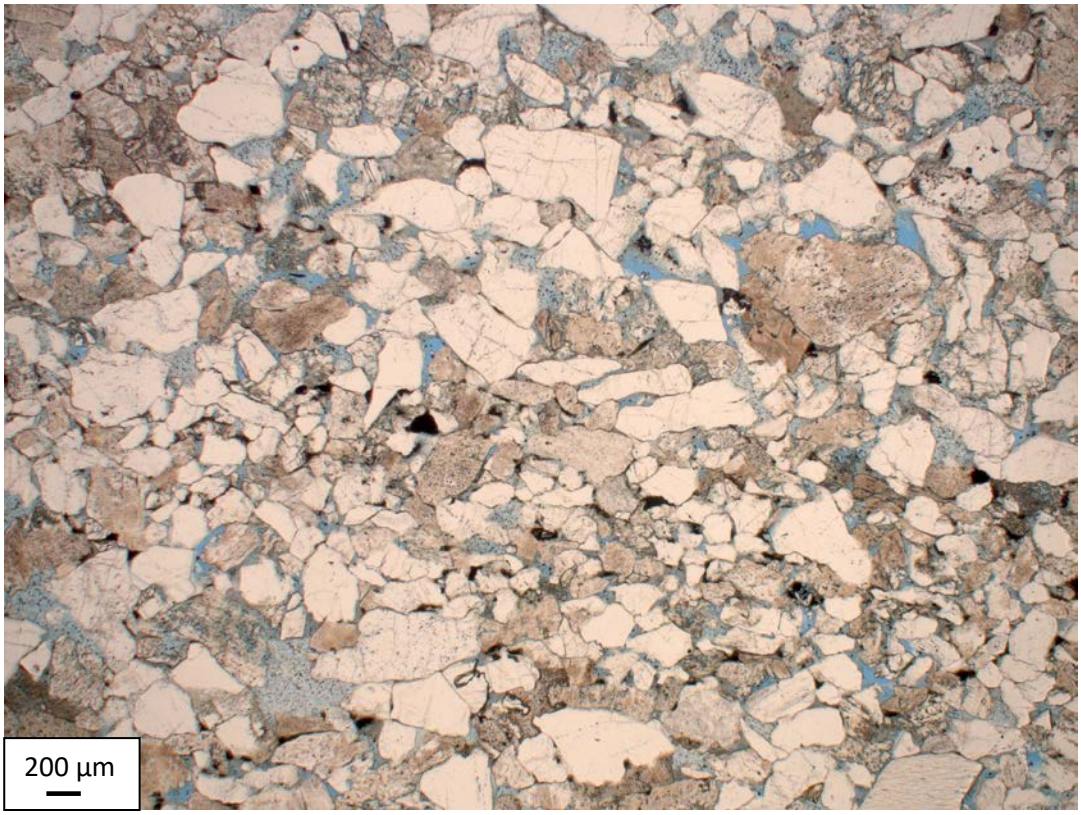

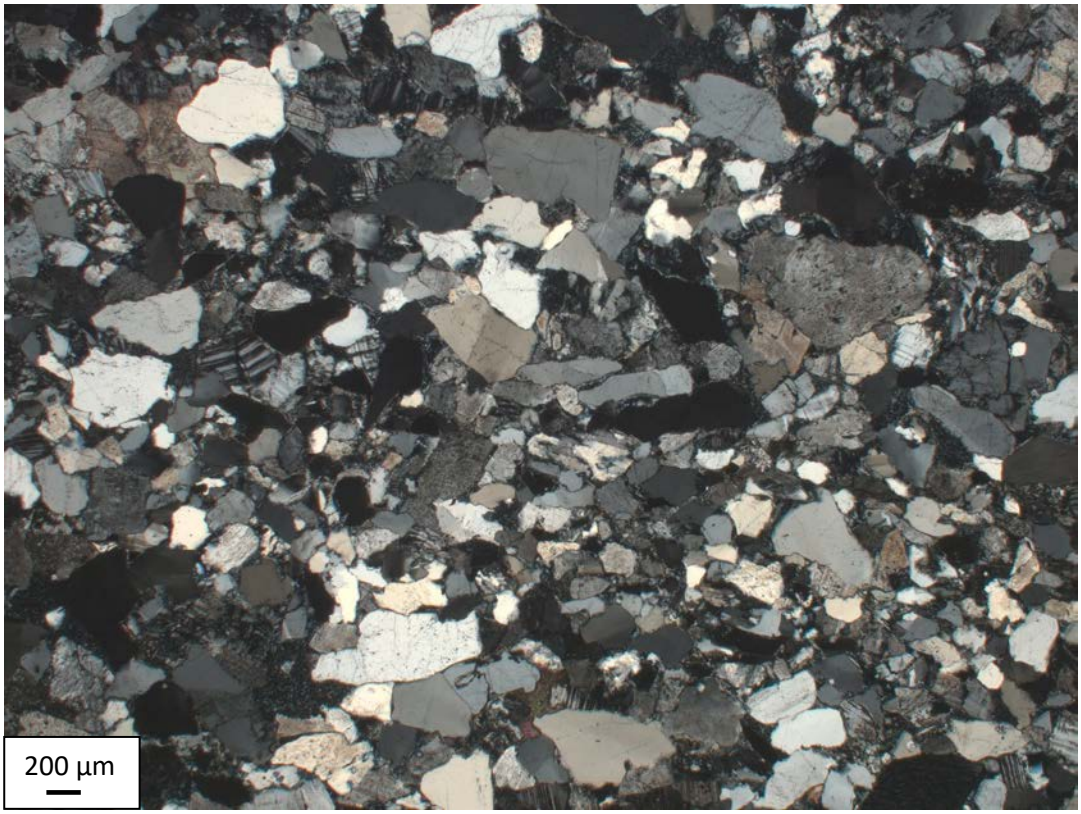

Aa1-Ga3318.10A Plug 10

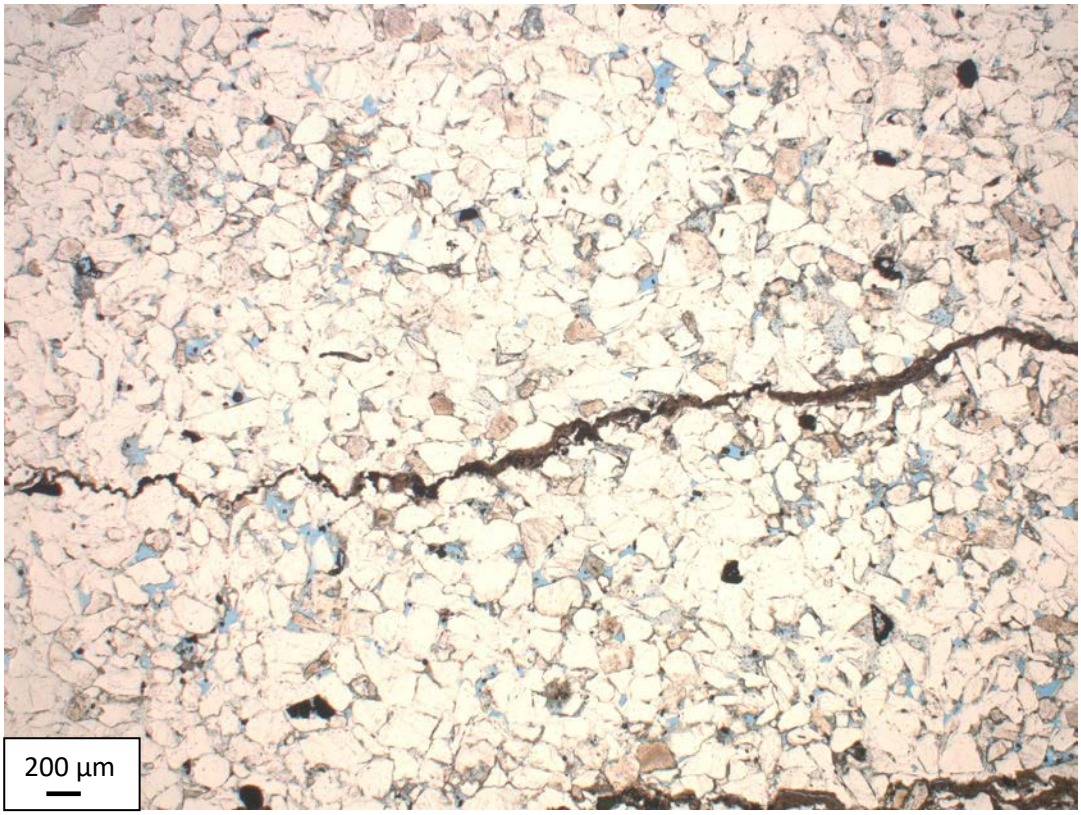

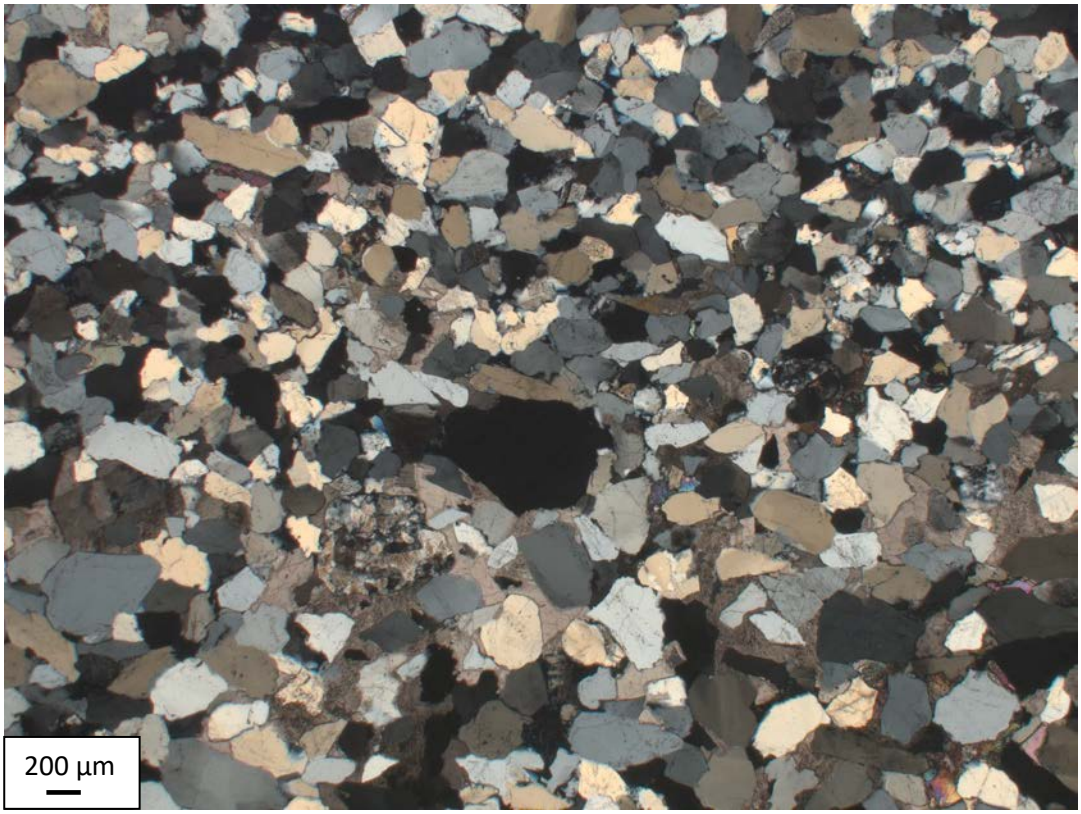

Th2-Sk2761.63A Plug 6

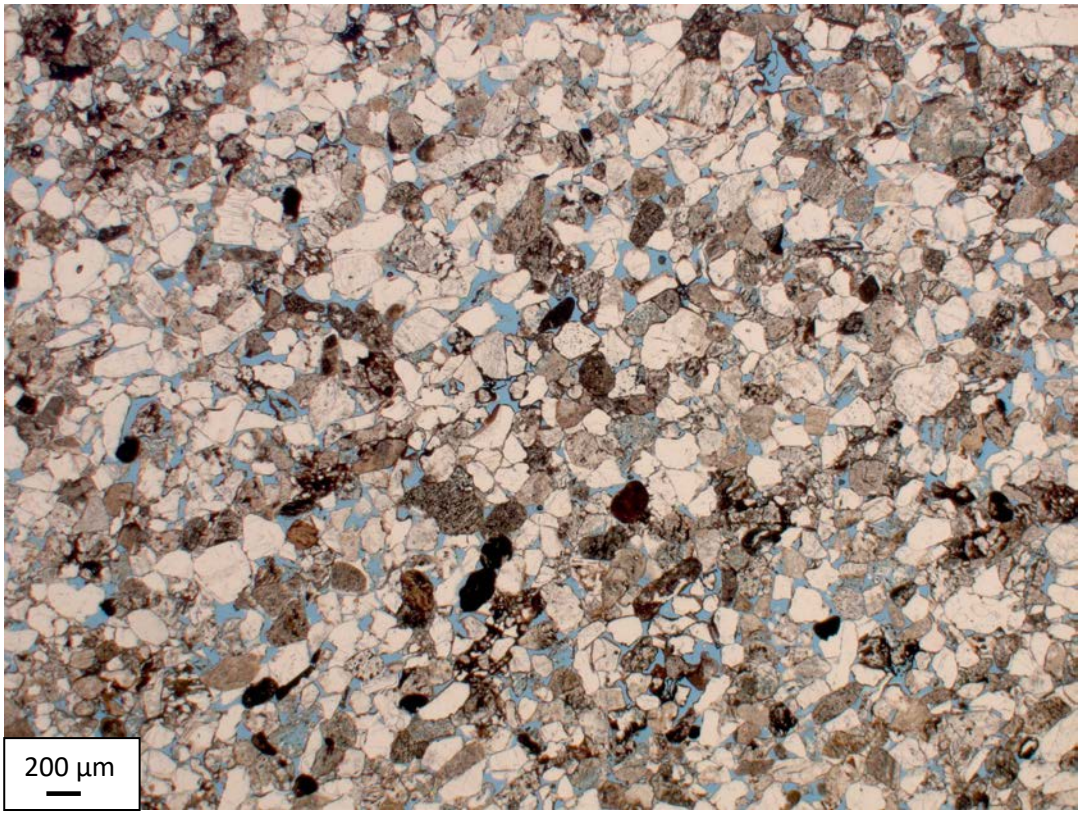

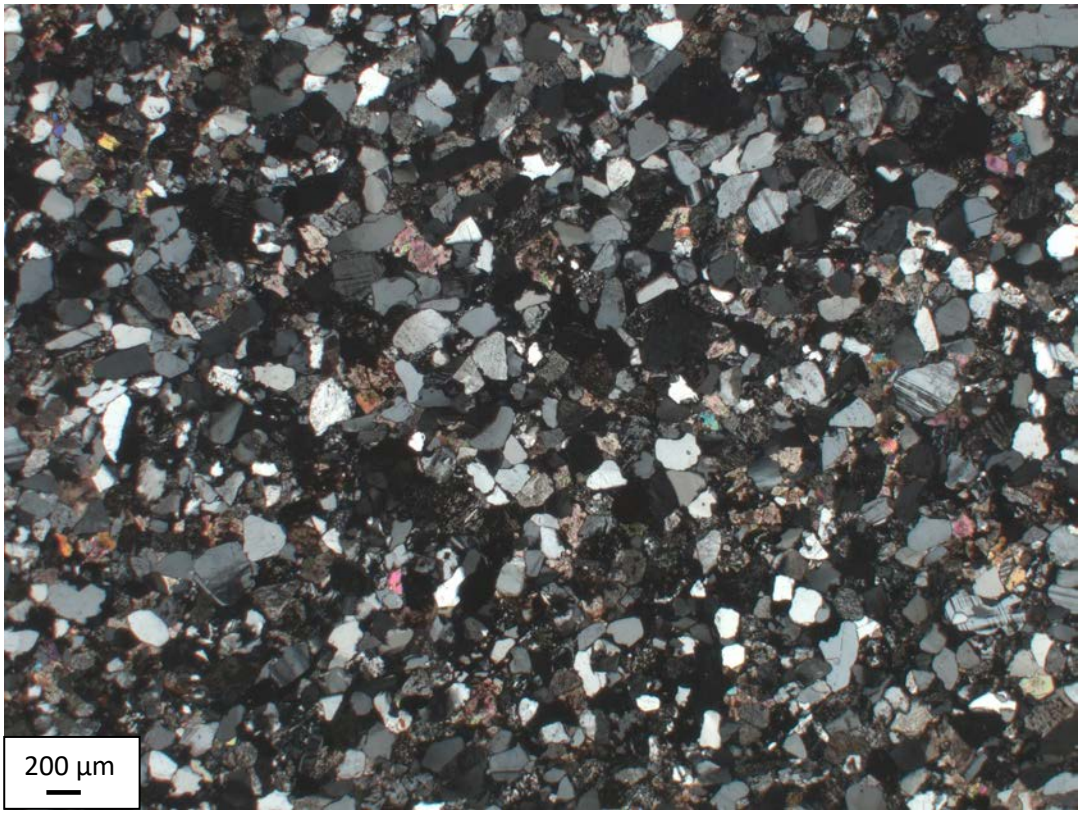

Th2-Sk2919.35B Plug 4A

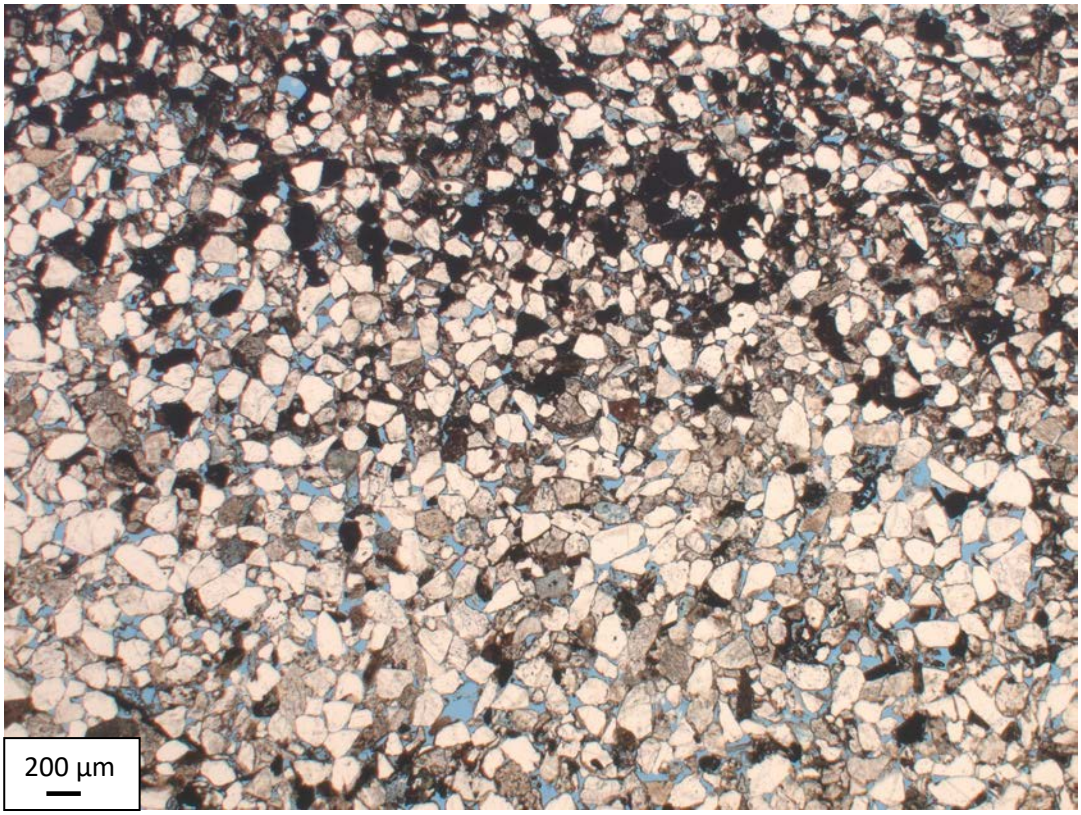

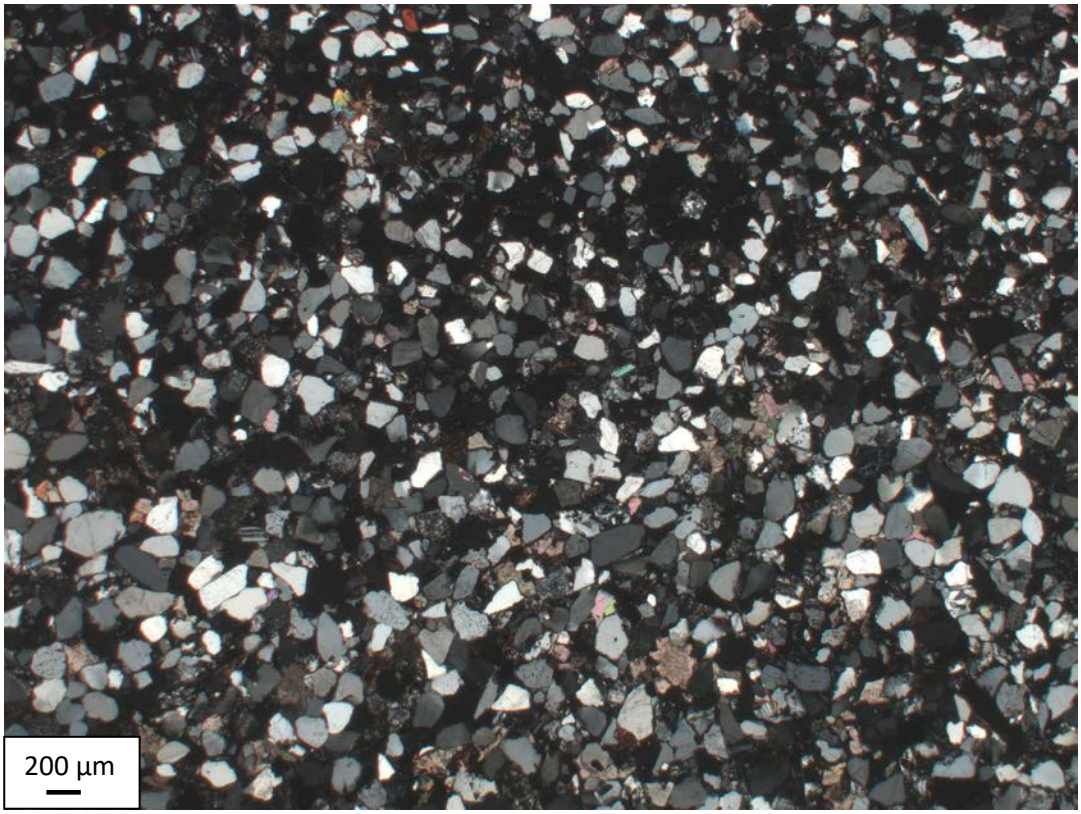

Mo1-Sk5034.24A Plug 15

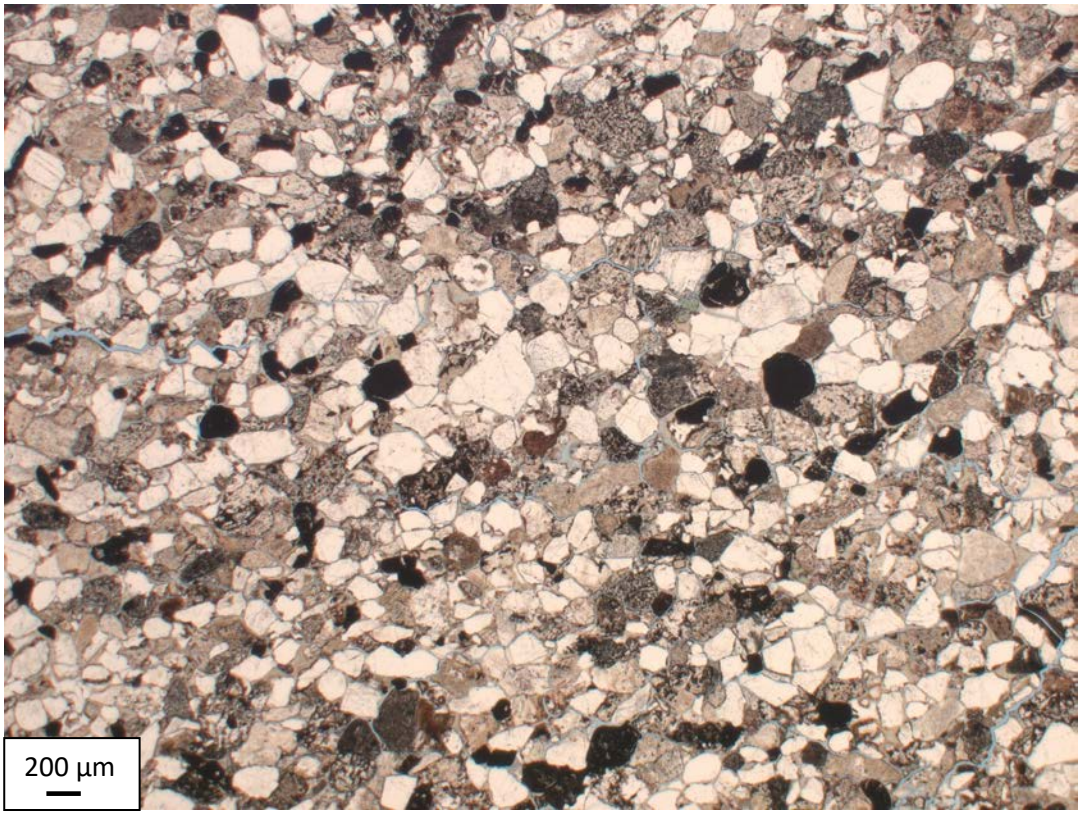

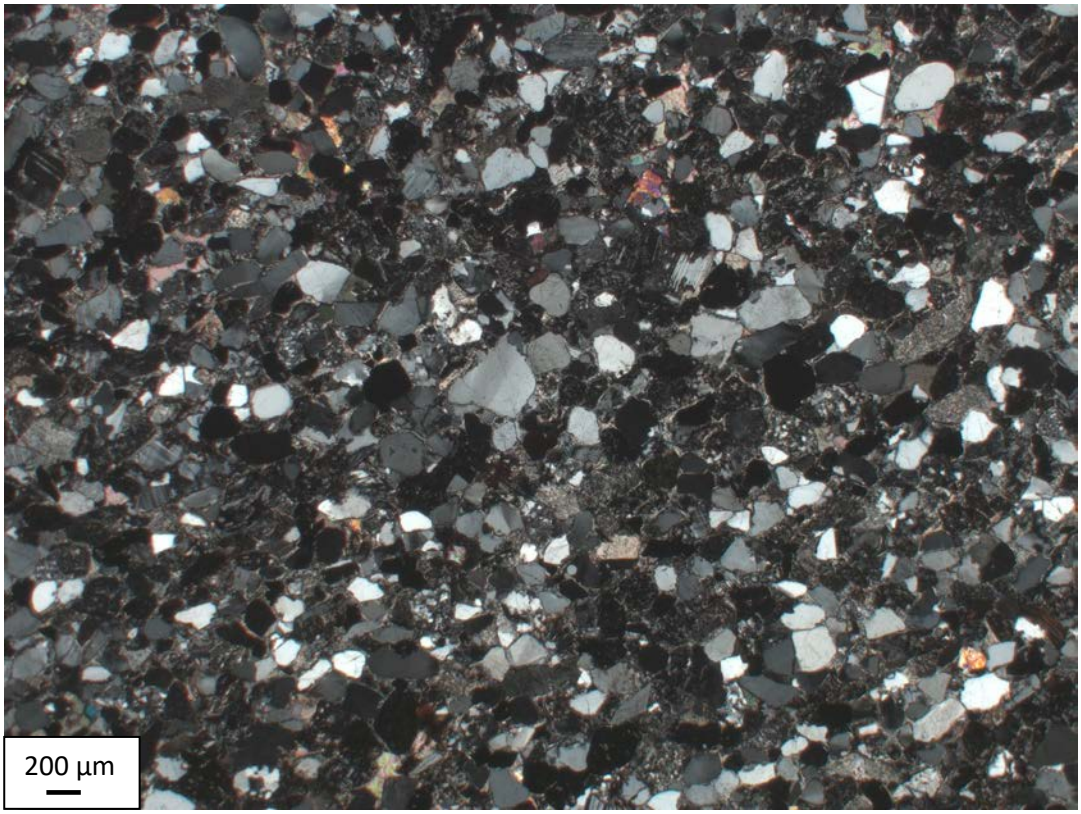

Th2-Sk2923.05A Plug 5

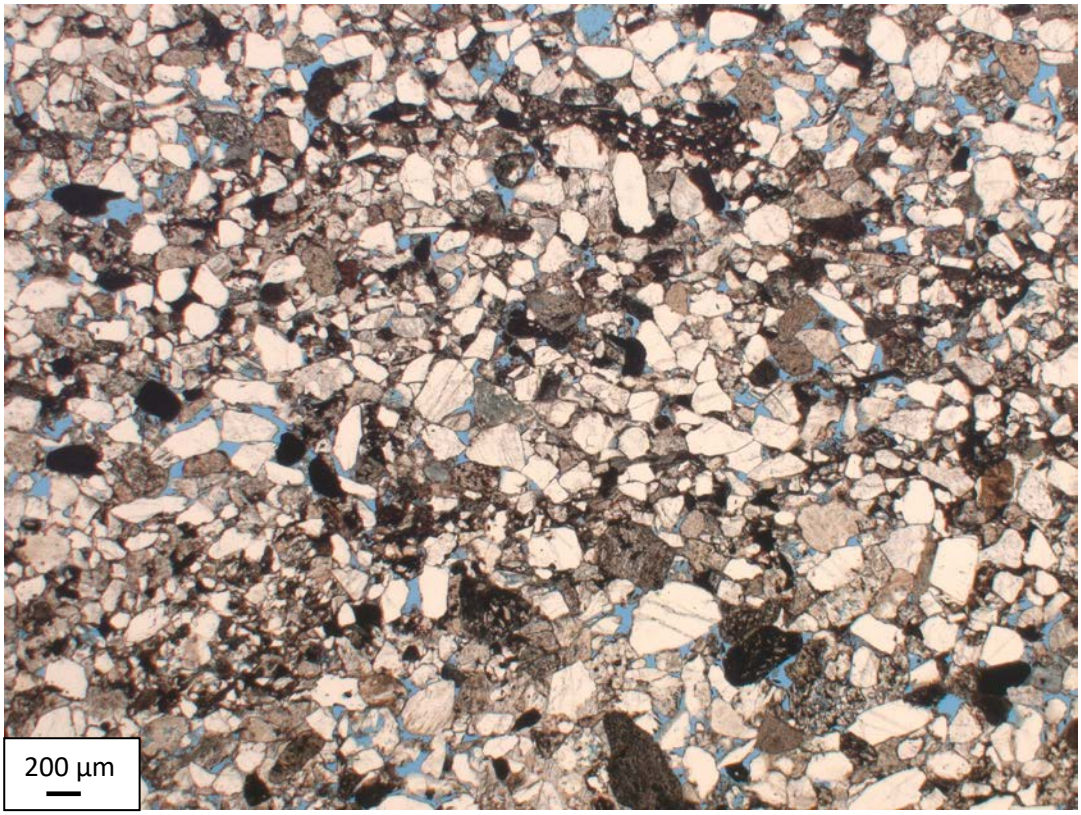

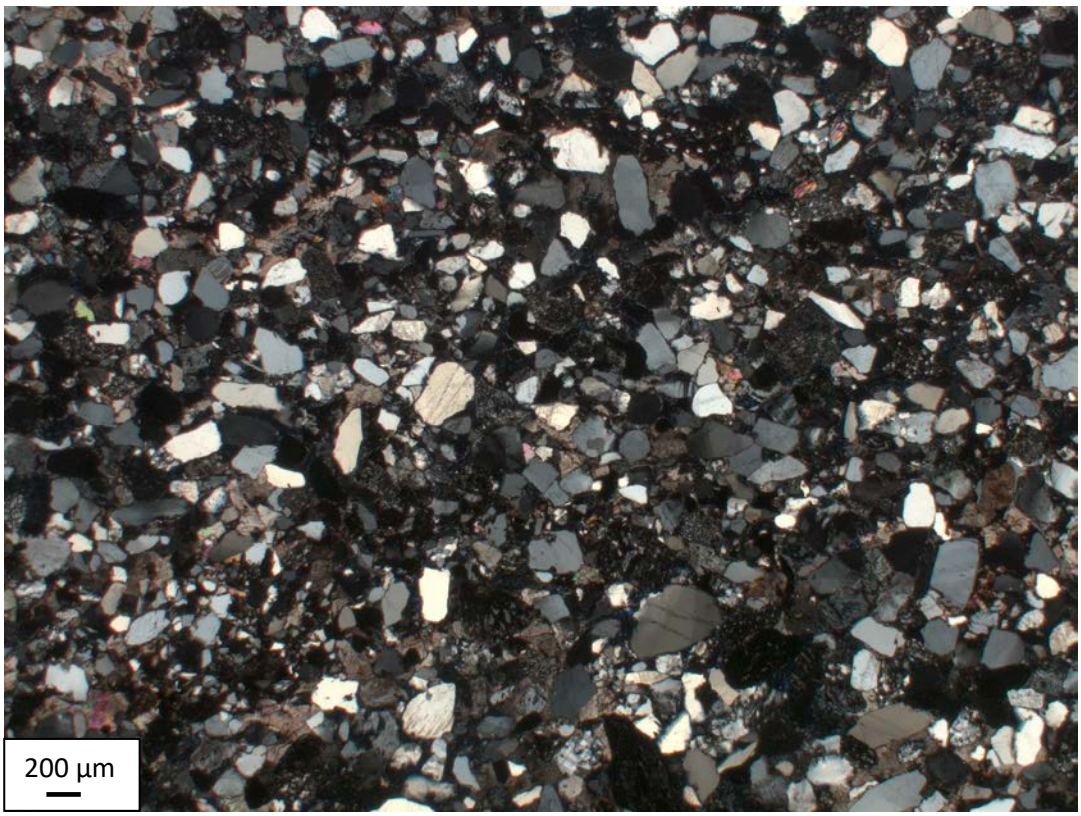

Mo1-Sk5089.57A Plug 3

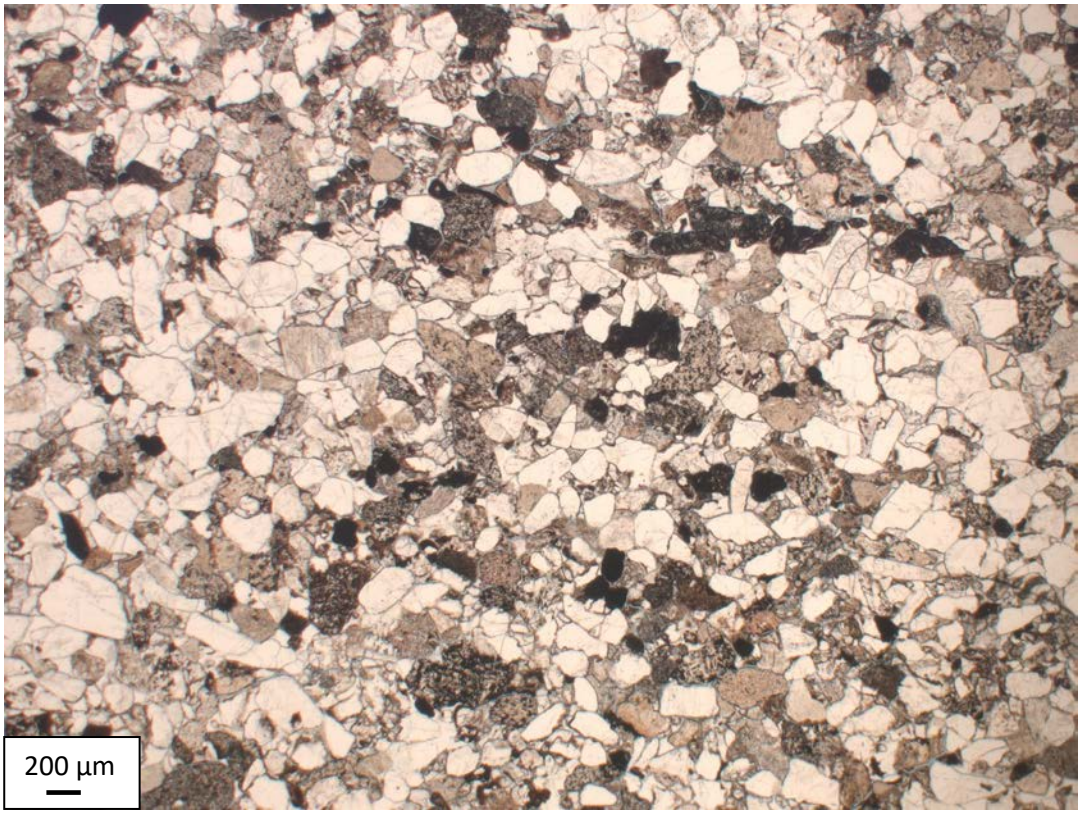

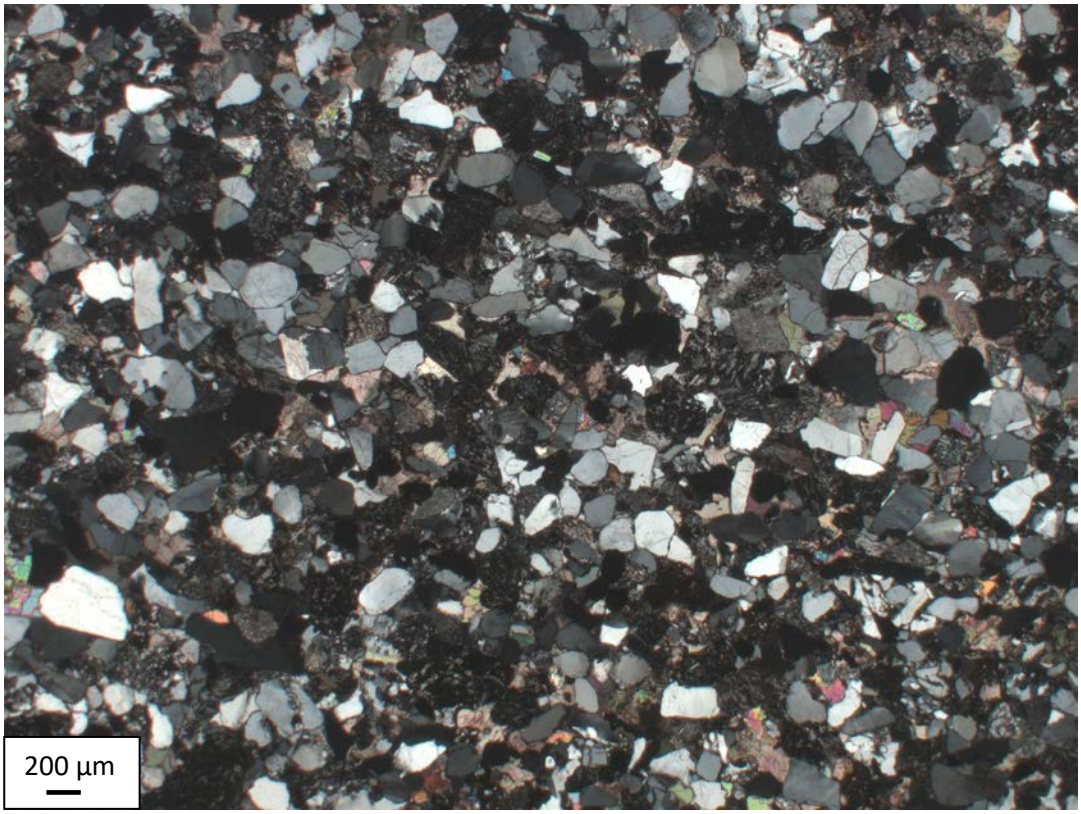

Ve1-Sk2062.92B Plug 7B

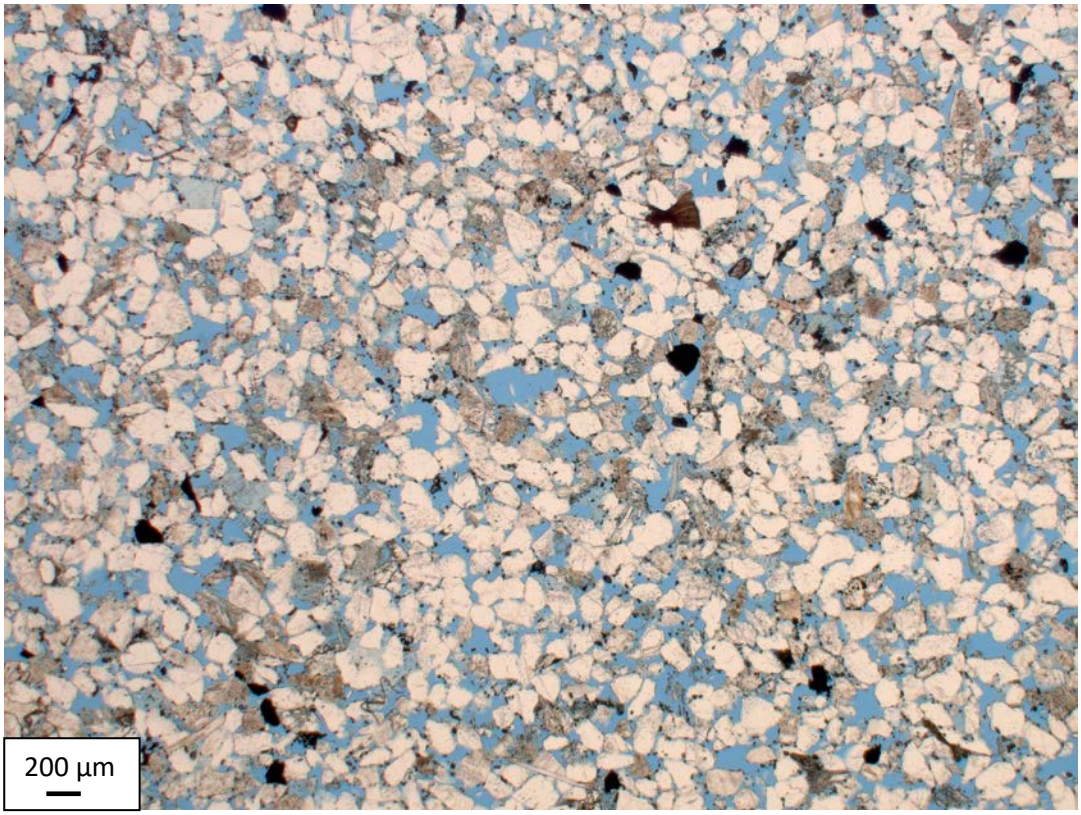

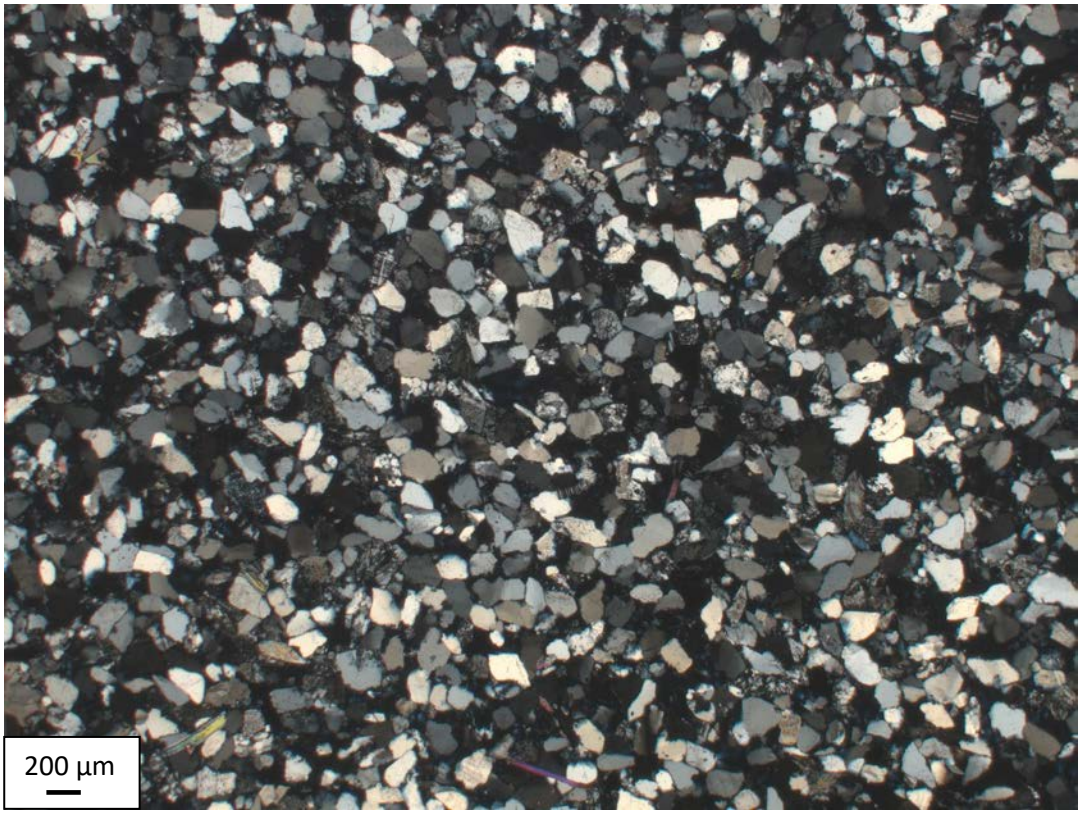
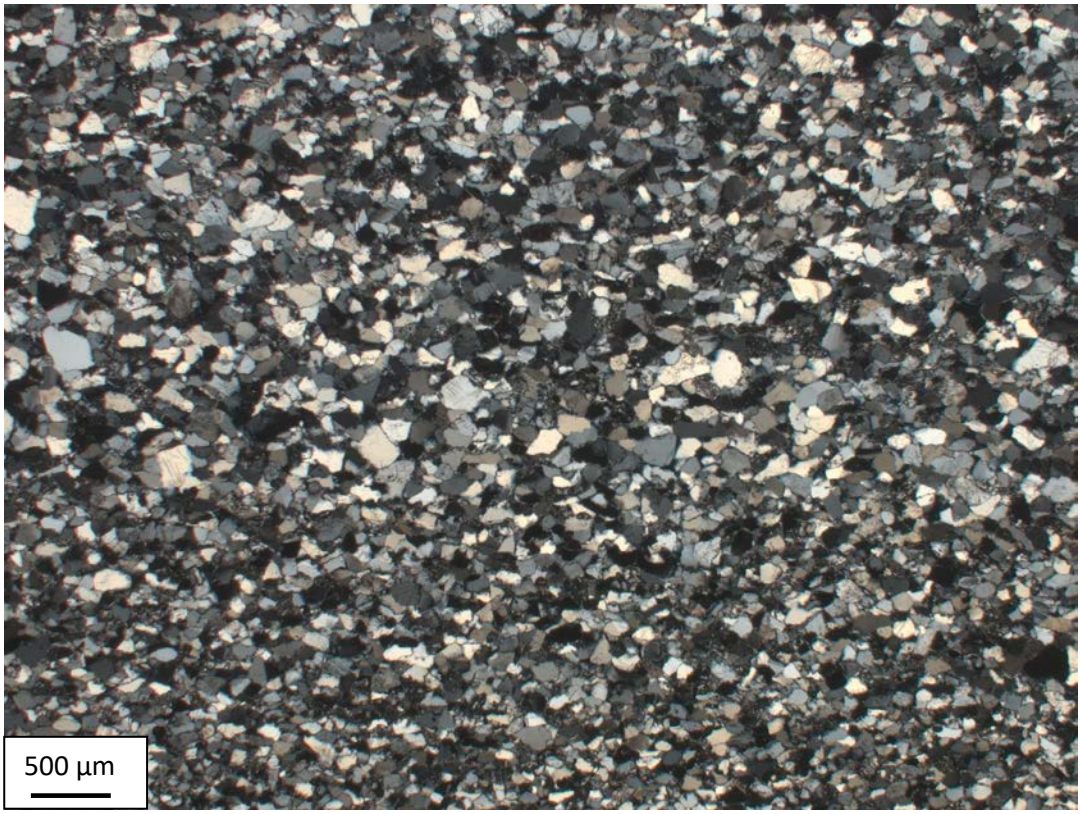
Ga1-Sk3032.42A Plug 1